

N3-TYPE RUTHENIUM RIGID ROD DYES AND N3-TYPE RUTHENIUM  
BIFUNCTIONAL DYES FOR STUDYING SOLAR CELL PROPERTIES

By Andrew Kopecky

A dissertation submitted to the  
Graduate School – Rutgers, Newark, The State University of New Jersey  
in partial fulfillment of requirements

for the degree of

Doctor of Philosophy

Graduate Program in Chemistry

Written under the direction of

Professor Elena Galoppini

and approved by

---

---

---

---

Newark, New Jersey  
May 2013

# Abstract of the Dissertation

## N3-Type Ruthenium Rigid Rod Dyes and N3-Type Ruthenium Bifunctional Dyes for Studying Solar Cell Properties

By Andrew Kopecky

Dissertation Director:

Professor Elena Galoppini

This thesis describes the synthesis and study of two types of ruthenium(II) bipyridyl complexes that were developed to study sensitization processes on  $\text{TiO}_2$  surfaces. The thesis will be separated into two parts: the synthesis, characterization, and study of rigid rod dyes to investigate  $V_{oc}$  and recombination, and the synthesis and preliminary results of thiol-substituted dyes that were developed to study the influence of platinum catalysis on redox mediator processes in dye-sensitized solar cells.

Rigid rod dyes, **AK0**, **AK1**, and **AK2**, a series of bis(bipyridyl) bis(thiocyanate) ruthenium(II) dyes (N3-type), were synthesized to study how dye structure affects voltage. Dyes **AK0-2** were synthesized through a one-pot complexation reaction with modified dipyrindyl ligands containing 0, 1, or 2 oligo(phenyleneethynylene) bridge units,

respectively, to study the effect of the chromophore-semiconductor distance. The dyes were characterized and their photophysical and photoelectrochemical properties were studied in solution and on  $\text{TiO}_2$  films. In DSSCs, the dyes showed an increase in  $V_{oc}$  due to decreased charge recombination rates with increasing semiconductor-chromophore distance. The recombination rate also showed decreased sensitivity to  $\text{TiO}_2$  electron concentrations as the chromophore-semiconductor distance increased. A second series of rigid-rod, N3-type dyes, **AK3** and **AK4**, was synthesized through a two-step complexation process proceeding through isolation of a *p*-cymene ruthenium(II) intermediate. These dyes contained long, saturated alkyl chain (nonyl) substituents on the ancillary bipyridyl ligand, with the goal of increasing solubility and facilitating solution characterization. These dyes were characterized synthetically and currently are being studied for  $\text{I}_2$ -adduct formation.

The modified thiol dyes were targeted for studying the catalytic process of redox mediator regeneration. As platinum has been shown to catalyze the  $\text{I}^-/\text{I}_3^-$  redox reaction, it was thought that by incorporating platinum nanoparticles into DSSCs the large overpotential for the  $\text{I}^-/\text{I}_3^-$  redox mediator could be reduced. A modified N3-type dye was designed with carboxylic acid groups for anchoring to  $\text{TiO}_2$  in the DSSC on one bipyridyl ligand and thiols on the other for attachment to platinum. The synthesis of the novel thiolane bipyridyl ligand was followed by a two-step complexation process and both ligand and dye were successfully synthesized and characterized. The dye, **AK6**, shows positive current and efficiencies of approximately 3% when used as a sensitizer in

an operational DSSC. It has also been shown to bind to platinum wire. These preliminary results suggest that this dye may allow for incorporation of platinum nanoparticles into the DSSC, which is currently being investigated.



# Acknowledgements

I would like to express my sincerest appreciation to my advisor, Dr. Elena Galoppini, for the gift of her time, assistance, and guidance. My appreciation also extends to everyone in our group, both past and present members: Dr. Olena Taratula, Dr. Sujatha Thyagarajan, Dr. Yongyi Zhang, Dr. Alfred Lee, Dr. Marina Kaiser, Dr. Elena Ruiz, Dr. Hao Tang, Keyur Chitre, Agnieszka Klimczak, Hao Fan, and Jessica Rivera. I would like to thank the undergraduate students who have worked with me on my projects for their time and contributions, Ardian Agushi, Alberto Batarseh, Hudifah Rabie, and Junaid Chaudhry. I would also like to thank the faculty and staff that have helped with collecting some of the data from the thesis: Dr. Lalancette for his work with crystallography and x-ray data, Dr. Kakalis for help with the NMR facilities, and Dr. Brukh for help with mass spectroscopy and other technical problems that may have arisen. Last, I would like to thank the members of my thesis committee, Dr. Pietrangelo, Dr. Lockard, and Dr. Agrios for their time and assistance.

I am grateful for the hard work and wonderful communication of our collaborators at Johns Hopkins University, Dr. Gerald Meyer and Dr. Patrik Johansson. Without their hard work, many of our wonderful results would not have been realized. I am also grateful for the work of our collaborators at the University of Connecticut, Dr. Alexander

Agrios and Guangliang Liu. Their work on the thiol project has been outstanding and I look forward to future interactions with their group.

Lastly, I would like to thank my family, especially my mother and sister for their support. My biggest thank you goes out to my wife, Yan Cao, both a member of our research group as well as the love of my life. I appreciate all the love and support both in the lab and outside on my way to completing my thesis. Thank you.

# Table of Contents

Abstract of the Dissertation .....	ii
Acknowledgements.....	v
List of Tables .....	ix
List of Schemes .....	x
List of Figures .....	xi
List of Acronyms/Abbreviations.....	xiii
Chapter 1: Ruthenium Dyes for Dye-Sensitized Solar Cells .....	1
Chapter 2: Rigid Rod N3-Type Dyes for Open-Circuit Photovoltage Studies .....	11
Introduction .....	12
Synthesis .....	17
Experimental .....	17
Discussion.....	45
Results and Discussion .....	54
Photophysical Measurements .....	54
Iodine Coordination .....	66
Conclusion.....	68
Chapter 3: Modified N3-Type Dyes for Coordination to Platinum Nanoparticles .....	70
Introduction .....	71
Synthesis .....	77
Experimental .....	77
Discussion.....	88
Results and Discussion .....	95
Conclusion.....	99
Conclusion.....	100
Appendix .....	102
Spectra .....	102
Additional figures.....	179
X-Ray Data:.....	182
References .....	212



# List of Tables

<b>Table 1</b> Charge Recombination Rates .....	57
<b>Table 2</b> Summary of Solution Data.....	59
<b>Table 3</b> Summary of TiO <sub>2</sub> Thin Film Data.....	60
<b>Table 4</b> Summary of Photophysical Properties .....	96

## List of Schemes

<b>Scheme 1</b> Synthesis of Anchor Ligands: <b>a.</b> NBS, H <sub>2</sub> SO <sub>4</sub> ; 90%; <b>b.</b> CuBr, PdCl <sub>2</sub> (PPh <sub>3</sub> ) <sub>2</sub> , Trimethylsilyl Acetylene, Diisopropyl Amine; 53%; <b>c.</b> TBAF, THF; 76%; <b>d.</b> Pd(PPh <sub>3</sub> ) <sub>4</sub> , Diisopropyl Amine, Benzene; 40%; <b>e.</b> Pd(PPh <sub>3</sub> ) <sub>4</sub> , Diisopropyl Amine, Benzene; 69% <b>f.</b> TBAF, THF; 50%; <b>g.</b> Pd(PPh <sub>3</sub> ) <sub>4</sub> , Diisopropyl Amine, Benzene; 83%; <b>h.</b> NaOH, MeOH, CH <sub>2</sub> Cl <sub>2</sub> ; 57%; <b>i.</b> NaOH, MeOH, CH <sub>2</sub> Cl <sub>2</sub> ; 80%.....	46
<b>Scheme 2</b> Synthesis of Dipyrityl ligands: <b>j.</b> HNO <sub>3</sub> , H <sub>2</sub> SO <sub>4</sub> ; 50%; <b>k.</b> H <sub>2</sub> (g), 10% Pd/C, MeOH; 91%; <b>l.</b> 1. NaNO <sub>2</sub> , H <sub>2</sub> SO <sub>4</sub> , 2. KI; 57% .....	46
<b>Scheme 3</b> General Scheme for One-Pot complexation reaction: stepwise addition of ligands followed by quenching with excess ammonium thiocyanate. ....	47
<b>Scheme 4</b> General scheme for hydrolysis of esters: sodium hydroxide in organic solvents. ....	49
<b>Scheme 5</b> General scheme for first step in two step complexation: addition of primary ligand. ....	52
<b>Scheme 6</b> General scheme for second step in two step complexation: addition of the secondary ligand followed by quenching with ammonium thiocyanate. ....	52
<b>Scheme 7</b> Initial synthetic process: targeting terminal alkyl thiol bipyridines .....	88
<b>Scheme 8</b> Adapted synthesis to achieve thiol bipyridines .....	91
<b>Scheme 9</b> Two-step complexation of lipoate bipyridine complex .....	92

# List of Figures

<b>Figure 1</b> Graetzel's dye, N3 .....	2
<b>Figure 2</b> Typical DSSC, adapted from reference 8 .....	3
<b>Figure 3</b> Electronic mechanism of DSSC .....	4
<b>Figure 4</b> IV curve for N3, depicts typical IV curve for two different dyes with $V_{oc}$ occurring when the curve intersects the x-axis, adapted from reference 4 .....	5
<b>Figure 5</b> Red arrows depict negative, competing recombination processes in solar cell mechanics .....	6
<b>Figure 6</b> Left: tripodal dyes; right: $V_{oc}$ vs. irradiance, $V_{oc}$ increases as distance increases, adapted from reference 21 .....	7
<b>Figure 7</b> Top left: dyes synthesized by Sun and coworkers; Bottom left: Solar cell properties of dyes; Top right: tuning HOMO and LUMO levels; Bottom right: dyes show increasing recombination rate with distance; adapted from references 22 and 23 .....	8
<b>Figure 8</b> More positive redox mediators show increasing $V_{oc}$ and faster recombination due to changes in the recombination and quasi-Fermi level of the semiconductor, adapted from reference 25 .....	10
<b>Figure 9</b> A sample of dyes studied in DSSCs that perform well, included is N3 .....	12
<b>Figure 10</b> Oligo(phenylene-ethynylene) (OPE) units .....	13
<b>Figure 11</b> DFT calculations of HOMO and LUMO for <b>AK2</b> ; LUMO calculations suggest dye to be capable of injection; adapted from reference 53 .....	14
<b>Figure 12</b> Targeted N3-type dyes, <b>AK0-2</b> , with calculated semiconductor-chromophore distance shown ..	15
<b>Figure 13</b> ORTEP diagram of Compound <b>17</b> showing the numbering scheme. Displacement ellipsoids are drawn at 30% probability level for non-H atoms .....	37
<b>Figure 14</b> Mechanism of the Sonogashira coupling reaction, adapted from reference 69 .....	45
<b>Figure 15</b> Two stereoisomers of <b>AK1-4</b> ; R is either <i>trans</i> from a thiocyanate group (left) or <i>trans</i> from a pyridyl group (right) .....	48
<b>Figure 16</b> $^1\text{H}$ NMR spectrum of Short Ester Rod. Signal from the methyl ester peaks at 3.8-4.2 ppm shows two peaks from the separate isomers present. ....	49
<b>Figure 17</b> $^{13}\text{C}$ NMR spectrum of Short Ester Rod. Signal from the methyl ester peaks at 52.5-53.0 ppm shows two peaks indicating separate isomers. ....	49
<b>Figure 18</b> ESI Spectra of <b>AK0</b> with different exposure times to DMSO. a. Spectrum of <b>AK0</b> with 0 day exposure to DMSO solution; b.-f. calculated ESI spectra for <b>AK0</b> (b. $[\text{M}+\text{H}]^+$ ; c. $[\text{M}+\text{Na}]^+$ ; d. $[\text{M}-(\text{NCS}^-)+(\text{DMSO})]^+$ ; e. $[\text{M}-(\text{NCS}^-)+(\text{DMSO})+\text{Na}]^+$ ; f. $[\text{M}-(\text{NCS}^-)]^+$ ; g. Spectrum of <b>AK0</b> after 1 day exposure to DMSO. ....	50
<b>Figure 19</b> ESI Spectra of <b>AK5</b> with different exposure times to DMSO. a. Spectrum of <b>AK5</b> with 0 day exposure to DMSO solution; b.-f. calculated ESI spectra for <b>AK5</b> (b. $[\text{M}]^+$ ; c. $[\text{M}+\text{Na}]^+$ ; d. $[\text{M}+\text{K}]^+$ ; e. $[\text{M}-(\text{NCS}^-)]^+$ ; f. $[\text{M}-(\text{NCS}^-)+(\text{DMSO})]^+$ ; g. Spectrum of <b>AK5</b> after 1 day exposure to DMSO .....	50
<b>Figure 20</b> Abs Spectra of <b>AK0</b> (black), <b>AK1</b> (red), and <b>AK2</b> (green) in Acetonitrile .....	54
<b>Figure 21</b> Photoluminescence Spectra of <b>AK0</b> (black), <b>AK1</b> (red), and <b>AK2</b> (green) in acetonitrile .....	54
<b>Figure 22</b> Absorption Spectra of dyes bound to $\text{TiO}_2$ ; solid line represents neat compound, dashed line represents neat compound plus $\text{Li}^+$ ; <b>AK0</b> (black), <b>AK1</b> (red), <b>AK2</b> (green) .....	55
<b>Figure 23</b> Photoluminescence spectra of <b>AK0</b> (black), <b>AK1</b> (red), and <b>AK2</b> (green) bound to $\text{TiO}_2$ . Darker colors show quenching of emission characteristic of injection in the presence of $\text{Li}^+$ .....	56
<b>Figure 24</b> Transient absorption spectrum of <b>13</b> in Acetonitrile solution .....	56
<b>Figure 25</b> Transient absorption spectrum of <b>13</b> on $\text{TiO}_2$ films .....	56
<b>Figure 26</b> Charge recombination. left: <b>AK0</b> (black), <b>13</b> (red), and <b>AK1</b> (blue) with KWW fit (white); right: <b>AK0</b> (black), <b>6</b> (red), and <b>AK1</b> (blue) on long time scale .....	57
<b>Figure 27</b> $V_{oc}$ as a function of irradiance for <b>AK0</b> (black), <b>13</b> (red), and <b>AK1</b> (green) .....	58
<b>Figure 28</b> $V_{oc}$ as a function of irradiance in the presence of $\text{Li}^+$ and $\text{I}^-$ , solar cell conditions; <b>AK0</b> (red), <b>AK1</b> (green), <b>AK2</b> (pale blue) .....	59
<b>Figure 29</b> IPCE for <b>AK0</b> (black), <b>AK1</b> (red), <b>AK2</b> (green) .....	59

<b>Figure 30</b> Transient absorption data monitored at 500 nm after pulsed 532 nm laser excitation of dyes on TiO <sub>2</sub> : <b>AK0</b> (black), <b>AK1</b> (red), and <b>AK2</b> (green) as laser power changes, from a to d: 0.15 mJ, 0.3 mJ, 0.7 mJ, 1.4 mJ.....	61
<b>Figure 31</b> Transient absorption data monitored at 500 nm after pulsed 532 nm laser excitation (0.2 mJ/pulse) of dyes on TiO <sub>2</sub> <b>AK0</b> (black), <b>AK1</b> (red), and <b>AK2</b> (green) with an applied bias of A) +150 mV; B) -150 mV; and C) -350 mV versus NHE. ....	62
<b>Figure 32</b> $k_{cr}$ as a function of distance with attenuation factor $\beta$ , fitted with and without <b>AK0</b> .....	63
<b>Figure 33</b> <b>AK0</b> (black), <b>AK1</b> (red), and <b>AK2</b> (green) on TiO <sub>2</sub> in the presence of 1.33 mM I <sub>2</sub> (dashed) and absence of I <sub>2</sub> (solid). Inset: Binding isotherm for <b>AK0-2</b> with $K = 2 \times 10^4 \text{ M}^{-1}$ .....	66
<b>Figure 34</b> DSSC electronic diagram; Redox mediator overpotential is the difference between HOMO level of the dye and the redox mediator potential. ....	71
<b>Figure 35</b> Cyclic voltammograms of I <sup>-</sup> /I <sub>3</sub> <sup>-</sup> oxidation in the presence (red) and absence (black) of platinum .....	73
<b>Figure 36</b> A variety of organometallic complexes attached to palladium nanoparticles; adapted from reference 103.....	75
<b>Figure 37</b> Targeted dye schematic, showing <b>AK6</b> .....	76
<b>Figure 38</b> ORTEP diagram of Compound <b>23</b> showing the numbering scheme. The other half of the molecule is generated by a center of symmetry. Displacement ellipsoids are drawn at the 30% probability level for non-H atoms.....	79
<b>Figure 39</b> ORTEP diagram of Compound <b>22</b> showing the numbering scheme. The image has been simplified to show only one molecule of the asymmetric unit. Displacement ellipsoids are drawn at the 30% probability level for non-H atoms.....	86
<b>Figure 40</b> Lipoate Bipyridine. This intermediate was not synthesized due to concerns that thiolane functional groups may coordinate to ruthenium. ....	93
<b>Figure 41</b> Absorption spectra for <b>AK6</b> at different concentrations. Inset: extinction coefficient calculation .....	95
<b>Figure 42</b> Emission spectrum of <b>AK6</b> , $\lambda_{exc} = 620 \text{ nm}$ .....	95
<b>Figure 43</b> Excitation spectrum for <b>AK6</b> , $\lambda_{emiss} = 764 \text{ nm}$ .....	96
<b>Figure 44</b> IV curve for DSSC with <b>AK6</b> under AM 1.5 radiation at $100 \text{ mW cm}^{-2}$ (1 sun) .....	96
<b>Figure 45</b> CV of <b>AK6</b> on Pt wire plus control experiments; Pt + <b>AK6</b> shows oxidation wave at +0.80 V vs. SCE suggesting binding of <b>AK6</b> to platinum wire .....	97
<b>Figure 46</b> IV curves for DSSC devices under simulated AM 1.5G sunlight at $1000 \text{ W/m}^2$ (1 sun) intensity ..	97



## List of Acronyms/Abbreviations

DSSC	Dye-sensitized solar cell
N3	Bis(bipyridyl) bis(thiocyanate) ruthenium(II)
TiO <sub>2</sub>	Titanium dioxide
FTO	Fluorine-doped tin oxide
E <sub>vb</sub> /E <sub>cb</sub>	Valence band/conduction band
HOMO	Highest occupied molecular orbital
LUMO	Lowest unoccupied molecular orbital
V <sub>oc</sub>	Open-circuit voltage
IV curve	Current-voltage curve
FF	Fill factor
J <sub>sc</sub> /I <sub>sc</sub>	Short-circuit current
OPE	Oligo(phenyleneethynylene)
DFT	Density functional theory
DMSO	Dimethyl sulfoxide
ESI	Electrospray Ionization
NMR	Nuclear magnetic resonance
THF	Tetrahydrofuran
HCl	Hydrochloric acid
DMF	N,N-Dimethylformamide
TBAF	Tetra-n-butyl ammonium fluoride
TMS	Trimethylsilyl
MLCT	Metal-to-ligand charge transfer band
TA	Transient absorption
KWW	Kolrausch-Williams-Watts function
IPCE	Incident photo-to-current efficiency
NHE	Normal hydrogen electrode
Pt	Platinum
SAM	Self-assembled monolayer
DCC	Dicyclohexylcarbodiimide
DMAP	Dimethyl aminopyridine
LDA	Lithium diisopropyl amide
NSF	National Science Foundation
DOE	Department of Energy

# **Chapter 1: Ruthenium Dyes for Dye-Sensitized Solar Cells**

## Introduction

With increased energy demands upon the world, there has been a global drive for the development of sustainable alternative fuel sources to replace fossil fuel use. Current estimates put the requirement for worldwide power production in the future over 6 TW.<sup>1</sup> Silicon-based solar cells have been operational for many years,<sup>2</sup> however, the cost and complexity of manufacture has led many to investigate other means of harnessing solar energy as a renewable source of power.

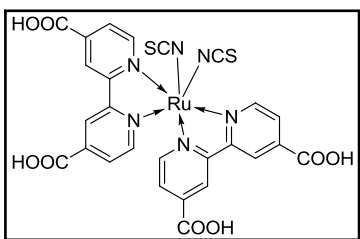


**Figure 1** Graetzel's dye, N3

In 1991, Graetzel and O'Regan developed the "Dye-Sensitized Solar Cell" (DSSC),<sup>3</sup> reporting over an order of magnitude improvement in efficiency compared to other previous attempts at dyed cells. Their main advance was the use of a nanocrystalline, mesoporous thin film semiconductor with high surface area to adsorb the organic dye. In 1993, Graetzel and coworkers developed a *cis*-ruthenium bis(bipyridyl) bis(thiocyanato) sensitizer for the DSSC with at-the-time record efficiencies of ~10%.<sup>4</sup> The dye, since dubbed N3 (Figure 1), has carboxylic acid modifications to the bipyridyl ligands for covalent attachment to the semiconductor surface, in this case titanium dioxide, TiO<sub>2</sub>.

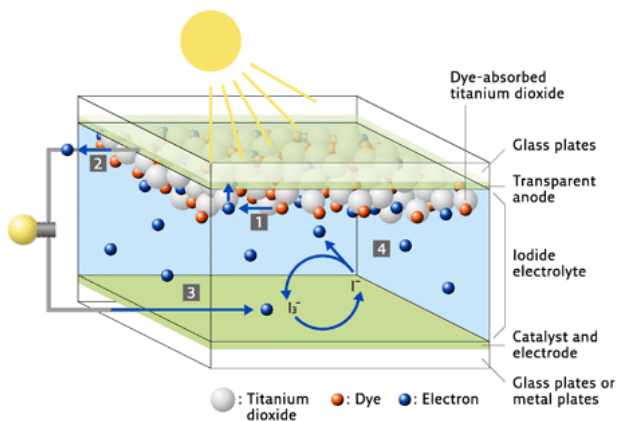


**Figure 2** Typical DSSC, adapted from reference 8

layer of nanocrystalline semiconductor (often  $\text{TiO}_2$  or another metal oxide, such as zinc oxide) cast across the surface. A chromophore is then attached to semiconductor nanoparticles, often through the use of an anchor group. The most frequently used anchor groups are carboxylic acids<sup>4,9</sup> and phosphonate groups,<sup>10-12</sup> and recent studies point at the acetylacetonate group as a strong anchor group.<sup>13</sup>

The counter electrode is a platinized piece of FTO glass. Separating the two electrodes is an electrolyte solution, typically in acetonitrile, with an external electron donor to reduce the oxidized dye (dye regeneration). This donor is termed the redox mediator and is conventionally  $\text{I}^-/\text{I}_3^-$ . This mediator is generated from  $\text{I}^-$  and  $\text{I}_2$  present in the solution, with an equilibrium constant of  $\sim 10^7 \text{ M}^{-1}$  for triiodide formation in acetonitrile.<sup>14,15</sup>

Since then, much has been studied about the DSSC, from the properties of electrons injected into  $\text{TiO}_2$ <sup>5,6</sup> to dye modifications.<sup>7</sup> A typical DSSC is shown in Figure 2.<sup>8</sup> It consists of a layer of conductive glass, typically fluorine-doped tin oxide (FTO) with a

A schematic diagram of electronic events occurring in a DSSC is shown in Figure 3.<sup>16</sup> In this case, the semiconductor is  $\text{TiO}_2$ . Depicted are the valence ( $E_{vb}$ ) and conduction ( $E_{cb}$ ) bands of the semiconductor. The energy levels of  $E_{cb}$  are very fluid depending upon the conditions of the semiconductor, for example the presence of cations or electrolyte solution.<sup>17</sup> When a ground state dye D, depicted here  $\text{Ru(II)}$ , is photoexcited, it forms an excited chromophore  $\text{D}^*$ ,  $\text{Ru(II)}^*$ . If the excited state possesses sufficient energy, in other words if the LUMO of the dye has a sufficiently more negative potential than the

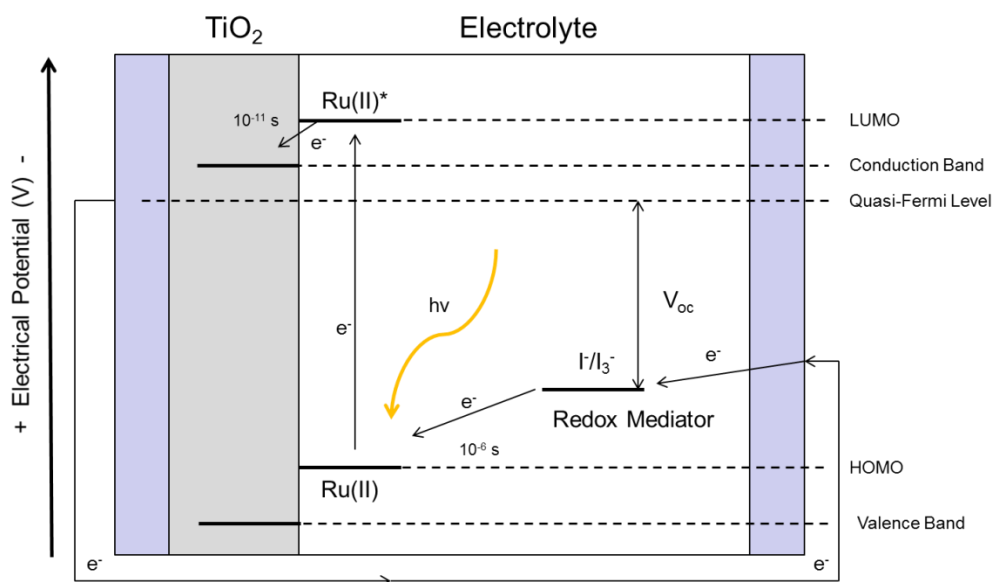


**Figure 3** Electronic mechanism of DSSC

conduction band of the semiconductor, an electron can transfer from  $\text{D}^*$  to the semiconductor's quasi-Fermi level leaving an oxidized dye  $\text{D}^+$  and an electron injected into the semiconductor,  $\text{TiO}_2(\text{e}^-)$ .

The electron in the semiconductor then migrates to the FTO glass electrode, Figure 2.<sup>8</sup> It then passes through a load to the counter electrode where it can reduce  $I_3^-$  to  $I^-$ . Iodide acts as an electron donor to reduce the oxidized dye  $D^+$  to its ground state yielding an iodine radical. The now-reduced dye is available to absorb another photon and begin the cycle again.

The potential required to reduce the oxidized mediator is the redox mediator overpotential. The difference between the redox mediator potential and the quasi-Fermi level of the semiconductor is the open-circuit photovoltage,  $V_{oc}$ .  $V_{oc}$  is the maximum Gibbs free energy available during steady state irradiances and occurs when

the current through the cell is 0. In a typical current-voltage (IV) curve, Figure 4,<sup>4</sup>  $V_{oc}$  is the point where the IV curve intersects the x-axis.

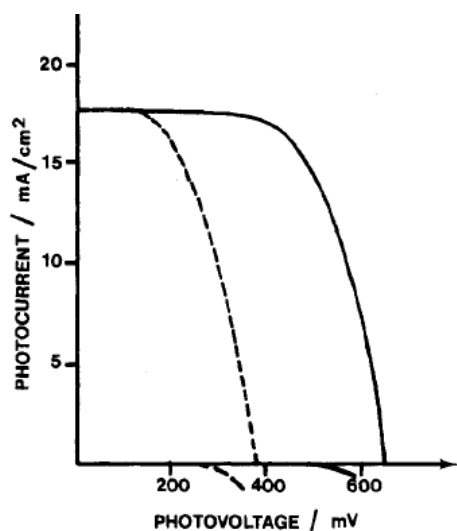


**Figure 4** IV curve for N3, depicts typical IV curve for two different dyes with  $V_{oc}$  occurring when the curve intersects the x-axis, adapted from reference 4

Theoretically, there are two ways to increase the open-circuit voltage in a solar cell. The first method is to raise the quasi-Fermi level and conduction band of the semiconductor surface. The conduction band changes

depending upon several factors, including the semiconductor morphology, the presence of ions, and the preparation. The other method to raise  $V_{oc}$  would be to lower the redox mediator potential.

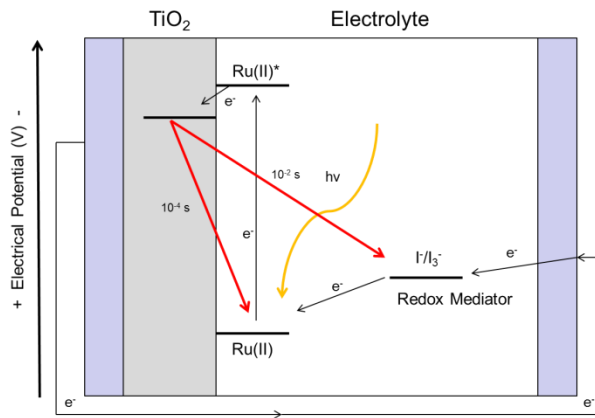


**Figure 5** Red arrows depict negative, competing recombination processes in solar cell mechanics

The efficacy of a solar cell is measured by its power output. This value is the product of its current and its voltage.

The light-to-current efficiency ( $\eta$ ) is a function of the short circuit current,  $J_{sc}$ ;  $V_{oc}$ ; and the fill-factor,  $FF$ , divided by

the maximum power,  $P_{in}$ , which is a function of irradiance and cell area, as in Equation 1.

$$\eta = \frac{|JV|_{\max}}{P_{in}} = \frac{J_{sc}V_{oc}FF}{P_{in}}$$

**Equation 1**

The fill factor,  $FF$ , is a measure of the “squareness” of the IV curve. It is a theoretical value that shows how well the IV curve fits to an optimal curve. It is related to the power point which is the maximum product of the output photovoltage and photocurrent of the cell.<sup>4,18</sup>

In a DSSC, there are competing processes that lead to loss of electrons in the semiconductor. Figure 5 shows the electronic diagram initially discussed. Once an electron has injected into the semiconductor, in addition to completion of the circuit, there are two notable competitive processes (red arrows). The first is direct interaction of the semiconductor electron with the redox mediator. In this case, the electron does not complete the circuit and instead reduces the  $I_3^-$  which then reduces the oxidized

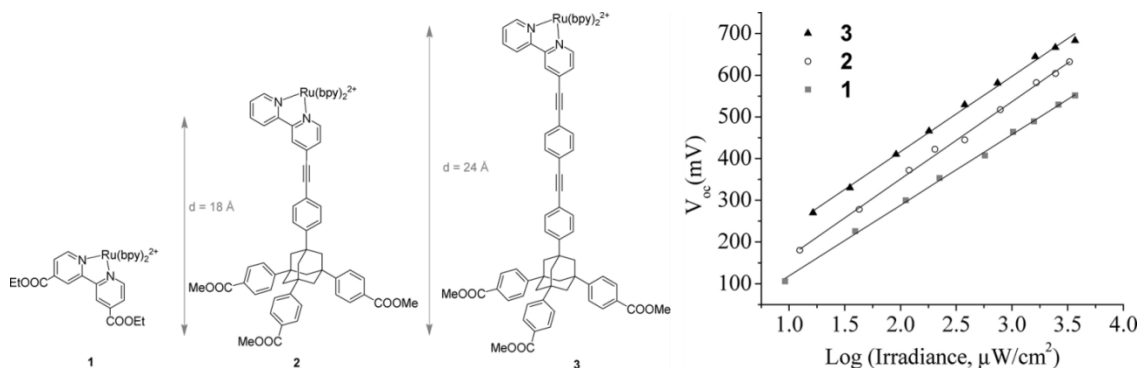


**Figure 6** Left: tripodal dyes; right:  $V_{oc}$  vs. irradiance,  $V_{oc}$  increases as distance increases, adapted from reference 21 dye. The second process is called charge recombination and occurs when an electron in the semiconductor directly recombines with the oxidized dye,  $D^+$  to regenerate the ground state dye. In this case, as well, potential power is lost. There are other competing processes that can be deleterious on the performance of the DSSC depending upon the specific aspect of which we are studying. One example is coordination of  $I_2^{19}$  with the dye that will be examined later.

In studying electronic mechanisms of DSSCs, one can tune specific aspects of the cell, such as the dye, to study a specific process. Previously, our group had synthesized a series of tris(bipyridyl)ruthenium dyes with ester anchor groups attached to one bipyridine group.<sup>20</sup> These adamantane tripod anchor groups were separated from the chromophore by a phenyleneethynylene spacer, Figure 6. As the chromophore-semiconductor distance increased, the open circuit voltage increased (Figure 6).<sup>21</sup> It was hypothesized that the increased distance of the chromophore from the semiconductor surface led to inhibited recombination of  $TiO_2(e^-)$  with the oxidized dye. However, these dyes were not tested under full solar cell conditions. One limiting factor was the poor



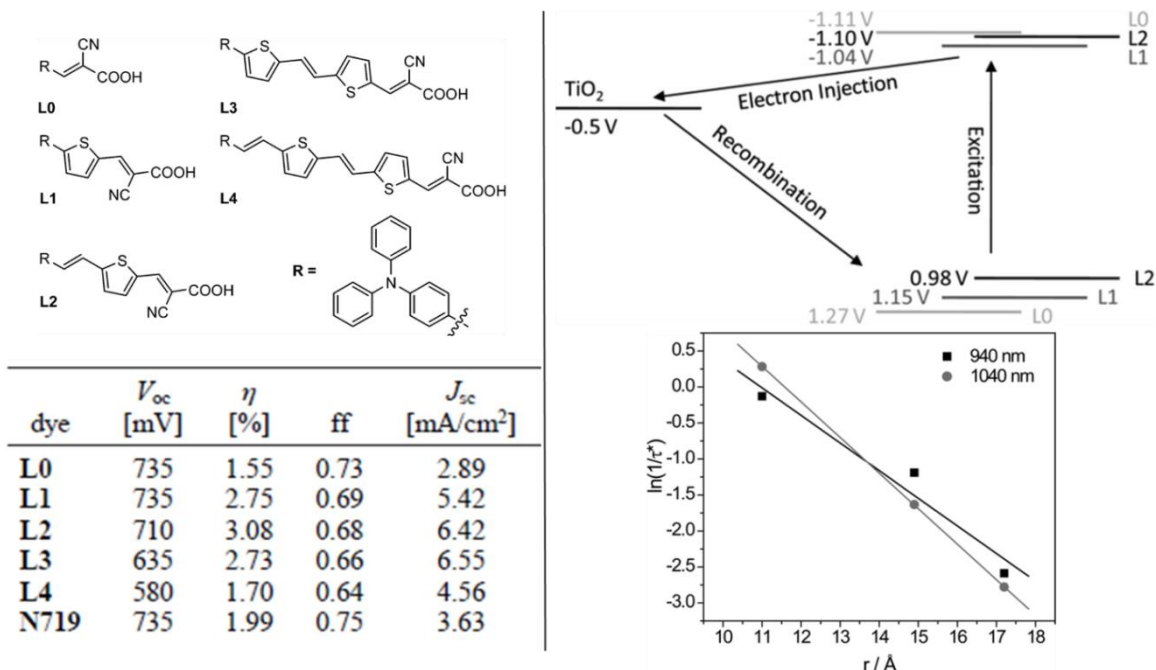


**Figure 7** Top left: dyes synthesized by Sun and coworkers; Bottom left: Solar cell properties of dyes; Top right: tuning HOMO and LUMO levels; Bottom right: dyes show increasing recombination rate with distance; adapted from references 22 and 23

injection of the tris(bipyridyl)ruthenium dyes and poor performance in high irradiance solar cells. Another factor was the use of dichloromethane as a solvent, which may have led to further separation of the redox mediator from the TiO<sub>2</sub> surface. This experiment, with all the limitations, suggested that  $V_{oc}$  can be controlled by limiting the negative, competing processes in recombination effects.

Other dyes with varying chromophore-semiconductor distances have been studied by other groups. Licheng Sun and coworkers developed a series of push-pull dyes (Figure 7) to study solar cell properties.<sup>22,23</sup> The length between the chromophore and the semiconductor was controlled by the incorporation of an increasing number of vinylthiophene units. The phenylamine group acted as an electron donor where the hole is located, and the push-pull design was used to increase charge separation. When

comparing the open-circuit voltages of the dyes (Figure 7, bottom left), it is apparent that as the vinylthiophene bridge length increases,  $V_{oc}$  decreases. Upon further examination of the mechanism, Sun and coworkers noted an increase in the recombination rate of their dyes as the length of the bridge increased (Figure 7, bottom right),<sup>23</sup> with this increase in the recombination rate resulted in the loss of  $V_{oc}$ . Rather than affecting the recombination and charge transfer rates by increasing distance, however, Sun and coworkers were actually modifying the chromophore unit of the dye. The HOMO and LUMO levels of the dye were changing, leading to different injection and recombination dynamics. As the chromophore properties were changing with increasing spacer length, accurate conclusions about the dependence of  $V_{oc}$  on charge separated distance are difficult to extract in this case. This study demonstrates the control of  $V_{oc}$  with HOMO, LUMO, and conduction band tuning through control of the chromophore.

The other method, adjusting the redox mediator potential, to control  $V_{oc}$  is illustrated through work of Hupp and coworkers.<sup>24,25</sup> In these papers, they developed a series of alternative redox mediators based upon nickel<sup>24</sup> or cobalt,<sup>25</sup>  $[\text{Co}(1,10\text{-phenanthroline})_3](\text{ClO}_4)_2$  and its derivatives, redox mediators. As more positive redox potentials for the cobalt mediator are employed,  $V_{oc}$  increases. Figure 8<sup>25</sup> depicts the change in potential and subsequent increase in  $V_{oc}$  as well as showing how the mediators with more positive potentials intercept electrons from the semiconductor leading to poor charge densities and low current. This paper suggests that modifying

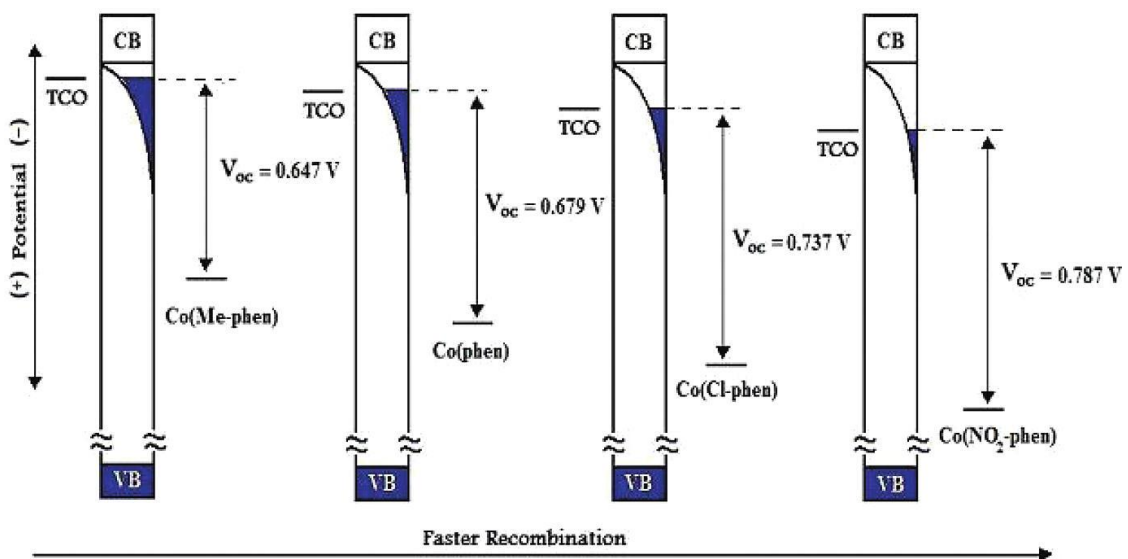


**Figure 8** More positive redox mediators show increasing  $V_{oc}$  and faster recombination due to changes in the recombination and quasi-Fermi level of the semiconductor, adapted from reference 25

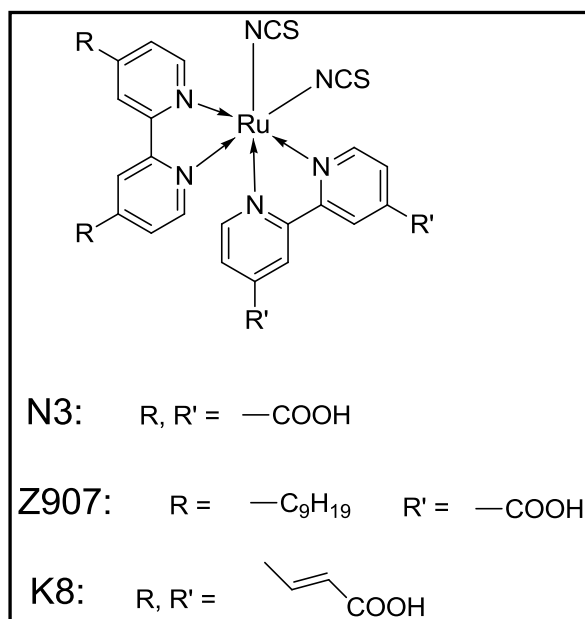
the redox mediator can lead to improvements in photovoltage. These results also stress the importance of inhibiting recombination processes.

In summary, when studying solar cell properties, such as  $V_{oc}$ , molecular control over a specific process to be studied is important. Careful design of a sensitizer through structural modifications can allow us to investigate specific processes in DSSCs. In the following sections, we will investigate the design and results for a series of N3-type dyes designed to study  $V_{oc}$  and its associated processes in DSSCs.

## **Chapter 2: Rigid Rod N3-Type Dyes for Open-Circuit Photovoltage Studies**

## Introduction

Previously our group had studied a series of rigid rod tris(bipyridyl) ruthenium dyes.<sup>21</sup> It was noted that these dyes showed increased  $V_{oc}$  with increasing semiconductor-chromophore distance. However, as these dyes were not optimal for DSSCs, we sought to develop a better series of dyes to investigate the properties associated with  $V_{oc}$  and



dye structure.

In 1993, Graetzel and coworkers developed a series of ruthenium bis(thiocyanate)bis(bipyridyl) dyes with efficiencies around 10%.<sup>4</sup> As these dyes continue to show excellent performance to-date in DSSCs, the N3-type dye seemed a logical transition to study  $V_{oc}$

**Figure 9** A sample of dyes studied in DSSCs that perform well, included is N3

and its processes through dye

modification. Other dyes of similar structures (Figure 9), such as Z907<sup>26-28</sup> and K8,<sup>29,30</sup> perform well in DSSCs. For N3, the two bipyridyl ligands are the same, both functionalized with carboxylic acids for attachment to  $TiO_2$ . The thiocyanate ligands are shown to have better DSSC performance than other ligands.<sup>4</sup>

In designing our series of dyes, **AKO-5**, our goal was to have a series of dyes where the chromophore was separated from the  $\text{TiO}_2$  at different distances by a conjugated bridge. The goal of the bridge was to allow facile injection of electrons from the excited chromophore, yet not affect the HOMO/LUMO levels of the chromophore. As previously mentioned,<sup>22,23</sup> Sun and coworkers have shown that increasing distance by modification of the chromophore can alter the chromophore properties thereby affecting  $V_{\text{oc}}$ .

When designing a dye molecule to study the chromophore-semiconductor distance effect on the open-circuit voltage and associated processes, there are a variety of conditions to consider when choosing which bridging group should be used. The bridge should be easily extended to allow the comparison of a variety of lengths. Second, it should have good electronic communication so that injection can occur. Third, it should not greatly affect the photophysical properties of the chromophore.

A variety of bridges have been studied for chromophore applications. Our group has

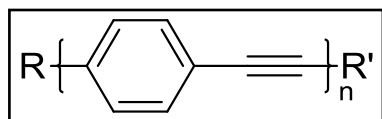


**Figure 10** Oligo(phenylene-ethynylene) (OPE) units

investigated tripodal anchors based on adamantane<sup>31</sup> and oligo(phenyleneethynylene) (OPE) bridges for both porphyrins<sup>32</sup> as well as tris(bipyridyl) ruthenium dyes.<sup>33</sup>

Other groups have studied dyes with polythiophene linkers,<sup>22,34</sup> dicyanovinyl groups,<sup>35</sup> and a variety of other bridges.<sup>36,37</sup> OPE bridges offer several advantages.

OPE bridges (Figure 10) have been studied for a variety of applications, ranging from biosensor and imaging devices<sup>38,39</sup> to molecular switches.<sup>40</sup> A typical OPE bridge acts as a rigid, linear connector between two systems, whether a donor-acceptor system or as a connection between a functional group and an anchor. These systems offer a simple, easy synthesis, which will be discussed later, as well as ease of potential modifications,<sup>41</sup> for example with modified functional groups such as alkoxy groups<sup>42</sup> or cholesterols.<sup>43</sup>

A second important aspect of OPEs applicable to DSSCs is the wealth of characterized electronic communication properties.<sup>44</sup> OPEs have been studied in a variety of donor-acceptor systems<sup>45</sup> showing fast electron transport<sup>46</sup> and properties desired for efficient

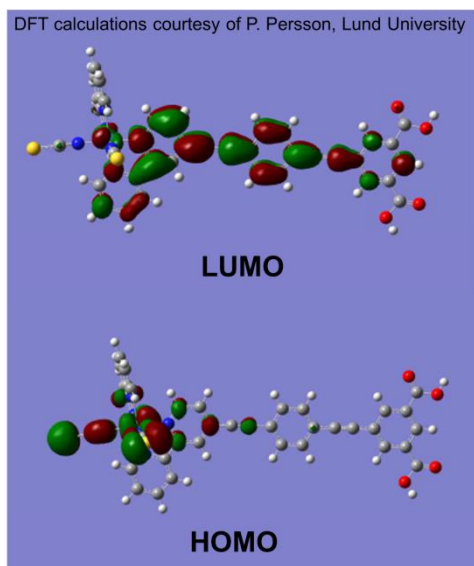


**Figure 11** DFT calculations of HOMO and LUMO for AK2; LUMO calculations suggest dye to be capable of injection; adapted from reference 53

electron injection. They have been studied as molecular wires and fully characterized for their electronic properties.<sup>47,48</sup> For example, the group of Wasielewski has studied the dynamics of electron and hole transfer across OPE bridges.<sup>49</sup>

The OPE bridge has also been shown to have excellent electronic communication,<sup>50,51</sup> while not affecting the chromophore properties,<sup>21,33,51-53</sup>

thus making it an optimal choice for utilization in our distance dependence study of the  $V_{oc}$  processes. DFT HOMO/LUMO calculations performed by Persson and coworkers indicating electron density from the LUMO extending to the isophthalic unit suggest that

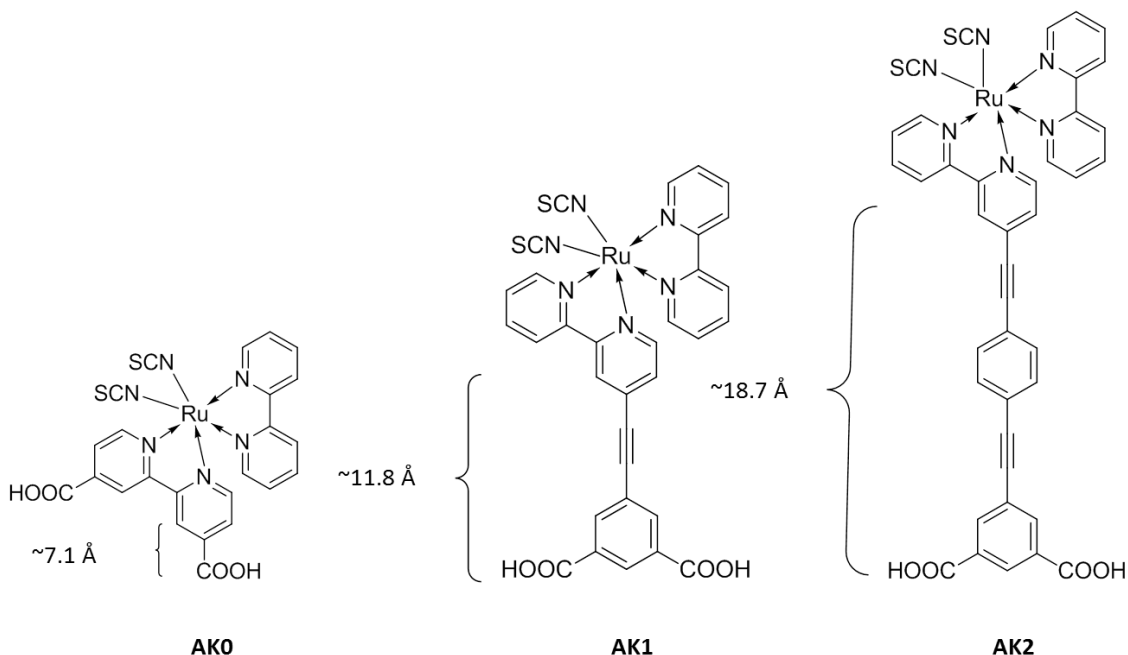


**Figure 12** Targeted N3-type dyes, **AK0-2**, with calculated semiconductor-chromophore distance shown

dyes containing OPE bridges should be capable of injection through the bridge, Figure 11.<sup>52,53</sup> We targeted a series of N3-type dyes with increasing OPE bridge length (Figure 12) to study the effect of distance on  $V_{oc}$  and recombination.

The synthesis of N3-type complexes occurs through several steps. The first component is synthesis of the target bipyridyl ligand. Once the ligand has been synthesized, the second step is complexation. Initially complexation was studied with a tetrakis(DMSO) ruthenium starting material.<sup>42,54,55</sup> These procedures require harsher conditions, have more required synthetic steps, have more difficult characterization of intermediates, as well as difficulty in purification. In 2003, Graetzel and coworkers published a paper utilizing a new ruthenium starting material, di- $\mu$ -chlorobis(*p*-cymene) ruthenium(II).<sup>26</sup> This starting material allowed for facile synthesis and characterization of N3-type complexes, especially heteroleptic complexes. The simplest method is a one-pot



synthesis where each ligand is sequentially added and the final product is purified. There is also a variation where a dichlororuthenium(II) bipyridyl *p*-cymene intermediate can be isolated.<sup>27,30</sup>

Z907, shown in Figure 9, was designed by Zakeeruddin and coworkers to address several of the shortcomings of N3.<sup>27</sup> It is similar to N3 with modifications to the ancillary ligand by the addition of alkyl chains. The alkyl chains can stabilize the DSSC to water induced desorption and increase the reversibility of the Ru(III/II) couple leading to enhanced stability. We also targeted these alkyl chains in the hopes that they would increase the solubility as the presence of the OPE bridges lowers the solubility of the already poorly soluble N3-type complex.

## Synthesis

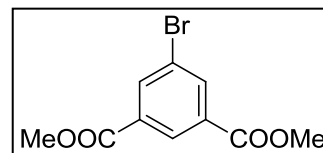
### Experimental

**Instrumentation.**  $^1\text{H}$  and  $^{13}\text{C}$  NMR spectra were recorded on a Varian INOVA NMR spectrometer operating at 499.896 MHz for  $^1\text{H}$  and 125.711 MHz for  $^{13}\text{C}$  using the solvent as an internal reference. The coupling constants ( $J$ ) for  $^1\text{H}$  NMR are recorded in Hz. High resolution mass spectra (ESI) were recorded on Bruker Daltonics Apex-Qe series, Fourier Transform Mass Spectrometer. X-ray data was collected at low temperature (100 K) as follows: Data collection: *APEX 2* (Bruker, 2006); cell refinement: *APEX 2*; data reduction: *SAINT* (Bruker, 2005); program(s) used to solve structure: *SHELXTL* (Sheldrick, 2008b); program(s) used to refine structure: *SHELXTL*; molecular graphics: *SHELXTL*; software used to prepare material for publication: *SHELXTL*.

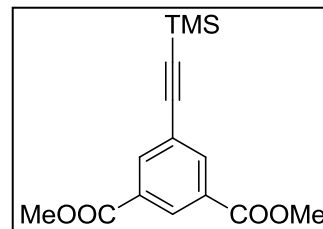
**Materials.** Solvents and concentrated acids were purchased from Pharmco. Diisopropyl amine and dichloromethane were distilled over calcium hydride under  $\text{N}_2$  atmosphere. THF was distilled with sodium and benzophenone while under  $\text{N}_2$  atmosphere or purified with an MBraun MB-SPS compact benchtop solvent purification system with purification columns for THF. Hexanes were distilled in air prior to use in column chromatography. All commercially available chemicals were used as received unless otherwise noted.  $\text{PdCl}_2(\text{PPh}_3)_2$ ,  $\text{Pd}(\text{PPh}_3)_4$ , and di- $\mu$ -chlorobis[(*p*-cymene)chlororuthenium (II)] were purchased from Strem. Anhydrous sodium sulfate,

N,N-dimethylformamide, 2,2'-dipyridyl, and sodium hydroxide were purchased from VWR. Dimethyl isophthalate, N-bromosuccinimide, tetra-N-butylammonium fluoride, [(4-bromophenyl)ethynyl](trimethyl)silane, 2,2'-dipyridyl-N-oxide, sodium borohydride, sodium nitrite, potassium iodide, ammonium thiocyanate, copper(I)bromide were purchased from Sigma-Aldrich. 10% Pd/C, sodium bisulfite, electrolytically reduced iron, and potassium dichromate were purchased from Fisher-Acros. 1.0 M tetra-N-butylammonium hydroxide in methanol solution, 4,4'-dimethyl-2,2'-bipyridine, and 4,4'-dinonyl-2,2'-bipyridine were purchased from Alfa Aesar. Trimethylsilyl acetylene was purchased from Oakwood chemicals. Silica gel (230-400 mesh) was purchased from Sorbent Technologies. Deuterated NMR solvents were purchased from Cambridge Isotopes.

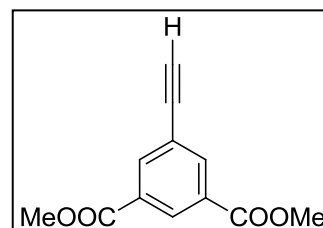
**Dimethyl-5-bromoisophthalate<sup>56</sup> (1):**



A solution of dimethyl isophthalate (21.0 g, 0.11 mol) in 18 M sulfuric acid (50 mL) was heated to 62 °C. Over one hour, N-bromosuccinimide (23.8 g, 0.13 mol) was added to the solution in three portions. After the last addition, heating and stirring was continued for 2 h. The solution was then poured onto crushed ice (150 g). After 15 minutes, a fine white precipitate formed. This was collected by vacuum filtration, washed with water, and then dissolved in dichloromethane. Ethyl acetate was added to the solution and allowed to slowly dry to form a thick white solid. Yield: 26.7 g, 90%. <sup>1</sup>H NMR (CDCl<sub>3</sub>) δ 8.61 (t, *J* = 1.6 Hz, 1H), 8.36 (d, *J* = 1.6 Hz, 2H), 3.97 (s, 6H).

**Dimethyl-5-((trimethylsilyl)ethynyl)isophthalate<sup>33,57</sup> (2):**

Compound **1** (5.06 g, 18.6 mmol), CuBr (540 mg, 3.77 mmol), and PdCl<sub>2</sub>(PPh<sub>3</sub>)<sub>2</sub> (396 mg, 0.56 mmol) were charged in a flame-dried round-bottom flask under N<sub>2</sub> atmosphere. Trimethylsilyl acetylene (23 mL, 161 mmol) and freshly distilled diisopropylamine (200 mL) were added to the flask via syringe. The reaction mixture was refluxed at 94 °C for 24 hours. The solvents were then removed under vacuum, and the brown crude product was purified by column chromatography using a hexane:ethyl acetate solvent mixture (9:1) to yield an off-white solid. Yield: 2.88 g, 53.5%. <sup>1</sup>H NMR (CDCl<sub>3</sub>) δ 8.60 (t, *J* = 1.4 Hz, 1H), 8.29 (d, *J* = 1.4 Hz, 2H), 3.95 (s, 6H), 0.26 (s, 9H). Spectral data were consistent with those previously reported.

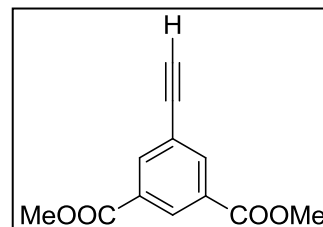
**Dimethyl 5-ethynylisophthalate (3): Method 1<sup>33</sup>**

A solution of **2** (4.12 g, 14.2 mmol) in THF (21 mL) was cooled in an ice bath. To this solution, a mixture of tetra-*n*-butylammonium fluoride (21 mL, 1.0 M in THF) diluted in THF (79 mL) was added over 10 minutes. After 2 hours, the solution was concentrated under vacuum. Water (100 mL) was added and the mixture was then extracted with dichloromethane (4 x 50 mL) and the combined organic layers were dried over anhydrous sodium sulfate. The brown crude was purified by column chromatography using a hexane:ethyl acetate solvent mixture (9:1) to yield an off-white solid. Yield: 2.37 g, 76.5%. <sup>1</sup>H NMR (CDCl<sub>3</sub>) δ 8.65 (t, *J* = 1.4 Hz, 1H), 8.33 (d, *J* = 1.5 Hz, 2H), 3.96 (s, 6H), 3.18 (s, 1H). This reaction was

repeated with yields varying from 40.3%-76.5%, most typically around 55%. Spectral data were consistent with those previously reported.

**Dimethyl 5-ethynylisophthalate (3): Method 2<sup>58</sup>**

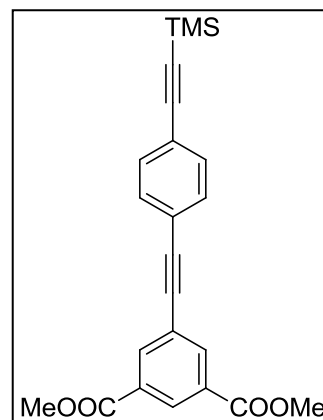
Compound **2** (1.01 g, 3.45 mmol) was dissolved in a premixed solution of methanol (23 mL), water (7 mL), and dichloromethane (38 mL). Silver(I) nitrate (72 mg, 0.424 mmol) was added and stirring was maintained for 22 h. A saturated aqueous ammonium chloride solution (75 mL) was added and the mixture was then extracted with dichloromethane (3 x 50 mL) and the combined organic layers were dried over anhydrous sodium sulfate. The brown crude was purified by column chromatography using a hexane:ethyl acetate solvent mixture (9:1) to yield an off-white solid. Yield: 0.404 g, 53.6%. <sup>1</sup>H NMR (CDCl<sub>3</sub>) δ 8.65 (t, *J* = 1.4 Hz, 1H), 8.33 (d, *J* = 1.5 Hz, 2H), 3.96 (s, 6H), 3.18 (s, 1H). Spectral data were consistent with those previously reported.



**Dimethyl 5-((4-**

**((trimethylsilyl)ethynyl)phenyl)ethynyl)isophthalate<sup>33,57</sup> (4):**

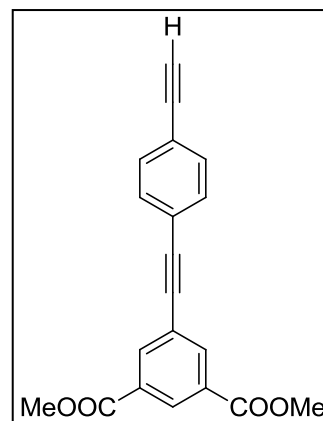
Compound **3** (1.029 g, 4.72 mmol), [(4-bromophenyl)ethynyl](trimethyl)silane (1.541g, 6.09 mmol), and Pd(PPh<sub>3</sub>)<sub>4</sub> (336 mg, 0.29 mmol) were charged in a flame-dried round-bottom flask under N<sub>2</sub> atmosphere. Freshly distilled diisopropylamine (90 mL) and benzene (105 mL) were added via syringe. The



solution was refluxed at 90 °C for 24 hours. The solvents were then removed under vacuum and the resulting brown crude was purified by column chromatography using a hexane:ethyl acetate solvent mixture (9:1) to yield an off-white solid. Yield: 0.744 g, 40.3%.  $^1\text{H}$  NMR ( $\text{CDCl}_3$ )  $\delta$  8.64 (t,  $J$  = 1.6 Hz, 1H), 8.36 (d,  $J$  = 1.6 Hz, 2H), 7.52 – 7.43 (m, 4H), 3.98 (s, 6H), 0.27 (s, 9H). Spectral data were consistent with those previously reported.

**Dimethyl 5-((4-ethynylphenyl)ethynyl)isophthalate<sup>33</sup> (5):**

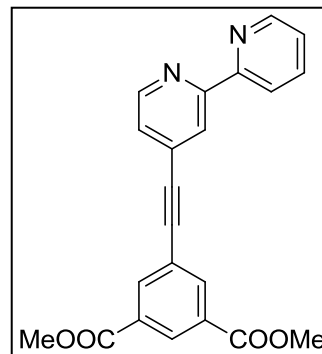
A solution of **4** (1.437 g, 3.68 mmol) in THF (100 mL) was cooled in an ice bath. To this solution, a mixture of tetra-*n*-butylammonium fluoride (5.0 mL, 1.0 M in THF) diluted in THF (25 mL) was added over 10 minutes. After 2 hours, the reaction was quenched by the addition of water (100 mL).



The mixture was then extracted with dichloromethane (4 x 50 mL) and the combined organic layers were dried over anhydrous sodium sulfate. The brown crude was purified by column chromatography using a hexane:ethyl acetate solvent mixture (9:1) to yield an off-white solid. Yield: 0.587 g, 50.3%.  $^1\text{H}$  NMR ( $\text{CDCl}_3$ )  $\delta$  8.64 (t,  $J$  = 1.4 Hz, 1H), 8.37 (d,  $J$  = 1.5 Hz, 2H), 7.50 (s, 4H), 3.98 (s, 6H), 3.21 (s, 1H). Spectral data were consistent with those previously reported.

**Dimethyl 5-([2,2'-bipyridin]-4-ylethynyl)isophthalate<sup>33,57</sup> (6):**

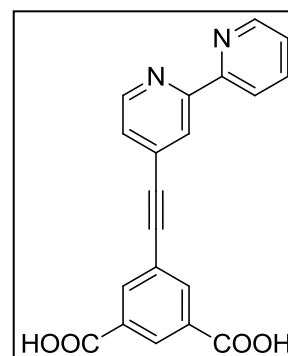
Compound **3** (180 mg, 0.826 mmol), 4-iodo-2,2'-bipyridine (200 mg, 0.710 mmol), and Pd(PPh<sub>3</sub>)<sub>4</sub> (50 mg, 0.043 mmol) were charged in a flame-dried round-bottom flask under N<sub>2</sub> atmosphere. Dry benzene (20 mL) and freshly distilled



diisopropylamine (20 mL) were added via syringe. The solution was heated for 24 hours at 86 °C. The solvents were then removed under vacuum and the crude was purified by column chromatography using a hexane:ethyl acetate solvent mixture (6:4) to yield an off-white solid. Yield: 0.182 g, 68.9%. <sup>1</sup>H NMR (CDCl<sub>3</sub>) δ 8.78 – 8.70 (m, 2H), 8.69 (t, *J* = 1.5 Hz, 1H), 8.59 (s, 1H), 8.45 (d, *J* = 8.0 Hz, 1H), 8.41 (d, *J* = 1.5 Hz, 2H), 7.87 (td, *J* = 7.8, 1.6 Hz, 1H), 7.44 (dd, *J* = 4.9, 1.4 Hz, 1H), 7.40 – 7.33 (m, 1H), 3.99 (s, 6H). <sup>13</sup>C NMR (CDCl<sub>3</sub>) δ 165.62, 149.40, 137.41, 136.98, 131.39, 131.13, 125.50, 124.40, 123.62, 123.51, 121.52, 88.83, 52.84.

**5-([2,2'-bipyridin]-4-ylethynyl)isophthalic acid<sup>59</sup> (L1):**

Compound **6** (100 mg, 0.269 mmol) was dissolved in freshly distilled dichloromethane (100 mL). To this solution, a 2 N solution of sodium hydroxide in methanol (10 mL) was added and stirred at room temperature for 4 days. Water (50 mL) was

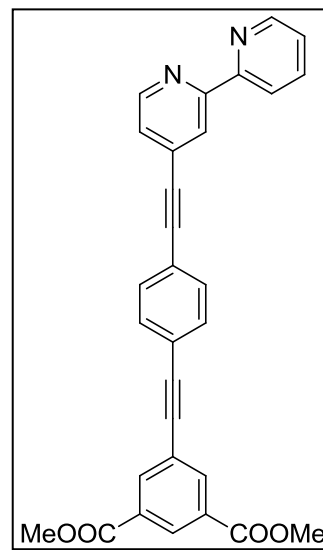


added and the mixture was extracted with water (2 x 50 mL). Dilute HCl (~ 0.5 M HCl) was used to neutralize the aqueous solution and precipitate the product. The product was then filtered and DMF was used to recover the product. Yield: 0.074 g, 79.9%. <sup>1</sup>H

NMR (DMSO-d<sub>6</sub>)  $\delta$  8.77 (d,  $J$  = 4.6 Hz, 1H), 8.72 (d,  $J$  = 3.7 Hz, 1H), 8.54 (s, 1H), 8.51 (s, 1H), 8.41 (d,  $J$  = 7.7 Hz, 1H), 8.34 (s, 2H), 7.98 (t,  $J$  = 7.5 Hz, 1H), 7.67 (d,  $J$  = 4.0 Hz, 1H), 7.50 (t,  $J$  = 6.2 Hz, 1H). <sup>13</sup>C NMR (DMSO-d<sub>6</sub>)  $\delta$  165.85, 162.25, 155.67, 154.34, 149.80, 149.79, 149.36, 137.46, 135.77, 132.71, 130.83, 130.55, 130.53, 125.53, 124.63, 122.08, 120.59, 91.76, 88.02. ESI<sup>+</sup>: calculated: 345.0870 [M+H]<sup>+</sup>, 367.0689 [M+Na]<sup>+</sup>; found: 345.0879 [M+H]<sup>+</sup>, 367.0700 [M+Na]<sup>+</sup>.

**Dimethyl 5-((4-([2,2'-bipyridin]-4-ylethynyl)phenyl)ethynyl)isophthalate<sup>33,57</sup> (7):**

Compound **5** (175 mg, 0.552 mmol), 4-iodo-2,2'-bipyridine (249 mg, 0.883 mmol), and Pd(PPh<sub>3</sub>)<sub>4</sub> (44 mg, 0.038 mmol) were charged in a flame-dried round-bottom flask under N<sub>2</sub> atmosphere. Freshly distilled THF (16 mL) and freshly distilled diisopropylamine (16 mL) were added via syringe. The solution was heated for 24 hours at 92 °C. The solvents



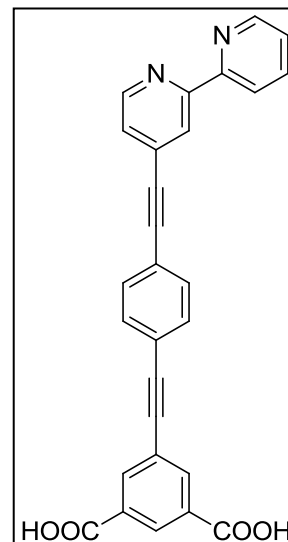
were then removed under vacuum and the crude was purified by column chromatography using a hexane:ethyl acetate solvent mixture (6:4) to yield an off-white solid. Yield: 0.216 g, 83.1%. <sup>1</sup>H NMR (CDCl<sub>3</sub>)  $\delta$  8.71 (d,  $J$  = 4.2 Hz, 1H), 8.68 (d,  $J$  = 4.9 Hz, 1H), 8.64 (t,  $J$  = 1.5 Hz, 1H), 8.56 (s, 1H), 8.44 (d,  $J$  = 7.9 Hz, 1H), 8.37 (d,  $J$  = 1.6 Hz, 2H), 7.85 (td,  $J$  = 7.8, 1.6 Hz, 1H), 7.56 (s, 4H), 7.43 – 7.38 (m, 1H), 7.38 – 7.31 (m, 1H), 3.97 (s, 6H). Spectral data were consistent with those previously reported.



**5-((4-([2,2'-bipyridine]-4-ylethynyl)phenyl)ethynyl)isophthalic**

**acid<sup>59</sup> (L2):**

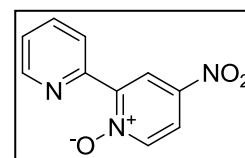
Compound **7** (150 mg, 0.318 mmol) was dissolved in dichloromethane (120 mL). To this solution, a 2 N solution of sodium hydroxide solution in methanol (12 mL) was added and stirred at room temperature for 4 days. Water (50 mL) was added and the mixture was extracted with water (2 x 50 mL). Dilute HCl (~ 0.5 M HCl) was used to neutralize the aqueous



solution and precipitate the product. The precipitate was collected by vacuum filtration. Yield: 0.081 g, 57.5%. <sup>1</sup>H NMR (DMSO-d<sub>6</sub>) δ 8.76 (d, *J* = 4.9 Hz, 1H), 8.73 (d, *J* = 3.9 Hz, 1H), 8.50 (s, 1H), 8.46 (t, *J* = 1.4 Hz, 1H), 8.41 (d, *J* = 7.9 Hz, 1H), 8.29 (d, *J* = 1.5 Hz, 2H), 7.99 (td, *J* = 7.8, 1.7 Hz, 1H), 7.74 (s, 4H), 7.62 (dd, *J* = 4.9, 1.4 Hz, 1H), 7.56 – 7.47 (m, 1H).

**4-Nitro-2,2'-dipyridyl-N-oxide<sup>60,61</sup> (8):**

A solution of 2,2'-dipyridyl-N-oxide (5.48 g, 31.8 mmol) in concentrated sulfuric acid (100 mL) was heated to 110 °C.

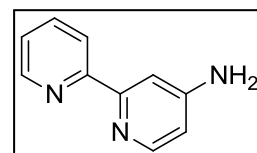


Concentrated nitric acid (7.8 mL) was added dropwise very slowly overnight while maintaining the temperature. Then, a second portion of concentrated nitric acid (6.2 mL) was added dropwise over 2 hours. Heating (110 °C) and stirring was maintained for an additional 1.5 hours. Fuming nitric acid (6.5 mL) was then added dropwise over 2 hours. The temperature (110 °C) was maintained for an additional 16 hours. The

concentrated acidic solution was allowed to cool and then poured onto ice (90 g). While being cooled in an ice bath, the acidic solution was neutralized with a concentrated aqueous solution of NaOH until basic to litmus leading to the formation of a fine yellow precipitate. The entire solution and precipitate was then extracted with dichloromethane (8 x 50 mL). The combined organic layers were dried over anhydrous sodium sulfate and the solvent removed under vacuum. Yield: 3.47 g, 50.0%.  $^1\text{H}$  NMR ( $\text{CDCl}_3$ )  $\delta$  9.17 (d,  $J$  = 3.4 Hz, 1H), 8.89 (d,  $J$  = 8.1 Hz, 1H), 8.79 (d,  $J$  = 3.9 Hz, 1H), 8.36 (d,  $J$  = 7.2 Hz, 1H), 8.06 (dd,  $J$  = 7.2, 3.3 Hz, 1H), 7.88 (td,  $J$  = 7.9, 1.9 Hz, 1H), 7.44 (dt,  $J$  = 7.9, 3.0 Hz, 1H). Yields of 48.0-54.2% were recorded when the reaction was repeated. Spectral data were consistent with those previously reported.

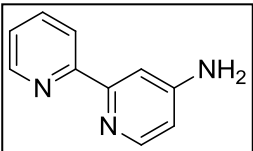
#### 4-Amino-2,2'-bipyridine (9): Method 1<sup>62</sup>

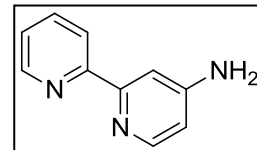
4-Nitro-2,2'-bipyridine-N-oxide (3.86 g, 17.7 mmol) and 10% palladium on carbon (800 mg) were suspended in methanol (300 mL). The reaction flask was placed in an ice bath and the suspension purged for 20 minutes with  $\text{N}_2$ . Sodium borohydride (8.03 g, 212 mmol) was added over 3 hours in small portions. When gas evolution ceased, the suspension was allowed to return to room temperature. The suspension was filtered through Celite to remove the Pd/C and a honey colored solution was recovered. The methanol was removed under vacuum and water (50 mL) was added. The aqueous layer was extracted with dichloromethane (4 x 50 mL) and then the combined organic layers were dried over anhydrous sodium sulfate and the solvent removed under vacuum. The resulting off-white product showed no relevant impurity



via NMR and was used without further purification. Yield: 1.12 g, 40.5%.  $^1\text{H}$  NMR ( $\text{CDCl}_3$ )  $\delta$  8.65 (d,  $J$  = 4.0 Hz, 1H), 8.36 (d,  $J$  = 8.0 Hz, 1H), 8.31 (d,  $J$  = 5.5 Hz, 1H), 7.79 (td,  $J$  = 7.8, 1.7 Hz, 1H), 7.68 (d,  $J$  = 2.2 Hz, 1H), 7.31 – 7.27 (m, 1H), 6.56 (dd,  $J$  = 5.5, 2.3 Hz, 1H), 4.23 (s, 2H). Yields of 40.2-80.4% were recorded when the reaction was repeated. Spectral data were consistent with those previously reported.

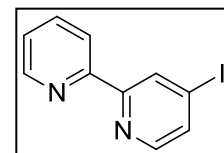
**4-Amino-2,2'-bipyridine (9): Method 2<sup>63</sup>**

4-Nitro-2,2'-bipyridine-N-oxide (0.500 g, 2.29 mmol) was  suspended in glacial acetic acid (15 mL) and water (2 mL). The suspension was then heated to reflux, dissolving all solids. Electrolytically reduced iron powder (0.640 g, 11.45 mmol) was added. The suspension was refluxed for 12 h upon which the suspension was filtered through a fritted-glass funnel to remove the iron filings. The deep red solution was neutralized with 20% aqueous sodium hydroxide and extracted with dichloromethane (4 x 50 mL). The combined organic layers were washed with water and dried over anhydrous sodium sulfate and the solvent removed under vacuum. Yield: 0.197 g, 50.2%.  $^1\text{H}$  NMR ( $\text{CDCl}_3$ )  $\delta$  8.65 (d,  $J$  = 4.0 Hz, 1H), 8.36 (d,  $J$  = 8.0 Hz, 1H), 8.31 (d,  $J$  = 5.5 Hz, 1H), 7.79 (td,  $J$  = 7.8, 1.7 Hz, 1H), 7.68 (d,  $J$  = 2.2 Hz, 1H), 7.31 – 7.27 (m, 1H), 6.56 (dd,  $J$  = 5.5, 2.3 Hz, 1H), 4.23 (s, 2H). Yields of 50.2-56.8% were recorded when the reaction was repeated. Spectral data were consistent with those previously reported.

**4-Amino-2,2'-bipyridine (9): Method 3<sup>64</sup>**

4-Nitro-2,2'-bipyridine-N-oxide (0.712 g, 3.26 mmol) and 10% palladium on carbon (70 mg) were suspended in methanol (60 mL).

H<sub>2</sub> gas was bubbled very slowly through the solution for 3 days. The resulting methanol solution was filtered through Celite to remove the Pd/C and the solvent removed under vacuum. The resulting off-white product showed no relevant impurity via NMR and was used without further purification. Yield: 0.508 g, 91.1%. <sup>1</sup>H NMR (CDCl<sub>3</sub>) δ 8.65 (d, *J* = 4.0 Hz, 1H), 8.36 (d, *J* = 8.0 Hz, 1H), 8.31 (d, *J* = 5.5 Hz, 1H), 7.79 (td, *J* = 7.8, 1.7 Hz, 1H), 7.68 (d, *J* = 2.2 Hz, 1H), 7.31 – 7.27 (m, 1H), 6.56 (dd, *J* = 5.5, 2.3 Hz, 1H), 4.23 (s, 2H). Yields of 88.8-99.8% were recorded when the reaction was repeated. Spectral data were consistent with those previously reported.

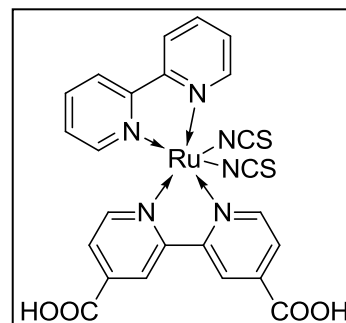
**4-Iodo-2,2'-bipyridine<sup>62,65,66</sup> (10):**

4-Amino-2,2'-bipyridine (1.339 g, 7.83 mmol) was dissolved in 7.5M sulfuric acid (35 mL) and cooled to -5 °C in an ice/acetone bath. Solutions of sodium nitrite (2.78 g, 40.3 mmol) in water (18 mL) and potassium iodide (18.1 g, 106 mmol) in water (25 mL) were precooled in an ice/acetone bath. The sodium nitrite solution was added to the solution of the bipyridine over a period of 3 minutes, yielding a blue-green solution of the azo-intermediate. This azo-intermediate is unstable and the low temperature was carefully monitored and maintained. After 2 minutes, the potassium iodide solution was added dropwise over 10 minutes. The solution was stirred and allowed to gradually reach ambient temperature (overnight). The resulting dark-colored

solution was then neutralized to pH 8 with first a 10% aqueous sodium hydroxide solution and then with sodium carbonate. The resulting aqueous solution was extracted with dichloromethane (4 x 50 mL). The combined organic layers were washed with a concentrated, aqueous solution of sodium bisulfite to remove residual iodine and then dried over anhydrous sodium sulfate. The resulting crude was purified by silica gel column chromatography using a hexane:ethyl acetate solvent mixture (9:1) to yield a white solid. Yield: 1.261 g, 57.1%.  $^1\text{H}$  NMR ( $\text{CDCl}_3$ )  $\delta$  8.84 (d,  $J$  = 1.2 Hz, 1H), 8.68 (ddd,  $J$  = 4.7, 1.6, 0.9 Hz, 1H), 8.39 (d,  $J$  = 8.0 Hz, 1H), 8.31 (d,  $J$  = 5.1 Hz, 1H), 7.83 (td,  $J$  = 7.8, 1.7 Hz, 1H), 7.69 (dd,  $J$  = 5.1, 1.7 Hz, 1H), 7.34 (ddd,  $J$  = 7.5, 4.8, 1.1 Hz, 1H). Yields of 57.1-67.0% were recorded when the reaction was repeated. Spectral data were consistent with those previously reported.

**$\text{Ru}(\text{NCS})_2[2,2'\text{-Bipyridine}][4,4'\text{-Dicarboxylic acid-2,2'-bipyridine}]^{26}$  (AK0):**

Di- $\mu$ -chlorobis[(*p*-cymene)chlororuthenium (II)] (303 mg, 0.496 mmol) and 4,4'-dicarboxylic acid-2,2'-bipyridine (248 mg, 1.00 mmol) were dissolved in DMF (87 mL) under  $\text{N}_2$

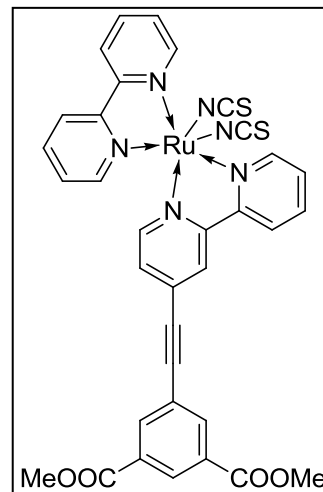


and heated to 70 °C for 4 hours. 2,2'-Dipyridyl (158 mg, 1.00 mmol) was added and heated to 160 °C for an additional 4 hours. Ammonium thiocyanate (578 mg, 7.605 mmol) was then added and heating maintained for an additional 4 hours. The reaction flask was allowed to cool to room temperature overnight and then the solvent was removed under vacuum. The resulting purple crude was washed with water, diethyl

ether, and hexane and dried under vacuum to yield a dark purple solid. Yield: 0.440 g, 70.6%.  $^1\text{H}$  NMR (DMSO- $d_6$ ):  $\delta_{\text{H}}$  9.43 (d,  $J = 5.7$ , 1H), 9.27 (d,  $J = 5.5$ , 1H), 9.07 (s, 1H), 8.91 (s, 1H), 8.77 (d,  $J = 8.1$ , 1H), 8.62 (d,  $J = 8.1$ , 1H), 8.28 (t,  $J = 7.3$ , 2H), 7.97 (t,  $J = 6.7$ , 1H), 7.91 (t,  $J = 8.2$ , 1H), 7.76 (d,  $J = 5.6$ , 1H), 7.61 (d,  $J = 5.5$ , 1H), 7.52 (d,  $J = 5.5$ , 1H), 7.29 – 7.18 (m, 1H).  $^{13}\text{C}$  NMR (DMSO- $d_6$ )  $\delta$  165.38, 164.95, 158.87, 157.98, 157.49, 156.69, 153.02, 152.26, 152.14, 151.69, 136.99, 136.28, 134.25, 133.69, 127.08, 126.33, 125.97, 125.17, 123.51, 123.37, 122.65, 122.39, 34.32. ESI $^+$ : calculated: 640.9615[M+Na] $^+$ ; found: 640.9793[M+Na] $^+$ .

**$\text{Ru}(\text{NCS})_2[2,2'\text{-Bipyridine}][\mathbf{6}]^{26}$  (**13**):**

Di- $\mu$ -chlorobis[(*p*-cymene)chlororuthenium (II)] (150 mg, 0.245 mmol) and compound **6** (182 mg, 0.489 mmol) were dissolved in DMF (43 mL) under  $\text{N}_2$  and heated to 70  $^\circ\text{C}$  for 4 hours. 2,2'-Dipyridyl (78 mg, 0.489 mmol) was added and heated to 160  $^\circ\text{C}$  for an additional 4 hours. Ammonium thiocyanate (250 mg, 3.2 mmol) was then added and heating

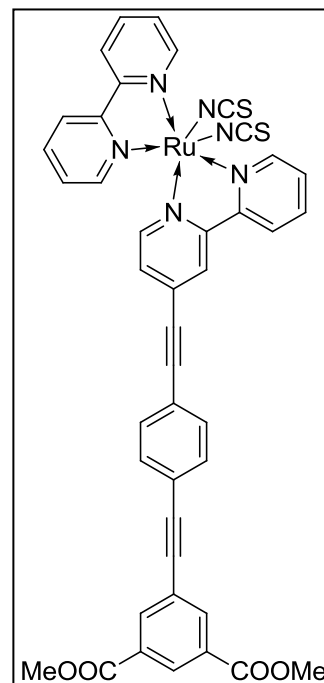


maintained for an additional 4 hours. The reaction flask was allowed to cool to room temperature overnight and then the solvent was removed under vacuum. The resulting purple crude was washed with water, diethyl ether, and hexane and dried under vacuum to yield a dark purple solid. Yield: 0.300 g, 82.12%.  $^1\text{H}$  NMR (DMSO- $d_6$ ):  $\delta_{\text{H}}$  9.33 (d,  $J = 5.8$ ), 9.29 (d,  $J = 4.7$ ), 9.02 (s), 8.87 (s), 8.85 (d,  $J = 8.0$ ), 8.79 – 8.73 (m), 8.71 (d,  $J = 8.1$ ), 8.65 – 8.58 (m), 8.54 (s), 8.48 (s), 8.46 (s), 8.33 (s), 8.30 – 8.19 (m), 8.10 (d,  $J$

= 5.8), 7.99 – 7.91 (m), 7.91 – 7.84 (m), 7.67 – 7.62 (m), 7.59 (d,  $J$  = 5.6), 7.57 – 7.51 (m), 7.37 (d,  $J$  = 5.8), 7.32 – 7.22 (m), 3.95 (s), 3.91 (s).  $^1\text{H}$  NMR data shows an integration ratio of 17.5:6 for protons in the aromatic region to protons on the methyl ester, with the proton peak for the two stereoisomers occurring at 3.95 and 3.91 ppm.  $^{13}\text{C}$  NMR (DMSO- $d_6$ ):  $\delta_{\text{C}}$  164.54, 164.47, 162.27, 159.12, 158.35, 158.19, 158.13, 157.85, 157.63, 157.04, 156.96, 156.77, 156.56, 152.28, 151.53, 151.48, 136.77, 136.65, 136.49, 136.12, 136.02, 135.92, 135.77, 133.58, 133.39, 131.22, 131.11, 128.84, 128.02, 127.96, 127.29, 127.04, 126.92, 126.34, 126.33, 126.25, 125.36, 125.12, 123.79, 123.69, 123.52, 123.50, 123.43, 123.39, 123.35, 123.31, 122.50, 122.37, 93.49, 88.43, 87.98, 52.82 (2C, -methyl ester), 52.77 (2C', -methyl ester). The presence of stereoisomers results in splitting of the 52.82 and 52.77 methyl ester. Due to the low solubility and the presence of stereoisomers (see Discussion), an accurate assignment of the NMR spectra is not possible. ESI $^+$ : calculated: 769.0244 [M+Na] $^+$ , 784.9983 [M+K] $^+$ ; found: 769.0328 [M+Na] $^+$ , 785.0070 [M+K] $^+$ .

**Ru(NCS) $_2$ [2,2'-Bipyridine][7] $^{26}$  (14):**

Compound **7** (357 mg, 0.758 mmol) and di- $\mu$ -chlorobis[(*p*-cymene)chlororuthenium (II)] (231 mg, 0.379 mmol) were dissolved in 200 proof ethanol (100 mL) under  $\text{N}_2$ . This suspension was heated to 82  $^\circ\text{C}$  for 4 hours. The ethanol was removed under vacuum and the resulting solid was dissolved in DMF (55 mL) and heated to 90  $^\circ\text{C}$  for 30 minutes. 2,2'-



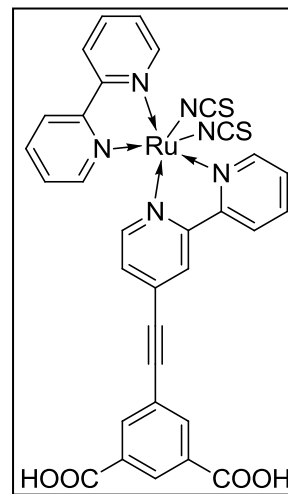
Dipyridyl (116 mg, 0.757 mmol) was added to the flask and the temperature was increased to 150 °C. After 4 hours, ammonium thiocyanate (432 mg, 5.69 mmol) was added and the heating was maintained for an additional 4 hours. The reaction flask was allowed to cool to room temperature and then the solvent was removed under vacuum. The resulting purple solid was purified with column chromatography using a dichloromethane/DMF solvent mixture (9:1) to yield a dark purple solid. Yield: 0.225 g, 33.6%.  $^1\text{H}$  NMR (DMSO- $d_6$ ):  $\delta_{\text{H}}$  9.31 (d,  $J$  = 5.9), 9.28 (dd,  $J$  = 7.9, 5.7), 8.95 (s), 8.85 (d,  $J$  = 8.4), 8.80 – 8.78 (m), 8.78 – 8.68 (m), 8.61 (dd,  $J$  = 13.2, 6.0), 8.46 (d,  $J$  = 9.8), 8.34 (d,  $J$  = 1.2), 8.31 (d,  $J$  = 1.2), 8.29 – 8.20 (m), 8.04 (dd,  $J$  = 6.1, 1.0), 7.99 – 7.85 (m), 7.79 (s), 7.72 (d,  $J$  = 8.3), 7.69 – 7.61 (m), 7.60 – 7.49 (m), 7.32 (dd,  $J$  = 6.0, 1.1), 7.31 – 7.23 (m), 3.93 (s), 3.91 (s).  $^1\text{H}$  NMR data shows an integration ratio of 22:6 for protons in the aromatic region to protons on the methyl ester, with the protons from the methyl ester appearing at 3.93 and 3.91 ppm for each stereoisomer. Due to the presence of stereoisomers and the low solubility (see Discussion), more accurate proton assignment was not possible.  $^{13}\text{C}$  NMR (DMSO- $d_6$ )  $\delta$  164.60, 164.57, 162.25, 159.03, 158.33, 158.17, 158.11, 157.83, 157.55, 157.02, 156.95, 156.77, 156.55, 152.41, 152.25, 152.13, 151.66, 151.45, 151.41, 136.70, 136.58, 136.43, 136.05, 135.95, 135.83, 135.73, 135.70, 133.60, 132.12, 132.07, 132.04, 131.98, 131.43, 131.35, 130.97, 130.95, 129.44, 129.28, 128.71, 128.61, 128.39, 127.91, 127.16, 126.99, 126.93, 126.83, 126.49, 126.26, 126.17, 124.98, 124.74, 123.75, 123.66, 123.43, 123.40, 123.36, 123.33, 123.31, 123.29, 123.27, 123.24, 122.88, 122.82, 121.63, 121.48, 95.54, 95.51, 90.67, 90.62, 89.53, 88.66, 88.23,



52.66, 52.64, 40.40, 35.71, 30.73. ESI<sup>+</sup>: calculated: 869.0559 [M+Na]<sup>+</sup>; found: 869.0550 [M+Na]<sup>+</sup>.

**Ru(NCS)<sub>2</sub>[2,2'-Bipyridine][L1]<sup>26</sup> (AK1):**

Di-μ-chlorobis[(*p*-cymene)chlororuthenium (II)] (76 mg, 0.125 mmol) and **L1** (86 mg, 0.250 mmol) were dissolved in DMF (22 mL) under N<sub>2</sub> and heated to 84 °C for 4 hours. 2,2'-Dipyridyl (39 mg, 0.250 mmol) was added and heated to 150 °C for an additional 4 hours. Ammonium thiocyanate (200 mg, 2.632 mmol) was then added and heating maintained for an additional

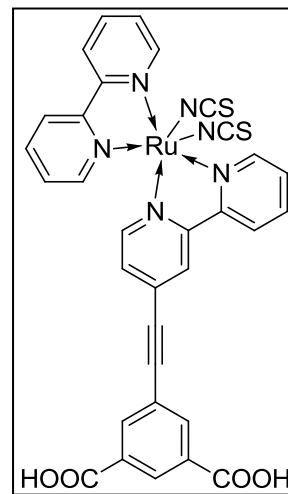


4 hours. The reaction flask was allowed to cool to room temperature overnight and then the solvent was removed under vacuum. To the resulting purple crude, water (50 mL) was added and the suspension was sonicated for 10 minutes. Using 0.2 M nitric acid, the pH was adjusted to approximately 2. The suspension was cooled in the refrigerator at 4 °C overnight. The suspension was then filtered and the purple solid was washed with water and subsequently dissolved in a minimal amount of 1.0 M tetra-n-butylammonium hydroxide in methanol solution. The crude was then purified on a Sephadex LH-20 column with methanol as the eluent collecting the main band. The methanol was removed under vacuum and the resulting solid was dissolved in water. The pH was adjusted to approximately 2 with 0.2 M nitric acid and the precipitate was collected. Yield: 0.054 g, 30.0%. NMR – see Appendix (Figure A 26 and Figure A 27) for

spectra. ESI<sup>+</sup>: calculated: 740.9930 [M+Na]<sup>+</sup>, 756.9669 [M+K]<sup>+</sup>; found: 741.0118 [M+Na]<sup>+</sup>, 756.9857 [M+K]<sup>+</sup>;

**Ru(NCS)<sub>2</sub>[2,2'-Bipyridine][L1]<sup>59</sup> (AK1):**

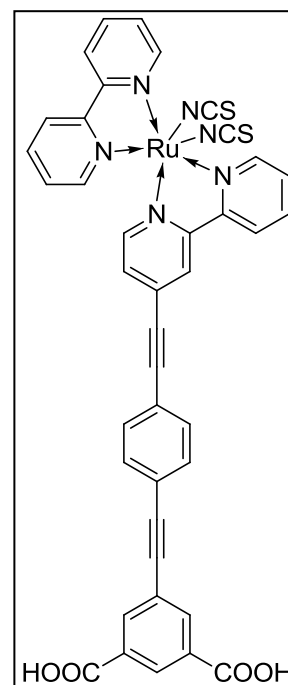
Compound **13** (23 mg, 0.031 mmol) was dissolved in freshly distilled dichloromethane (55 mL). To this solution, a 2 N solution of sodium hydroxide in methanol (7 mL) was added and was stirred at room temperature for 4 days. Water (50 mL) was added and the mixture was extracted with water (2 x 50 mL). Dilute HCl (~ 0.5 M HCl) was used to neutralize the aqueous



solution and precipitate the product. The product was then filtered and DMF was used to recover the dark purple product. Yield: 0.013 g, 58.5%. ESI<sup>+</sup>: calculated: 740.9930 [M+Na<sup>+</sup>], 756.9669 [M+K<sup>+</sup>]; found: 741.0118 [M+Na<sup>+</sup>], 756.9857 [M+K<sup>+</sup>].

**Ru(NCS)<sub>2</sub>[2,2'-Bipyridine][L2]<sup>26</sup> (AK2):**

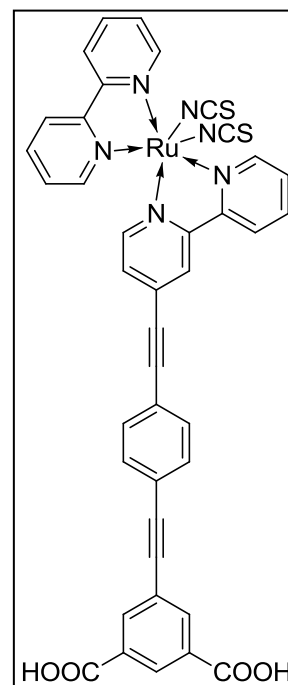
Di-μ-chlorobis[(*p*-cymene)chlororuthenium (II)] (90 mg, 0.145 mmol) and **L2** (128 mg, 0.290 mmol) were dissolved in DMF (25 mL) under N<sub>2</sub> and heated to 84 °C for 4 hours. 2,2'-Dipyridyl (50 mg, 0.320 mmol) was added and heated to 150 °C for an additional 4 hours. Ammonium thiocyanate (167 mg, 2.175 mmol) was then added and heating maintained for an additional 4 hours. The reaction flask was allowed to cool to room



temperature overnight and then the solvent was removed in vacuum. To the resulting purple crude, water (50 mL) was added and the suspension was sonicated for 10 minutes. Using 0.2 M nitric acid, the pH was adjusted to approximately 2. The suspension was cooled in the refrigerator at 4 °C overnight. The suspension was then filtered and the purple solid washed with water and subsequently dissolved in a minimal amount of 1.0 M tetra-n-butylammonium hydroxide in methanol solution. The crude was then purified on a Sephadex LH-20 column with methanol as the eluent collecting the main band. The methanol was removed under vacuum and the resulting purple solid was dissolved in water. The pH was adjusted to approximately 2 with 0.2 M nitric acid and the dark purple precipitate was collected by vacuum filtration. Yield: 0.132 g, 55.8%. NMR – see Appendix (Figure A 29) for spectra. ESI<sup>+</sup>: calculated: 841.0245 [M+Na]<sup>+</sup>; found: 841.0397 [M+Na]<sup>+</sup>. The ESI<sup>+</sup> spectrum showed some exchange of –NCS ligands with DMSO during extended exposure to DMSO solvent prior to ESI<sup>+</sup> data collection (see Discussion).

**Ru(NCS)<sub>2</sub>[2,2'-Bipyridine][L2]<sup>59</sup> (AK2):**

Compound **14** (18 mg, 0.021 mmol) was dissolved in freshly distilled dichloromethane (50 mL). To this solution, a 2 N solution of sodium hydroxide in methanol (6 mL) was added and was stirred at room temperature for 4 days. Water (50 mL) was added and the mixture was extracted with water (2 x 50 mL). Dilute HCl (~ 0.5 M HCl) was used to neutralize the aqueous



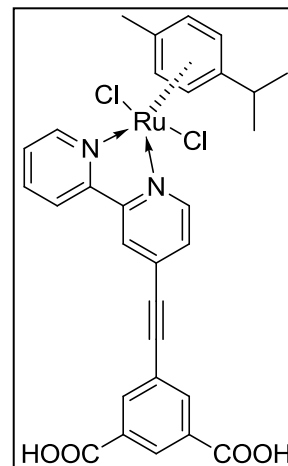
solution and precipitate the product. The product was then collected by vacuum filtration and DMF was used to recover the dark purple product. Yield: 0.005 g, 29.3%.

ESI<sup>+</sup>: calculated: 841.0245 [M+Na]<sup>+</sup>; found: 841.0250 [M+Na]<sup>+</sup>.

**RuCl<sub>2</sub>[*p*-cymene][L1]<sup>27,29</sup> (15):**

**L1** (40 mg, 0.116 mmol) and di-μ-chlorobis[(*p*-cymene)chlororuthenium (II)] (36 mg, 0.059 mmol) were dissolved in 200 proof ethanol (15 mL) under N<sub>2</sub> atmosphere.

The suspension was refluxed at 84 °C for 2 hours. The suspension fully dissolved after approximately 1.5 hours and

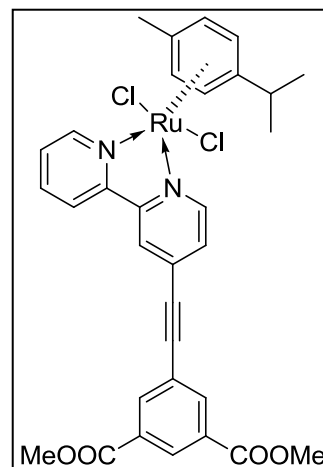


then heating was maintained for an additional half hour to insure completion of the reaction. The solution was then cooled to room temperature upon which the solvent was removed under vacuum to yield an orange-yellow solid: 58 mg, 0.089 mmol, 76.7%

<sup>1</sup>H NMR (CD<sub>3</sub>OD) δ 9.53 – 9.42 (m, 2H), 8.72 (d, *J* = 6.3 Hz, 2H), 8.59 (d, *J* = 7.8 Hz, 1H), 8.47 (s, 2H), 8.26 (t, *J* = 7.8 Hz, 1H), 7.88 (d, *J* = 5.5 Hz, 1H), 7.79 (t, *J* = 6.6 Hz, 1H), 6.14 (d, *J* = 6.3 Hz, 2H), 5.89 (d, *J* = 6.3 Hz, 2H), 2.67 (p, 6.8 Hz, 1H), 2.29 (s, 3H), 1.08 (d, *J* = 6.8 Hz, 6H). <sup>13</sup>C NMR (CD<sub>3</sub>OD) δ 167.70, 157.09, 156.81, 156.75, 156.07, 141.40, 138.03, 135.99, 133.76, 133.15, 130.23, 129.33, 127.05, 125.51, 123.50, 106.58, 106.09, 97.61, 88.47, 88.41, 87.45, 85.89, 32.55, 22.44, 19.10.

**$\text{RuCl}_2[\textit{p}\text{-cymene}][\textbf{6}]^{27,29}$  (**16**):**

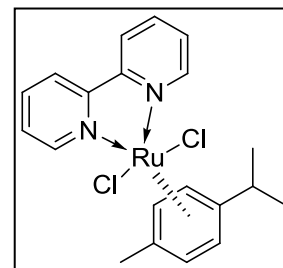
Compound **6** (180 mg, 0.484 mmol) and di- $\mu$ -chlorobis[(*p*-cymene)chlororuthenium (II)] (150 mg, 0.245 mmol) were dissolved in 200 proof ethanol (50 mL) under  $\text{N}_2$ . This suspension was heated to 82 °C for 4 hours. The ethanol was removed under vacuum to obtain an orange-yellow solid



used without further purification. Yield: 0.256 g, 77.9%.  $^1\text{H}$  NMR ( $\text{CDCl}_3$ )  $\delta$  9.91 (d,  $J$  = 5.0 Hz, 1H), 9.85 (d,  $J$  = 4.0 Hz, 1H), 8.71 (s, 1H), 8.40 (s, 2H), 8.21 (s, 2H), 8.12 (t,  $J$  = 7.4 Hz, 1H), 7.82 (s, 2H), 6.33 (dd,  $J$  = 15.4, 5.2 Hz, 2H), 6.18 (d,  $J$  = 4.9 Hz, 2H), 3.99 (s, 6H), 2.74 (p,  $J$  = 6.5 Hz, 1H), 2.32 (s, 3H), 1.07 (d,  $J$  = 6.8 Hz, 6H).  $^{13}\text{C}$  NMR ( $\text{CDCl}_3$ )  $\delta$  165.35, 157.80, 157.66, 154.67, 154.19, 139.86, 137.27, 134.47, 132.06, 131.65, 130.08, 129.07, 125.03, 123.48, 122.18, 105.56, 104.78, 97.28, 88.36, 88.30, 86.63, 85.78, 85.75, 53.00, 31.55, 29.90, 22.65, 19.64.  $\text{ESI}^+$ : calculated: 643.0938  $[\text{M}-\text{Cl}]^+$ ; found: 643.0993  $[\text{M}-\text{Cl}]^+$ .

**$\text{RuCl}_2[\textit{p}\text{-cymene}][\textbf{2,2'}\text{-bipyridine}]^{27,29}$  (**17**):**

2,2'-Bipyridine (49 mg, 0.313 mmol) and di- $\mu$ -chlorobis[(*p*-cymene)chlororuthenium (II)] (98 mg, 0.160 mmol) were dissolved in 200 proof ethanol (10 mL) under  $\text{N}_2$  atmosphere.



The solution was heated to 82 °C for 4 hours upon which the solvent was removed under vacuum to yield yellow-brown solid: 143 mg, 0.309 mmol, 98.7%  $^1\text{H}$  NMR ( $\text{CD}_3\text{OD}$ )  $\delta$  9.48 (d,  $J$  = 5.5 Hz, 2H), 8.50 (d,  $J$  = 8.5 Hz, 2H), 8.23 (t,  $J$  = 8.5 Hz, 2H), 7.91 –

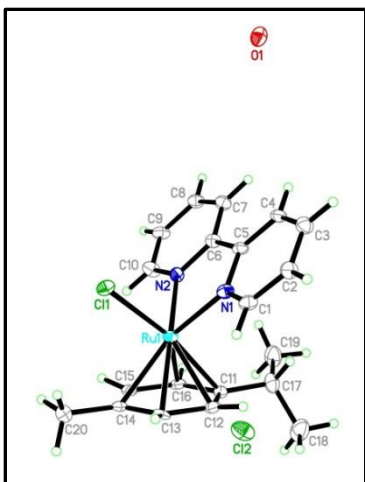


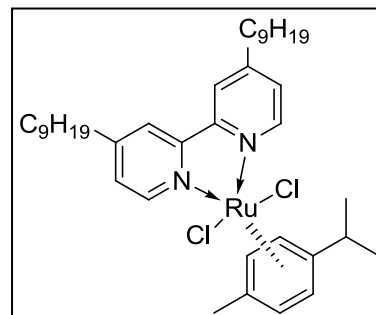
**Figure 13** ORTEP diagram of Compound 17 showing the numbering scheme. Displacement ellipsoids are drawn at 30% probability level for non-H atoms

7.59 (m, 2H), 6.12 (d,  $J = 6.3$  Hz, 2H), 5.87 (d,  $J = 6.3$  Hz, 2H), 2.64 (p,  $J = 6.9$  Hz, 1H), 2.27 (s, 3H), 1.04 (d,  $J = 6.9$  Hz, 6H).  $^{13}\text{C}$  NMR ( $\text{CD}_3\text{OD}$ )  $\delta$  157.05, 156.51, 141.33, 129.05, 125.10, 106.22, 105.97, 88.38, 85.71, 32.51, 22.43, 19.11. ESI $^+$ : calculated: 869.0559  $[\text{M}+\text{Na}]^+$ ; found: 869.0550  $[\text{M}+\text{Na}]^+$ . X-ray quality crystals were yielded from

methanol. See Figure 13 for x-ray structure and Appendix for crystallographic data.

**$\text{RuCl}_2[\text{p-cymene}][4,4'\text{-dinonyl-2,2'-bipyridine}]^{27,29}$  (12):**

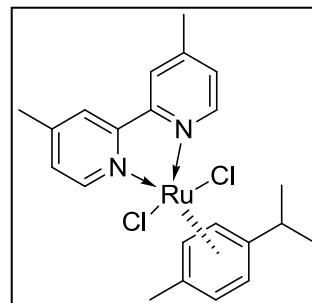
General Procedure: 4,4'-Dinonyl-2,2'-bipyridine (2 equivalents) and di- $\mu$ -chlorobis[(*p*-cymene)chlororuthenium (II)] (1 equivalent) were



dissolved in 200 proof ethanol under  $\text{N}_2$  atmosphere. The solution was heated to 82  $^\circ\text{C}$  for 6 hours upon which the solvent was removed under vacuum to yield a dark-orange oil used as-is without calculation of yield.  $^1\text{H}$  NMR ( $\text{CDCl}_3$ )  $\delta$  9.64 (d,  $J = 5.5$  Hz, 2H), 7.88 (s, 2H), 7.57 (d,  $J = 4.9$  Hz, 2H), 6.24 (d,  $J = 5.8$  Hz, 2H), 6.09 (d,  $J = 5.8$  Hz, 2H), 2.83 – 2.76 (m, 4H), 2.72 (p,  $J = 6.9$  Hz, 1H), 2.28 (s, 3H), 1.70 (p,  $J = 7.6$  Hz, 6H), 1.44 – 1.18 (m, 24H), 1.05 (d,  $J = 6.8$  Hz, 6H), 0.87 (t,  $J = 6.7$  Hz, 6H). Spectral data were consistent with those previously reported.

**$\text{RuCl}_2[p\text{-cymene}][4,4'\text{-dimethyl-2,2'-bipyridine}]^{27,29}$  (**18**):**

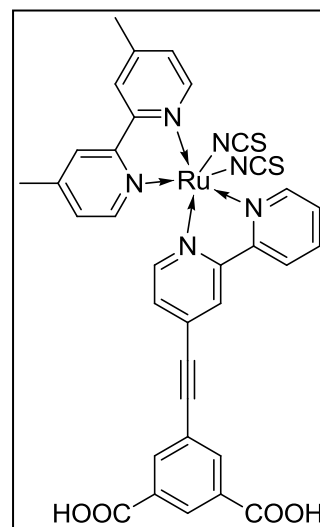
4,4'-Dimethyl-2,2'-bipyridine (28 mg, 0.152 mmol) and di- $\mu$ -chlorobis[(*p*-cymene)chlororuthenium (II)] (46 mg, 0.075 mmol) were dissolved in 200 proof ethanol (10 mL) under  $\text{N}_2$



atmosphere. The solution was heated to 82 °C for 6 hours upon which the solvent was removed under vacuum to yield yellow-orange solid used as-is without calculation of yield.  $^1\text{H}$  NMR ( $\text{CDCl}_3$ )  $\delta$  9.56 (d,  $J$  = 5.8 Hz, 2H), 8.11 (s, 2H), 7.49 (d,  $J$  = 5.8 Hz, 2H), 6.15 (d,  $J$  = 6.2 Hz, 2H), 5.99 (d,  $J$  = 6.2 Hz, 2H), 2.57 (d,  $J$  = 6.9 Hz, 1H), 2.47 (s, 6H), 2.20 (s, 3H), 0.94 (d,  $J$  = 6.9 Hz, 6H).  $^{13}\text{C}$  NMR ( $\text{CDCl}_3$ )  $\delta$  155.78, 154.08, 151.87, 128.86, 124.06, 104.22, 103.86, 87.12, 84.00, 31.02, 22.17, 21.41, 19.05, 18.45. Spectral data were consistent with those previously reported.

**$\text{Ru}(\text{NCS})_2[4,4'\text{-dimethyl-2,2'-bipyridine}][\text{L1}]^{67}$  (AK5):**

Compound **18** (from above) and **L1** (51 mg, 0.152 mmol) were dissolved in  $\text{N}_2$  de-gassed DMF (16 mL) under  $\text{N}_2$  atmosphere. The resulting orange solution was heated to 150 °C for 4 hours. A solution of ammonium thiocyanate (95 mg, 1.24 mmol) in degassed DMF (16 mL) was added to the original reaction mixture and the heating was maintained for an

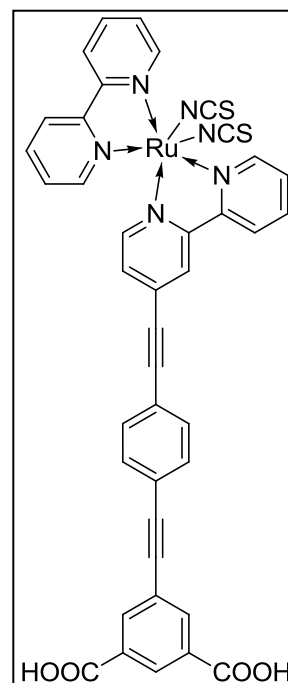


additional 4 hours. Upon cooling of the reaction flask, the solvent was removed under vacuum and water (100 mL) was added to the resulting purple crude. This purple suspension was then sonicated for 10 minutes. Using 0.2 M nitric acid (approximately 5

mL), the pH was adjusted to approximately 2 by litmus. The crude suspension was then cooled to 4 °C in a refrigerator overnight. The suspension was filtered to collect the purple crude and the solid was dissolved in a 1.0 M tetra-n-butylammonium hydroxide in methanol solution (0.51 mL) and methanol (10 mL). This solution was concentrated under vacuum and charged to a column of Sephadex LH-20 using methanol as an eluent. The first band (main band) was collected and concentrated under vacuum. Water (50 mL) was added and the resulting solution neutralized with 0.2 M nitric acid to pH 2 by litmus. The precipitate was collected via vacuum filtration to yield a purple solid: 30 mg, 0.040 mmol, 26.4%. NMR – see Appendix (Figure A 45 and Figure A 46) for spectra. ESI<sup>+</sup>: calculated: 746.0346 [M+Na]<sup>+</sup>; found: 746.0558 [M+Na]<sup>+</sup>.

**Ru(NCS)<sub>2</sub>[2,2'-Bipyridine][L2]<sup>67</sup> (AK2):**

Compound **17** (9.5 mg, 0.0204 mmol) and **L2** (9.0 mg, 0.0204 mmol) were dissolved in N<sub>2</sub> de-gassed DMF (10 mL) under N<sub>2</sub> atmosphere. The resulting brown solution was heated to 150 °C for 4 hours. A solution of ammonium thiocyanate (12 mg, 0.158 mmol) in degassed DMF (5 mL) was added to the original reaction mixture and the heating was maintained for an additional 4 hours. Upon cooling of the reaction flask, the solvent was removed under vacuum and water (50 mL) was added to the resulting purple crude. This purple suspension was then sonicated for 10 minutes. Using 0.2 M nitric acid, the pH was adjusted to approximately 2 by litmus. The

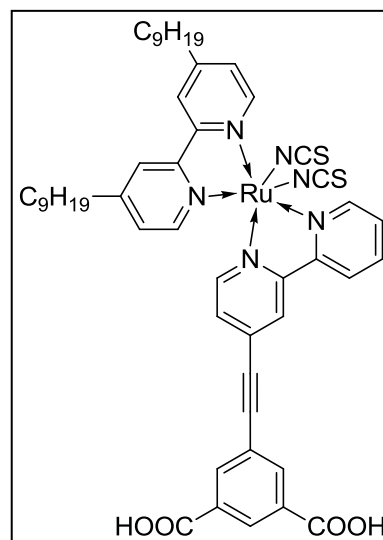




crude suspension was then cooled to 4 °C in a refrigerator overnight. The suspension was filtered to collect the purple crude and the solid was dissolved in a 1.0 M tetra-*n*-butylammonium hydroxide in methanol solution (0.2 mL) and methanol (1 mL). This solution was concentrated under vacuum and charged to a column of Sephadex LH-20 using methanol as an eluent. The first band (main band) was collected and concentrated under vacuum. Water (50 mL) was added and the resulting solution neutralized with 0.2 M nitric acid to pH 2 by litmus. The precipitate was collected via filtration to yield a purple solid: 5 mg, 0.005 mmol, 25.0%. NMR – see Appendix (Figure A 29) for spectra. ESI<sup>+</sup>: calculated: 841.0245 [M+Na]<sup>+</sup>; found: 841.0250 [M+Na]<sup>+</sup>.

**Ru(NCS)<sub>2</sub>[4,4'-dinonyl-2,2'-Bipyridine][L1]<sup>67</sup> (AK3):**

Compound **15** (57 mg, 0.088 mmol) and 4,4'-dinonyl-2,2'-bipyridine (36 mg, 0.088 mmol) were dissolved in DMF (15 mL) under N<sub>2</sub> atmosphere. The resulting orange solution was heated to 150 °C for 4 hours. After several minutes of reflux, the solution had become a dark purple color. A solution of ammonium thiocyanate (50 mg, 0.66

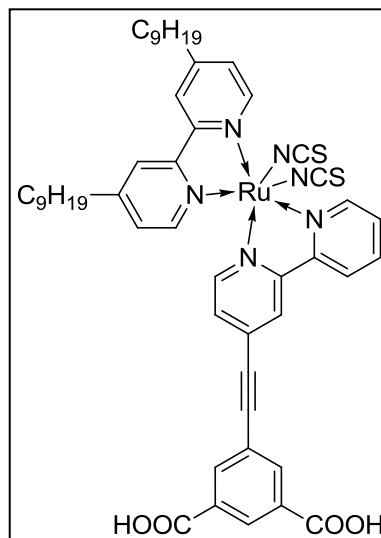


mmol) in degassed DMF (11 mL) was added to the original reaction mixture and the heating was maintained for an additional 4 hours. Upon cooling of the reaction flask, the solvent was removed under vacuum and water (50 mL) was added to the resulting purple crude. This purple suspension was then sonicated for 10 minutes. Using 0.2 M nitric acid (approximately 2.5 mL), the pH was adjusted to approximately 2 by litmus.

The crude suspension was then cooled to 4 °C in a refrigerator for 3 days (over a weekend). The suspension was filtered to collect the purple crude and the solid was dissolved in acetone and refiltered. The acetone was removed under vacuum and the resulting purple solid dissolved in a tetra-n-butylammonium hydroxide in methanol solution (1 mL of 1 M solution). This solution was concentrated under vacuum and charged to a column of Sephadex LH-20 using methanol as an eluent. The first band (main band) was collected and concentrated under vacuum. H<sub>2</sub>O (50 mL) was added to the concentrated product and the resulting solution neutralized with 0.2 M nitric acid to pH 2 by litmus. The precipitate was collected via filtration to yield a purple solid. This solid was collected via acetone from the filter paper: 36.1 mg, 0.037 mmol, 42.3%. <sup>1</sup>H NMR (DMSO-d<sub>6</sub>) δ 9.36 – 9.22 (m, 2H), 9.16 – 9.03 (m, 2H), 8.97 (s, 1H), 8.84 (d, *J* = 11.3 Hz, 1H), 8.71 (d, *J* = 6.2 Hz, 1H), 8.65 (s, 2H), 8.55 – 8.44 (m, 3H), 8.35 (s, 2H), 8.22 (s, 2H), 8.14 (s, 1H), 8.11 (s, 1H), 8.06 (d, *J* = 5.7 Hz, 1H), 7.94 (s, 2H), 7.88 (t, *J* = 7.1 Hz, 1H), 7.80 (t, *J* = 5.0 Hz, 1H), 7.62 (d, *J* = 5.9 Hz, 1H), 7.57 (d, *J* = 5.4 Hz, 1H), 7.51 (s, 1H), 7.43 (d, *J* = 5.8 Hz, 1H), 7.36 (d, *J* = 5.9 Hz, 1H), 7.32 (d, *J* = 5.3 Hz, 1H), 7.30 – 7.25 (m, 1H), 7.14 – 7.07 (m, 1H), 1.88 – 1.76 (m, 6H), 1.62 – 1.51 (m, 6H), 1.50 – 1.35 (m, 4H), 1.35 – 1.07 (m, 36H), 0.93 (t, *J* = 7.3 Hz, 4H), 0.90 – 0.73 (m, 24H). <sup>13</sup>C NMR not recorded due to low solubility. ESI<sup>+</sup>: calculated: 993.2752 [M+Na]<sup>+</sup>, 1009.2491 [M+K]<sup>+</sup>; found: 993.2718 [M+Na]<sup>+</sup>, 1009.2458 [M+K]<sup>+</sup>.

**$\text{Ru}(\text{NCS})_2[4,4'\text{-dinonyl-2,2'-Bipyridine}][\text{L1}]^{27,29,67}$  (AK3):**

Compound **12**: 4,4'-Dinonyl-2,2'-bipyridine (57 mg, 0.145 mmol) and di- $\mu$ -chlorobis[(*p*-cymene)chlororuthenium (II)] (45 mg, 0.073 mmol) were dissolved in 200 proof Ethanol (10 mL) under  $\text{N}_2$  atmosphere. The solution was heated to 82 °C for 6 hours upon which the solvent was removed under vacuum to yield a dark orange oil that was used as-is without calculation of yield.



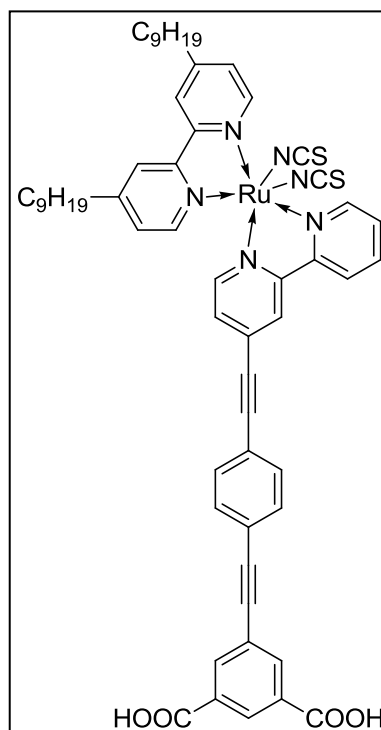
**AK3:** Compound **12** (from above) and **L1** (55 mg, 0.146 mmol) were dissolved in  $\text{N}_2$  degassed DMF (15 mL) under  $\text{N}_2$  atmosphere. The resulting orange solution was heated to 150 °C for 4 hours. A solution of ammonium thiocyanate (113 mg, 1.49 mmol) in degassed DMF (8 mL) was added to the original reaction mixture and the heating was maintained for an additional 4 hours. Upon cooling of the reaction flask, the solvent was removed under vacuum and water (100 mL) was added to the resulting purple crude. This purple suspension was then sonicated for 10 minutes. Using 0.2 M nitric acid (approximately 5 mL), the pH was adjusted to approximately 2 by litmus. The crude suspension was then cooled to 4 °C in a refrigerator overnight. The suspension was filtered to collect the purple crude and the solid was dissolved in a tetra-*n*-butylammonium hydroxide in methanol solution (1M in methanol). This solution was concentrated under vacuum and charged to a column of Sephadex LH-20 using methanol as an eluent. The first band (main band) was collected and the resulting solution neutralized with 0.2 M nitric acid to pH 2 by litmus. The precipitate was

collected via vacuum filtration to yield a purple solid: 97 mg, 0.100 mmol, 68.8%.  $^1\text{H}$  NMR (DMSO- $d_6$ )  $\delta$  9.36 – 9.22 (m, 2H), 9.16 – 9.03 (m, 2H), 8.97 (s, 1H), 8.84 (d,  $J$  = 11.3 Hz, 1H), 8.71 (d,  $J$  = 6.2 Hz, 1H), 8.65 (s, 2H), 8.55 – 8.44 (m, 3H), 8.35 (s, 2H), 8.22 (s, 2H), 8.14 (s, 1H), 8.11 (s, 1H), 8.06 (d,  $J$  = 5.7 Hz, 1H), 7.94 (s, 2H), 7.88 (t,  $J$  = 7.1 Hz, 1H), 7.80 (t,  $J$  = 5.0 Hz, 1H), 7.62 (d,  $J$  = 5.9 Hz, 1H), 7.57 (d,  $J$  = 5.4 Hz, 1H), 7.51 (s, 1H), 7.43 (d,  $J$  = 5.8 Hz, 1H), 7.36 (d,  $J$  = 5.9 Hz, 1H), 7.32 (d,  $J$  = 5.3 Hz, 1H), 7.30 – 7.25 (m, 1H), 7.14 – 7.07 (m, 1H), 1.88 – 1.76 (m, 6H), 1.62 – 1.51 (m, 6H), 1.50 – 1.35 (m, 4H), 1.35 – 1.07 (m, 36H), 0.93 (t,  $J$  = 7.3 Hz, 4H), 0.90 – 0.73 (m, 24H).  $^{13}\text{C}$  NMR not recorded due to low solubility. ESI $^+$ : calculated: 993.2752  $[\text{M}+\text{Na}]^+$ , 1009.2491  $[\text{M}+\text{K}]^+$ ; found: 993.2718  $[\text{M}+\text{Na}]^+$ , 1009.2458  $[\text{M}+\text{K}]^+$ .

**$\text{Ru}(\text{NCS})_2[4,4'\text{-dinonyl-2,2'}\text{-Bipyridine}][\text{L2}]^{27,29,67}$  (AK4):**

Compound **12**: 4,4'-Dinonyl-2,2'-bipyridine (60 mg, 0.147 mmol) and di- $\mu$ -chlorobis[(*p*-cymene)chlororuthenium (II)] (45 mg, 0.074 mmol) were dissolved in 200 proof ethanol (10 mL) under  $\text{N}_2$  atmosphere. The solution was heated to 82  $^\circ\text{C}$  for 6 hours upon which the solvent was removed under vacuum to yield a dark orange oil that was used as-is without calculation of yield.

**AK4**: Compound **12** (from above) and **L2** (65 mg, 0.147



mmol) were dissolved in  $\text{N}_2$  de-gassed DMF (10 mL) under  $\text{N}_2$  atmosphere. The resulting

orange solution was heated to 150 °C for 4 hours. A solution of ammonium thiocyanate (94 mg, 1.24 mmol) in degassed DMF (11 mL) was added to the original reaction mixture and the heating was maintained for an additional 4 hours. Upon cooling of the reaction flask, the solvent was removed under vacuum and water (100 mL) was added to the resulting purple crude. This purple suspension was then sonicated for 10 minutes. Using 0.2 M nitric acid (approximately 5 mL), the pH was adjusted to approximately 2 by litmus. The crude suspension was then cooled to 4 °C in a refrigerator overnight. The suspension was filtered to collect the purple crude and the solid was dissolved in a minimal amount of tetra-n-butylammonium hydroxide in methanol solution (1 M in methanol). This solution was concentrated under vacuum and charged to a column of Sephadex LH-20 using methanol as an eluent. The first band (main band) was collected and concentrated under vacuum. Water (50 mL) was added and the resulting solution neutralized with 0.2 M nitric acid to pH 2 by litmus. The precipitate was collected via vacuum filtration to yield a purple solid: 100 mg, 0.093 mmol, 63.6%. See Appendix (Figure A 51 and Figure A 53) for NMR spectra. ESI<sup>+</sup>: calculated: 1093.3068 [M+Na]<sup>+</sup>; found: 1093.3467 [M+Na]<sup>+</sup>.

## Discussion

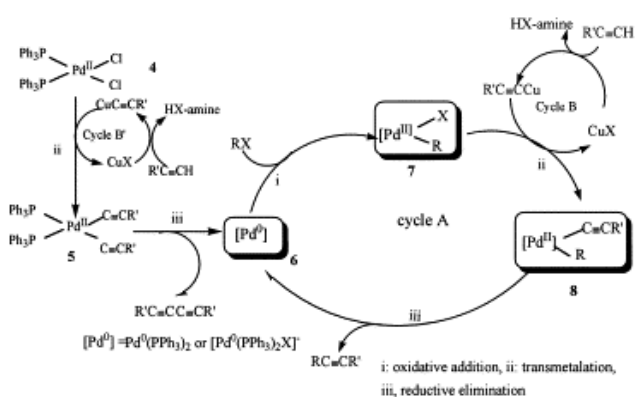
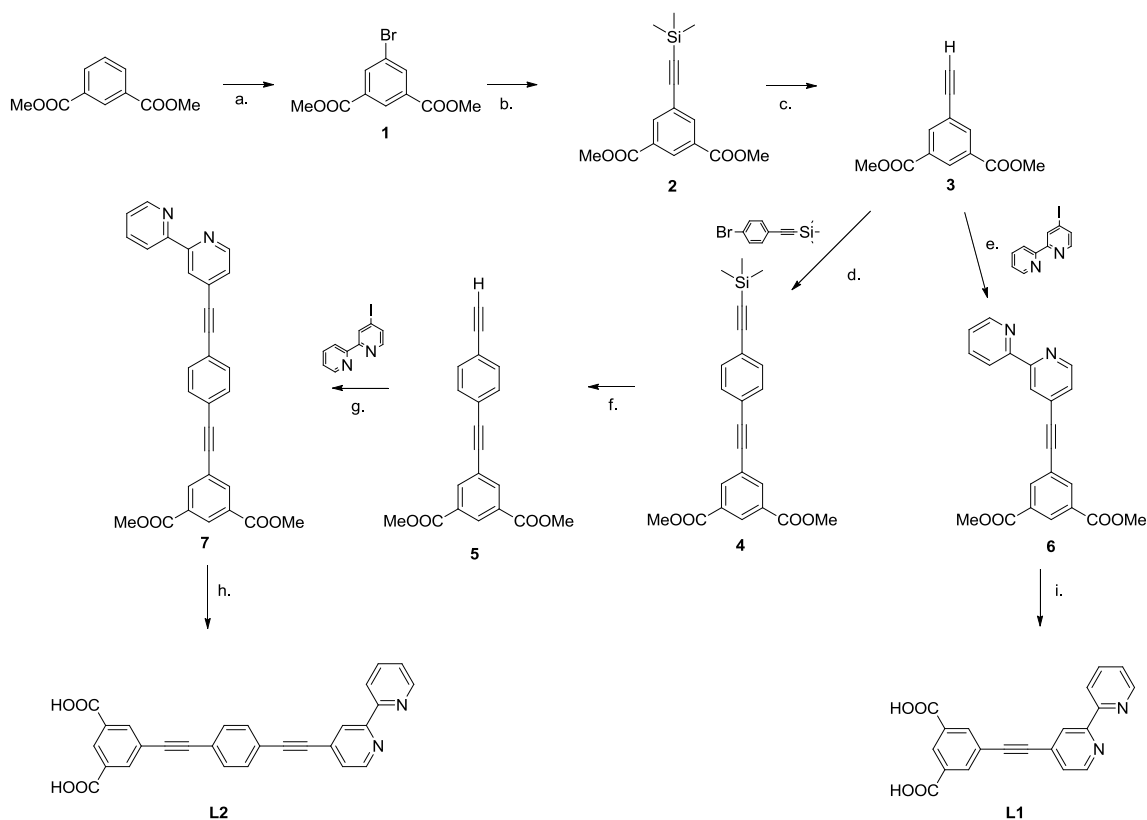


**Figure 14** Mechanism of the Sonogashira coupling reaction, adapted from reference 69

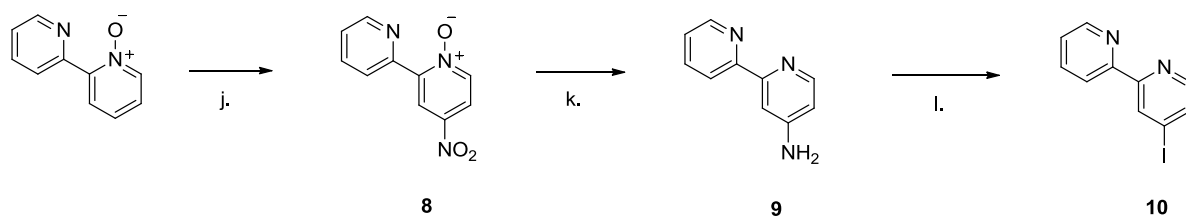
OPE bridge synthesis frequently is achieved through one of two coupling mechanisms. Suzuki-Miyaura coupling or Sonogashira coupling are used to couple an alkyne and an aryl halide. In Suzuki-Miyaura, the coupling occurs between a boronic

acid and the aryl halide. Thus, the alkyne must be first modified to contain a terminal boronic acid. This reaction is promoted through the use of an organometallic catalyst, frequently a palladium(0) catalyst with various ligands.<sup>68</sup>

Sonogashira coupling also proceeds with the use of a palladium catalyst (either Pd(0) or Pd(II)) but requires instead a terminal alkyne and a base. These reactions are also often run in the presence of a co-catalyst, a Cu(I) halide. The typical mechanism of the Sonogashira coupling reaction is shown in Figure 14.<sup>69</sup> The aryl halide is coordinated to the Pd(0) first through oxidative addition, followed by transmetalation transferring the terminal alkyne to the palladium. This is followed by reductive elimination yielding Pd(0) and the coupled product. Through this method, it is possible to easily and efficiently construct modified OPE units. The exact synthesis of **AK0-5** will be discussed below.



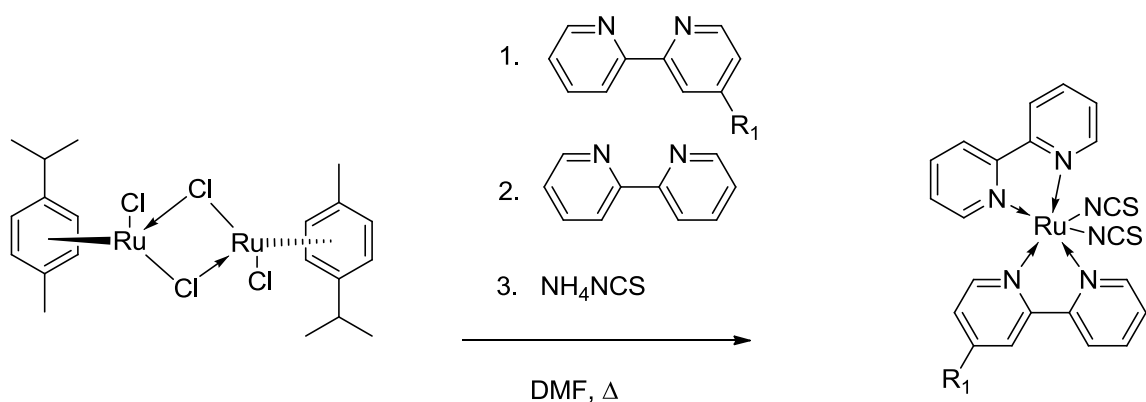
**Scheme 1** Synthesis of Anchor Ligands: **a.** NBS,  $\text{H}_2\text{SO}_4$ ; 90%; **b.**  $\text{CuBr}$ ,  $\text{PdCl}_2(\text{PPh}_3)_2$ , Trimethylsilyl Acetylene, Diisopropyl Amine; 53%; **c.** TBAF, THF; 76%; **d.**  $\text{Pd}(\text{PPh}_3)_4$ , Diisopropyl Amine, Benzene; 40%; **e.**  $\text{Pd}(\text{PPh}_3)_4$ , Diisopropyl Amine, Benzene; 69% **f.** TBAF, THF; 50%; **g.**  $\text{Pd}(\text{PPh}_3)_4$ , Diisopropyl Amine, Benzene; 83%; **h.**  $\text{NaOH}$ ,  $\text{MeOH}$ ,  $\text{CH}_2\text{Cl}_2$ ; 57%; **i.**  $\text{NaOH}$ ,  $\text{MeOH}$ ,  $\text{CH}_2\text{Cl}_2$ ; 80%



**Scheme 2** Synthesis of Dipyriddy ligands: **j.**  $\text{HNO}_3$ ,  $\text{H}_2\text{SO}_4$ ; 50%; **k.**  $\text{H}_2$  (g), 10%  $\text{Pd/C}$ ,  $\text{MeOH}$ ; 91%; **l.** 1.  $\text{NaNO}_2$ ,  $\text{H}_2\text{SO}_4$ , 2.  $\text{KI}$ ; 57%

The synthesis of two rigid rod ligands, **L1** and **L2**, was achieved through a Sonogashira coupling reaction between 4-iodo-2,2'-bipyridine and an alkynyl isophthalate anchor group, by modification of methods previously used in our group (Scheme 1 and Scheme

2).<sup>33,70,71</sup> 4-Iodo-2,2'-bipyridine was synthesized from 2,2-dipyridyl-N-oxide first by nitration<sup>60,61</sup> followed by reduction of the nitro group to an amino group. The reduction was first achieved through use of sodium borohydride.<sup>62</sup> However, when the reaction was repeated, yields were very inconsistent, leading to the need to use more reproducible methods of reduction. An iron-catalyzed reduction using electrolytically reduced iron powder and acetic acid<sup>63</sup> gave yields consistently around 50%; however the extraction was an arduous task where the formation of an emulsion made it difficult to cleanly isolate the product. A third method, catalytic hydrogenation, was then investigated. With almost quantitative yields of reduction from Pd/C and H<sub>2</sub> gas, this became the preferred method for reduction of the nitro group.<sup>64</sup> Following the formation of 4-amino-2,2'-bipyridine, the Sandmeyer reaction was employed to convert the amino group to an iodo group through an diazonium salt intermediate.<sup>62,65,66</sup> The reaction was repeated many times with consistent yields. Variation of the concentrated acid used (either hydrochloric acid or sulfuric acid) showed no impact upon the yield.



**Scheme 3** General Scheme for One-Pot complexation reaction: stepwise addition of ligands followed by quenching with excess ammonium thiocyanate.



The synthesis of the isophthalic anchor group began with dimethyl isophthalate, which was first brominated with N-bromosuccinimide, in a step adapted from a method for isophthalic acid.<sup>56</sup> This radical reaction had almost quantitative yield and though the product was slightly impure, it was used directly in the next step. Following bromination, the Sonogashira coupling reaction was used to couple trimethylsilylacetylene with the brominated anchor group.<sup>33,57</sup> The next step involved removal of the trimethylsilyl protective group, typically through the use of tetra-n-butylammonium fluoride (TBAF).<sup>33</sup> While this reaction should have yields upward of 80%, our typical yields were around 50%. Different attempts were made to increase the yield: anhydrous or wet solvent, the presence of N<sub>2</sub> atmosphere, diluting the TBAF, or using freshly ordered batches of TBAF. However, none of these factors had a significant

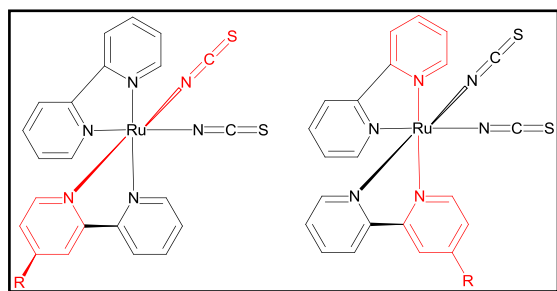


**Figure 15** Two stereoisomers of **AK1-4**; R is either *trans* from a thiocyanate group (left) or *trans* from a pyridyl group (right)

impact. A second method, using silver nitrate (AgNO<sub>3</sub>) was attempted for the deprotection, however, this method had similar yields (~50%) and long reaction

times and was thus not further pursued.<sup>58</sup> At this point, the Sonogashira

coupling was employed to couple the anchor group and the iodobipyridine completing the synthesis of the short rigid rod, **L1**. Alternatively, the Sonogashira coupling was made between compound **3** and [(4-bromophenyl)ethynyl](trimethyl)silane followed by the deprotection of the TMS group and Sonogashira coupling with iodobipyridine to form the long rigid rod, **L2**. Either the ester version of the ligands was isolated here, or

an additional step of hydrolysis (Scheme 4) using sodium hydroxide in organic solvents was employed to isolate the corresponding carboxylic acids.<sup>59</sup>

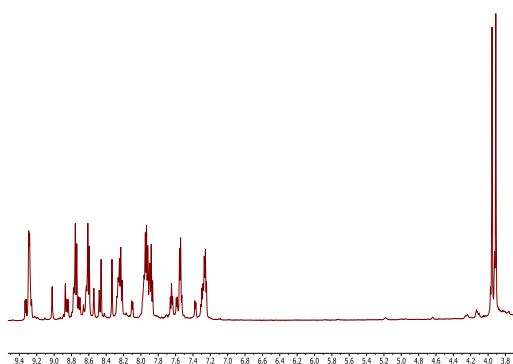
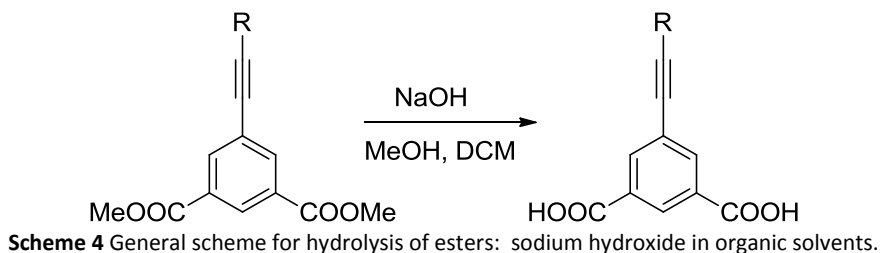


**Figure 16**  $^1\text{H}$  NMR spectrum of Short Ester Rod. Signal from the methyl ester peaks at 3.8-4.2 ppm shows two peaks from the separate isomers present.

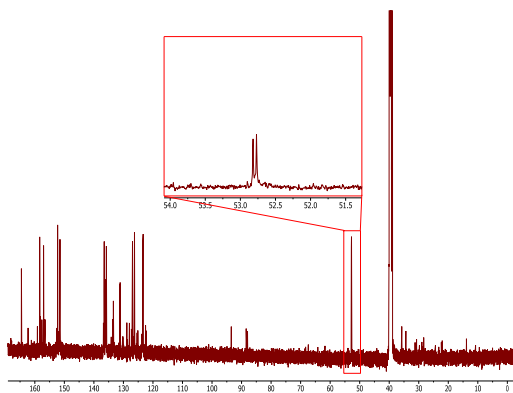


**Figure 17**  $^{13}\text{C}$  NMR spectrum of Short Ester Rod. Signal from the methyl ester peaks at 52.5-53.0 ppm shows two peaks indicating separate isomers.

Following the synthesis of the ligands, complexation was employed to form complexes **AK0-5**, and the two ester rigid rod compounds, **13** and **14**. **AK0** and the two ester

complexes were synthesized via a one-pot reaction (Scheme 3) with di- $\mu$ -chlorobis[(*p*-cymene)chlororuthenium (II)] and stepwise addition of each target ligand followed by quenching with an excess of ammonium thiocyanate.<sup>26</sup> These reactions were carried out in DMF with heating (150 °C). Due to the asymmetry of the rigid rod complexes, each complex (other than **AK0**) has two stereoisomers. One stereoisomer occurs

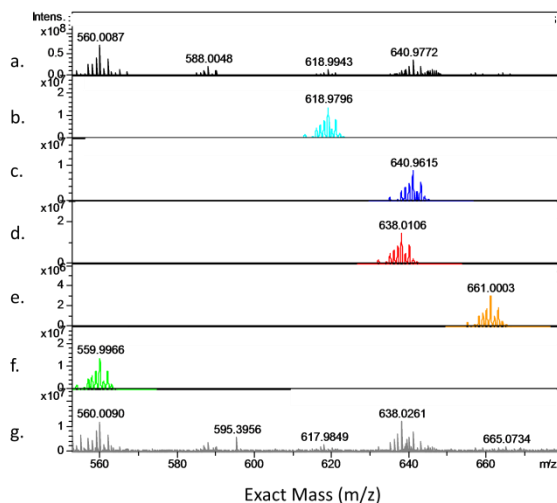


**Figure 18** ESI Spectra of **AKO** with different exposure times to DMSO. a. Spectrum of **AKO** with 0 day exposure to DMSO solution; b.-f. calculated ESI spectra for **AKO** (b.  $[M+H]^+$ ; c.  $[M+Na]^+$ ; d.  $[M-(NCS^-)+(DMSO)]^+$ ; e.  $[M-(NCS^-)+(DMSO)+Na]^+$ ; f.  $[M-(NCS^-)]^+$ ); g. Spectrum of **AKO** after 1 day exposure to DMSO.

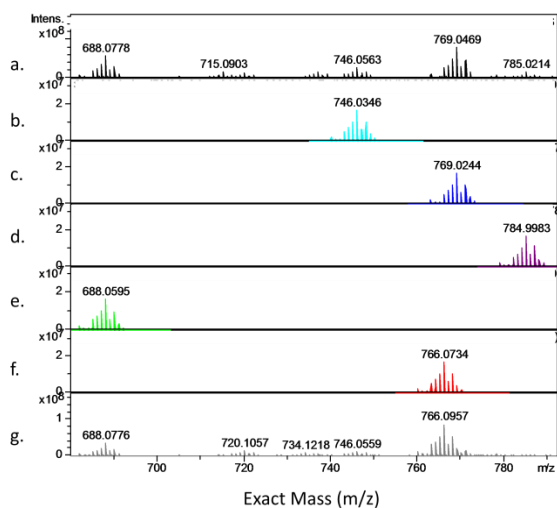


**Figure 19** ESI Spectra of **AK5** with different exposure times to DMSO. a. Spectrum of **AK5** with 0 day exposure to DMSO solution; b.-f. calculated ESI spectra for **AK5** (b.  $[M]^+$ ; c.  $[M+Na]^+$ ; d.  $[M+K]^+$ ; e.  $[M-(NCS^-)]^+$ ; f.  $[M-(NCS^-)+(DMSO)]^+$ ); g. Spectrum of **AK5** after 1 day exposure to DMSO.

when the anchor group of the bipyridine ligand is *trans* to a thiocyanate ligand, whereas the other isomer occurs when the anchor group is *trans* to a pyridyl unit, Figure 15.

This is most readily apparent in the  $^1H$  and  $^{13}C$  NMR spectra of the two ester complexes, Figure 16 and Figure 17. The presence of these two *cis*-Ru isomers, as well as low solubility of N3-type complexes in general, and the exchange of thiocyanate with DMSO (the solvent required for the NMR spectra) led to difficulties in assigning the signals in the NMR spectra, both proton and carbon.

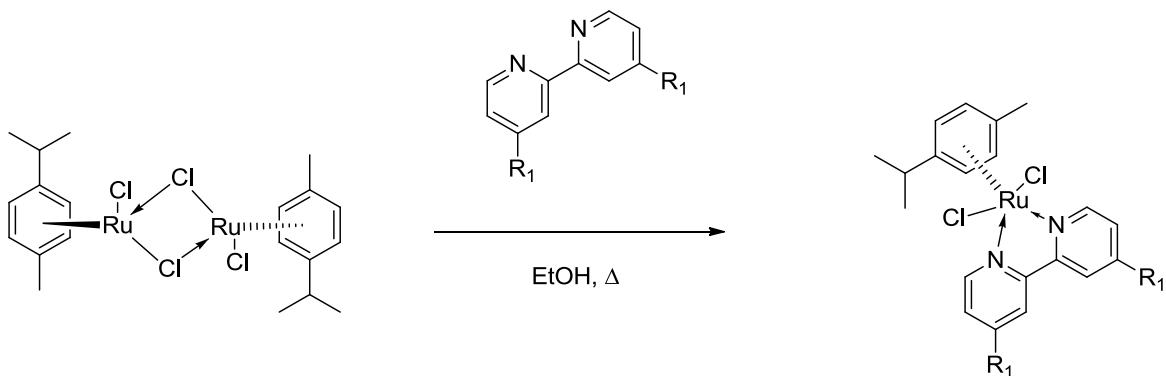
Hara and coworkers also found the presence of isomers in asymmetric N3-type complexes complicated NMR

assignment and that it was not possible to separate these isomers.<sup>72</sup> Graetzel and coworkers also noted the presence of the isomers.<sup>55</sup>

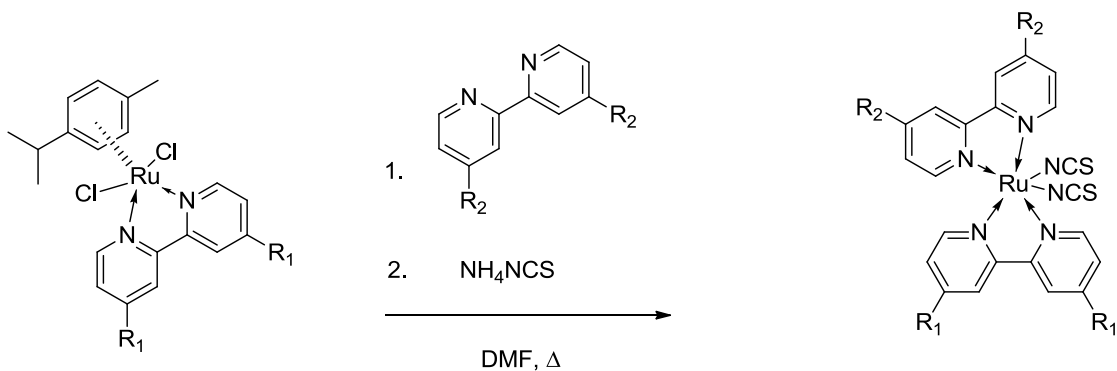
The thiocyanate-DMSO exchange was monitored by ESI spectra. Spectra were taken in DMSO with a drop of formic acid added to assist in ionization of the complex. If the sample was freshly prepared, the spectrum of the N3-type complex was easily obtained, without apparent ligand exchange. However, the longer the sample had been exposed to DMSO, the more exchange of DMSO with the thiocyanate ligand was observed. The spectra shown here were collected under two conditions. Figure 18 and Figure 19 show freshly prepared samples of **AK0** and **AK5** in DMSO in spectra a. (top, black). Both spectra do not show exchange with DMSO, with peaks for both compounds as well as for the compounds minus a thiocyanate ligand. However, spectra g. in both figures (bottom, grey) show samples that have been prepared a day prior to data collection. In these spectra (both prepared from the same batch of compounds in Figure 18 and Figure 19) a new set of peaks is apparent:  $[M-(NCS^-)+(DMSO)]^+$ . This clearly highlights the fact that DMSO can exchange with the thiocyanate ligands, further complicating the characterization of the compounds. The presence of literature reports indicating that DMSO coordinates to ruthenium further supports our observation.<sup>73</sup>

Due in part to the low solubility of the compounds as well as the desire to have another practical solvent for characterization (other than DMSO), we devised a second generation of N3-type rigid rod dyes, where we modified the ancillary bipyridyl ligand to possess alkyl chains in the hopes of increasing solubility. Unexpectedly, the solubility increase was minor at best with the exception of compound **AK3** which is soluble in

acetone. However, acetone is also known to be weakly coordinating to ruthenium<sup>74,75</sup> and thus is still not an ideal solvent.



**Scheme 5** General scheme for first step in two step complexation: addition of primary ligand.



**Scheme 6** General scheme for second step in two step complexation: addition of the secondary ligand followed by quenching with ammonium thiocyanate.

To aid in confirmation of successful, sequential ligand coordination in the ruthenium complexes, we investigated other methods of synthesis to confirm that the complexes were synthesized. Graetzel and coworkers had developed a process by which they first added one bipyridyl ligand and isolated a RuCl<sub>2</sub>[LL][*p*-cymene] intermediate and characterized it.<sup>27,29</sup> Our hypothesis was that we could isolate two intermediates, one for each target ligand on our final N<sub>3</sub>-type complex, and then, once characterized, carry out the final complexation with the other ligand to achieve the formation of the same final complex through two distinct intermediates. In the synthesis of **AK3**, this was

achieved, where we isolated the 4,4'-dinonyl-2,2'-bipyridine intermediate and the **L1** intermediate (Scheme 5). The *p*-cymene intermediates were isolated and characterized prior to the second step of complexation to yield the N3-type complexes. Both of these intermediates are quite soluble in organic solvents leading to easy characterization by NMR and ESI. The second step of complexation, in DMF, with stepwise addition of the second bipyridyl ligand and an excess of ammonium thiocyanate (Scheme 6) yielded consistent NMR and ESI for both compounds.<sup>67</sup>

## Results and Discussion

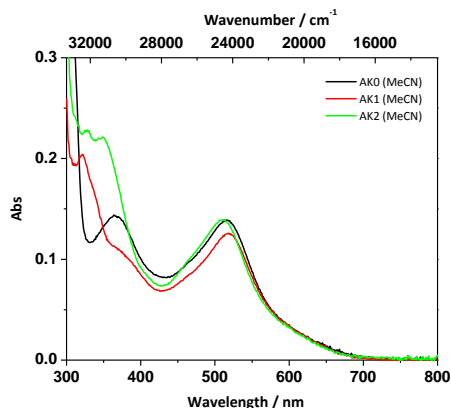


**Figure 20** Abs Spectra of **AK0** (black), **AK1** (red), and **AK2** (green) in Acetonitrile

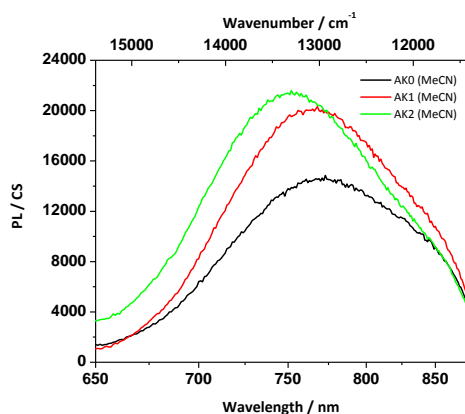


**Figure 21** Photoluminescence Spectra of **AK0** (black), the metal-to-ligand-charge-transfer band **AK1** (red), and **AK2** (green) in acetonitrile

(MLCT). Intense  $\pi$ -to- $\pi^*$  transitions were observed at 300 nm.<sup>76</sup> An additional absorption band at 340-360 nm is present for **AK1** and **AK2**, attributed to the absorption of the phenyleneethynylene (OPE) bridge.<sup>33</sup> When excited in the MLCT (Figure 21), compounds **AK0-2** showed characteristic weak photoluminescence,<sup>54</sup> with  $\lambda_{\text{max}} = 770$  nm for **AK0**, **AK1** and  $\lambda_{\text{max}} = 750$  nm for **AK2**.

### Photophysical Measurements

*The results in this section would not be possible without the effort of our collaborators at Johns Hopkins University, especially Patrik Johansson.*

Ruthenium complexes **AK0-2** were synthesized and characterized spectroscopically. Solution absorption spectra are shown in Figure 20. All three complexes exhibited characteristic absorption from 450-700 nm attributed to

The compounds were then anchored to nanocrystalline  $\text{TiO}_2$  thin films by immersion into a dye solution (0.5 – 2 mM) in *t*-butanol/acetonitrile (1:1). Absorption and emission

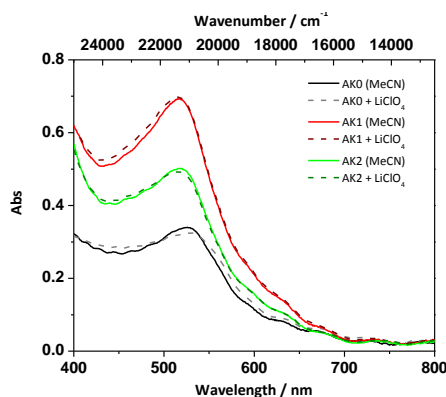


**Figure 22** Absorption Spectra of dyes bound to  $\text{TiO}_2$ ; solid line represents neat compound, dashed line represents neat compound plus  $\text{Li}^+$ ; **AK0** (black), **AK1** (red), **AK2** (green)

spectra were obtained on films as well (see Figure 22 and Figure 23). The  $\text{TiO}_2$  films were base pre-treated to both assist in binding (especially when the anchor groups are esters)<sup>21</sup> and to raise the quasi-Fermi level of

the conduction band to a more negative potential.<sup>77</sup> Small cations ( $\text{Li}^+$ ) were added to

the electrolyte to help shift the acceptor states in the  $\text{TiO}_2$  to a more positive level (away from the vacuum) resulting in more favorable energetics for charge transfer.<sup>78</sup> Meyer and coworkers theorized that the oxygen ligands on the  $\text{TiO}_2$  surface coordinate to the  $\text{Li}^+$  cations which acts as Lewis acids to draw electron density away from the  $\text{Ti(IV)}$  center facilitating easier electron transfer to the  $\text{Ti(IV)}$  center, thus lowering the energy. In the presence of  $\text{Li}^+$ , **AK0-2** showed no noticeable change in their absorption spectra when anchored to  $\text{TiO}_2$ . However, the effect of the cation is readily apparent in the photoluminescence spectra for **AK0-2** on  $\text{TiO}_2$  (Figure 23). In the absence of the cation, the quasi-Fermi level of the semiconductor is not favorable for interfacial charge transfer as evidenced by the photoluminescence (black, red, and green). In the presence of  $\text{Li}^+$ , photoluminescence (when excited in the MLCT) was quenched suggesting electron transfer from the excited dye to the  $\text{TiO}_2$ .



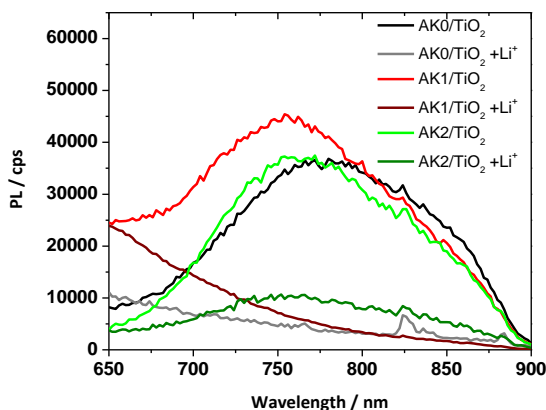


**Figure 23** Photoluminescence spectra of **AK0** (black), **AK1** (red), and **AK2** (green) bound to  $\text{TiO}_2$ . Darker colors show quenching of emission characteristic of injection in the presence of  $\text{Li}^+$

The next experiment was to further probe the electron transfer dynamics of the rigid rod dyes. Transient absorption (TA)<sup>79</sup> is a technique employed in the study of excited state

dynamics. It is a technique where a film or solution of dye is pulsed with

light to form the excited state and then the change in absorption when compared to the ground state absorption is observed. The subsequent increase or decrease in absorption correlates to the change in absorption due to the excited state. A typical solution-based TA spectrum for the dyes is shown in Figure 24. This spectrum was conducted on compound **13** as that compound had the highest solubility. Solubility is an issue for solution based transient absorption as high concentrations of dye are required. For N3-type dyes, the compound **13** shows the characteristic bleaching of the MLCT band around 550 nm and long lived excited state lifetimes (55 ns).<sup>80,81</sup> Upon anchoring to  $\text{TiO}_2$ , the TA spectrum exhibits some important changes, Figure 25. On  $\text{TiO}_2$ , the

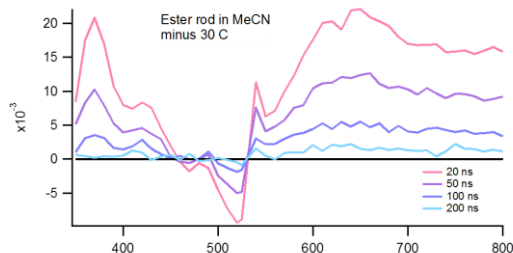


**Figure 24** Transient absorption spectrum of **13** in Acetonitrile solution

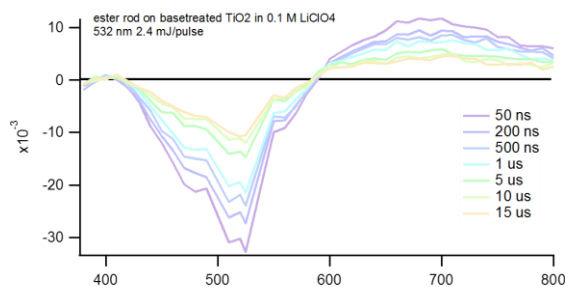


**Figure 25** Transient absorption spectrum of **13** on  $\text{TiO}_2$  films

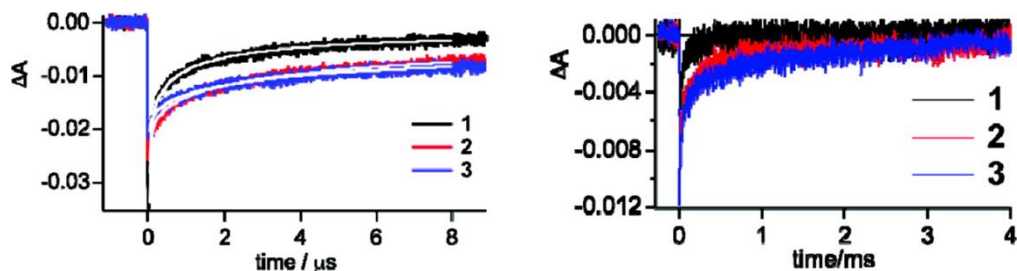


**Figure 26** Charge recombination. left: **AK0** (black), **13** (red), and **AK1** (blue) with KWW fit (white); right: **AK0** (black), **6** (red), and **AK1** (blue) on long time scale

excited state dye injects an electron into the semiconductor and shows bleaching of the dye without the increased absorbance around 400 nm. There is also evidence of a long-lived charge separated state. The increase in absorption after 700 nm is frequently attributed to the absorbance of the oxidized sensitizer<sup>80</sup> beginning around 700 nm, and  $\text{TiO}_2(e^-)$ ,<sup>82</sup> centered around 900 nm.

From the transient absorption data, our collaborators were able to extract the charge recombination rate,  $k_{\text{cr}}$ . Initially we probed the short rigid rod compounds, **AK0**, **13**, and **AK1**.<sup>80</sup> Figure 26 shows the spectra for **AK0**, **13**, and **AK1** where the left figure has been fit with an exponential model based upon the Kolraush-Williams-Watt function (KWW).<sup>83</sup> The data are summarized in Table 1:

**Table 1** Charge Recombination Rates

Sensitizer	<b>AK0</b> (black)	<b>6</b> (red)	<b>AK1</b> (blue)
$k_{\text{cr}} \text{ (s}^{-1}\text{)}$	$7.1 \pm 3.6 \times 10^5$	$2.8 \pm 1.4 \times 10^5$	$2.6 \pm 1.3 \times 10^5$

The charge recombination rate constant for **AK0**, the shortest compound, is much greater than **AK1**.

We then investigated the effect that rigid rod length had upon  $V_{oc}$ . Figure 27 shows the open-circuit voltage for **AK0** and **AK1** thin films. These films are dye-TiO<sub>2</sub> films, not fully operational solar cells, i.e. they contain no iodide. At all irradiances, **AK1** has much better  $V_{oc}$  than **AK0** and at higher irradiances, it has increased  $V_{oc}$  as evident by the slope of the fitting line. The diode equation, Equation 2,

$$V_{oc} = i \times \frac{(kT)}{e} \times \ln\left[\frac{I_{inj}}{n \sum_j k_{cr}[A]_j}\right]$$

Equation 2

models the open-circuit voltage, where  $i$  is the ideality factor,  $kT/e$  is a constant dependent upon temperature,  $I_{inj}$  represents the influx of electrons into the semiconductor, and the bottom term represents the charge recombination between electrons in the semiconductor and acceptor states,  $[A]_j$ . The slope of  $V_{oc}$  vs. irradiance

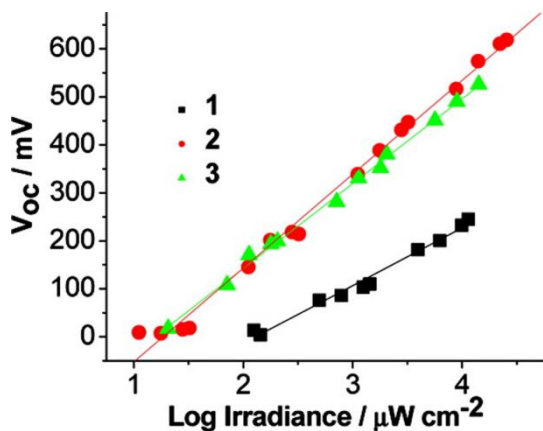
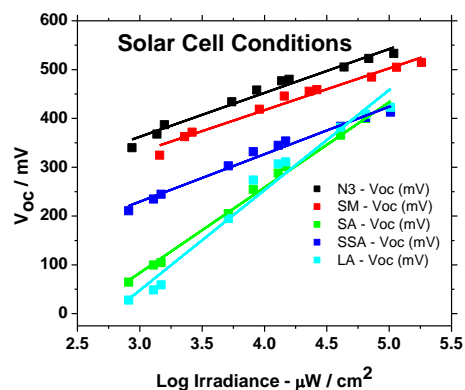


Figure 27  $V_{oc}$  as a function of irradiance for **AK0** (black), **13** (red), and **AK1** (green)

is  $i$ , the ideality factor and it shows how the open-circuit voltage is dependent upon irradiance for a specific dye. Ideality factors typically reported for N3-type compounds are approximately  $i = 2$ ;<sup>84</sup> however, **AK1** and **AK2** (see Figure 28) have unusually high ideality factors of  $i = 2.90$  and  $i = 3.47$

respectively. This implies that at high irradiances **AK1** and **AK2** should outperform N3 in solar cell applications.



**Figure 28**  $V_{oc}$  as a function of irradiance in the presence of  $Li^+$  and  $I^-$ , solar cell conditions; **AK0** (red), **AK1** (green), **AK2** (pale blue)

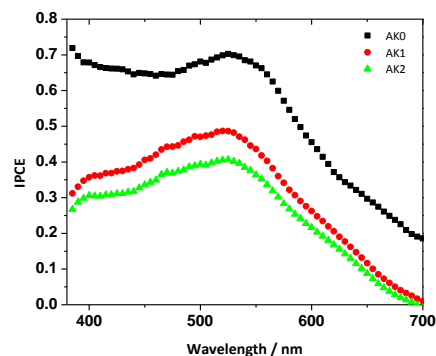


**Figure 29** IPCE for **AK0** (black), **AK1** (red), **AK2** (green)

When the incident-photon-to-current-efficiency (IPCE) is examined, however, with IPCE of 0.48 and 0.39, respectively **AK1** and **AK2** are significantly less efficient than **AK0** (Figure 29), with IPCE of 0.78. Also, under solar cell conditions, the open-circuit voltage for **AK1** and **AK2** is considerably worse than when compared to similar films in the absence of the redox mediator (Figure 28); however, the ideality factors remain the same. The difference here arises from the presence of iodine and iodide. These results imply that **AK1** and **AK2** interact with iodine, which will be discussed further in this section.

A summary of the relevant solution (Table 2) and  $TiO_2$  film data (Table 3) can be found below.

**Table 2** Summary of Solution Data

Compound	$\tau_0$ ns	$\lambda_{abs}$ (MLCT) nm	$\lambda_{PL}$ nm
<b>AK0</b>	$27 \pm 0.1$	515	770
<b>AK1</b>	$31 \pm 0.1$	510	770
<b>AK2</b>	$26 \pm 0.1$	510	750

**Table 3** Summary of TiO<sub>2</sub> Thin Film Data

Compound	$\lambda_{\text{abs}}$ (MLCT) nm	$k_{\text{inj}} \text{ s}^{-1} \times 10^{10}$	$\phi_{\text{inj}}$
<b>AK0</b>	530	$7.6 \pm 1.9$	$0.98 \pm 0.03$
<b>AK1</b>	510	$0.7 \pm 0.2$	$0.93 \pm 0.03$
<b>AK2</b>	520	$0.2 \pm 0.1$	$0.70 \pm 0.03$

Of note is the high excited state lifetime ( $\tau_0$ ) for all compounds in solution. This is typical of all N3-type complexes.<sup>4,27</sup> This is important as it implies a stable excited state with good characteristics for electron injection. Also of note is the  $k_{\text{inj}}$ , the excited state injection rate constant, for **AK0-2**. As the distance the chromophoric unit increases from the anchor group of the dyes,  $k_{\text{inj}}$  decreases implying that electron injection occurs through the bridge. However, injection occurs fast enough that there is nearly quantitative yield of injection ( $\phi_{\text{inj}}$ ) for the compounds.

Electron transfer from the chromophore to the semiconductor was further investigated through experiments with variable laser fluency and applied bias. With decreased charge recombination and injection rate constants ( $k_{\text{cr}}$  and  $k_{\text{inj}}$ ) and higher  $V_{\text{oc}}$  for increased spacer length, it is clear that the structure of the dye has an effect on the electronic communication properties. When we investigate the effect that different concentrations of electrons in the TiO<sub>2</sub> has upon recombination, we can look at either increasing the number of charge separated states by creating more excited dyes (variable laser fluency) or by adding electrons directly to the TiO<sub>2</sub> (applied bias).

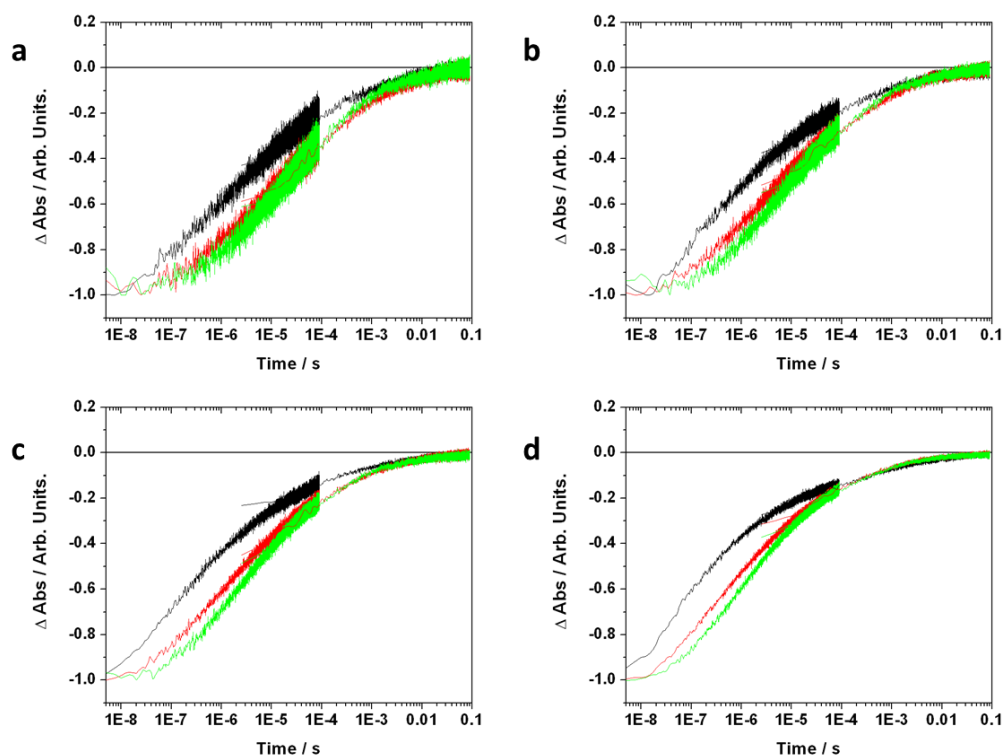


**Figure 30** Transient absorption data monitored at 500 nm after pulsed 532 nm laser excitation of dyes on  $\text{TiO}_2$ : **AK0** (black), **AK1** (red), and **AK2** (green) as laser power changes, from **a** to **d**: 0.15 mJ, 0.3 mJ, 0.7 mJ, 1.4 mJ

When analyzing the effect of structure on recombination, the difference in the charge recombination rates on **AK0-2** can be compared as the number of charge separated states is increased. To achieve this, the power of the laser is increased from 0.15 mJ per pulse to 1.4 mJ per pulse and the effect on recombination is observed. The recombination can be broken into two approximate regions (Figure 30), a fast component ( $10^{-7}$  to  $10^{-4}$  s) and a slow component ( $10^{-4}$  to  $10^{-1}$  s). As the laser power increases, the effect from the  $\text{TiO}_2(e^-)$  increases and affects the fast component of charge recombination. From the weakest power and thus lowest concentration of  $\text{TiO}_2(e^-)$ , there is the slowest recombination. As the concentration of charge separated states increased, charge recombination rates increase as well. However, rather than

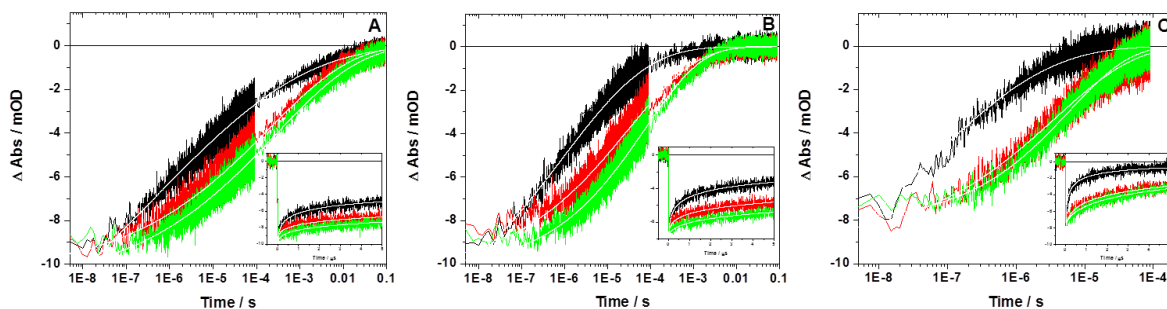


**Figure 31** Transient absorption data monitored at 500 nm after pulsed 532 nm laser excitation (0.2 mJ/pulse) of dyes on TiO<sub>2</sub> **AK0** (black), **AK1** (red), and **AK2** (green) with an applied bias of A) +150 mV; B) -150 mV; and C) -350 mV versus NHE.

increase consistently across **AK0-2**, a larger change in laser power is required to affect the same change in the recombination rate as the chromophore-semiconductor distance increases. This effect is only apparent in the “fast” region of recombination, as the structural effects on recombination do not affect the “slow” component. This, as well as low temperature studies performed by our collaborators, suggests that the slow component of the charge recombination kinetics occurs through a tunneling mechanism, such as that suggested by Furube.<sup>85</sup> The slow mechanism would be suppressed due to the increased TiO<sub>2</sub>(e<sup>-</sup>) concentration filling the trap states in the TiO<sub>2</sub> required for tunneling. Thus, the “fast” mechanism of electron transfer depends upon dye structure.

The effect of structure on the recombination rate can also be probed through applied bias where the TiO<sub>2</sub>(e<sup>-</sup>) concentration is increased. Durrant<sup>81</sup> and O'Regan<sup>86</sup> have shown that by increasing the concentration of TiO<sub>2</sub>(e<sup>-</sup>) through an applied bias, fast recombination is achieved across all time scales and for all chromophores studied. Instead, **AK0-2** show that with increased TiO<sub>2</sub>(e<sup>-</sup>) concentrations, recombination is affected on the “fast” component (Figure 31) but not on the “slow” component. If a

large enough potential was applied, recombination could be affected to occur on the “fast” time scale, removing any observable long-time scale recombination. In order to obtain a 20% increase in charge recombination rates for **AK0**, an applied bias of approximately +50 mV was required. To obtain the same change in **AK1** and **AK2**, applied biases of -50 mV and -150 mV were needed respectively.

Taken together, these data imply that charge recombination can be inhibited by distance, even when  $\text{TiO}_2(e^-)$  concentrations are high. This is particularly relevant to solar cell applications when under typical irradiances, each  $\text{TiO}_2$  nanoparticle is expected to house over 20 electrons.<sup>87</sup> This data explains the high  $V_{oc}$  present at high irradiances for **AK1** and **AK2** (Figure 27).

As dye structure plays an important part in injection and recombination dynamics, as

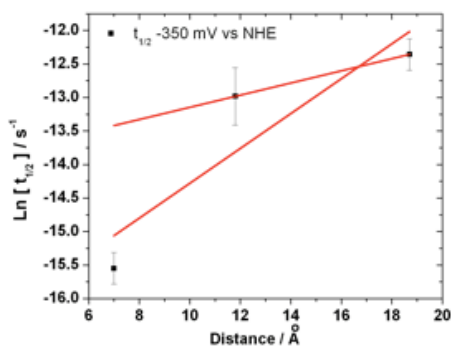


**Figure 32**  $k_{cr}$  as a function of distance with attenuation factor  $\beta$ , fitted with and without **AK0**

well as two different apparent mechanisms for recombination, the communication through the OPE bridge must be investigated. Typically, electron transfer through a distance is monitored by the attenuation factor,  $\beta$ , which is a model of the charge transfer rate constants with dependence upon distance.

With typical measurements for  $\beta$  for the OPE spacer reported at  $\beta = 0.25 \text{ Å}^{-1}$  for injection and  $\beta = 0.20 \text{ Å}^{-1}$  for recombination,<sup>50</sup> the values for **AK0-2** were investigated.



$$k = A \exp(-\beta R_{DA})$$

Equation 3

$R_{DA}$  was calculated with the distance between the pyridyl nitrogen and the carboxylate oxygen as the chromophore-semiconductor distance. With approximate distances of 7.1 Å for **AK0**, 11.8 Å for **AK1**, and 18.7 Å for **AK2**, the recombination constants were plotted as a function of distance (Figure 32) using Equation 3.  $\beta$  was abstracted two ways: fitting **AK0-2** and a second fitting using only **AK1** and **AK2**. For the first method, our  $\beta = 0.25 \text{ Å}^{-1}$  corresponds closely with the typical values reported by Albinsson and coworkers.<sup>50</sup> The second method was employed due to the lack of correlation between **AK0** with **AK1/AK2** due to the coupling factor associated with the bridge. The value of  $\beta$  for this method is  $\beta = 0.12 \text{ Å}^{-1}$ . While this value was abstracted from only two data points and is subject to a rather large uncertainty, previously published data indicate that the mesoporous nature of the  $\text{TiO}_2$  thin films likely preclude analysis over larger distances.<sup>88</sup>

Minor differences in the compounds **AK0-2** should also be considered when evaluating the data due to chromophore-semiconductor distance. The difference in the anchor groups of **AK0** with **AK1** or **AK2** suggests that a model of distance, while relevant, also presents some holes in the evaluation of the data. **AK0** has a carboxylic acid anchor group attached to each pyridyl ring, whereas **AK1** and **AK2** have two anchor groups attached to the isophthalic unit. This difference in the anchor group, and therefore

charge transfer, should lead to careful characterization of the charge transfer mechanisms.

## Iodine Coordination

As previously mentioned, **AK1** and **AK2** did not perform well in solar cell conditions. We consider the possibility that this poor performance arises from a dye-iodine interaction. O'Regan and coworkers have examined N3-type dye-iodine interactions to determine that  $I_2$  coordinates with thiocyanate ligands in the dye.<sup>19</sup> This suggests that the additional chromophore-semiconductor distance in **AK1** and **AK2** coupled with iodine coordination may lead to poor injection from those chromophores and thus poor solar

cell performance. The interaction of **AK0-2** with  $I_2$  was studied as well.

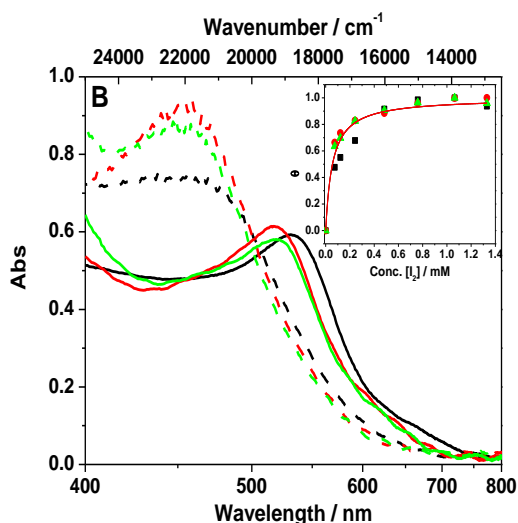


**Figure 33** AK0 (black), AK1 (red), and AK2 (green) on TiO<sub>2</sub> in the presence of 1.33 mM I<sub>2</sub> (dashed) and absence of I<sub>2</sub> (solid). Inset: Binding isotherm for **AK0-2** with  $K = 2 \times 10^4 \text{ M}^{-1}$ .

N3-type complexes and  $I_2$  of  $K = 4.0 \times 10^4 \text{ M}^{-1}$ . **AK0-2** showed behavior consistent with that reported by O'Regan with both the blue shift in the MLCT as well as the presumed one-to-one binding isotherm of  $K = 2 \times 10^4 \text{ M}^{-1}$ , see Figure 33, which shows the absorbance spectra once changes in the solution absorbance have been subtracted. One dye that O'Regan and coworkers looked at contained an amino functional group

which was shown to have additional interactions with  $I_2$ . These additional interactions are theorized to be responsible for a large increase in the recombination rate of their dye resulting in a decrease in  $V_{oc}$  and overall efficiency of their dye. For **AK1** and **AK2**, the formation of an iodine adduct lowered the injection yield by about 80%. There was no noticeable change in the injection yield for **AK0**. Iodine is an electron acceptor and has been shown to quench the excited state, a process which could account for the change in the injection yields.<sup>89,90</sup> O'Regan's results coupled with results from our dye suggest that the increased  $TiO_2$ -chromophore distance for **AK1** and **AK2** and  $I_2$  interaction are largely responsible for the poor solar cell performance of **AK1** and **AK2** when compared to **AK0** and N3.

Initial results show  $I_2$ -adduct formation for **AK3** and **AK4** consistent with that found for **AK1** and **AK2**. However, the binding isotherm for **AK4** shows a much higher affinity for  $I_2$  compared to **AK2**. Currently, the origin of this binding affinity is being investigated. Ligand modifications and subsequent effect on the formation of the  $I_2$  adduct could lead to modification of the ancillary bipyridyl ligand to inhibit the coordination with  $I_2$ . This result could allow longer N3-type dyes to be viable for solar cell applications and stresses the importance of molecular design in a variety of aspects in the dye-sensitized solar cell. At the time that this thesis was written, further experiments were being conducted by Dr. Hao Tang in our group to study how the structural differences of the anchor group as well as the presence of alkyl chains on the ancillary ligand affect the  $I_2$  interaction.

## Conclusion

Compounds **AK0-4** were successfully synthesized and characterized. These compounds exhibit difficult physical characterizations due to low solubility, the presence of stereoisomers, and the occurrence of thiocyanate-DMSO ligand exchange. Long chain alkyl substituents were added to the ancillary ligands for compounds **AK3** and **AK4** to increase solubility and characterizability.

The photophysical properties of the dyes, **AK0-2**, were studied in solution and on  $\text{TiO}_2$ . In solution, the dyes exhibited photophysical and electrochemical properties similar to those exhibited by N3, long excited state lifetimes and characteristic strong absorption to the near IR.

When bound to  $\text{TiO}_2$ , the dyes also exhibited similar photophysical properties to N3, showing fast electron injection into the semiconductor as well as slower charge recombination. Communication through the OPE bridge for **AK1** and **AK2** was also studied. The bridge length dependence for charge injection and recombination was studied through attenuation factor,  $\beta$ , and was consistent with values previously reported for OPE spacers. The dyes also showed increased  $V_{oc}$  as a function of OPE bridge length due to a decreased charge recombination rate. The increased spacer length lowered the effect of the  $\text{TiO}_2(e^-)$  on the chromophore leading to lower effect at

higher electron concentrations. This result suggests that increasing the chromophore-TiO<sub>2</sub> distance can inhibit recombination, leading to higher  $V_{oc}$ . This is of practical interest because high irradiances are typical of cells under working conditions.

However, under when incorporated into DSSCs, **AK1** and **AK2** did not outperform the model, **AK0**, even though they had previously exhibited better  $V_{oc}$ . This was most likely due to formation of an I<sub>2</sub>-adduct, which has been shown to form with N3-type dyes. Currently, the origin of this binding affinity is being investigated. Ligand modifications and subsequent effect on the formation of the I<sub>2</sub> adduct could lead to modification of the ancillary bipyridyl ligand to inhibit the coordination with I<sub>2</sub>. This result could allow longer N3-type dyes to be viable for solar cell applications and stresses the importance of molecular design in a variety of aspects in the dye-sensitized solar cell.

## **Chapter 3: Modified N3-Type Dyes for Coordination to Platinum Nanoparticles**

## Introduction

As previously mentioned,  $V_{oc}$  can be controlled through two predominant methods, increasing the quasi-Fermi level of the semiconductor or lowering the potential of the redox mediator. The overpotential is the difference between the HOMO level of the dye and the redox potential of the mediator. The redox mediator is involved in the DSSC regenerative process (see Figure 34) when it reduces the oxidized sensitizer.  $I^-/I_3^-$  is

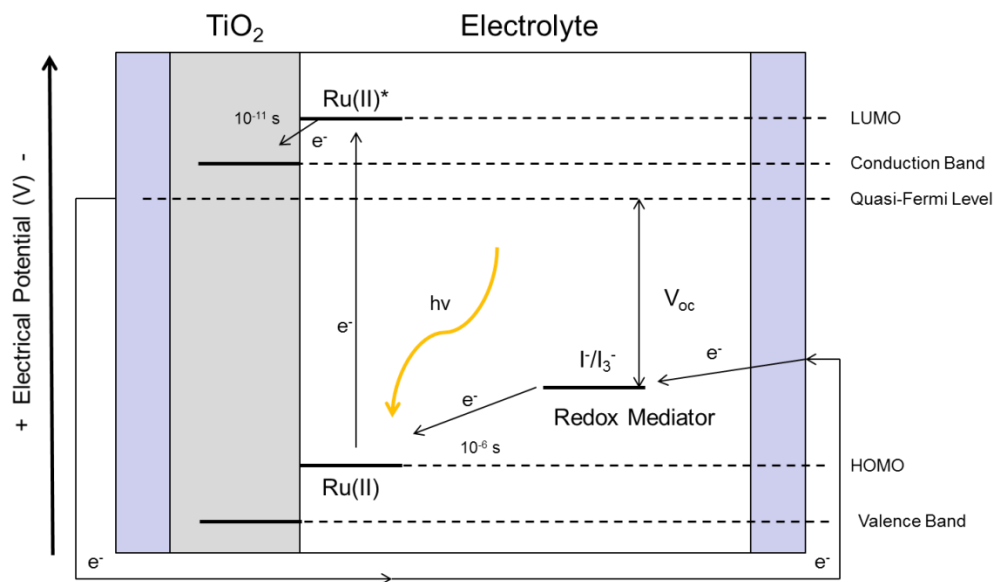


**Figure 34** DSSC electronic diagram; Redox mediator overpotential is the difference between HOMO level of the dye and the redox mediator potential.

currently the mediator of choice for DSSCs. Many of the electronic losses in DSSCs occur due to the large overpotential required for the  $I^-/I_3^-$  mediator. Theoretically, there are two ways to lower the loss of voltage from this large overpotential. One could change from the  $I^-/I_3^-$  couple to another mediator with a lower overpotential, or one could develop a method of lowering the large overpotential currently required for  $I^-/I_3^-$ .



$\text{I}^-/\text{I}_3^-$  has a standard electrochemical potential of +0.35 V vs. NHE (normal hydrogen electrode).<sup>91</sup> Theoretically, any dye with a more positive electrochemical potential could be reduced by the  $\text{I}^-/\text{I}_3^-$  mediator. However, in practice, this regeneration process occurs quite sluggishly if there is not at least a 0.5 V overpotential from the  $\text{I}^-/\text{I}_3^-$  redox mediator compared to the dye's potential. In the DSSC, a fast regeneration of the dye is desired as this can generate a higher current. N3 shows typical oxidation potentials between 0.5 V<sup>92</sup> and 0.75 V<sup>91</sup> more positive than the  $\text{I}^-/\text{I}_3^-$  redox mediator. When Lewis and coworkers compared a series of ruthenium dyes, one of which was N3, with a series of osmium analogs,<sup>92</sup> they showed that with a sufficient redox mediator overpotential the osmium analogs could perform comparably to the ruthenium dyes. However, the osmium analog of N3 only had an oxidation potential about 0.35 V more positive than the  $\text{I}^-/\text{I}_3^-$  mediator. This led to much lower currents, 11.1 mA/cm<sup>2</sup> for N3 compared to 2.2 mA/cm<sup>2</sup> for the osmium analog, and poor solar cell performance.<sup>92</sup> Further investigation spectroscopically showed that the poor performance of the osmium analog was due to the poor regeneration from  $\text{I}^-$ .<sup>93</sup> These results showed the large required overpotential for the  $\text{I}^-/\text{I}_3^-$  mediator.

The  $\text{I}^-/\text{I}_3^-$  mediator is typically used despite the 0.5 V overpotential because it has slow recombination kinetics preventing recombination of electrons in the  $\text{TiO}_2$  directly with the redox mediator. One alternative redox couple already discussed, the use of a cobalt mediator developed by Hupp and coworkers,<sup>24,25</sup> exhibited fast recombination of  $\text{TiO}_2(\text{e}^-)$

) which led to poor DSSC performance. Other alternative redox couples investigated

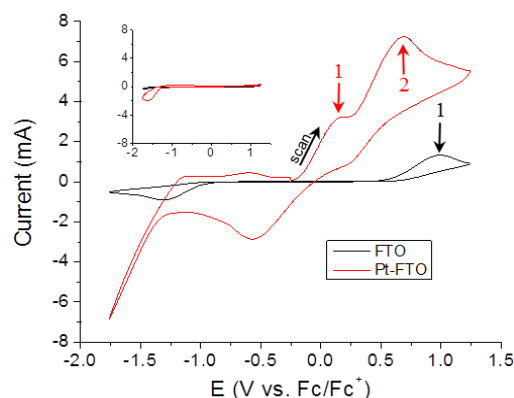


**Figure 35** Cyclic voltammograms of  $I^-/I_3^-$  oxidation in the presence (red) and absence (black) of platinum

include ferrocene/ferrocenium<sup>94</sup> and other cobalt complexes.<sup>95,96</sup>

Previously, Professor Agrios's group tested the catalytic effect of platinum, Pt, on the

oxidation of  $I^-$  to  $I_3^-$ .<sup>i</sup> Figure 35 shows the oxidation potential required to oxidize  $I^-$  to  $I_3^-$  at about +0.6 V vs. Fc/Fc<sup>+</sup> (ferrocene/ferrocenium) for plain conductive glass. When compared to a platinized electrode, the voltage required for the same oxidation occurred at +0.14 V. In fact, under the same required potential for plain conductive glass, a second process attributed to the oxidation of  $I_3^-$  to  $I_2$  is apparent. Our goal was then to incorporate platinum to catalyze the reduction of the oxidized sensitizer by  $I^-$  and hence lower the overpotential.

A sensitizer was targeted with dual functionality: the capability to perform in a DSSC, as well as the ability to coordinate to a Pt nanoparticle to study the catalytic reaction. When choosing a sensitizer, we turned to the most consistent types of ruthenium dyes which are known to perform well in DSSCs, i.e., N3-type dyes.<sup>16</sup> Further investigation was required for modification of the dye ligands for metal nanoparticle coordination.

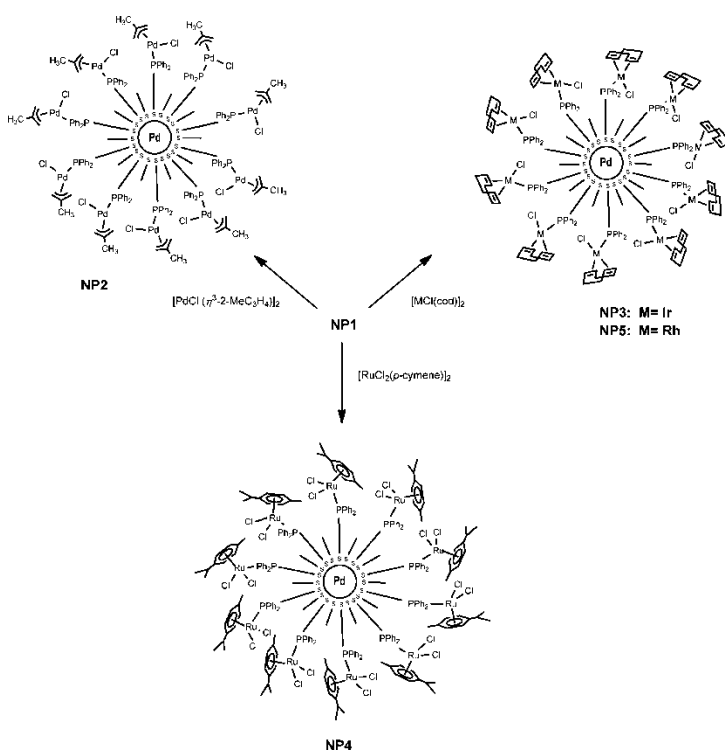
<sup>i</sup> The outline of this discussion was adapted from a grant proposal submitted to NSF in September 2012 by Galoppini and Agrios

Coordination of organometallic complexes to metal surfaces has numerous precedents. For instance, Yamada and coworkers looked at self-assembled monolayers (SAMs) of ruthenium tris(bipyridyl) dyes<sup>97</sup> and phthalocyanines anchored to gold electrodes. They synthesized these dyes with a modified terminal alkylthiol functional group for anchoring to gold electrodes. Their goal was to control the direction of a generated photocurrent through changing irradiance wavelength.<sup>98,99</sup> These results support the hypothesis that dye molecules can still be photoactive when anchored to metal surfaces.

Thiol-modified bipyridines have been employed in sensor devices anchored to gold nanoparticles. Thomas and coworkers used these modified bipyridines to coordinate to europium ions for phosphorescence detection.<sup>100</sup> With the thiol modifications, Thomas was able to achieve a high density of chelating ligands (the bipyridines) to act as “ion sponges.” Synthesis was achieved from a methyl-substituted bipyridine converted to an alkyl thiol bipyridine. Once the target ligand was achieved, coordination to the gold nanoparticles followed through the thiol groups. This study, as well as the previous, suggest that organometallic complexes can be both assembled prior to and following coordination with metal surfaces. It also suggests that modification of bipyridyl units in a dye molecule should be achievable.

Both of the previously mentioned examples show metal surface coordination through alkylthiol functional groups. Lipoic acid derivatives have also been shown to coordinate

to metal surfaces. Isied and coworkers studied SAMs on gold surfaces with two different anchor groups: lipoic acid groups and alkylthiol groups.<sup>101</sup> The group of Nicholas Fletcher examined the binding of rhenium complexes onto silver through lipoic acid modified bipyridines.<sup>102</sup> Their group showed that once the organometallic complex has been made, it is possible to coordinate to other metal surfaces and characterize the functionalized metal nanoparticles.



Llorca and coworkers studied palladium nanoparticles for use in organometallic functionalization.<sup>103</sup> They developed a stabilized palladium nanoparticle with alkylthiol groups on the coordinating ligand for palladium functionalization.

**Figure 36** A variety of organometallic complexes attached to palladium nanoparticles; adapted from reference 103

also modified with a phosphine ligand for organometallic complexation. Once the palladium nanoparticles were synthesized, Llorca's group functionalized the nanoparticles with a variety of metal complexes. Figure 36 shows a variety of organometallic complexes that have been coordinated to the palladium nanoparticles. One in particular, the ruthenium complex **NP4**, is a dichloro(*p*-cymene) ruthenium(II)

complex very similar to the intermediates isolated by Graetzel and coworkers,<sup>27,29</sup> suggesting it may be possible to further functionalize the nanoparticles after coordination.

The work of Zhao and coworkers suggests that it is possible to bridge two metals with an organic complex.<sup>104</sup> They develop a method for connecting platinum nanoparticles and

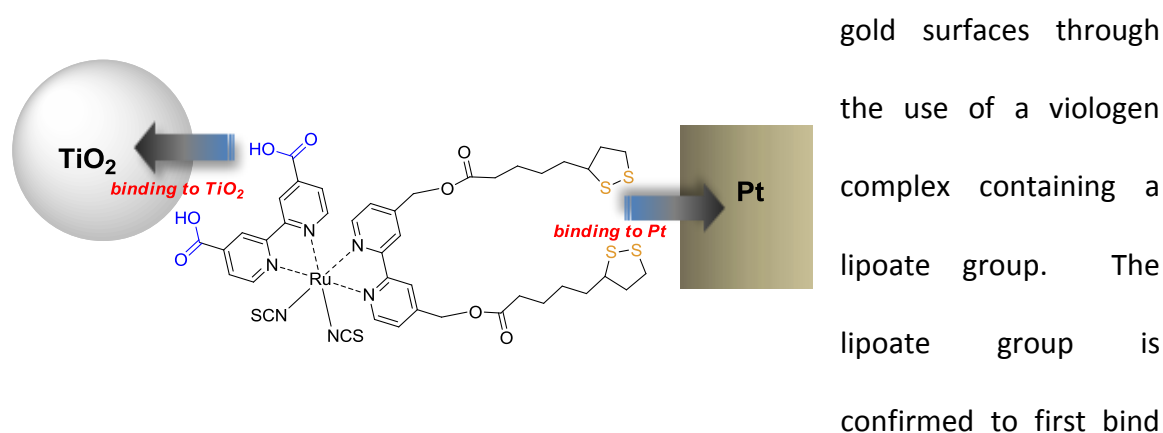


**Figure 37** Targeted dye schematic, showing **AK6**

to the metal, in this case, targeting the gold surface. This is followed by sequential addition of the platinum nanoparticles. This work suggests it should be possible to design a dye that can bridge platinum nanoparticles and the  $\text{TiO}_2$  semiconductor surface (Figure 37).

In summary, based on this background, we designed an N3-type ruthenium sensitizer for DSSCs that has functional modifications for binding to metal surfaces. Our target dye is ruthenium(II) bis(thiocyanate)bis(bipyridyl) (N3 type) where one bipyridyl unit has been modified with carboxylic acid groups for anchoring to  $\text{TiO}_2$  and the other has been modified with alkyl thiol or lipoic acid groups for binding to platinum.

## Synthesis

### Experimental

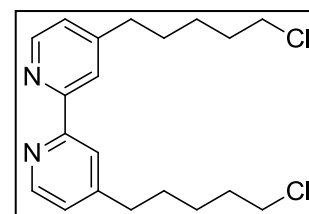
**Instrumentation.**  $^1\text{H}$  and  $^{13}\text{C}$  NMR spectra were recorded on a Varian INOVA NMR spectrometer operating at 499.896 MHz for  $^1\text{H}$  and 125.711 MHz for  $^{13}\text{C}$  using the solvent as an internal reference. The coupling constants ( $J$ ) for  $^1\text{H}$  NMR are recorded in Hz. High resolution mass spectra (ESI) were recorded on a Bruker Daltonics Apex-Qe series, Fourier Transform Mass Spectrometer. UV–Vis spectra were recorded on a Varian Cary 50 UV-Vis spectrophotometer using 1 cm quartz cuvettes. Solar cell current–voltage measurements were made using a Newport Oriel Sol2A Class ABA solar simulator and a Keithley 2400 source meter. Cyclic voltammetry (CV) was recorded on a CHInstruments 600D potentiostat. X-ray data was collected at low temperature (100 K) as follows: Data collection: *APEX 2* (Bruker, 2006); cell refinement: *APEX 2*; data reduction: *SAINT* (Bruker, 2005); program(s) used to solve structure: *SHELXTL* (Sheldrick, 2008b); program(s) used to refine structure: *SHELXTL*; molecular graphics: *SHELXTL*; software used to prepare material for publication: *SHELXTL*.

**Materials.** Solvents and concentrated acids were purchased from Pharmco. Triethyl amine and dichloromethane were distilled over calcium hydride under  $\text{N}_2$  atmosphere. THF was distilled with sodium and benzophenone while under  $\text{N}_2$  atmosphere or purified with an MBraun MB-SPS compact benchtop solvent purification system with

purification columns for THF. Hexanes were distilled in air prior to use in column chromatography. All commercially available chemicals were used as received unless otherwise noted. Di- $\mu$ -chlorobis[(*p*-cymene)chlororuthenium (II)] was purchased from Strem. Anhydrous sodium sulfate, sodium iodide, N,N-dimethylformamide, 2,2'-dipyridyl, ammonium thiocyanate, ammonium chloride, and sodium hydroxide were purchased from VWR. Lithium diisopropyl amide, sodium borohydride, dicyclohexylcarbodiimide (DCC), dimethyl aminopyridine (DMAP), thionyl chloride, and bis(trimethylsilyl)sulfide were purchased from Sigma-Aldrich. Thionyl chloride was distilled under N<sub>2</sub> atmosphere prior to use. 4,4'-Dimethyl-2,2'-bipyridine, lipoic acid, and potassium dichromate were purchased from Fisher-Acros. 1-Bromo-4-chlorobutane and thiourea were purchased from Alfa Aesar. Silica gel (230-400 mesh) and neutral alumina gel (50-200  $\mu$ m) was purchased from Sorbent Technologies. Deuterated NMR solvents were purchased from Cambridge Isotopes.

**4,4'-Dichloropentyl-2,2'-bipyridine<sup>105,106</sup> (23):**

4,4'-dimethyl-2,2'-bipyridine (990 mg, 5.37 mmol) was dissolved in freshly distilled THF (50 mL) under a nitrogen



atmosphere in a flame-dried flask. This colorless solution was cooled to -10 °C in an ice/acetone bath. After complete cooling, Lithium Diisopropyl Amide (6.80 mL of 2.0 M solution in Hexanes and THF, 13.60 mmol) was added dropwise via syringe over 5 minutes. The dark brown solution was stirred for 30 minutes while maintaining cooling. 1-Bromo-4-chlorobutane (12.5 mmol, 1.48 mL) was added via syringe and stirring and

cooling were maintained for an additional 5 hours. The reaction was allowed to reach room temperature overnight and was then quenched by the addition of brine (50 mL). The suspension was concentrated under vacuum and then extracted with dichloromethane (3 x 50 mL). The combined organic extracts were dried over anhydrous sodium sulfate and concentrated under vacuum. The crude was purified via Silica Gel column chromatography with hexane/ethyl acetate mixture (4:1) used as the eluent. A colorless oil was yielded: 1.374 g, 69.6%.  $^1\text{H}$  NMR ( $\text{CDCl}_3$ )  $\delta$  8.57 (d,  $J$  = 5.0 Hz, 2H), 8.24 (s, 2H), 7.15 – 7.11 (m, 2H), 3.53 (t,  $J$  = 6.7 Hz, 4H), 2.72 (t,  $J$  = 7.8 Hz, 4H), 1.82 (d,  $J$  = 6.7 Hz, 4H), 1.73 (p,  $J$  = 7.7 Hz, 4H), 1.52 (p,  $J$  = 7.6 Hz, 4H).  $^{13}\text{C}$  NMR ( $\text{CDCl}_3$ )  $\delta$

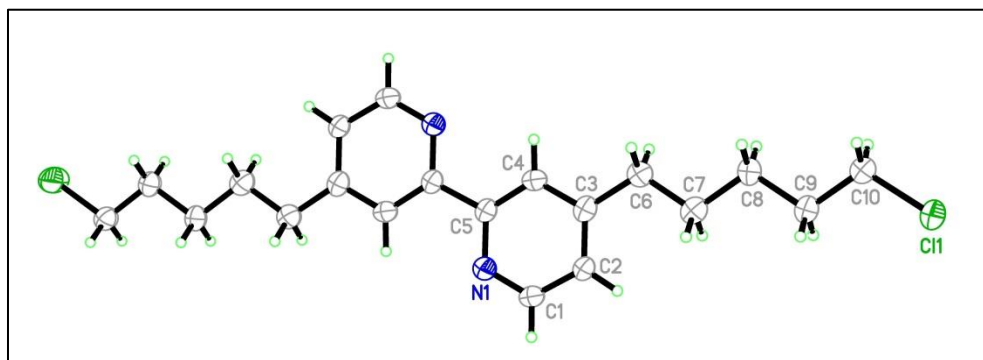


**Figure 38** ORTEP diagram of Compound **23** showing the numbering scheme. The other half of the molecule is generated by a center of symmetry. Displacement ellipsoids are drawn at the 30% probability level for non-H atoms.

156.33, 152.47, 149.23, 124.07, 121.39, 45.02, 35.49, 32.54, 29.86, 26.71. For crystal structure, see Figure 38.

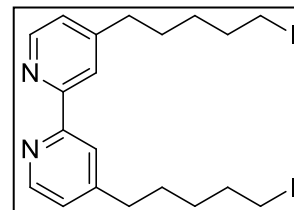
The mono-substituted byproduct was also recovered, 4-Chloropentyl-4'-methyl-2,2'-bipyridine.  $^1\text{H}$  NMR ( $\text{CDCl}_3$ )  $\delta$  8.55 (d,  $J$  = 4.9 Hz, 1H), 8.53 (d,  $J$  = 4.9 Hz, 1H), 8.22 (s, 2H), 7.12 (d,  $J$  = 4.7 Hz, 2H), 3.52 (t,  $J$  = 6.7 Hz, 2H), 2.70 (t,  $J$  = 7.8 Hz, 2H), 2.43 (s, 3H), 1.80 (p,  $J$  = 6.8 Hz, 2H), 1.72 (p,  $J$  = 7.8 Hz, 2H), 1.50 (p,  $J$  = 7.7 Hz, 2H).  $^{13}\text{C}$  NMR ( $\text{CDCl}_3$ )  $\delta$



156.35, 156.16, 152.43, 149.21, 149.09, 148.30, 124.83, 124.03, 122.18, 121.35, 45.01, 35.48, 32.53, 29.85, 26.71, 21.36.

**4,4'-Diiodopentyl-2,2'-bipyridine<sup>105,106</sup> (24):**

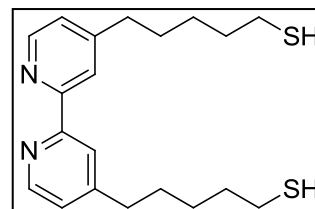
4,4'-Dichloropentyl-2,2'-bipyridine (1.08 g, 2.95 mmol) and sodium iodide (1.91 g, 11.8 mmol) were dissolved in acetone



(7.6 mL). The colorless solution was stirred for 16 hours at room temperature following which water (20 mL) was added. The aqueous layer was extracted with dichloromethane (3 x 25 mL). The combine organic extracts were dried over anhydrous sodium sulfate and the solvent removed under vacuum to yield a pale yellow solid which was used as-is without further purification or characterization: 1.180 g, 72.5%.

**4,4'-Dithiopentyl-2,2'-bipyridine<sup>105,107</sup> (25):**

4,4'-Diiodopentyl-2,2'-bipyridine (690 mg, 1.25 mmol) was dissolved in freshly distilled THF (6 mL) under nitrogen

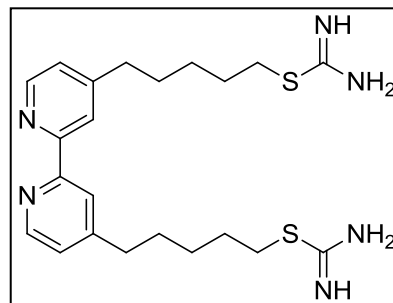


atmosphere and cooled to -10 °C in an ice/acetone bath. Bis(trimethylsilyl)sulfide (0.640 mL, 3.01 mmol) and TBAF (2.80 mL, 1.0 M in THF) were added via syringe. The bis(trimethylsilyl)sulfide was kept in a well-ventilated location for storage and measurement. The reaction was allowed to reach room temperature after addition of reagents, and then progress was monitored by TLC. After 12 hours, no further progress was noted via TLC, so reaction was quenched by addition of dichloromethane (50 mL). The organic layer was washed with brine (50 mL) and then dried under vacuum. The

resulting pale yellow crude was purified with silica gel column chromatography using hexane/ethyl acetate (3:1) mixture as the eluent. A colorless oil was yielded: 214 mg, 47.1%.  $^1\text{H}$  NMR ( $\text{CDCl}_3$ )  $\delta$  8.55 (d,  $J$  = 4.9 Hz, 2H), 8.23 (s, 2H), 7.12 (d,  $J$  = 3.6 Hz, 2H), 2.70 (t,  $J$  = 7.7 Hz, 4H), 2.52 (q,  $J$  = 7.4 Hz, 4H), 1.76 – 1.57 (m, 8H), 1.46 (p,  $J$  = 7.5 Hz, 4H), 1.33 (t,  $J$  = 7.8 Hz, 2H).  $^{13}\text{C}$  NMR ( $\text{CDCl}_3$ )  $\delta$  156.34, 152.64, 149.22, 124.09, 121.45, 35.55, 33.96, 30.04, 28.17, 24.66. Note: This colorless oil is very unstable in air – it rapidly degrades and/or polymerizes.

**4,4'-Dithiourealpentyl-2,2'-bipyridine<sup>106</sup> (26):**

4,4'-Diiodopentyl-2,2'-bipyridine (1.60 g, 2.91 mmol) and thiourea (465 mg, 6.11 mmol) were dissolved in ethanol (15 mL) under a nitrogen atmosphere. This colorless

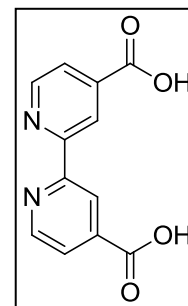


solution was refluxed overnight. The solvent was removed under vacuum to yield a sticky, white crude. This crude was dissolved in water (1 mL) with three drops of concentrated HCl added. Ethanol was added dropwise until the solution became cloudy and then 1 additional drop of concentrated HCl was added. This solution was cooled overnight in a refrigerator at 4 °C. The solution forms two layers, a pale yellow aqueous layer and a viscous orange oil at the bottom. The aqueous layer was collected and neutralized with 10% sodium hydroxide solution till basic to litmus yielding a fine white precipitate. The precipitate was collected by vacuum filtration and washed with 10% aqueous sodium hydroxide, water, and then hexanes to yield a fine white solid: 330 mg, 25.5%.  $^1\text{H}$  NMR ( $\text{DMSO}-d_6$ )  $\delta$  8.54 (d,  $J$  = 4.9 Hz, 2H), 8.22 (s, 2H), 7.28 (d,  $J$  = 4.8 Hz, 2H),

6.41 (s, 6H), 2.81 (t,  $J = 7.2$  Hz, 4H), 2.68 (t,  $J = 7.6$  Hz, 4H), 1.70 – 1.51 (m, 8H), 1.39 (p,  $J = 7.5, 7.1$  Hz, 4H).  $^{13}\text{C}$  NMR (DMSO- $d_6$ )  $\delta$  160.55, 155.24, 152.10, 148.97, 124.07, 120.41, 34.39, 29.51, 29.30, 28.90, 27.71.

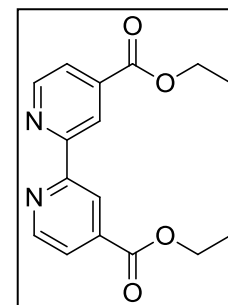
**[2,2'-bipyridine]-4,4'-Dicarboxylic acid<sup>108-110</sup> (11):**

A solution of 4,4'-dimethyl-2,2'-bipyridine (2.00 g, 10.9 mmol) in concentrated sulfuric acid (50 mL) was heated to 70 °C. Potassium dichromate (9.63 g, 32.6 mmol) was added very slowly. Heating and stirring were maintained for 1 h, and then the hot solution was poured onto ice (300 g) and stirred for 1 h. A fine yellow solid formed. This solid was collected via vacuum filtration and washed with water. The crude product was suspended in 50% aqueous nitric acid (50 mL) and heated to 120 °C for 4 h. The suspension was allowed to cool to room temperature and then poured onto ice (300 g). The suspension was allowed to sit overnight, and the resulting white solid was collected by vacuum filtration and washed with water. The solid was then thoroughly dried in a flask under vacuum to yield a white solid: 2.195 g, 81.2% yield.  $^1\text{H}$  NMR (DMSO- $d_6$ )  $\delta$  8.92 (d,  $J = 4.9$  Hz, 2 H), 8.85 (s, 2 H), 7.91 (dd,  $J = 4.9, 1.3$  Hz, 2 H). Spectral data were consistent with those previously reported.



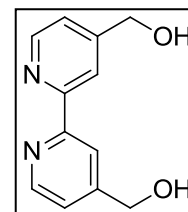
**[2,2'-bipyridine]-4,4'-Diethyl carboxylate<sup>109,110</sup> (19):**

Compound **11** (1.00 g, 4.11 mmol) was suspended in ethanol (80 mL). Concentrated sulfuric acid (1 mL) was added and the suspension was



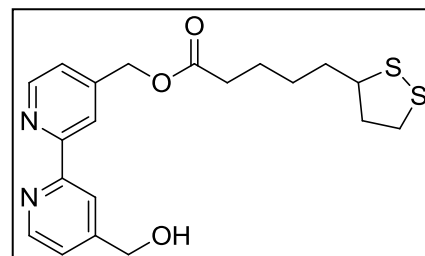
refluxed for 5 days, then cooled to room temperature. Water (80 mL) was added and ethanol was removed under vacuum. The aqueous layer was neutralized with 10% aqueous sodium hydroxide solution to yield a white precipitate that was collected by vacuum filtration. The crude product was washed with water and dried to yield a white solid: 1.12 g, 91.2% yield.  $^1\text{H}$  NMR ( $\text{CDCl}_3$ )  $\delta$  8.96 (s, 2H), 8.87 (d,  $J$  = 4.9 Hz, 2H), 7.92 (dd,  $J$  = 4.9, 1.6 Hz, 2H), 4.47 (q,  $J$  = 7.1 Hz, 4H), 1.45 (t,  $J$  = 7.1 Hz, 6H).  $^{13}\text{C}$  NMR ( $\text{CDCl}_3$ )  $\delta$  165.36, 156.75, 150.28, 139.21, 123.44, 120.77, 62.11, 14.49.

**4,4'-Dihydroxymethyl-2,2'-bipyridine<sup>109,110</sup> (20):**



Compound **19** (1.02 g, 3.40 mmol) was suspended in 200 proof ethanol (67 mL). Sodium borohydride (2.80 g, 74.0 mmol) was added and the suspension was refluxed at 90 °C for 3 h. After cooling, saturated aqueous ammonium chloride (75 mL) was added and ethanol was removed under vacuum. Water was added until all white solid was dissolved. The aqueous layer was extracted with ethyl acetate (4 x 50 mL) and the combined organic layers were dried over anhydrous sodium sulfate. The solvent was removed under vacuum to yield a white solid: 638 mg, 87.7% yield.  $^1\text{H}$  NMR ( $\text{CD}_3\text{OD}$ )  $\delta$  8.59 (d,  $J$  = 5.0 Hz, 2H), 8.27 (s, 2H), 7.44 (d,  $J$  = 4.9 Hz, 2H), 4.75 (s, 4H).  $^{13}\text{C}$  NMR ( $\text{CD}_3\text{OD}$ )  $\delta$  158.06, 155.16, 151.01, 123.54, 121.05, 64.46.

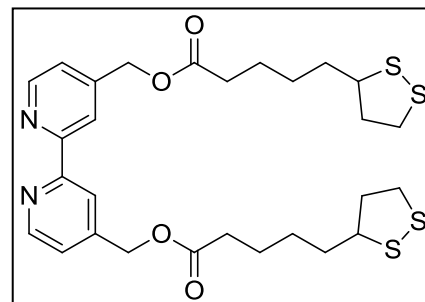
**4-Methyl lipolate-4'-Hydroxymethyl-2,2'-bipyridine<sup>102</sup> (21):**



4,4'-Dihydroxymethyl-2,2'-bipyridine (285 mg, 1.32 mmol), lipoic Acid (680 mg, 3.30 mmol), and dicyclohexylcarbodiimide (DCC; 817 mg, 3.96 mmol) were dissolved in DMF (15 mL) under nitrogen atmosphere. This pale yellow solution was cooled to 0 °C in an ice bath and stirred for 45 minutes. A solution of N,N-dimethyl aminopyridine (DMAP; 97 mg, 0.79 mmol) in DMF (15 mL) was created under nitrogen atmosphere and added via cannula to the solution with the bipyridine. Stirring and cooling were maintained for an additional 1 hour, whereupon the reaction was allowed to reach room temperature and stirring maintained for 36 hours. Water (25 mL) was added to the resulting cloudy yellow solution whereupon a yellow precipitate was formed. The THF was removed under vacuum and dichloromethane (50 mL) was added. The organic solution was washed with water (2 x 50 mL) and dried under vacuum. The resulting yellow crude was purified by neutral alumina gel column chromatography using hexane/ethyl acetate (2:1) mixture as the eluent to yield a yellow wax: 253 mg, 47.4%. ESI<sup>+</sup>: calculated: 427.1121 [M+Na]<sup>+</sup>; found: 427.1168 [M+Na]<sup>+</sup>. Compound was only characterized by ESI as it was not the desired compound. Further characterization was not carried out.

**4,4'-Di[Methyl lipoate]-2,2'-bipyridine<sup>111</sup> (L3):**

Freshly distilled thionyl chloride (1.02 mL, 14.0 mmol) was diluted with freshly distilled dichloromethane (15 mL) under N<sub>2</sub> atmosphere and the solution, cooled to



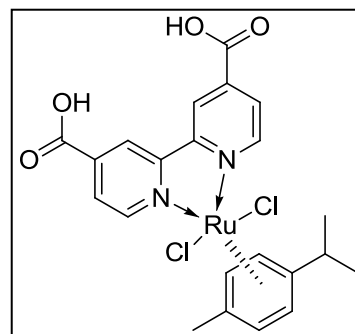
0 °C, was added dropwise via syringe over 2 minutes to a cold (0 °C) solution of lipoic acid (1.94 g, 9.36 mmol) in freshly distilled dichloromethane (25 mL) under N<sub>2</sub>

atmosphere. The solution was stirred at 0 °C for 1 hour, then the ice bath was removed and the solution was allowed to reach room temperature over 1 hour. The solvents were removed under vacuum to leave lipoyl chloride as a brown residue. This was dissolved in dry toluene (25 mL) and added dropwise over 30 min to a flask charged with a cold (0 °C) solution of Compound **20** (200 mg, 0.936 mmol) and freshly distilled triethylamine (4.50 mL) in dry toluene (20 mL). The reaction was stirred overnight. Water (75 mL) was added, resulting in the formation of a brown precipitate. The mixture was filtered, the solid was discarded, and the organic layer was washed with water (2 x 50 mL) and dried over anhydrous sodium sulfate. The solvent was removed under vacuum, to obtain a yellow crude product. This was purified by column chromatography using neutral alumina and hexane/ethyl acetate (2:1) as the eluent. After the less polar fraction (mostly lipoic acid) was separated, the eluent was changed to hexane/ethyl acetate (1:4) to collect the fractions with the product. The solvent was removed under vacuum and the product was obtained as a yellow solid: 67 mg, 12.1% yield. <sup>1</sup>H NMR (CDCl<sub>3</sub>) δ 8.67 (d, J = 5.0 Hz, 2H), 8.38 (s, 2 H), 7.29 (dd, J = 5.0 Hz, 2 H), 5.21 (s, 4 H), 3.56 (m, 2 H), 3.23 – 3.12 (m, 2H), 3.12 – 3.04 (m, 2 H), 2.49 – 2.37 (m, 6 H), 1.89 (dq, J = 13.6, 6.9 Hz, 2 H), 1.79 – 1.62 (m, 8 H), 1.58 – 1.40 (m, 4H). <sup>13</sup>C NMR (CDCl<sub>3</sub>) δ 173.10, 156.26, 149.59, 146.23, 122.26, 119.60, 64.51, 56.38, 40.30, 38.60, 34.69, 34.04, 28.84, 24.76. ESI<sup>+</sup>: calculated: 593.1631 [M]<sup>+</sup>, 615.1540 [M+Na]<sup>+</sup>, 631.1189 [M+K]<sup>+</sup>; found: 593.1654 [M]<sup>+</sup>, 615.1483 [M+Na]<sup>+</sup>, 631.1437 [M+K]<sup>+</sup>.

**Ru[4,4'-Dicarboxylic acid-2,2'-Bipyridine][*p*-**

**Cymene]Cl<sub>2</sub><sup>27,29</sup> (**22**):**

Compound **11** (150 mg, 0.614 mmol) and Di- $\mu$ -chlorobis[(*p*-cymene)chlororuthenium(II)] (188 mg, 0.307 mmol) were suspended in ethanol (75 mL) under a nitrogen



atmosphere. The solution was heated to 90 °C for four hours. The red-colored solution was then cooled to room temperature and the solvent was removed under vacuum.

The crude product was crystallized from methanol to yield an orange solid: 300 mg,

88.8%. <sup>1</sup>H NMR (CD<sub>3</sub>OD)  $\delta$  9.66 (d, *J* = 5.8 Hz, 2H), 8.99

(s, 2H), 8.23 (d, *J* = 5.8 Hz, 2H), 6.20 (d, *J* = 6.0 Hz, 2H),

5.95 (d, *J* = 6.0 Hz, 2H), 2.68 (hept, *J* = 6.8 Hz, 1H), 2.27

(s, 3H), 1.07 (d, *J* = 6.8 Hz, 6H). <sup>13</sup>C NMR (CD<sub>3</sub>OD)  $\delta$

178.09, 165.85, 157.95, 156.83, 143.72, 128.24,

124.78, 107.47, 106.34, 88.73, 86.47, 22.49, 19.10,

18.51. ESI<sup>+</sup>: calculated: 515.0309 [M-Cl]<sup>+</sup>; found:

515.0378 [M-Cl]<sup>+</sup> X-ray quality crystals were obtained

from methanol. See Figure 39 for crystal structure and

Appendix for crystallographic data.

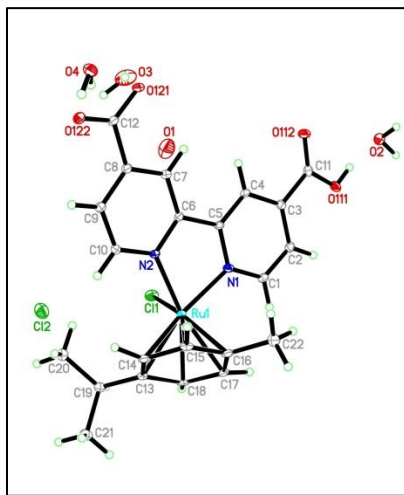


**Figure 39** ORTEP diagram of Compound **22** showing the numbering scheme. The image has been simplified to show only one molecule of the asymmetric unit. Displacement ellipsoids are drawn at the 30% probability level for non-H atoms.

**$\text{Ru}(\text{NCS})_2[4,4'\text{-Dicarboxylic acid-}$**

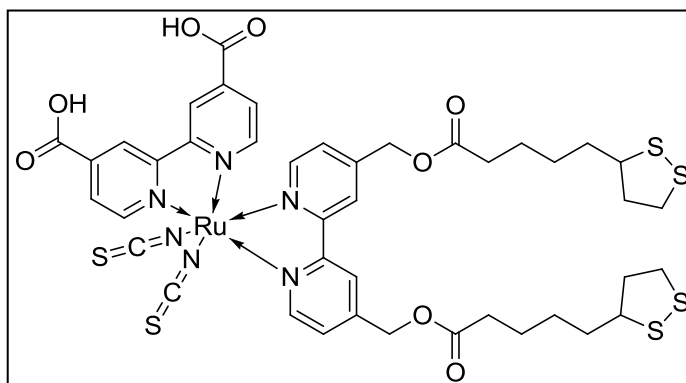
**$2,2'\text{-Bipyridine}][4,4'\text{-}$**

**$\text{Dimethylthiophosphate-2,2'-}$**

**$\text{Bipyridine}]^{67}$  (AK6):**

Compound **22** (122 mg, 0.222

mmol) and **L3** (132 mg, 0.222



mmol) were dissolved in nitrogen degassed DMF (20 mL) under nitrogen atmosphere.

The dark orange solution was heated to 150 °C for 3 h, upon which a solution of ammonium thiocyanate (145 mg, 1.91 mmol) in DMF (15 mL) was added. Heating and stirring was maintained for an additional 3 h. The reaction was allowed to cool overnight and then the solvent was removed under vacuum. Water (50 mL) was added to the dark purple crude and the suspension was sonicated for 10 minutes. The purple suspension was stored at 4 °C for several hours and the product, a purple solid, was collected by vacuum filtration. The filtrate was washed with water and dichloromethane to yield a dark purple solid: 133 mg, 56.8%.  $^1\text{H}$  NMR (DMSO- $d_6$ )  $\delta$  9.45 (d,  $J$  = 5.8 Hz, 1H), 9.21 (d,  $J$  = 5.7 Hz, 1H), 9.11 (s, 1H), 8.96 (s, 1H), 8.74 (s, 1H), 8.59 (s, 1H), 8.31 (d,  $J$  = 5.8 Hz, 1H), 7.96 (d,  $J$  = 5.9 Hz, 1H), 7.86 (d,  $J$  = 5.7 Hz, 1H), 7.63 (d,  $J$  = 5.9 Hz, 1H), 7.49 (d,  $J$  = 5.9 Hz, 1H), 7.20 (d,  $J$  = 5.9 Hz, 1H), 5.47 (s, 2H), 5.20 (s, 2H), 3.58 – 3.48 (m, 2H), 3.22 – 3.01 (m, 4H), 2.61 – 2.53 (m, 2H), 2.47 – 2.26 (m, 4H), 1.95 – 1.76 (m, 2H), 1.76 – 1.41 (m, 8H), 1.42 – 1.24 (m, 4H). The solution was too diluted to obtain a satisfactory  $^{13}\text{C}$  NMR (see Appendix, Figure A 76). ESI $^+$ : calculated: 1077.0488  $[\text{M}+\text{Na}]^+$ ; found: 1077.0515  $[\text{M}+\text{Na}]^+$ .

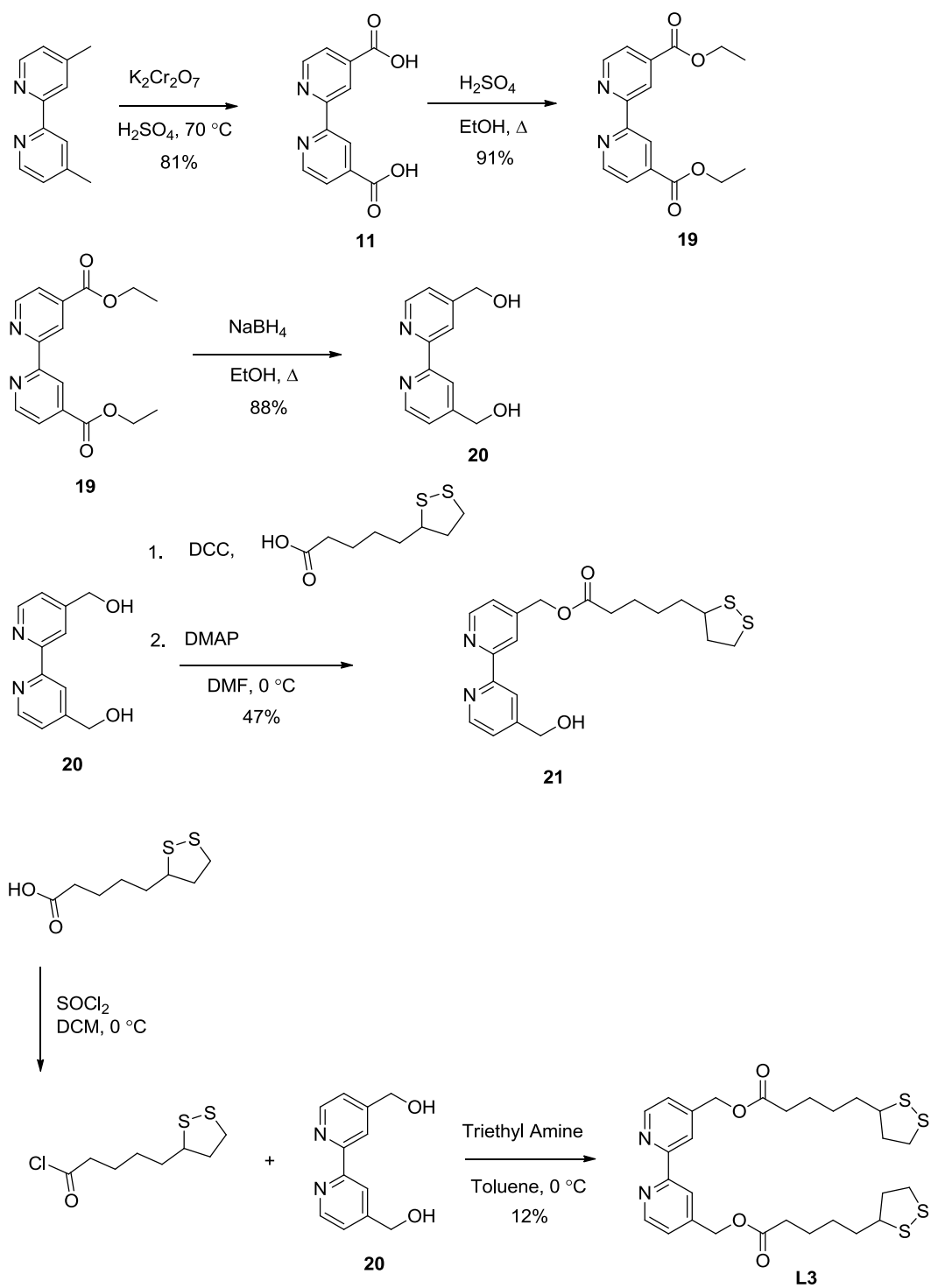




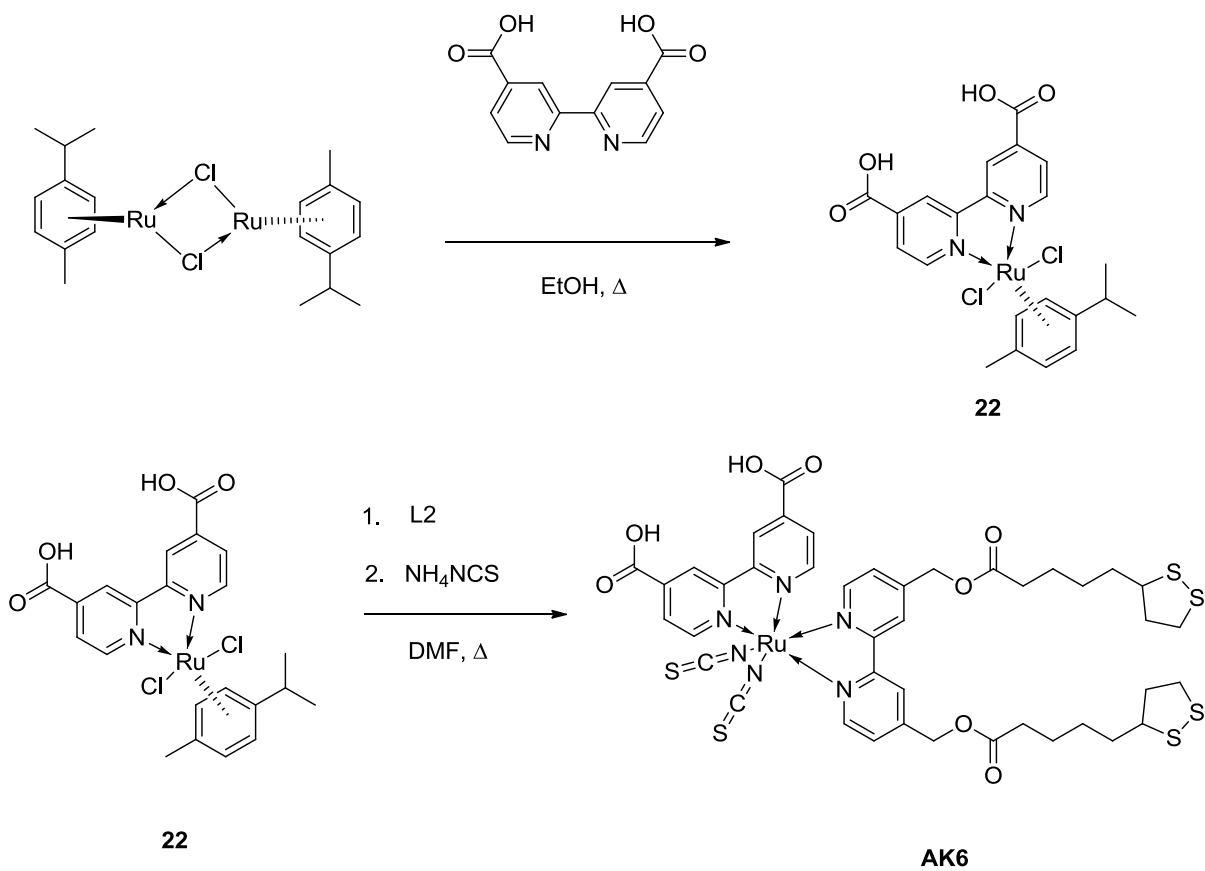
Our target was an N3-type ruthenium complex containing one bipyridine substituted with carboxylic acid groups to bind with  $\text{TiO}_2$  and one substituted with alkyl chains capped with thiol groups for binding with Pt. The synthesis of the carboxylic acid bipyridine was achieved through oxidation of 4,4'-dimethyl-2,2'-bipyridine with potassium dichromate in concentrated sulfuric acid.<sup>108-110</sup> The synthesis of the alkylthiol bipyridine (Scheme 7) began with the di-lithiation of 4,4'-dimethyl-2,2'-bipyridine with LDA, followed by a nucleophilic substitution with 1-bromo-4-chlorobutane.<sup>105,106</sup> When a slight excess of LDA was used, a mix of di- and tri-substituted products were obtained. The mixture did not separate with silica or alumina gel column chromatography. When a limiting quantity of LDA was used (1.8 equivalents), mono- and di-substituted products were observed. Through the use of a long column and slow, careful elution, these products were separated, with the mono-substituted product eluting first. Both compounds are colorless oils at room temperature. A pure sample of 4,4'-dichloropentyl-2,2'-bipyridine stored under air at room temperature for several weeks, formed crystals from the oil (R >12%; refer to the crystal structure in Experimental Section 2, Figure 38). In the following step, iodine was substituted for the chlorine groups to enhance reactivity.<sup>105,106</sup> This substitution reaction was carried out with sodium iodide in acetone and was driven by the low solubility of sodium chloride in acetone.

Following isolation of 4,4'-diiodopentyl-2,2'-bipyridine, two different methods were used to prepare the target alkylthiol bipyridine. The first method involved the

substitution of the iodine with thiourea.<sup>106</sup> This method led to the formation of a thioureal bipyridine intermediate which was characterized. However, we were unable to cleave the urea groups and when complexation was attempted with the thioureal bipyridine, coordination to the ruthenium center appears to occur between the bipyridyl nitrogens as well as the urea groups. Others have reported urea functional groups coordinating to ruthenium.<sup>112,113</sup> A second method, involving the direct substitution of the iodine groups in 4,4'-diiodopentyl-2,2'-bipyridine with thiols through the use of bis(trimethylsilyl)sulfide using TBAF,<sup>105,107</sup> led to successful synthesis of the target bipyridine. This compound, unfortunately, was extremely unstable in air. After several hours exposed to air, this compound became insoluble and appears to have polymerized. Schubert and coworkers noted that their polypyridyl dyes were synthesized as a mixture of free thiols and dimers,<sup>114</sup> where the major the product is the dimer. This further supports the existence of multiple products, in our case unwanted byproducts. While characterization was achieved, this compound appeared to be a poor target for an easy-to-handle N3-type complex.



**Scheme 8** Adapted synthesis to achieve thiol bipyridines



**Scheme 9** Two-step complexation of lipocate bipyridine complex

Given the difficulty in obtaining a stable ruthenium complex with free thiol groups, we decided to synthesize a bipyridine with thiolane groups (Scheme 8). Lipoic acid and 4,4'-dihydroxymethyl-2,2'-bipyridine were targeted to form an ester bond for the formation of the target bipyridine, **L3**. 2,2'-Bipyridine-4,4'-dicarboxylic acid, **11**, was converted to diethylcarboxylate bipyridine through Fisher esterification,<sup>109</sup> followed by reduction to dihydroxymethyl bipyridine with sodium borohydride.<sup>109</sup> Initially, we attempted to prepare the ester using DCC and DMAP.<sup>102</sup> Only a monosubstituted product was obtained via this method, and the purification was difficult due to the presence of large quantities of insoluble byproducts. Lipoyl chloride in the presence of base was then

used in the esterification step.<sup>111</sup> A large (14-fold) excess of lipoyl chloride was necessary to obtain the diester ligand, **L3**. This product, while considerably more stable than the alkylthiol bipyridine, decomposed after several months when stored under air at room temperature. While we do not know whether the degradation involves the ester or the thiolane group, it is known that benzyl esters are labile to hydrolysis, even used as protecting groups for alcohols,<sup>115</sup> and future work should focus on synthesis of a

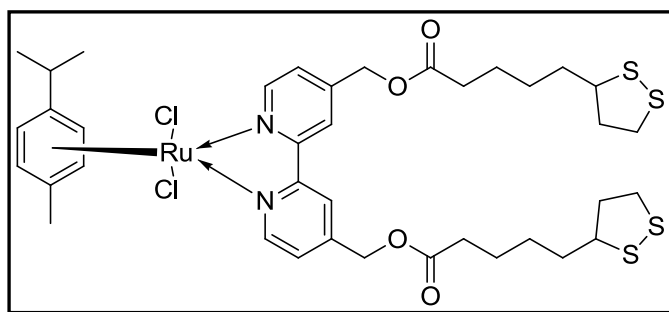


**Figure 40** Lipoate Bipyridine. This intermediate was not synthesized due to concerns that thiolane functional groups may coordinate to ruthenium.

ligand without the benzyl ester functionality.

The formation of the N3-type

complex, **AK6**, was achieved through the stepwise method,

involving the isolation of a  $\text{RuCl}_2[\mathbf{11}][p\text{-cymene}]$  intermediate (Scheme 9).<sup>27</sup> The dilipoate bipyridine intermediate (Figure 40) was not synthesized due to concerns that the thiolane groups may coordinate with the ruthenium center. The second step of the complexation was achieved through stepwise addition of the dilipoate bipyridine followed by quenching with excess ammonium thiocyanate in DMF with heat. Typical purifications of N3-type complexes involve isolation of a tetra-n-butylammonium carboxylate prior to purification on Sephadex, in our case typically Sephadex LH-20. However, benzyl esters are very susceptible to base-induced hydrolysis, even in the presence of mild bases such as potassium bicarbonate. Thus most traditional purification techniques were avoided with the synthesis of complex **AK5**. The complex

also appeared much more stable to oxidation by air when compared to dilipoate bipyridine, as insoluble byproducts were not observed.

## Results and Discussion

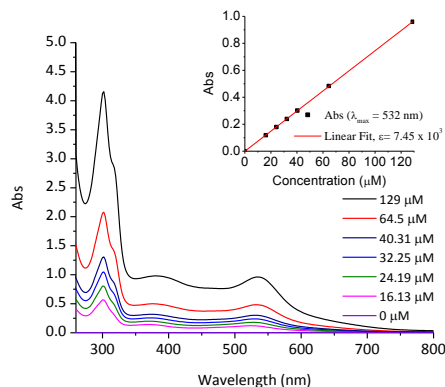


**Figure 41** Absorption spectra for **AK6** at different concentrations. **Inset:** extinction coefficient calculation

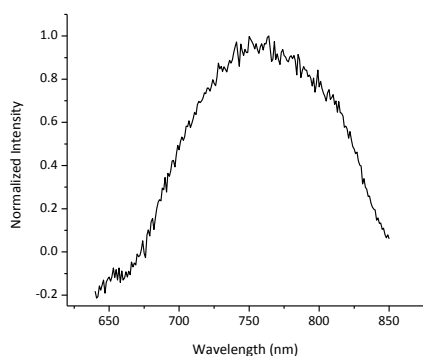


**Figure 42** Emission spectrum of **AK6**,  $\lambda_{\text{exc}} = 620$  nm

*The results in this section would not be possible without the effort of our collaborators at the University of Connecticut, especially Dr. Alexander Agrios and Guanliang Liu.*

The photophysical characterization of **AK6** in solution and bound to surfaces (metal and metal oxide) was carried out. Figure 41 shows the absorption spectra of **AK6** in DMSO solution and was utilized to calculate the extinction coefficient,  $\varepsilon = 7.45 \times 10^3 \text{ M}^{-1}\text{cm}^{-1}$  (inset). The absorption spectra show the characteristic MLCT band at 550 nm and the intense  $\pi$ -to- $\pi^*$  transition at 300 nm for N3-

type complexes. Emission and excitation spectra were also recorded for **AK6**. Characteristic weak emission occurs through excitation in the MLCT band ( $\lambda_{\text{exc}} = 620$ ) and is shown in Figure 42. The excitation spectrum for emission at 764 nm clearly shows the MLCT band from 450 nm to 550 nm (Figure 43).

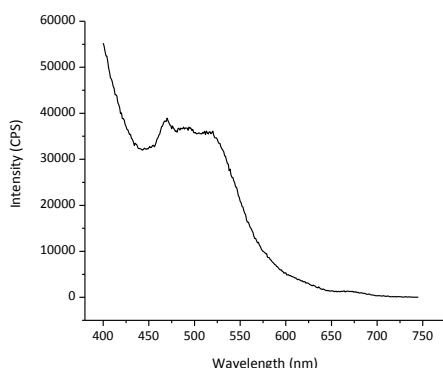


**Table 4** Summary of Photophysical Properties

Compound	$\lambda_{\text{max}}$ MLCT (nm)	$\lambda_{\text{max}}$ Emission (nm)	Ru <sup>III/II</sup> oxidation vs. SCE (V)
<b>AK6</b>	533	764	1.09
N3	534	755	0.85
Z907	526	769	0.75

The relevant photophysical properties of **AK6**

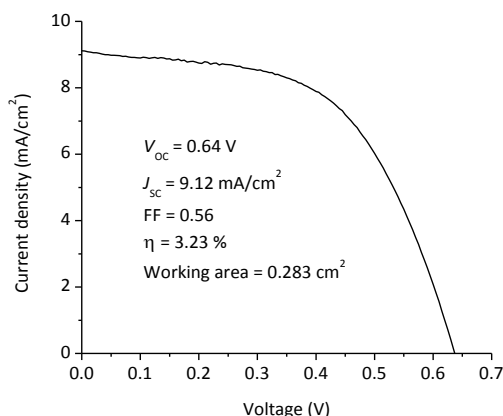
are summarized in Table 4. N3<sup>4</sup> and Z907<sup>27</sup> are shown for comparison. For cyclic voltammograms from which the oxidation potentials were abstracted, see Appendix (Figure A 78).

**Figure 43** Excitation spectrum for **AK6**,  $\lambda_{\text{emiss}} = 764$  nm

**AK6** was synthesized to be a bi-coordinate dye,

with functional groups to attach to both a semiconductor surface, TiO<sub>2</sub>, as well as to a metal surface, Pt, and to function in solar cell conditions. As proof of binding to both

substrates, several experiments were undertaken.

**Figure 44** IV curve for DSSC with **AK6** under AM 1.5 radiation at 100 mW cm<sup>-2</sup> (1 sun)

First, to provide evidence of semiconductor binding and positive solar cell activity, **AK6** was adsorbed

onto a TiO<sub>2</sub> film ca. 10 μm thick and assembled into a standard DSSC device. **AK6** performed well, with a short circuit current density better than 9 mA/cm<sup>2</sup>. The IV curve and a summary of the DSSC data

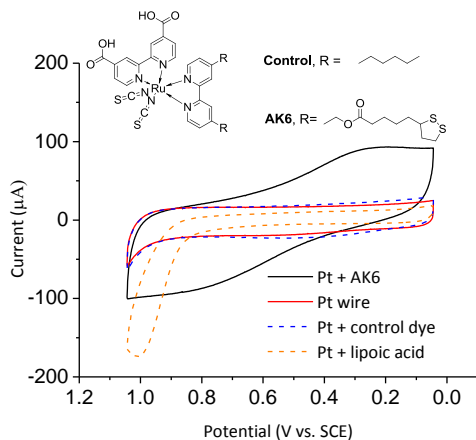


**Figure 45** CV of **AK6** on Pt wire plus control experiments; Pt + **AK6** shows oxidation wave at +0.80 V vs. SCE suggesting binding of **AK6** to platinum wire

are shown in Figure 44, and clearly suggest that **AK6** is capable of injecting electrons into  $\text{TiO}_2$ . This indicates that the LUMO level of **AK6** resides above the quasi-Fermi level of the semiconductor.

THF and then cyclic voltammetry measurements were performed using that wire as the working electrode (see Figure 45). On the wire dyed with **AK6**, an oxidation wave occurs at +0.80 V vs. SCE, with a reduction wave at +0.30 V vs. SCE. Both waves are attributed to **AK6** as they do not appear in either control experiment – that of a platinum wire dipped in a control dye without thiols for platinum coordination or the naked platinum

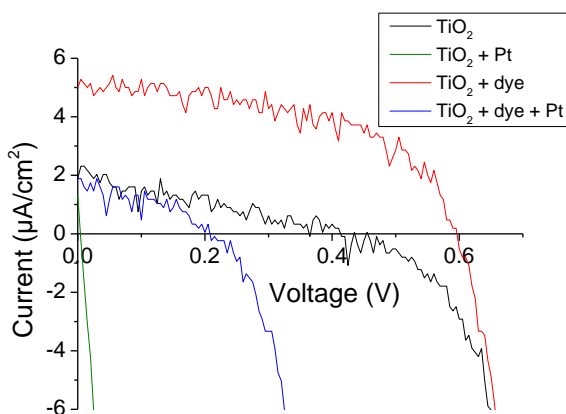


**Figure 46** IV curves for DSSC devices under simulated AM 1.5G sunlight at  $1000 \text{ W/m}^2$  (1 sun) intensity

wire. These results suggest that **AK6** could act as a solar cell dye to tether platinum nanoparticles to  $\text{TiO}_2$  surfaces.

Our collaborators constructed DSSCs with **AK6** as a sensitizer to study the effect

the performance of the cell. DSSCs constructed in the absence of a sensitizer exhibit a dark current (Figure 46, black) that is quenched in the presence of Pt nanoparticles

(Figure 46, green). The Pt nanoparticles appear to adsorb to the surface of the  $\text{TiO}_2$  thin films and induce significant recombination. When the DSSC is constructed with **AK6** as the sensitizer, there is a noticeable improvement in performance (Figure 44 and Figure 46, red). The addition of Pt nanoparticles to the DSSC (Figure 46, blue) exhibits far less recombination and thus a higher solar cell performance when compared to the cells with the nanoparticles in the absence of the sensitizer (Figure 46, green). This suggests that the Pt nanoparticles are attached to the dyes' sulfur atoms and thus held at an increased distance from the semiconductor. However, it cannot be ruled out that the observed recombination is due simply to a smaller amount of Pt nanoparticles that adhere to the surface of the semiconductor.<sup>ii</sup>

---

<sup>ii</sup> Adapted from a grant proposal submitted to NSF in September 2012 by Galoppini and Agrios

## Conclusion

In conclusion, we have synthesized a bifunctional N3-type dye for use in DSSCs to coordinate to metal surfaces with the goal of lowering the redox overpotential through incorporation of catalytic platinum. The dye was synthesized through the modification of two bipyridyl ligands. The first ligand was modified with two carboxylic acid groups for binding to  $\text{TiO}_2$ . The second ligand was modified with lipoic acid groups for coordination to metal surfaces. This dye was characterized synthetically and photophysically.

A DSSC prepared from **AK6** exhibited efficiency of about 3%. Binding to platinum was probed through a series of cyclic voltammetry experiments on a platinum wire. When incorporated into solar cells in the presence of platinum nanoparticles, a small increase in current was observed, which was tentatively attributed to a reduced quenching from the platinum nanoparticles, as a result of the increased distance of the platinum nanoparticles from the  $\text{TiO}_2$  surface due to the presence of the saturated linker. These preliminary results are promising, and additional experiments are being carried out by our collaborators at the University of Connecticut.

## Conclusion

Two series of N3-type dyes have been synthesized to study the effect that structural modifications of the dye have on  $V_{oc}$ . The first series of three dyes (**AK0-2**) investigated the issue of  $TiO_2(e^-)$  recombination with the oxidized dye through an increasing chromophore-semiconductor distance. The dyes showed two notable results as a function of increasing chromophore-semiconductor distance: decreased recombination rates and less sensitivity to  $TiO_2(e^-)$  concentrations. Both of effects led to increased  $V_{oc}$  as the chromophore was further separated from the semiconductor surface. However, while the observed properties should have led to better DSSC performance, the two rigid rod dyes did not perform well under actual solar cell conditions (IPCEs of xx-xx). The poor performance is speculated to arise due to the formation of an  $I_2$ -adduct with N3-type dyes. Currently this association behavior and effect on DSSC performance is being investigated.

A second series of dyes was synthesized in the attempt to overcome some of the shortcomings of the first generation. Dyes **AK3** and **AK4** were structurally similar to **AK1** and **AK2**, but carried two, long saturated alkyl chains (nonyl) on the ancillary bipyridine ligand. These modifications were made in the attempt to increase solubility and make the solution characterization easier. A modification to the synthetic procedure, involving a two-step process to isolate and characterize a ruthenium *p*-cymene

intermediate, also aided in the characterization of the N3-type dyes. Currently, these dyes are being studied for their  $I_2$  interaction by another member of our group, Dr. Hao Tang.

A third type of N3-type dye was synthesized to study alternative methods of controlling  $V_{oc}$ . The goal of this project was to synthesize a dye that could lower the large required overpotential for the  $I^-/I_3^-$  redox couple through incorporation of platinum, a known catalyst for the  $I^-/I_3^-$  redox reaction. An N3-type dye was targeted with modification to one of the bipyridyl ligands with thiol functionality for coordination to metals, in particular platinum nanoparticles. The dye, **AK6**, has performed well in DSSC conditions with efficiency >3% and has been shown to bind to platinum wire through the thiol groups and to the  $TiO_2$  through the carboxylic groups. Additional work coordinating platinum nanoparticles within the DSSC (incorporating the platinum nanoparticles to the dye within the active DSSC) is currently being conducted by collaborators in the group of Alexander Agrios at the University of Connecticut.

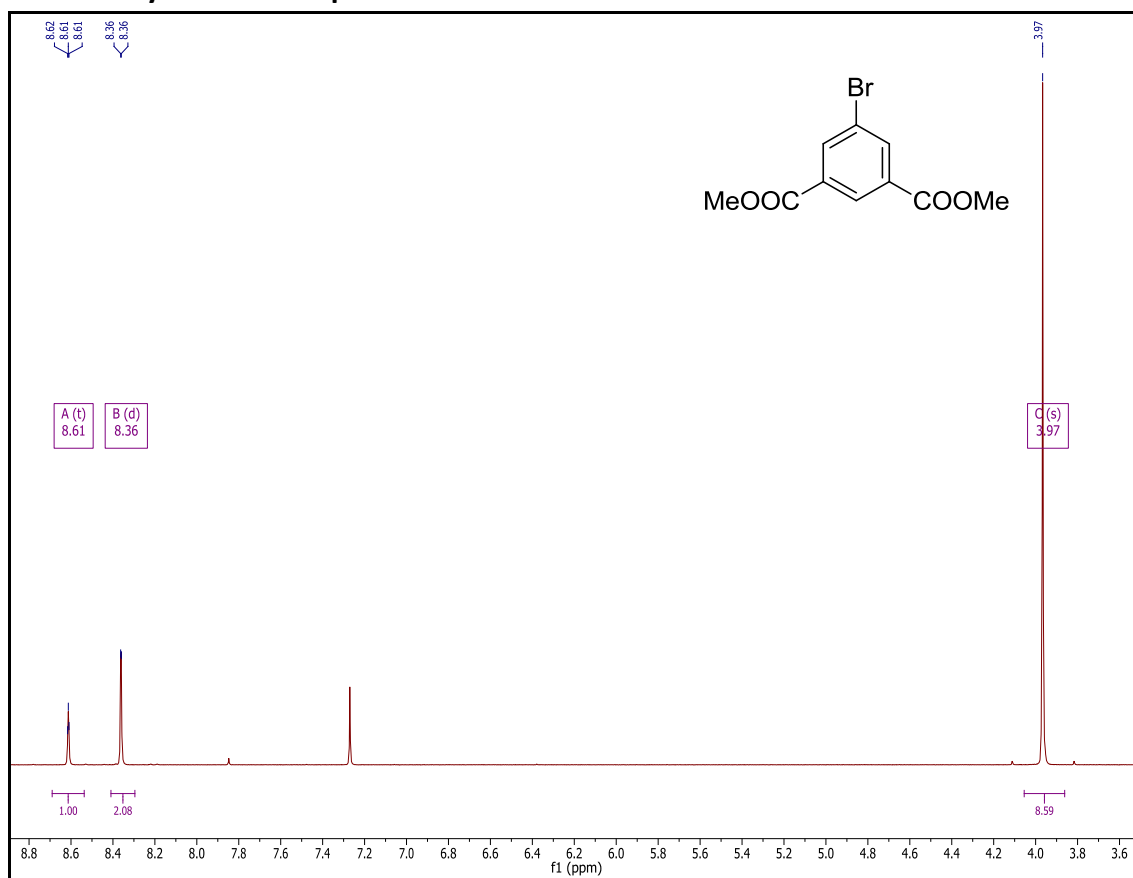
## Appendix

### Spectra

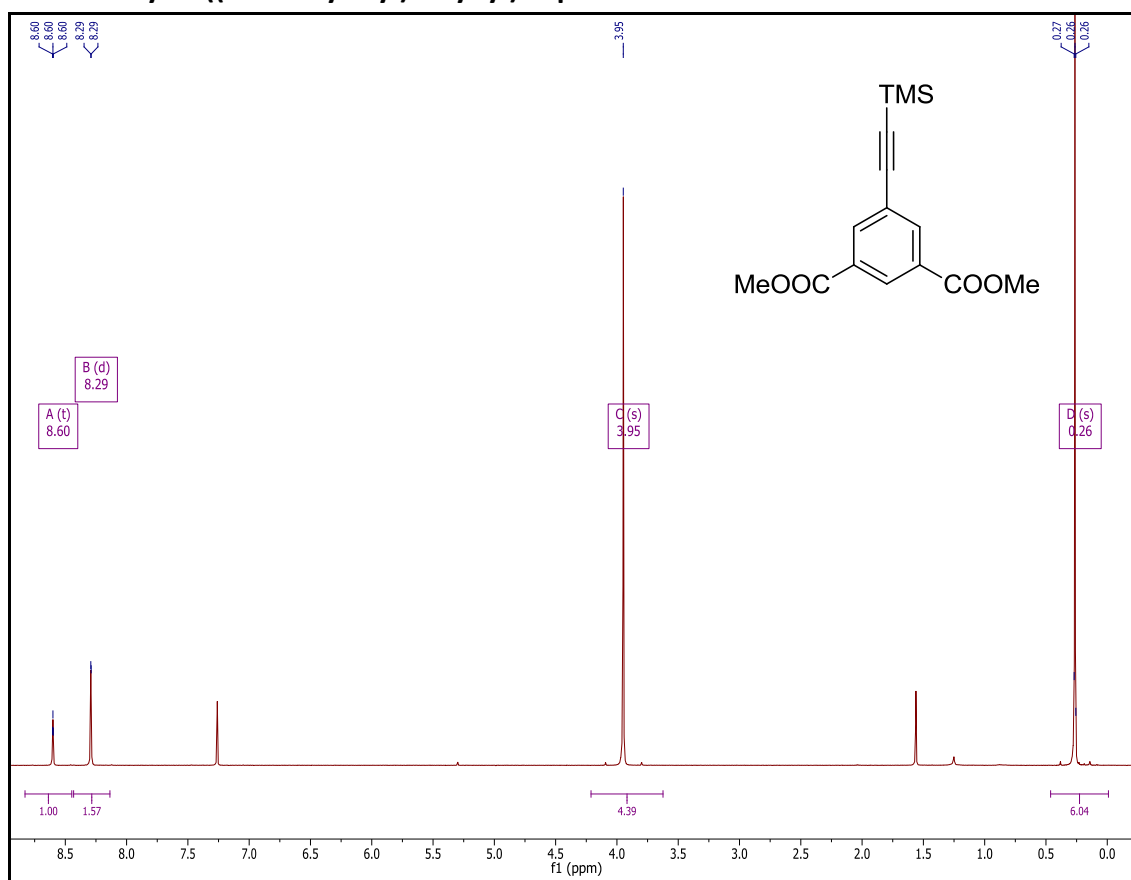
#### Characterizations

Here are the NMR and ESI spectra for each compound characterized in the experimental sections.

##### 1. Dimethyl-5-bromoisophthalate: **1**

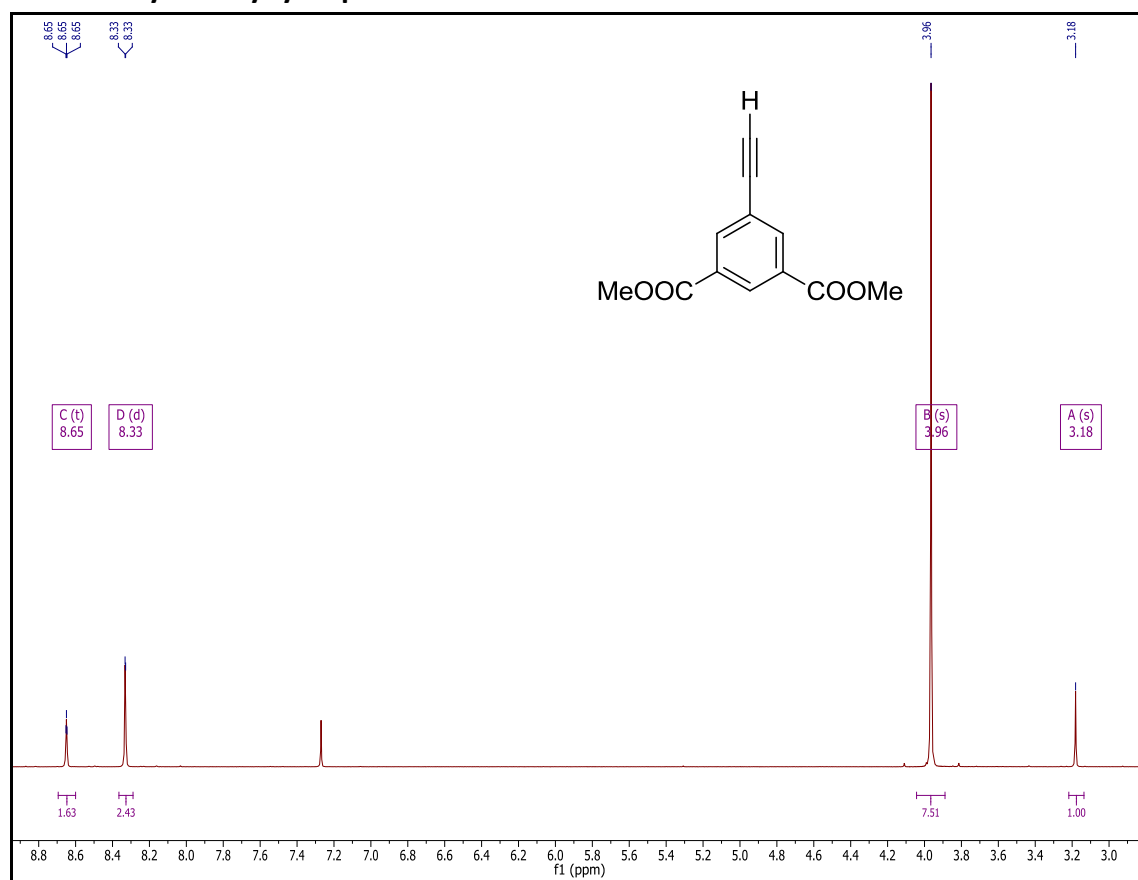


**Figure A 1**  $^1\text{H}$  NMR ( $\text{CDCl}_3$ )  $\delta$  8.61 (t,  $J$  = 1.6 Hz, 1H), 8.36 (d,  $J$  = 1.6 Hz, 2H), 3.97 (s, 6H).

**2. Dimethyl-5-((trimethylsilyl)ethynyl)isophthalate: 2**

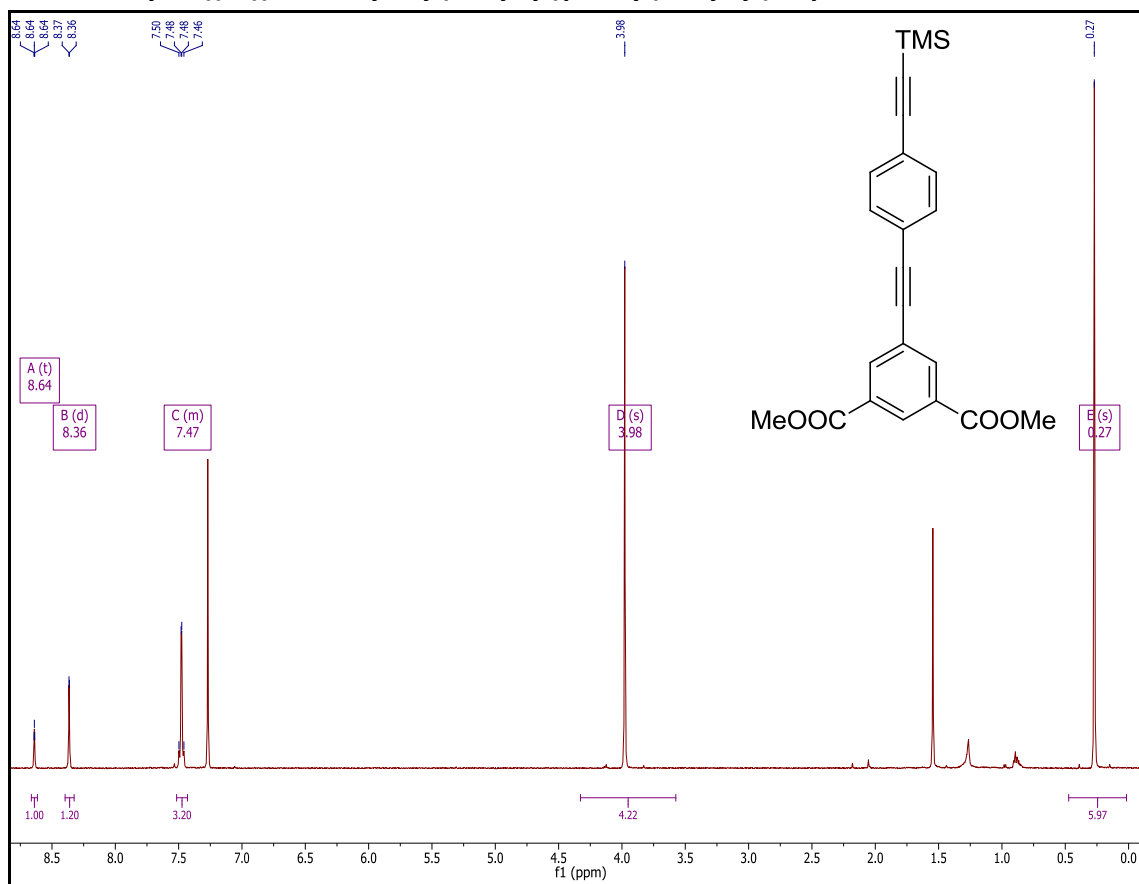
**Figure A 2**  $^1\text{H}$  NMR ( $\text{CDCl}_3$ )  $\delta$  8.60 (t,  $J = 1.4$  Hz, 1H), 8.29 (d,  $J = 1.4$  Hz, 2H), 3.95 (s, 6H), 0.26 (s, 9H).



**3. Dimethyl 5-ethynylisophthalate: 3**

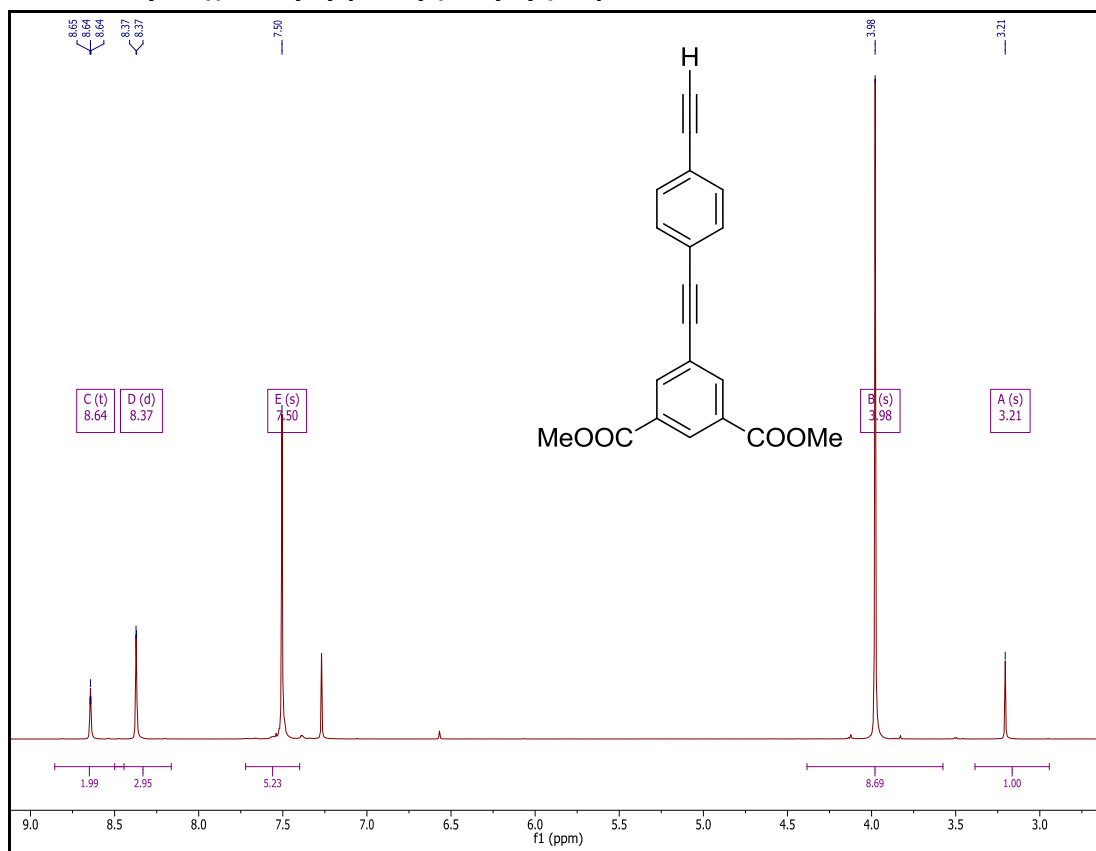
**Figure A 3**  $^1\text{H}$  NMR ( $\text{CDCl}_3$ )  $\delta$  8.65 (t,  $J$  = 1.4 Hz, 1H), 8.33 (d,  $J$  = 1.5 Hz, 2H), 3.96 (s, 6H), 3.18 (s, 1H).

#### 4. Dimethyl 5-((4-((trimethylsilyl)ethynyl)phenyl)ethynyl)isophthalate : **4**



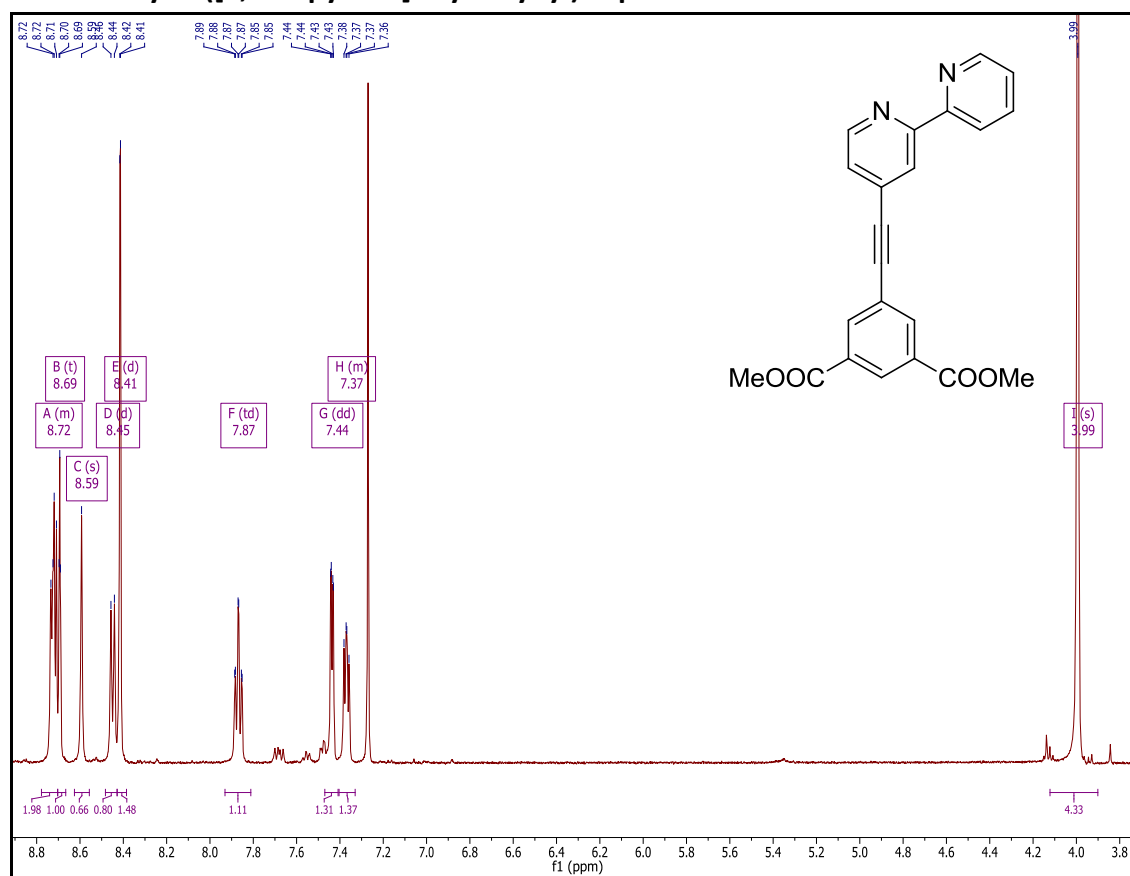
**Figure A 4**  $^1\text{H}$  NMR ( $\text{CDCl}_3$ )  $\delta$  8.64 (t,  $J = 1.6$  Hz, 1H), 8.36 (d,  $J = 1.6$  Hz, 2H), 7.52 – 7.43 (m, 4H), 3.98 (s, 6H), 0.27 (s, 9H).

### 5. Dimethyl 5-((4-ethynylphenyl)ethynyl)isophthalate: 5

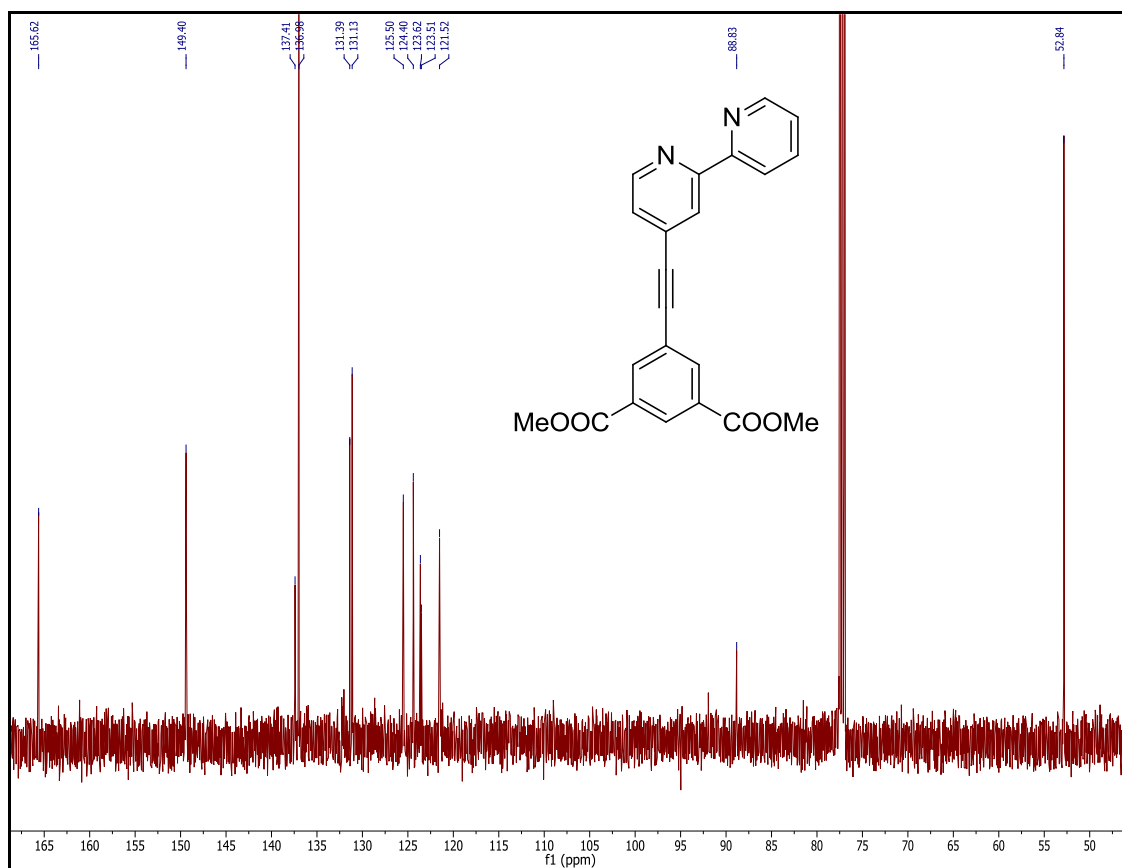


**Figure A 5**  $^1\text{H}$  NMR ( $\text{CDCl}_3$ )  $\delta$  8.64 (t,  $J = 1.4$  Hz, 1H), 8.37 (d,  $J = 1.5$  Hz, 2H), 7.50 (s, 4H), 3.98 (s, 6H), 3.21 (s, 1H).

# 6. Dimethyl 5-([2,2'-bipyridin]-4-ylethynyl)isophthalate: **6**

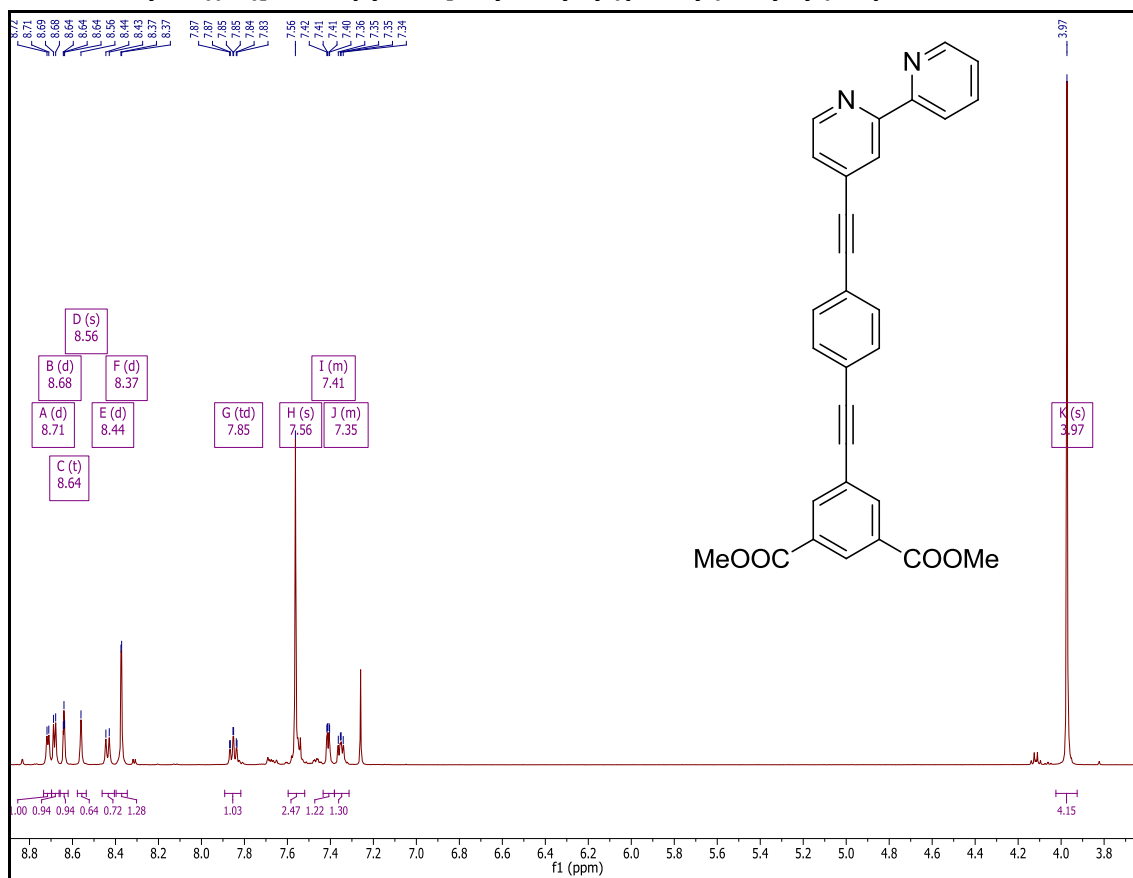


**Figure A 6** <sup>1</sup>H NMR (CDCl<sub>3</sub>) δ 8.78 – 8.70 (m, 2H), 8.69 (t, *J* = 1.5 Hz, 1H), 8.59 (s, 1H), 8.45 (d, *J* = 8.0 Hz, 1H), 8.41 (d, *J* = 1.5 Hz, 2H), 7.87 (td, *J* = 7.8, 1.6 Hz, 1H), 7.44 (dd, *J* = 4.9, 1.4 Hz, 1H), 7.40 – 7.33 (m, 1H), 3.99 (s, 6H).



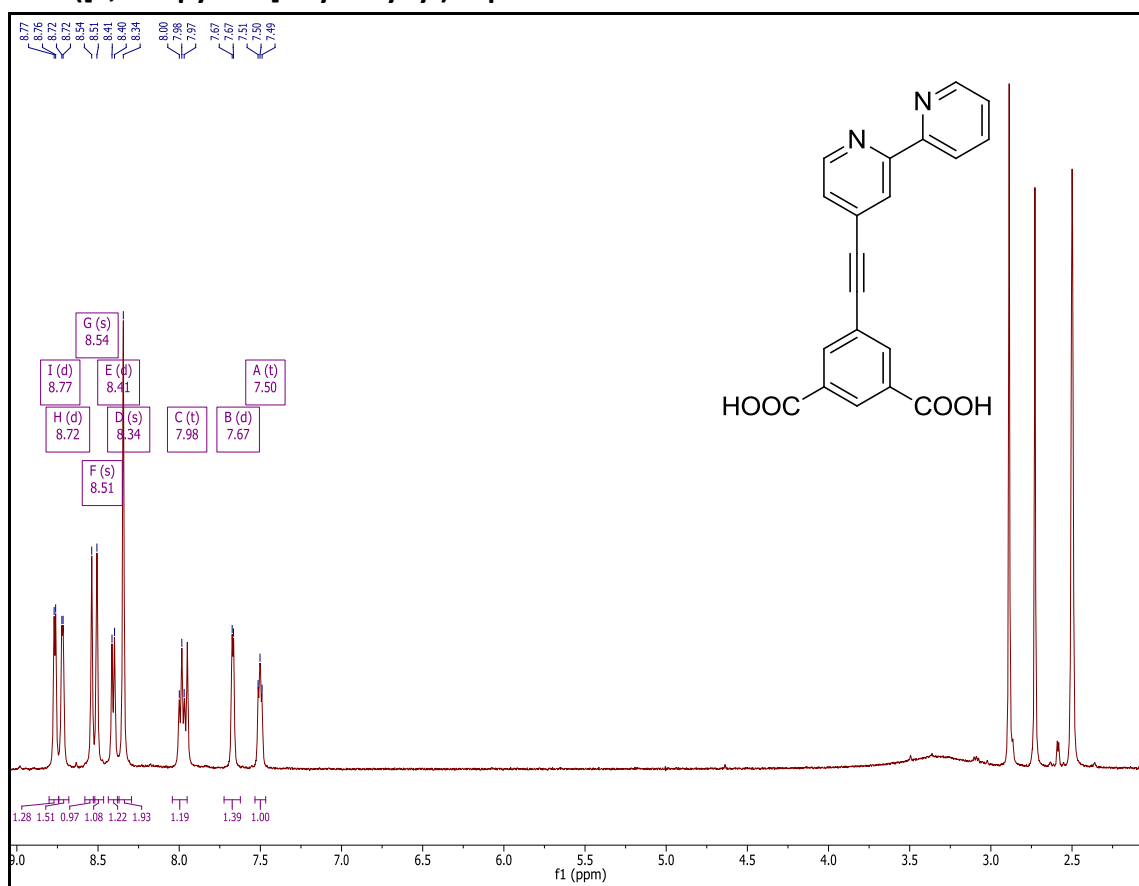
**Figure A 7**  $^{13}\text{C}$  NMR ( $\text{CDCl}_3$ )  $\delta$  165.62, 149.40, 137.41, 136.98, 131.39, 131.13, 125.50, 124.40, 123.62, 123.51, 121.52, 88.83, 52.84.

7. Dimethyl 5-((4-([2,2'-bipyridin]-4-ylethynyl)phenyl)ethynyl)isophthalate: **7**

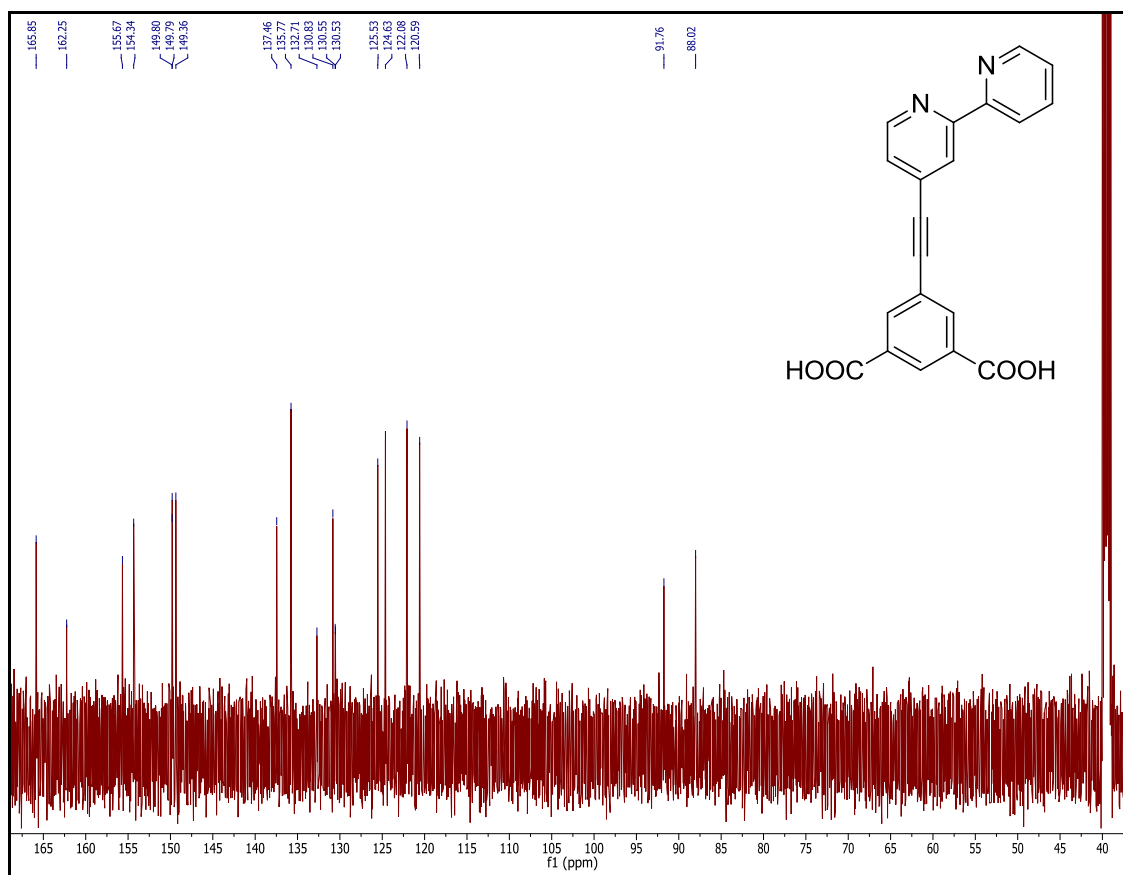


**Figure A 8** <sup>1</sup>H NMR (CDCl<sub>3</sub>) δ 8.71 (d, *J* = 4.2 Hz, 1H), 8.68 (d, *J* = 4.9 Hz, 1H), 8.64 (t, *J* = 1.5 Hz, 1H), 8.56 (s, 1H), 8.44 (d, *J* = 7.9 Hz, 1H), 8.37 (d, *J* = 1.6 Hz, 2H), 7.85 (td, *J* = 7.8, 1.6 Hz, 1H), 7.56 (s, 4H), 7.43 – 7.38 (m, 1H), 7.38 – 7.31 (m, 1H), 3.97 (s, 6H).

## 8. 5-([2,2'-bipyridin]-4-ylethynyl)isophthalic acid: L1

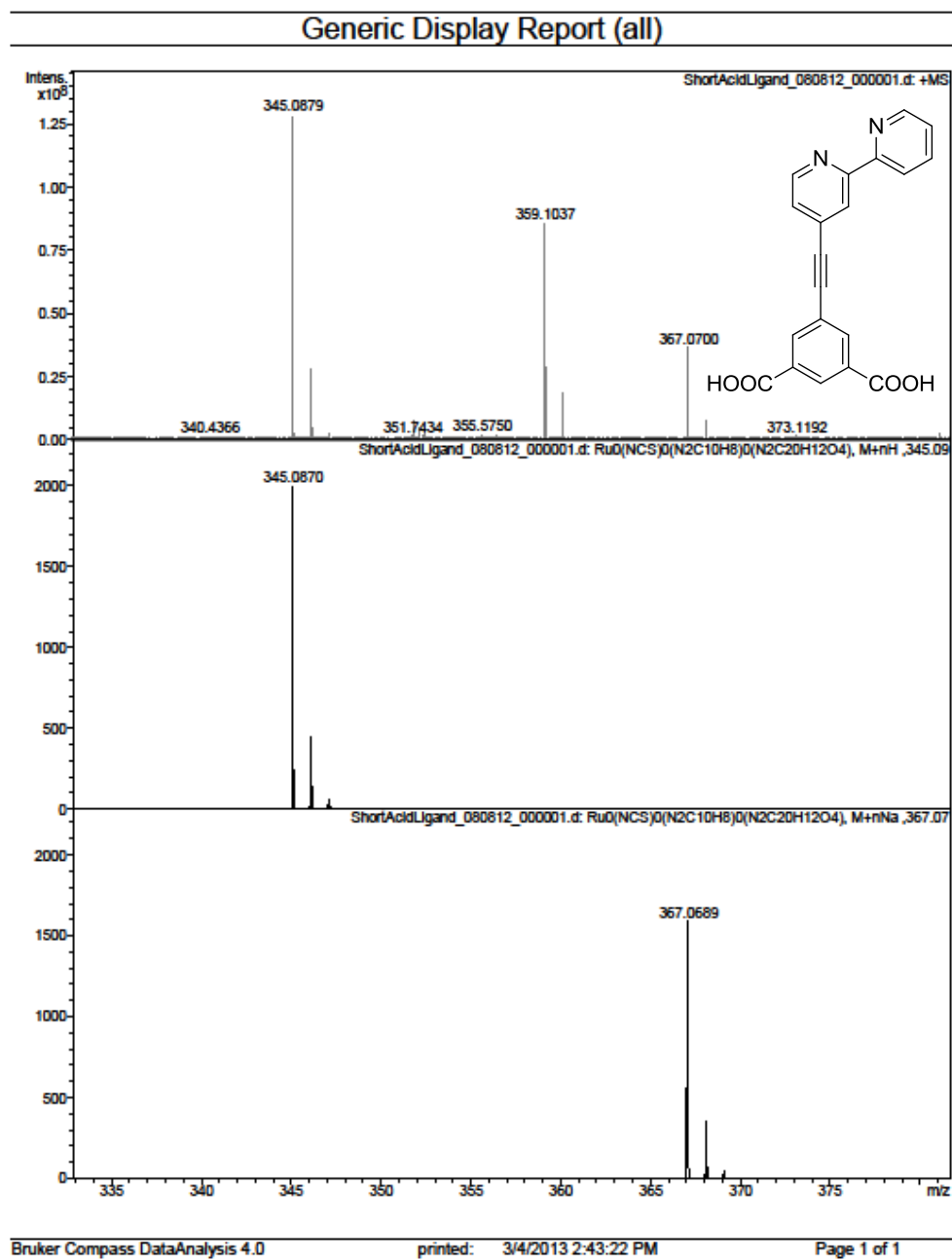


**Figure A 9** <sup>1</sup>H NMR (DMSO-d<sub>6</sub>) δ 8.77 (d, *J* = 4.6 Hz, 1H), 8.72 (d, *J* = 3.7 Hz, 1H), 8.54 (s, 1H), 8.51 (s, 1H), 8.41 (d, *J* = 7.7 Hz, 1H), 8.34 (s, 2H), 7.98 (t, *J* = 7.5 Hz, 1H), 7.67 (d, *J* = 4.0 Hz, 1H), 7.50 (t, *J* = 6.2 Hz, 1H).



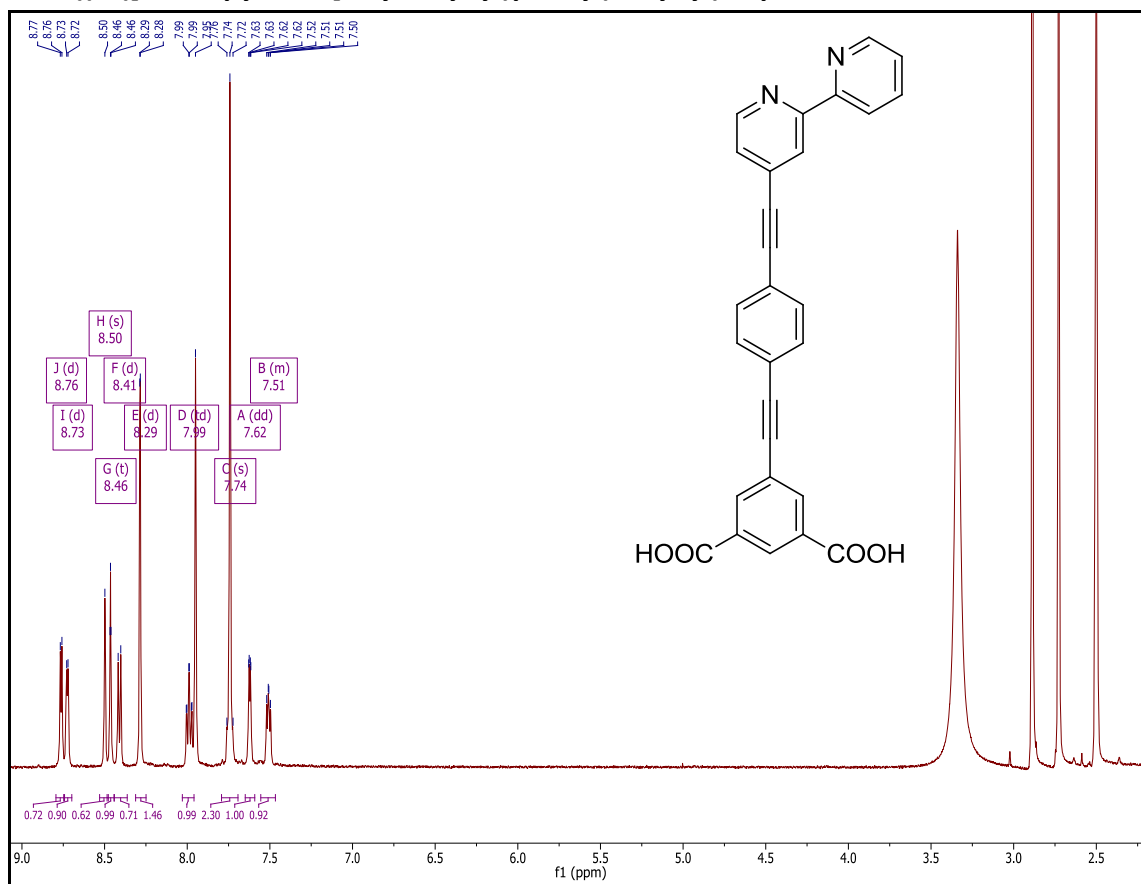
**Figure A 10**  $^{13}\text{C}$  NMR (DMSO- $d_6$ )  $\delta$  165.85, 162.25, 155.67, 154.34, 149.80, 149.79, 149.36, 137.46, 135.77, 132.71, 130.83, 130.55, 130.53, 125.53, 124.63, 122.08, 120.59, 91.76, 88.02.



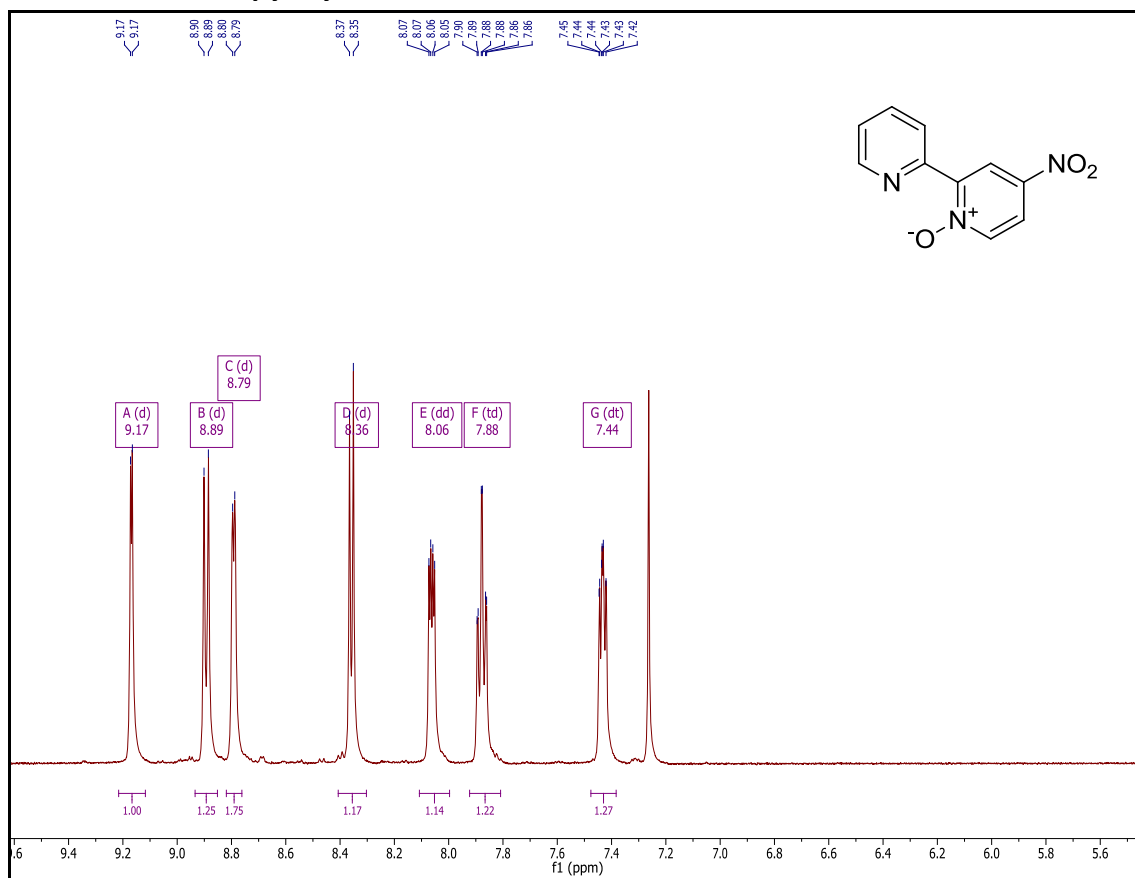


**Figure A 11** Top: Actual spectrum; mid: calculated:  $[M+H]^+$ ; bottom: calculated:  $[M+Na]^+$

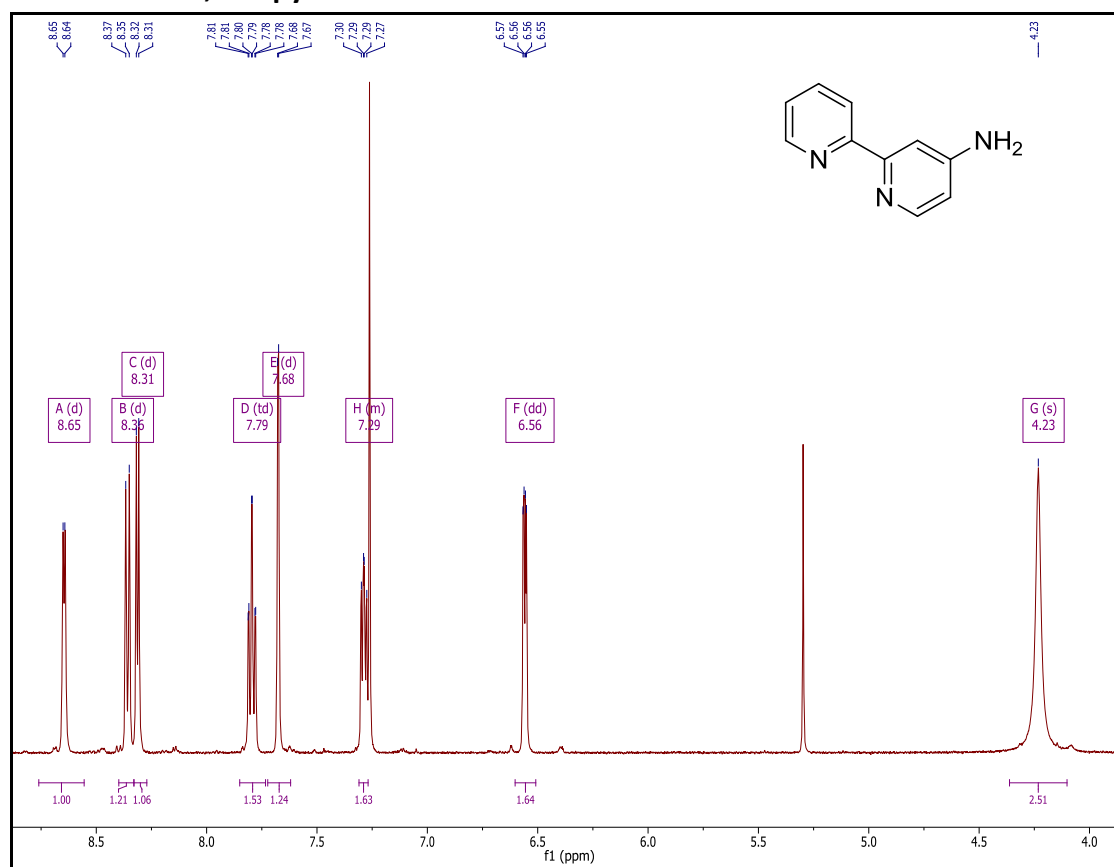
9. 5-((4-([2,2'-bipyridine]-4-ylethynyl)phenyl)ethynyl)isophthalic acid: L2



**Figure A 12** <sup>1</sup>H NMR (DMSO-d<sub>6</sub>) δ 8.76 (d, *J* = 4.9 Hz, 1H), 8.73 (d, *J* = 3.9 Hz, 1H), 8.50 (s, 1H), 8.46 (t, *J* = 1.4 Hz, 1H), 8.41 (d, *J* = 7.9 Hz, 1H), 8.29 (d, *J* = 1.5 Hz, 2H), 7.99 (td, *J* = 7.8, 1.7 Hz, 1H), 7.74 (s, 4H), 7.62 (dd, *J* = 4.9, 1.4 Hz, 1H), 7.56 – 7.47 (m, 1H).

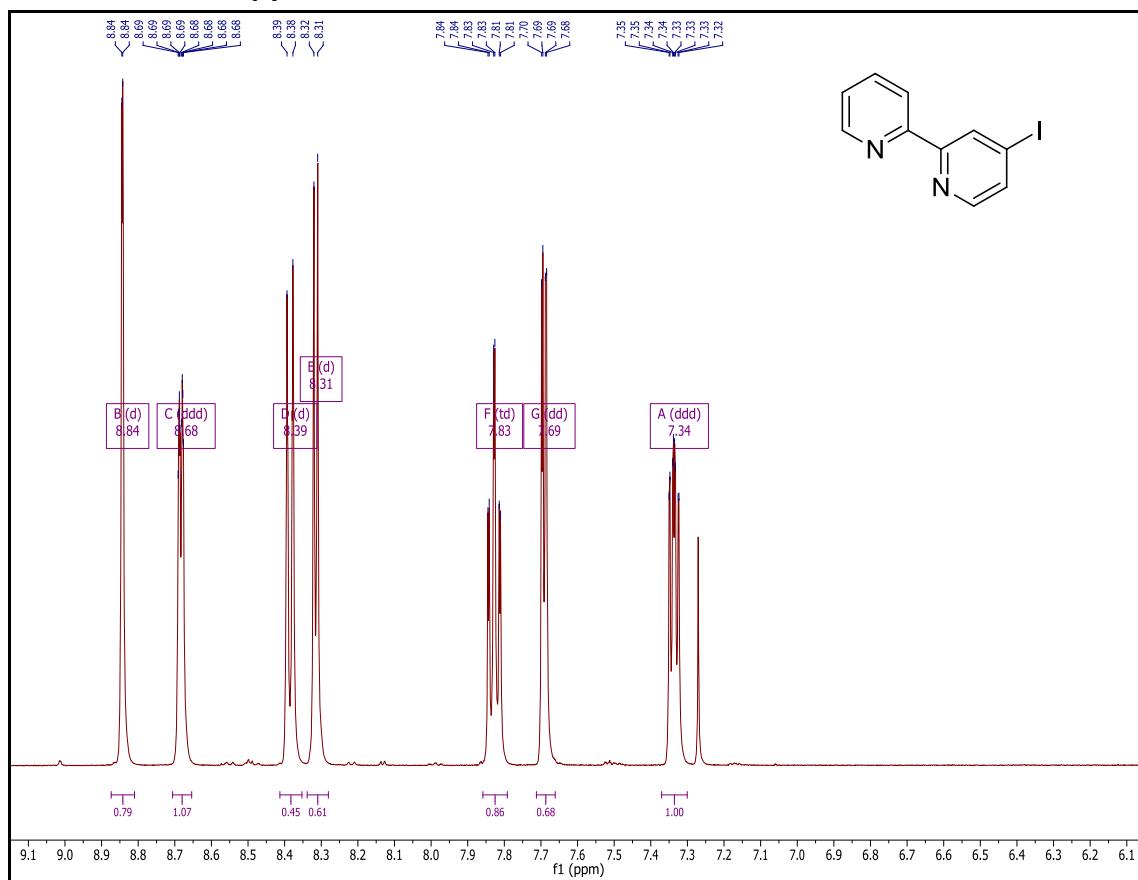
10. 4-Nitro-2,2'-dipyridyl-N-oxide: **8**

**Figure A 13**  $^1\text{H}$  NMR ( $\text{CDCl}_3$ )  $\delta$  9.17 (d,  $J = 3.4$  Hz, 1H), 8.89 (d,  $J = 8.1$  Hz, 1H), 8.79 (d,  $J = 3.9$  Hz, 1H), 8.36 (d,  $J = 7.2$  Hz, 1H), 8.06 (dd,  $J = 7.2, 3.3$  Hz, 1H), 7.88 (td,  $J = 7.9, 1.9$  Hz, 1H), 7.44 (dt,  $J = 7.9, 3.0$  Hz, 1H).

11. 4-Amino-2,2'-bipyridine: **9**

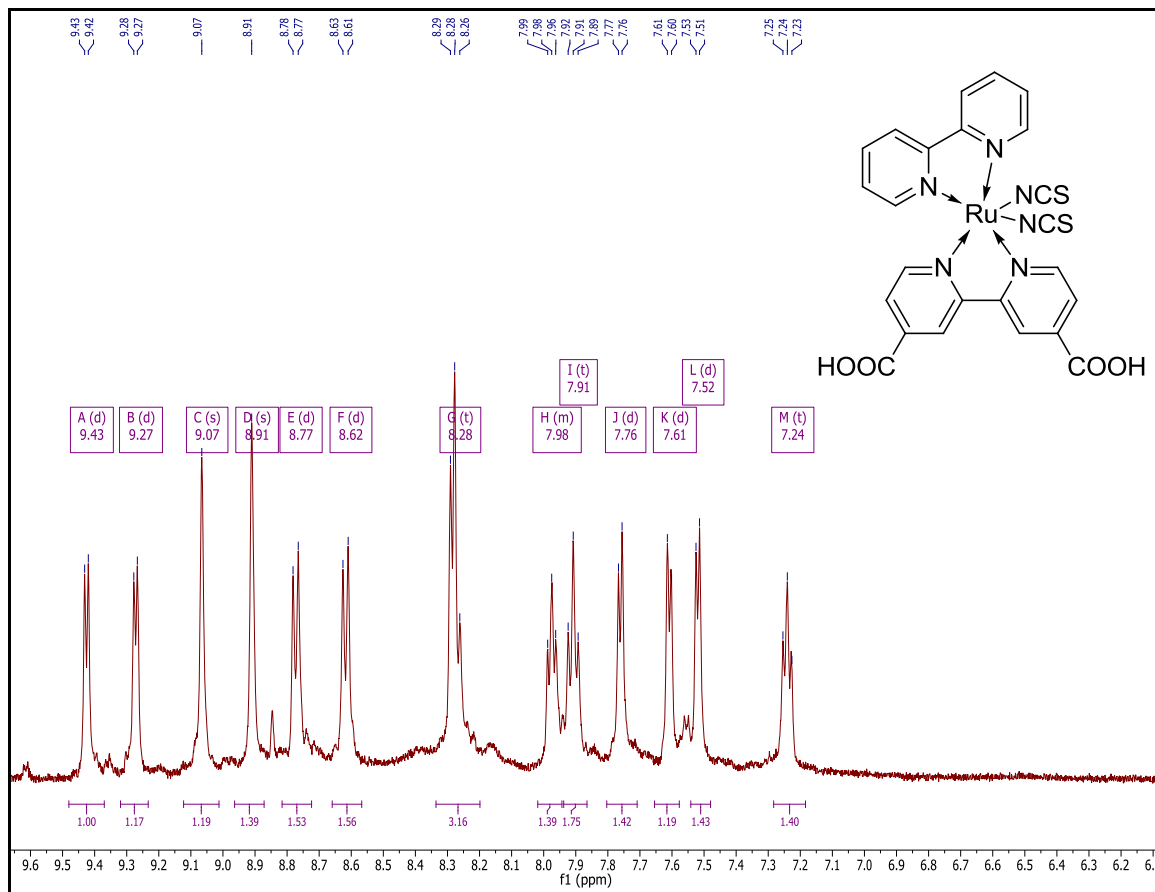
**Figure A 14** <sup>1</sup>H NMR (CDCl<sub>3</sub>) δ 8.65 (d, *J* = 4.0 Hz, 1H), 8.36 (d, *J* = 8.0 Hz, 1H), 8.31 (d, *J* = 5.5 Hz, 1H), 7.79 (td, *J* = 7.8, 1.7 Hz, 1H), 7.68 (d, *J* = 2.2 Hz, 1H), 7.31 – 7.27 (m, 1H), 6.56 (dd, *J* = 5.5, 2.3 Hz, 1H), 4.23 (s, 2H).

## 12. 4-Iodo,-2,2'-bipyridine: 10

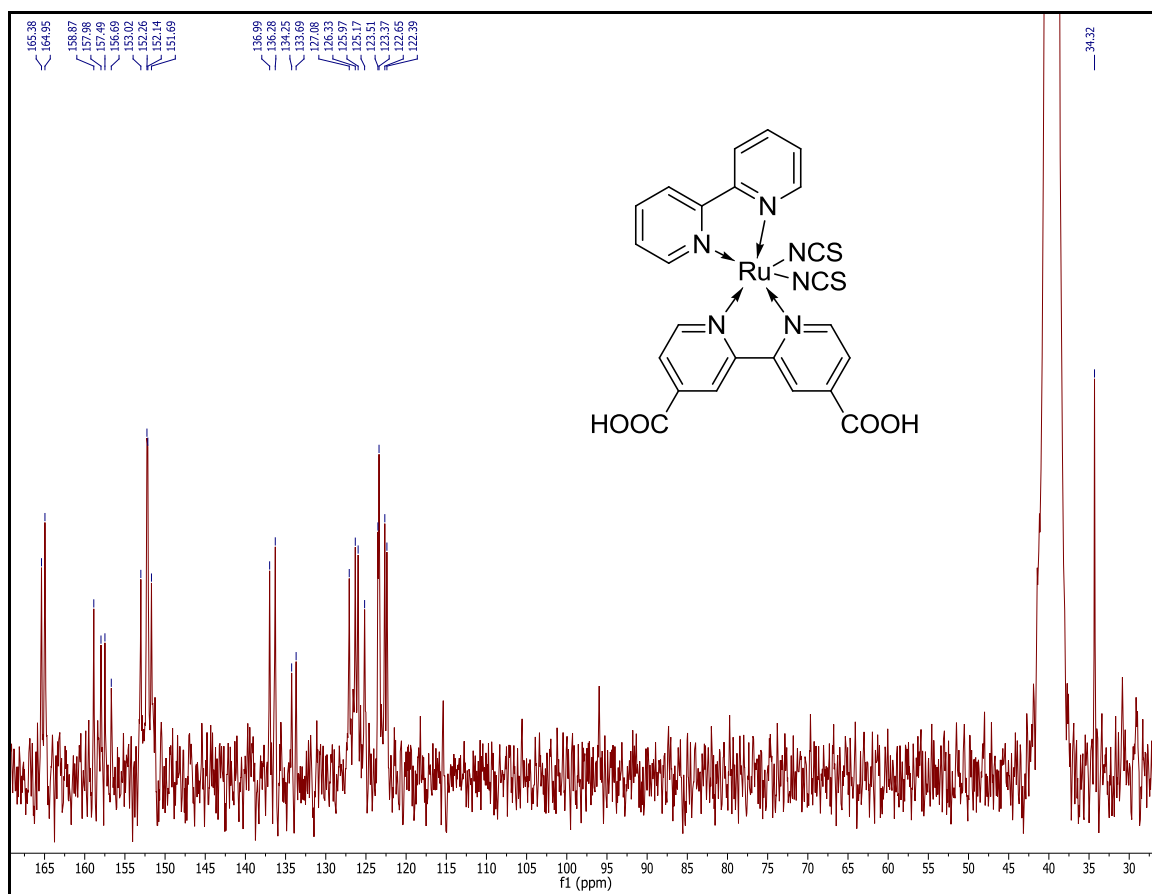


**Figure A 15** <sup>1</sup>H NMR (CDCl<sub>3</sub>) δ 8.84 (d, *J* = 1.2 Hz, 1H), 8.68 (ddd, *J* = 4.7, 1.6, 0.9 Hz, 1H), 8.39 (d, *J* = 8.0 Hz, 1H), 8.31 (d, *J* = 5.1 Hz, 1H), 7.83 (td, *J* = 7.8, 1.7 Hz, 1H), 7.69 (dd, *J* = 5.1, 1.7 Hz, 1H), 7.34 (ddd, *J* = 7.5, 4.8, 1.1 Hz, 1H).

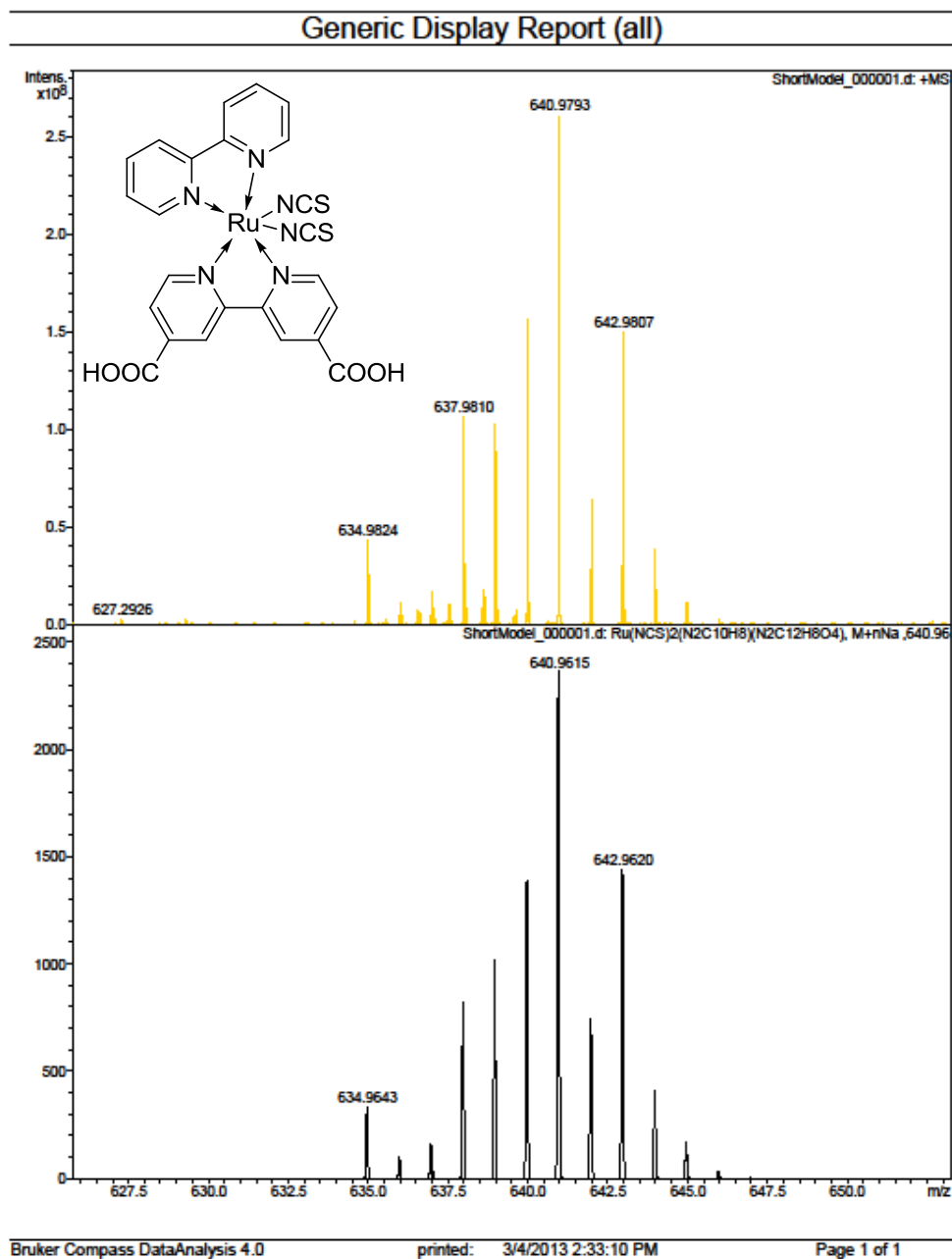
13.  $\text{Ru}(\text{NCS})_2[2,2'\text{-Bipyridine}][4,4'\text{-Dicarboxylic acid-2,2'-bipyridine}]$ : AKO



**Figure A 16**  $^1\text{H}$  NMR ( $\text{DMSO-d}_6$ ):  $\delta_{\text{H}}$  9.43 (d,  $J = 5.7$ , 1H), 9.27 (d,  $J = 5.5$ , 1H), 9.07 (s, 1H), 8.91 (s, 1H), 8.77 (d,  $J = 8.1$ , 1H), 8.62 (d,  $J = 8.1$ , 1H), 8.28 (t,  $J = 7.3$ , 2H), 7.97 (t,  $J = 6.7$ , 1H), 7.91 (t,  $J = 8.2$ , 1H), 7.76 (d,  $J = 5.6$ , 1H), 7.61 (d,  $J = 5.5$ , 1H), 7.52 (d,  $J = 5.5$ , 1H), 7.29 – 7.18 (m, 1H).

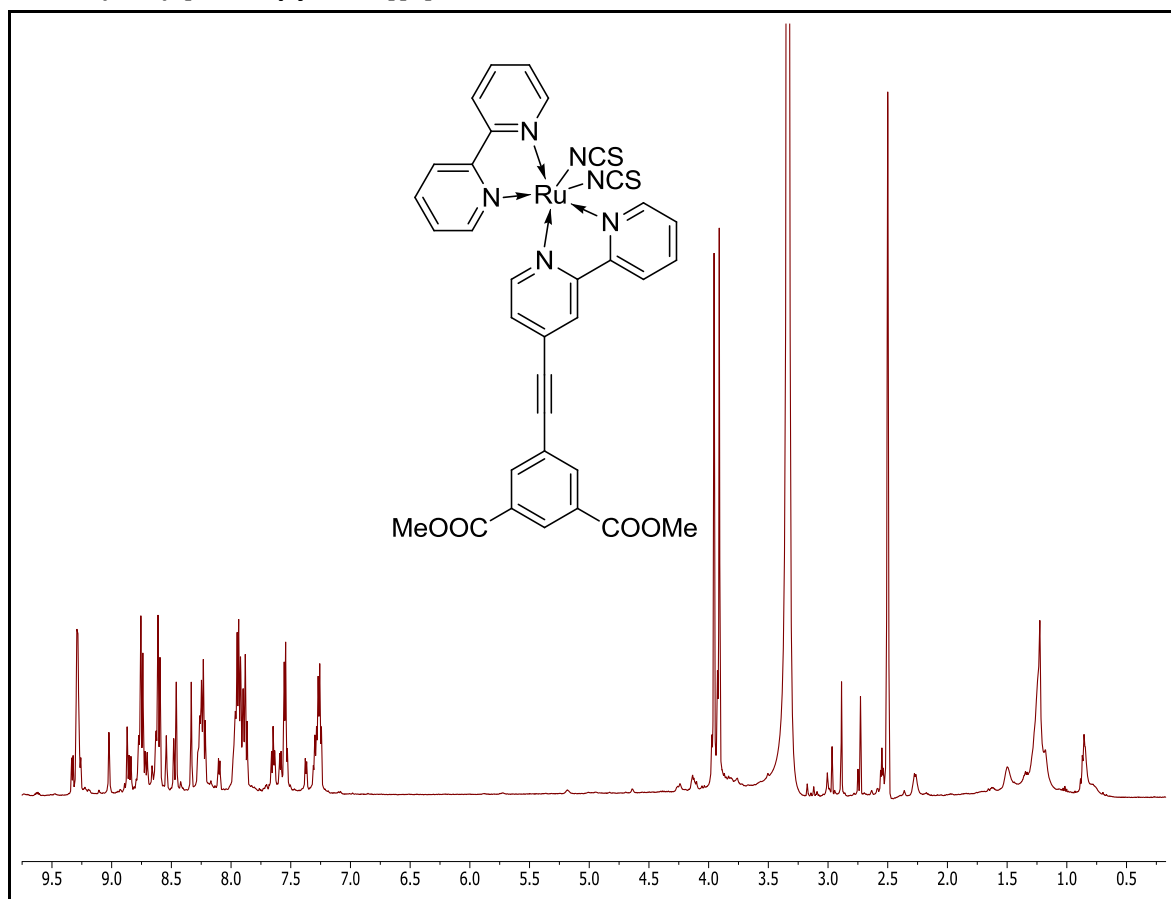


**Figure A 17**  $^{13}\text{C}$  NMR ( $\text{DMSO-d}_6$ )  $\delta$  165.38, 164.95, 158.87, 157.98, 157.49, 156.69, 153.02, 152.26, 152.14, 151.69, 136.99, 136.28, 134.25, 133.69, 127.08, 126.33, 125.97, 125.17, 123.51, 123.37, 122.65, 122.39, 34.32.



**Figure A 18** Top: Actual spectrum; bottom: calculated:  $[M+Na]^+$



14.  $\text{Ru}(\text{NCS})_2[2,2'\text{-Bipyridine}][6]$ : 13Figure A 19  $^1\text{H}$  NMR in  $\text{DMSO-d}_6$

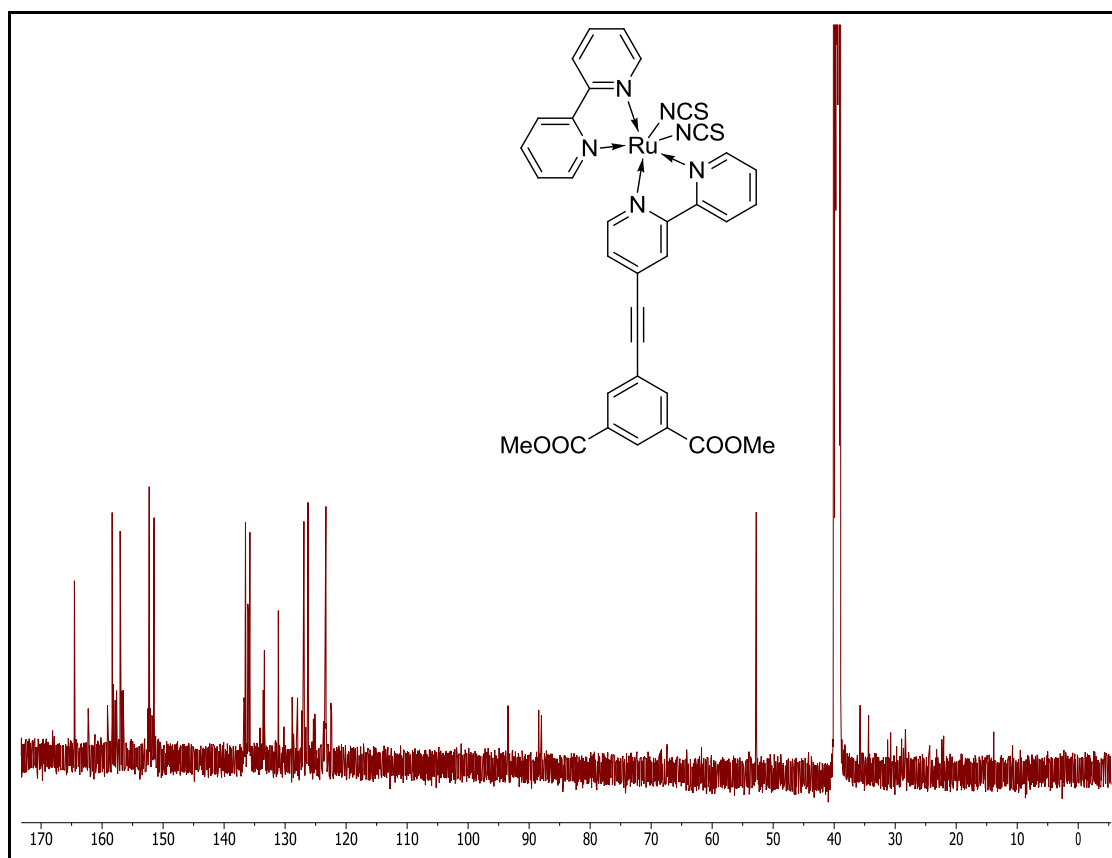
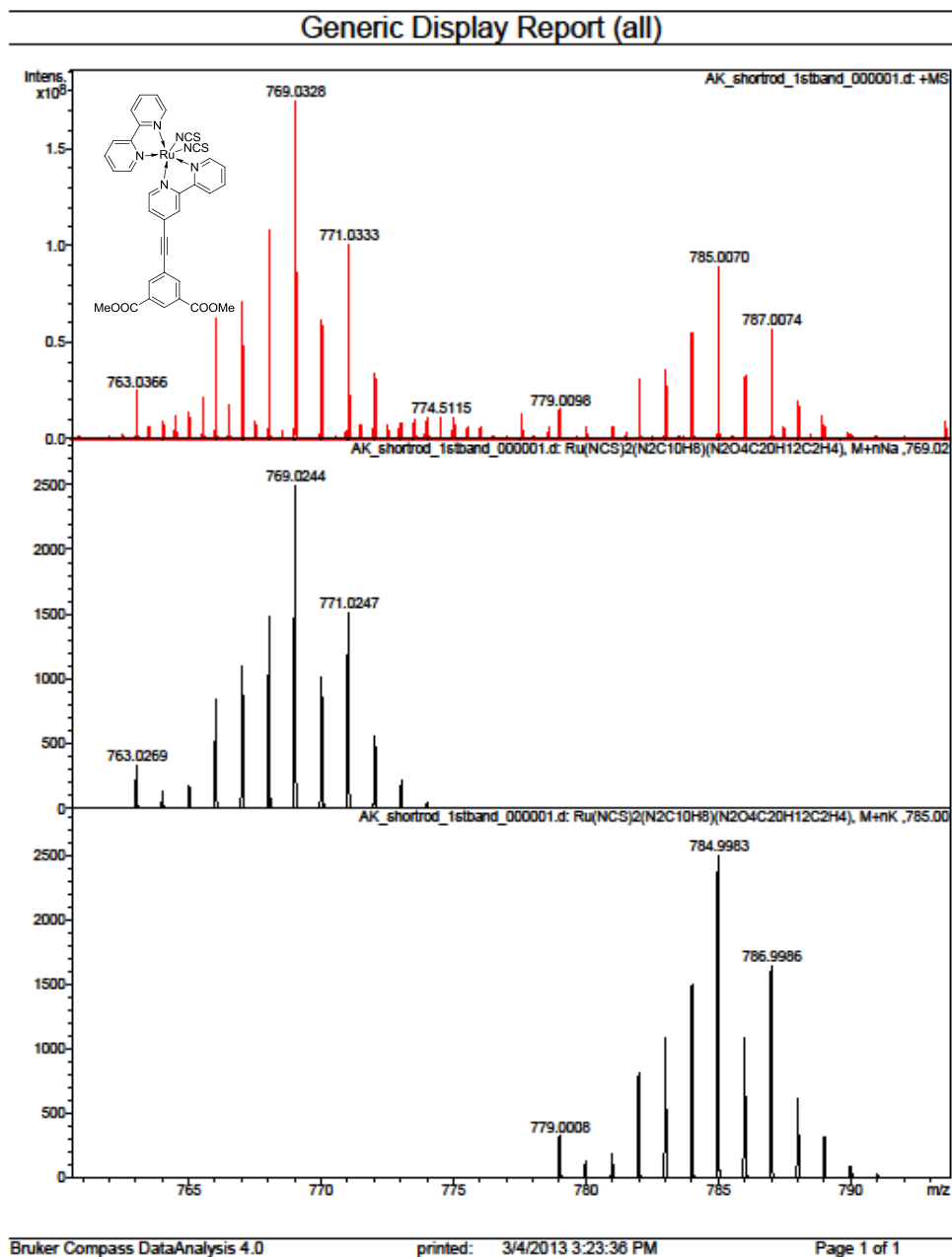
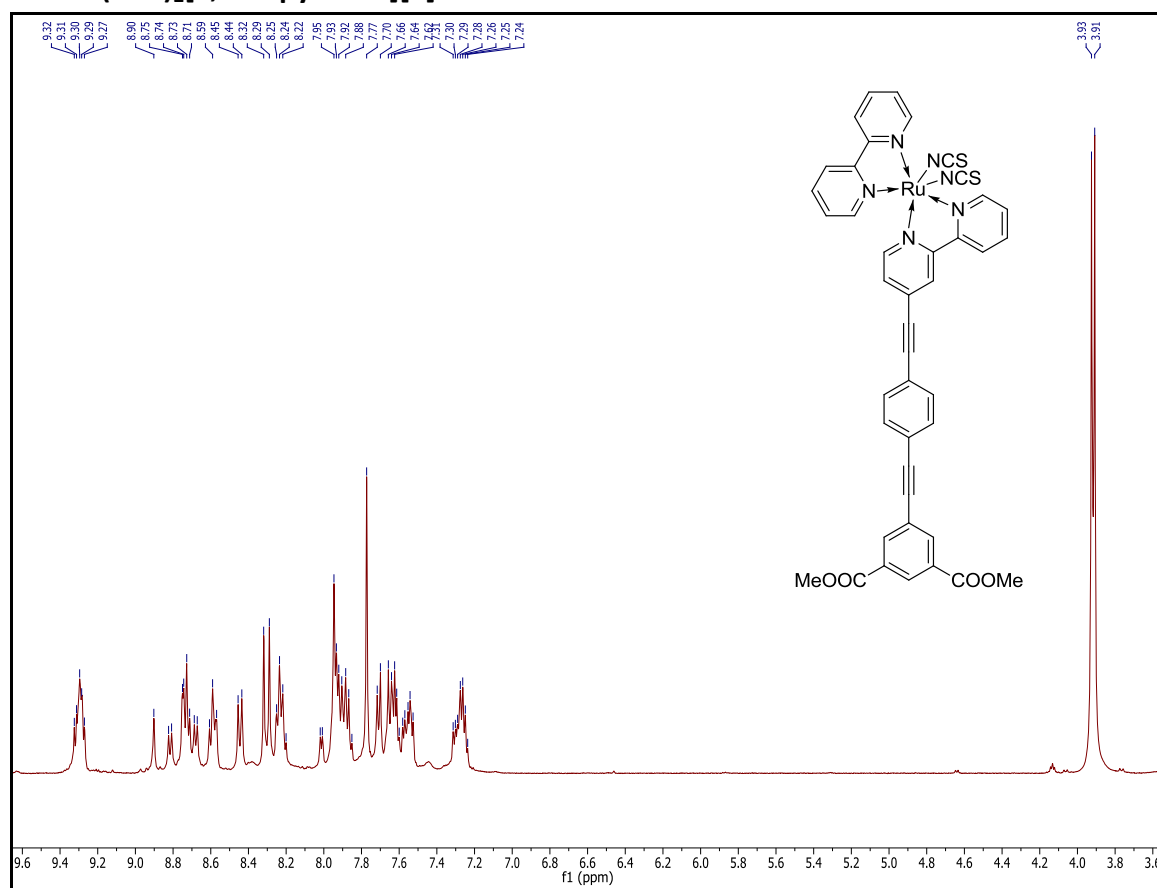


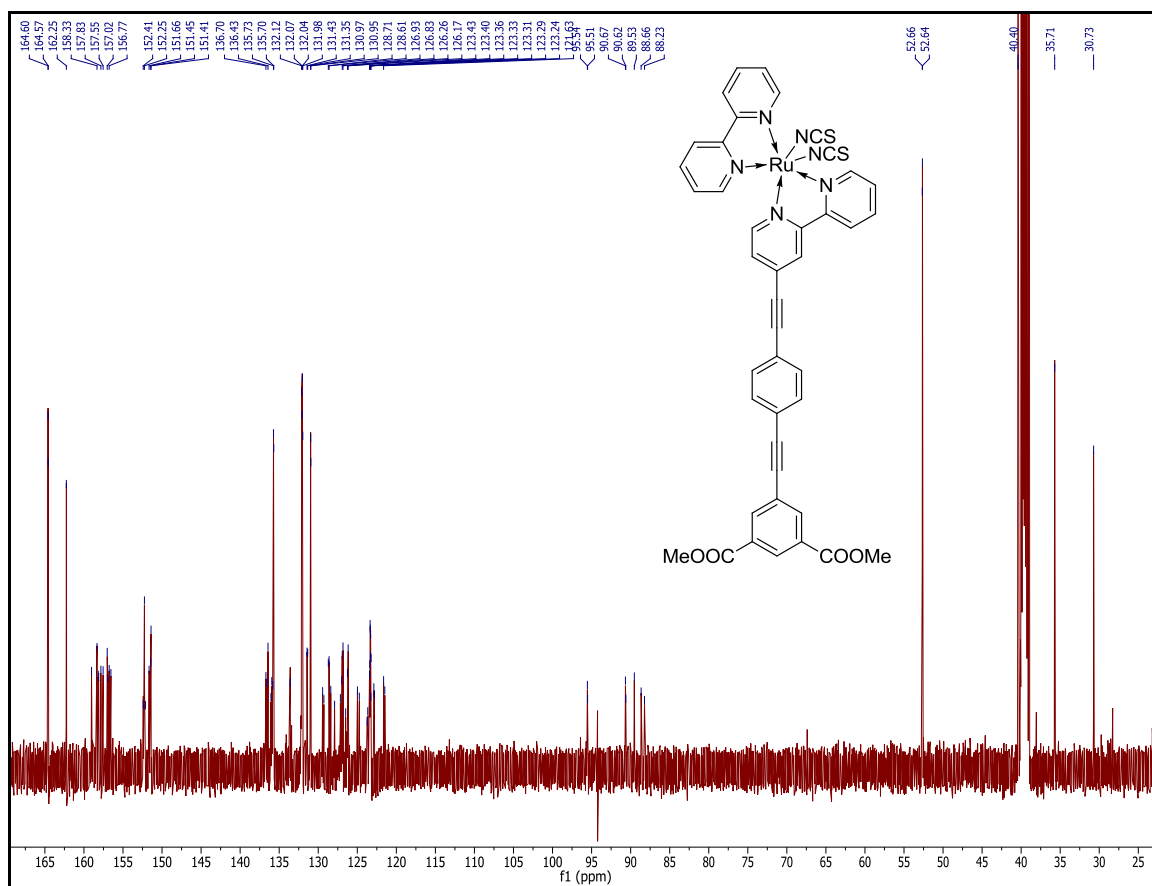
Figure A 20  $^{13}\text{C}$  NMR in  $\text{DMSO-d}_6$



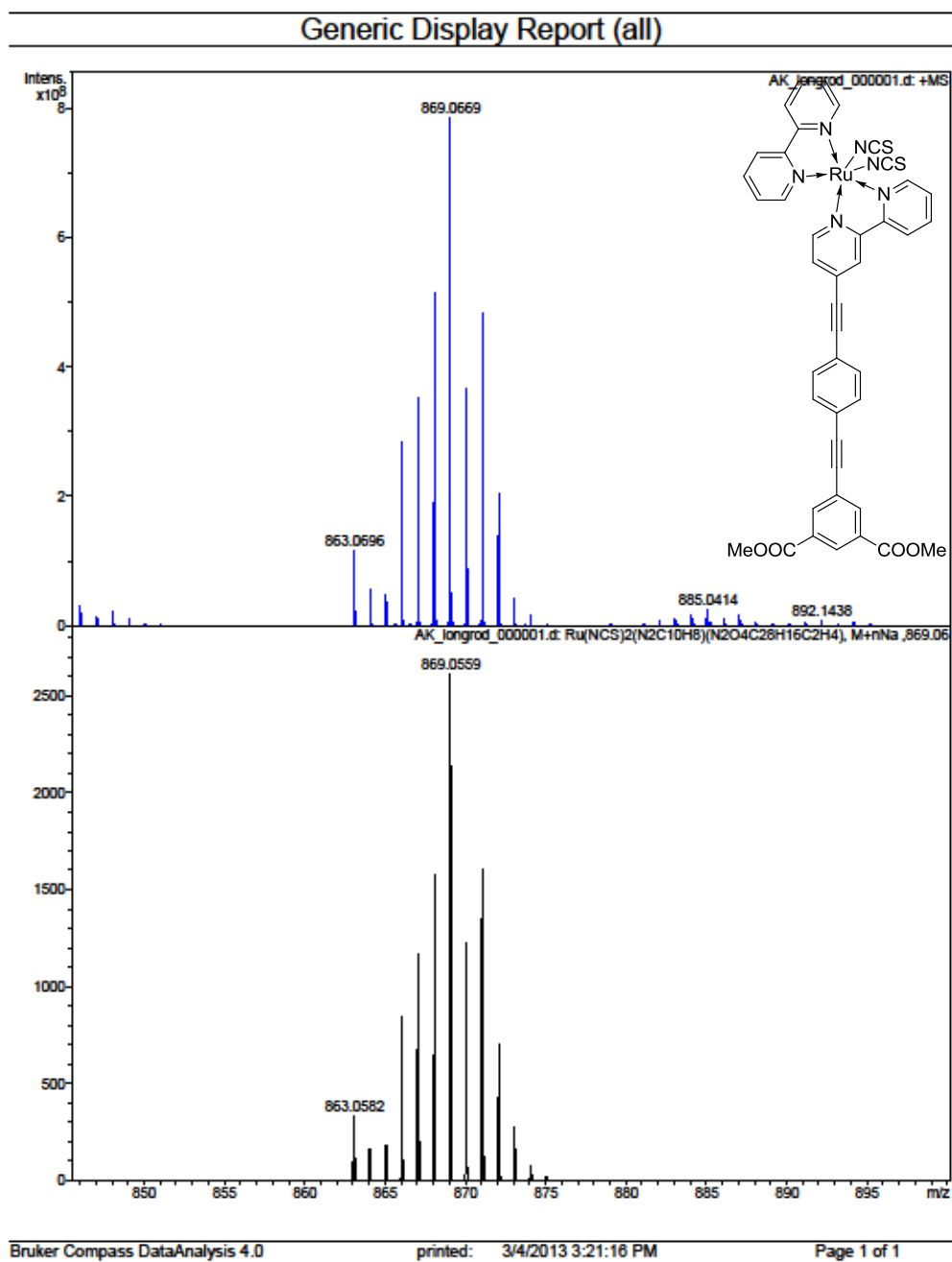
**Figure A 21** Top: Actual spectrum; mid: calculated:  $[M+Na]^+$ ; bottom: calculated:  $[M+K]^+$

15.  $\text{Ru}(\text{NCS})_2[2,2'\text{-Bipyridine}][7]$ : 14

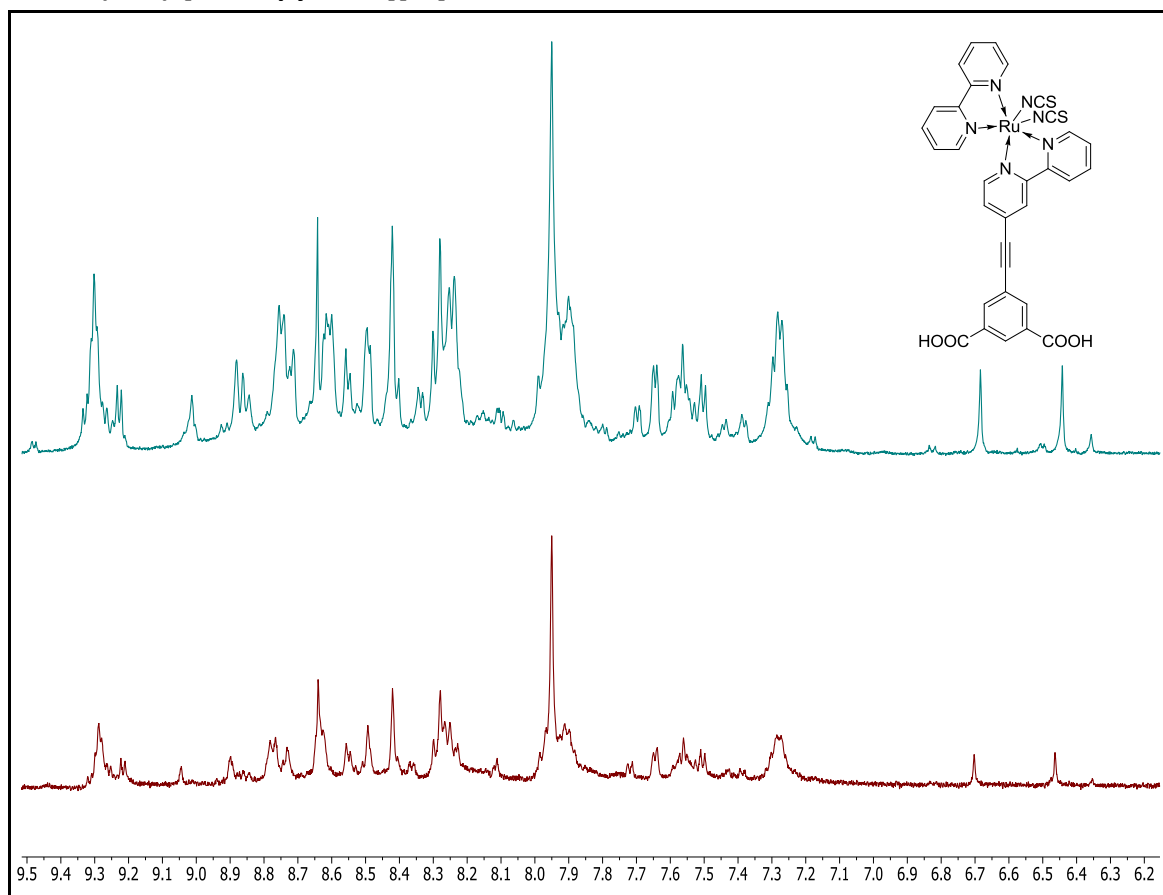
**Figure A 22**  $^1\text{H}$  NMR ( $\text{DMSO-d}_6$ )  $\delta$  9.32, 9.31, 9.30, 9.29, 9.27, 8.90, 8.82, 8.81, 8.75, 8.74, 8.73, 8.71, 8.69, 8.67, 8.61, 8.59, 8.57, 8.45, 8.44, 8.32, 8.29, 8.25, 8.24, 8.22, 8.20, 8.02, 8.01, 7.95, 7.93, 7.92, 7.90, 7.88, 7.87, 7.85, 7.77, 7.72, 7.70, 7.66, 7.64, 7.62, 7.61, 7.60, 7.58, 7.57, 7.55, 7.54, 7.53, 7.31, 7.30, 7.29, 7.28, 7.26, 7.25, 7.24, 3.93, 3.91.

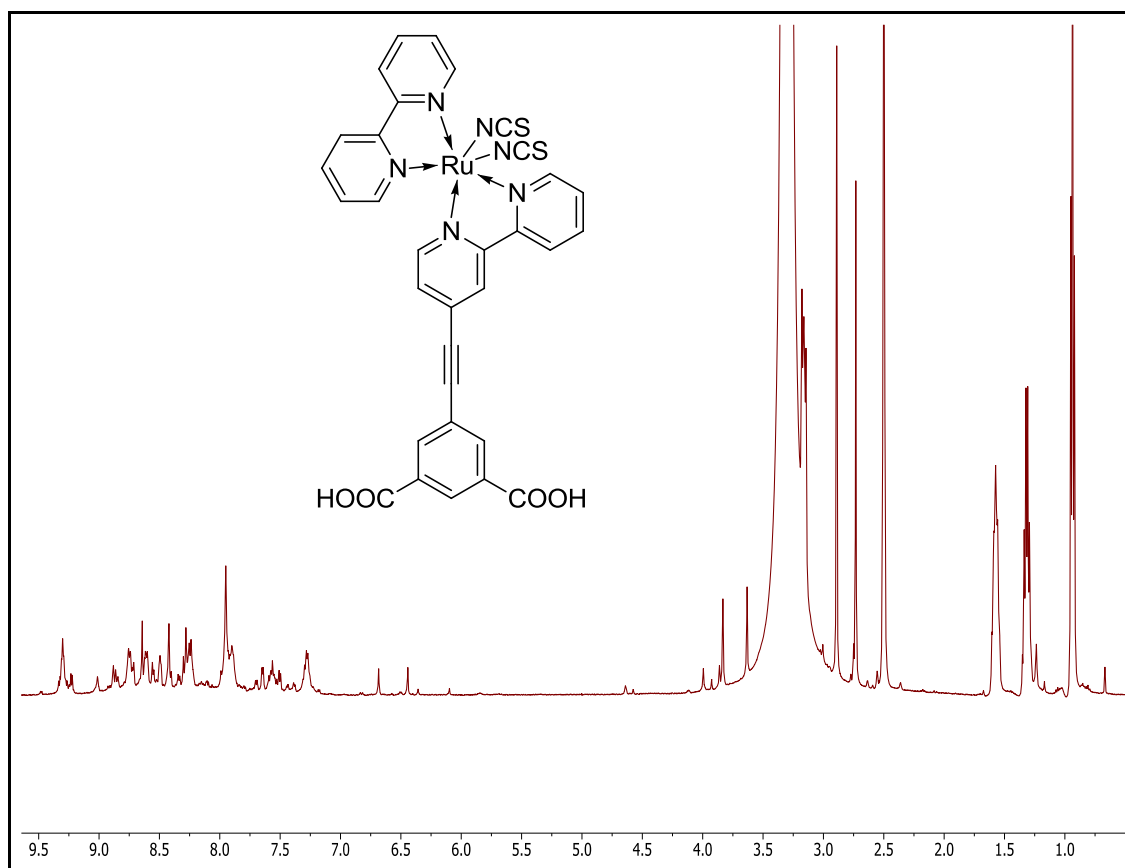


**Figure A 23** <sup>13</sup>C NMR (DMSO-d<sub>6</sub>) δ 164.60, 164.57, 162.25, 159.03, 158.33, 158.17, 158.11, 157.83, 157.55, 157.02, 156.95, 156.77, 156.55, 152.41, 152.25, 152.13, 151.66, 151.45, 151.41, 136.70, 136.58, 136.43, 136.05, 135.95, 135.83, 135.73, 135.70, 133.60, 132.12, 132.07, 132.04, 131.98, 131.43, 131.35, 130.97, 130.95, 129.44, 129.28, 128.71, 128.61, 128.39, 127.91, 127.16, 126.99, 126.93, 126.83, 126.49, 126.26, 126.17, 124.98, 124.74, 123.75, 123.66, 123.43, 123.40, 123.36, 123.33, 123.31, 123.29, 123.27, 123.24, 122.88, 122.82, 121.63, 121.48, 95.54, 95.51, 90.67, 90.62, 89.53, 88.66, 88.23, 52.66, 52.64, 40.40, 35.71, 30.73.



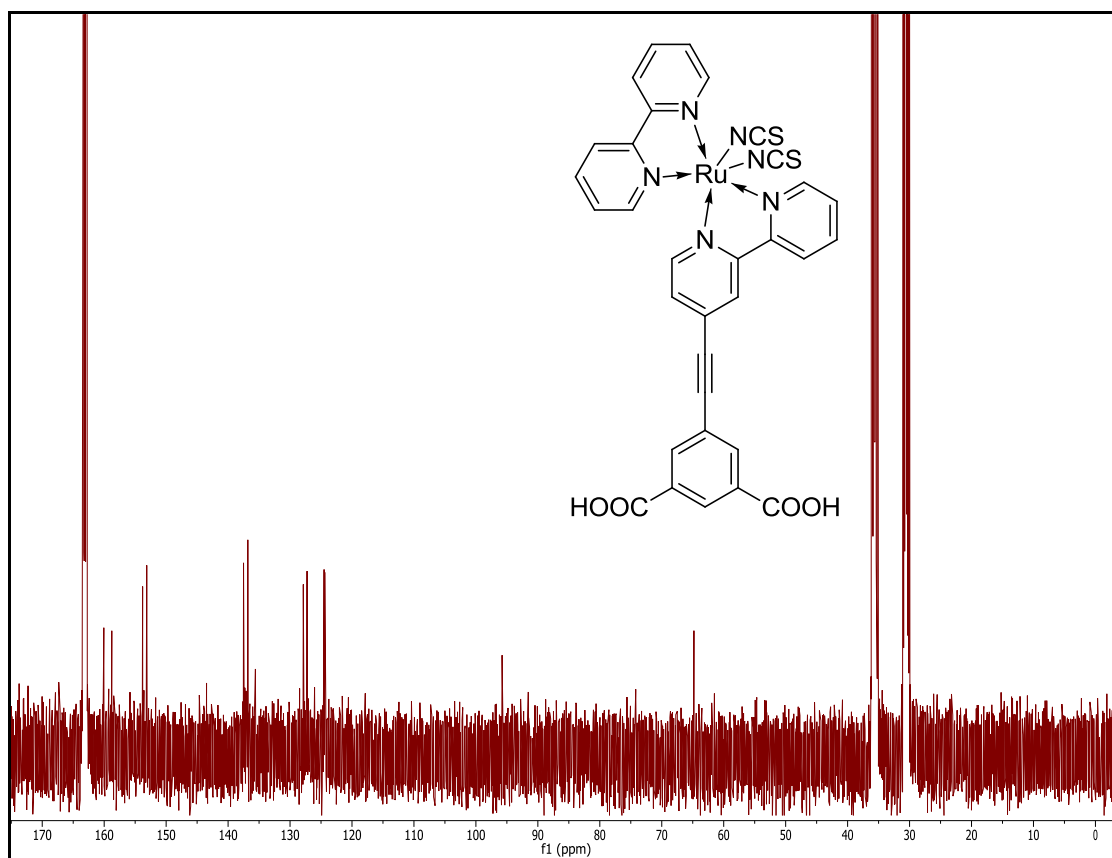
**Figure A 24** Top: Actual spectrum; bottom: calculated:  $[M+Na]^+$

16.  $\text{Ru}(\text{NCS})_2[2,2'\text{-Bipyridine}][\text{L1}]$ : AK1Figure A 25  $^1\text{H}$  NMR of two separate samples of AK1 in  $\text{DMSO-d}_6$

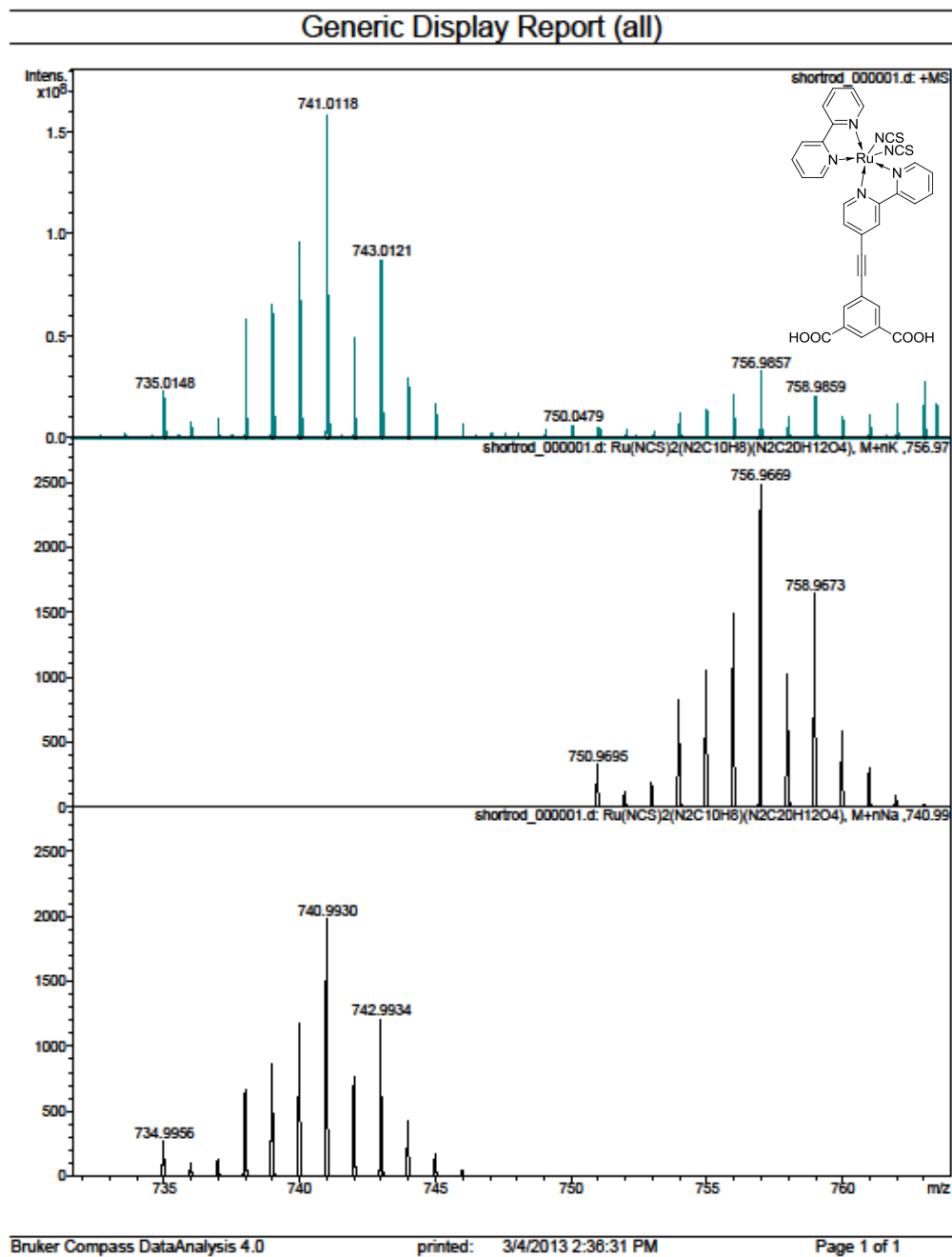


**Figure A 26**  $^1\text{H}$  NMR in DMSO- $d_6$  with DMF present in spectrum

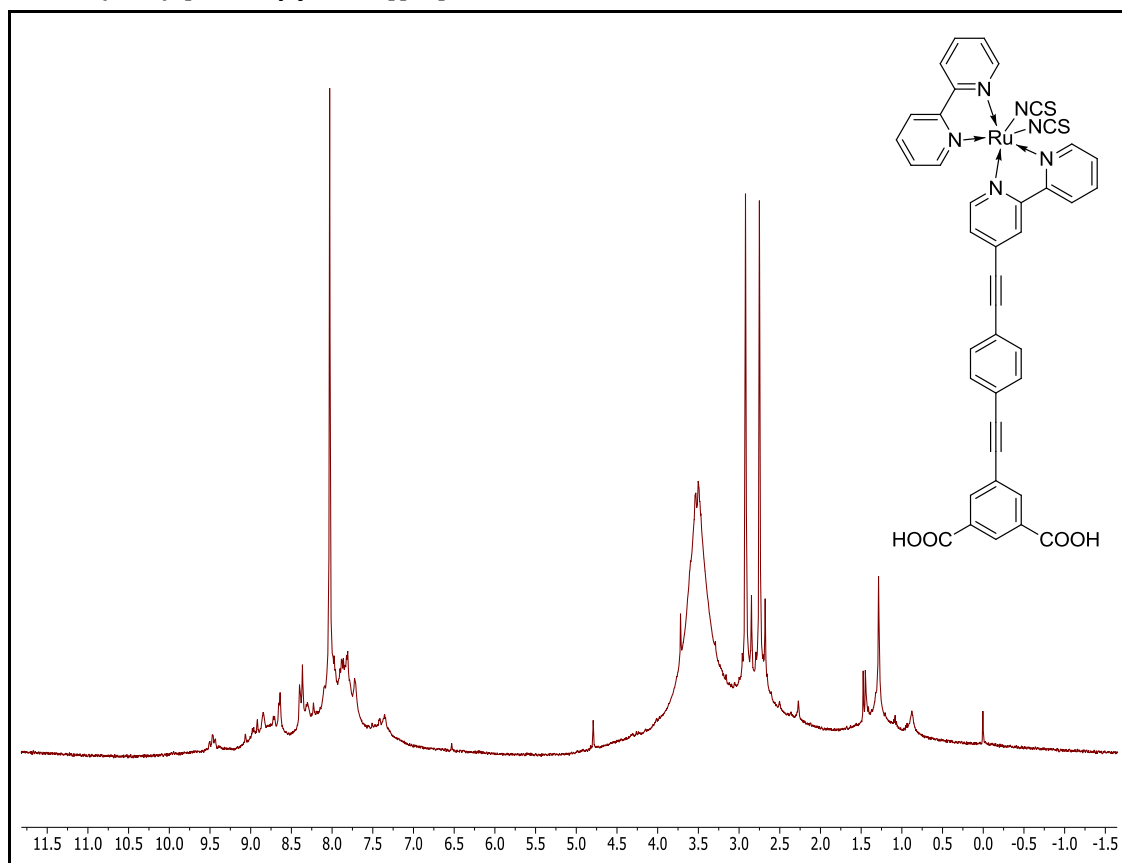




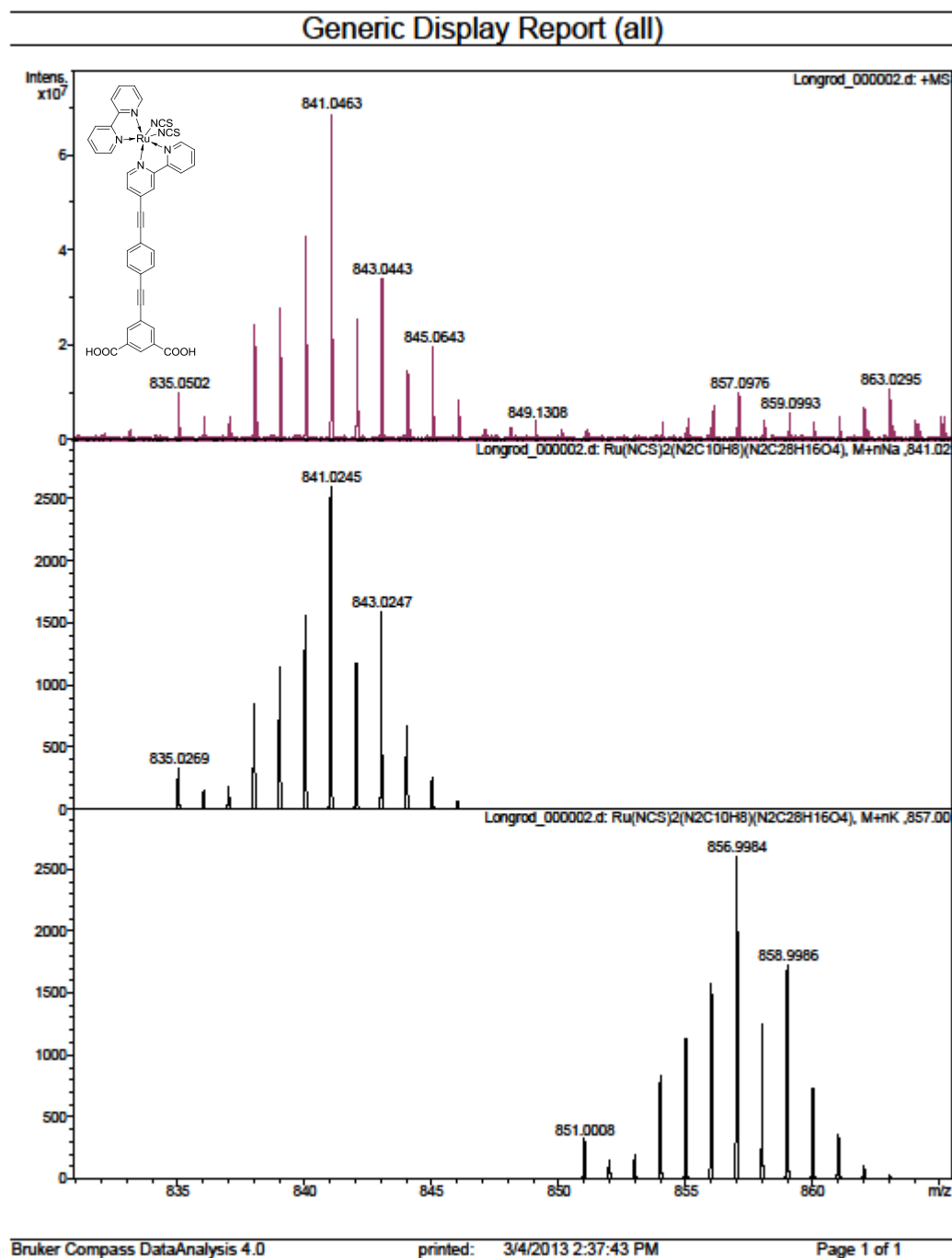
**Figure A 27**  $^{13}\text{C}$  NMR (DMF- $d_7$ )  $\delta$  160.06, 158.77, 153.80, 153.13, 137.51, 136.81, 135.59, 127.86, 127.26, 126.04, 124.40, 95.77, 64.81, 35.10.



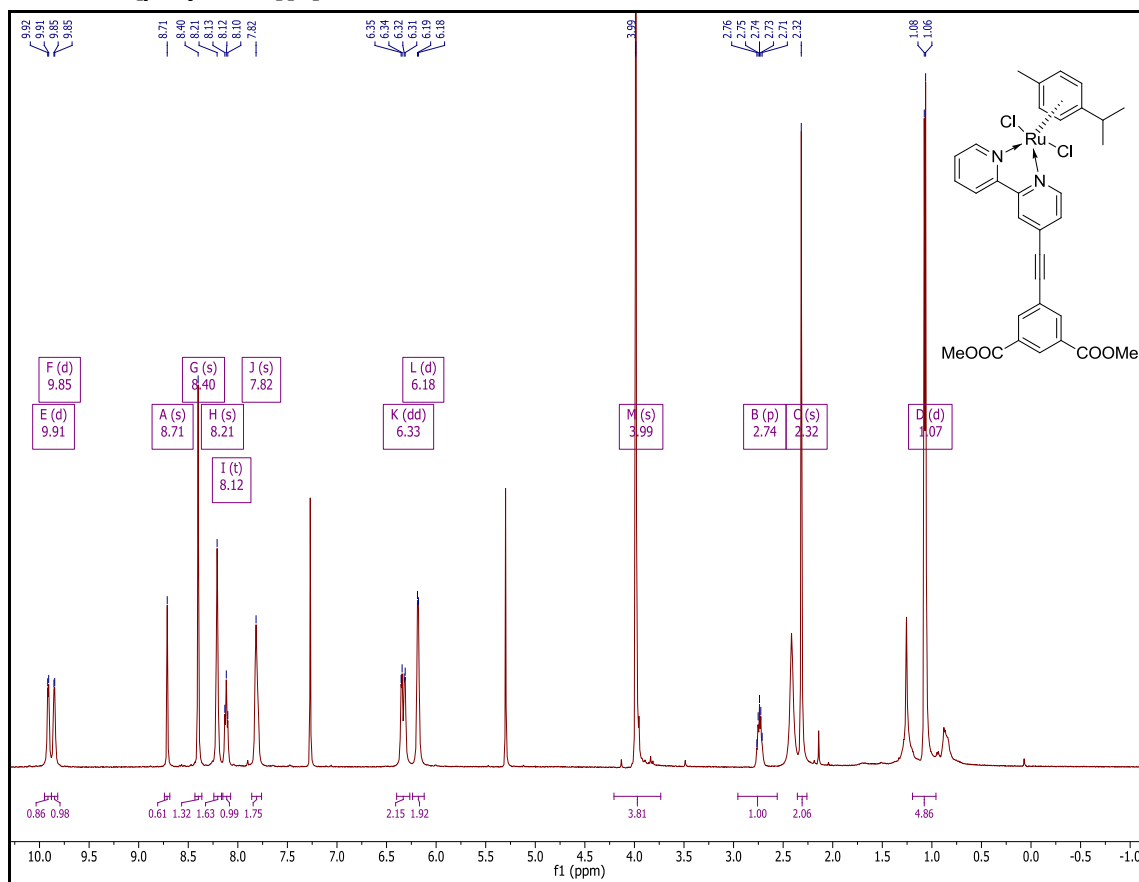
**Figure A 28** Top: Actual spectrum; middle: calculated:  $[M+K]^+$ ; bottom: calculated:  $[M+Na]^+$

17.  $\text{Ru}(\text{NCS})_2[2,2'\text{-Bipyridine}][\text{L2}]$ : AK2**Figure A 29**  $^1\text{H}$  NMR in  $\text{DMSO-d}_6$ 

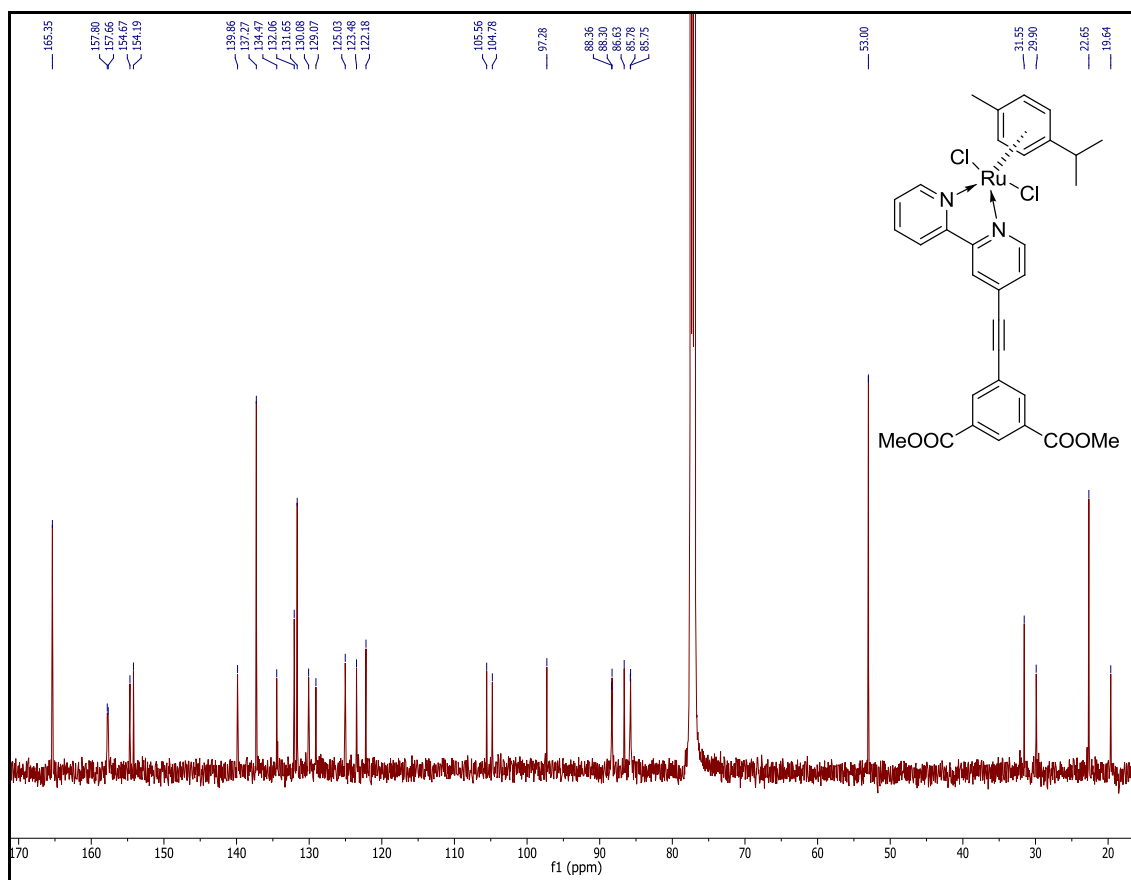
$^{13}\text{C}$  NMR not recorded due to low solubility.



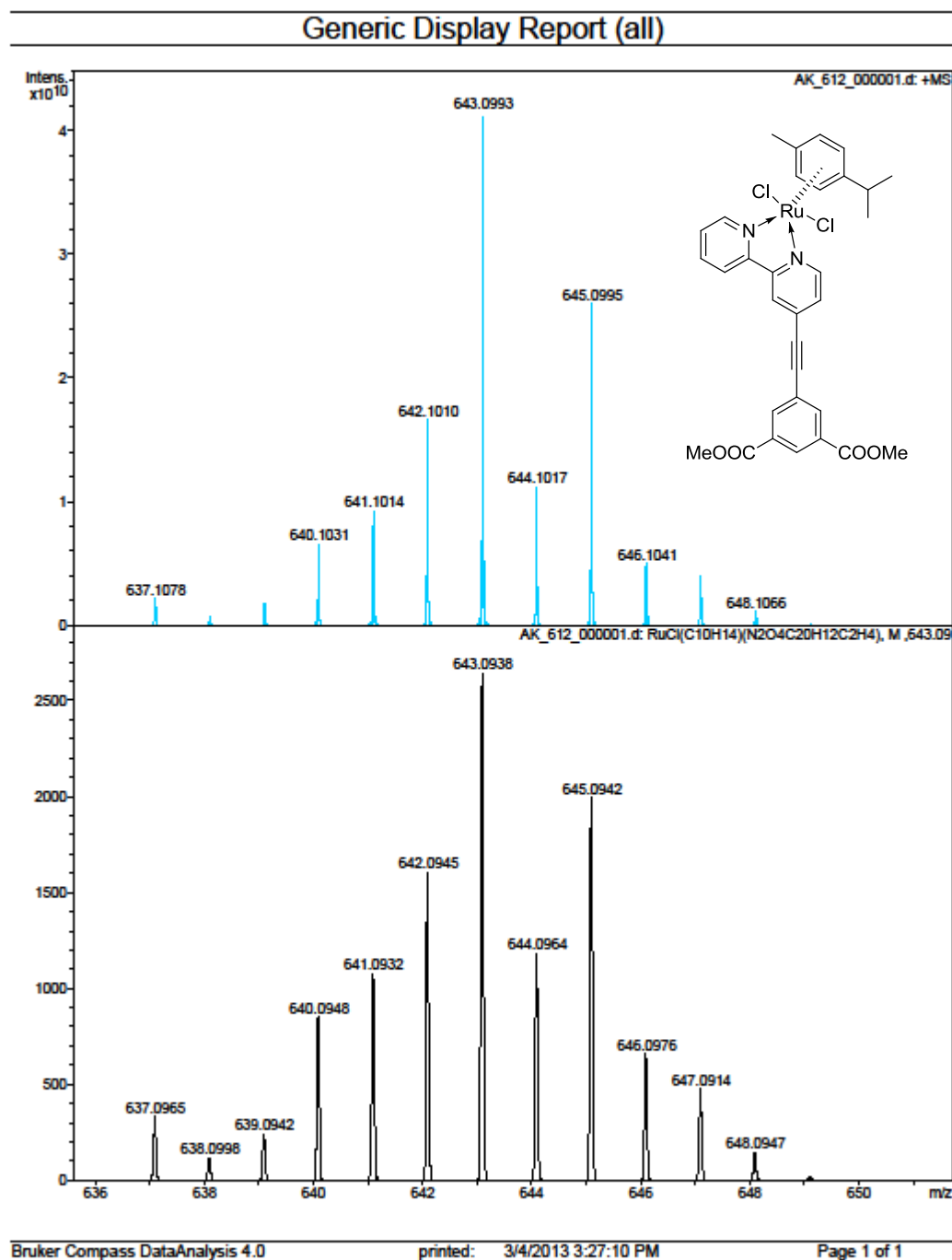
**Figure A 30** Top: Actual spectrum; middle: calculated:  $[M+Na]^+$ ; bottom: calculated:  $[M+K]^+$

18.  $\text{RuCl}_2[\text{p-cymene}][6]$ : 16

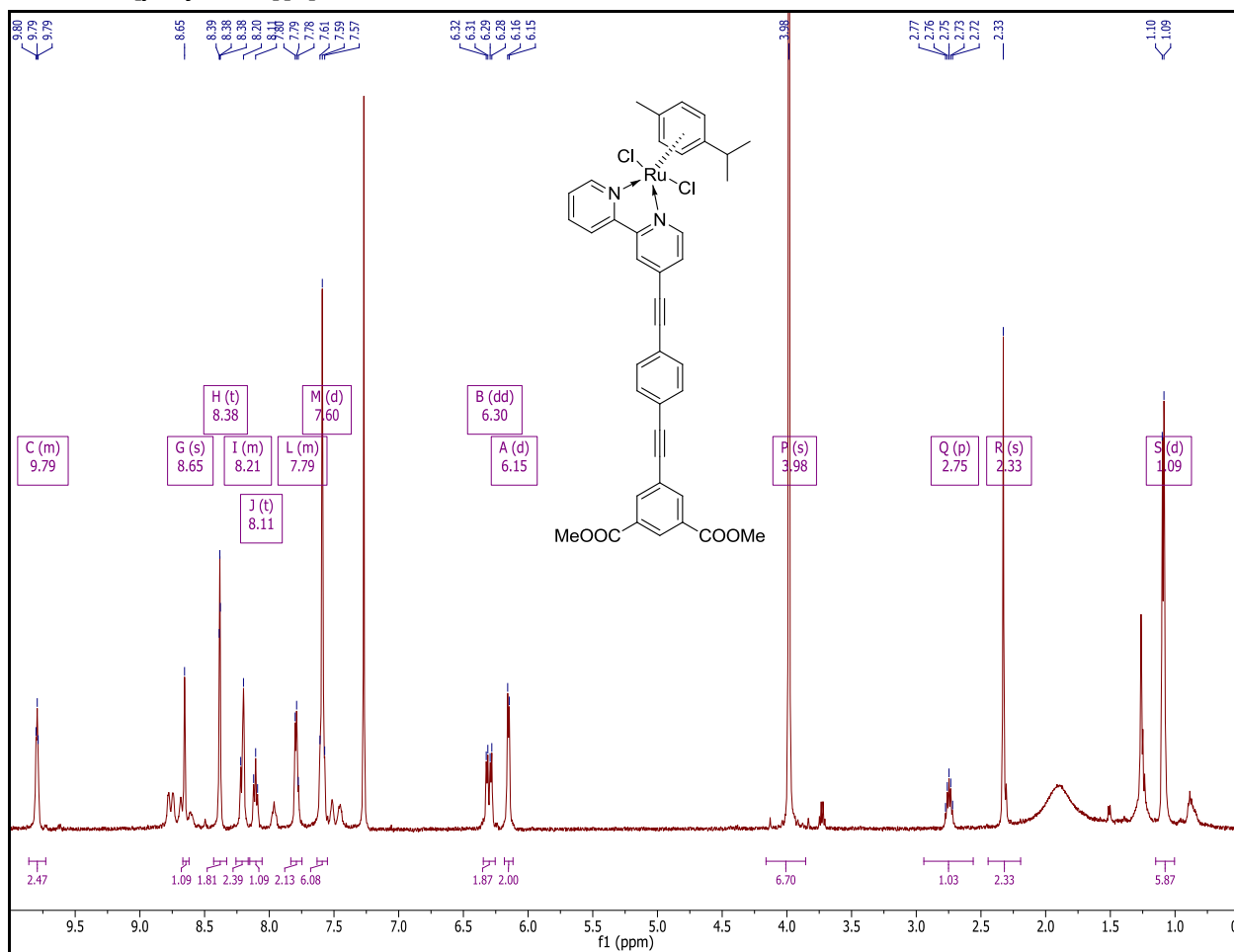
**Figure A 31**  $^1\text{H}$  NMR ( $\text{CDCl}_3$ )  $\delta$  9.91 (d,  $J = 5.0$  Hz, 1H), 9.85 (d,  $J = 4.0$  Hz, 1H), 8.71 (s, 1H), 8.40 (s, 2H), 8.21 (s, 2H), 8.12 (t,  $J = 7.4$  Hz, 1H), 7.82 (s, 2H), 6.33 (dd,  $J = 15.4, 5.2$  Hz, 2H), 6.18 (d,  $J = 4.9$  Hz, 2H), 3.99 (s, 6H), 2.74 (p,  $J = 6.5$  Hz, 1H), 2.32 (s, 3H), 1.07 (d,  $J = 6.8$  Hz, 6H).



**Figure A 32**  $^{13}\text{C}$  NMR ( $\text{CDCl}_3$ )  $\delta$  165.35, 157.80, 157.66, 154.67, 154.19, 139.86, 137.27, 134.47, 132.06, 131.65, 130.08, 129.07, 125.03, 123.48, 122.18, 105.56, 104.78, 97.28, 88.36, 88.30, 86.63, 85.78, 85.75, 53.00, 31.55, 29.90, 22.65, 19.64.

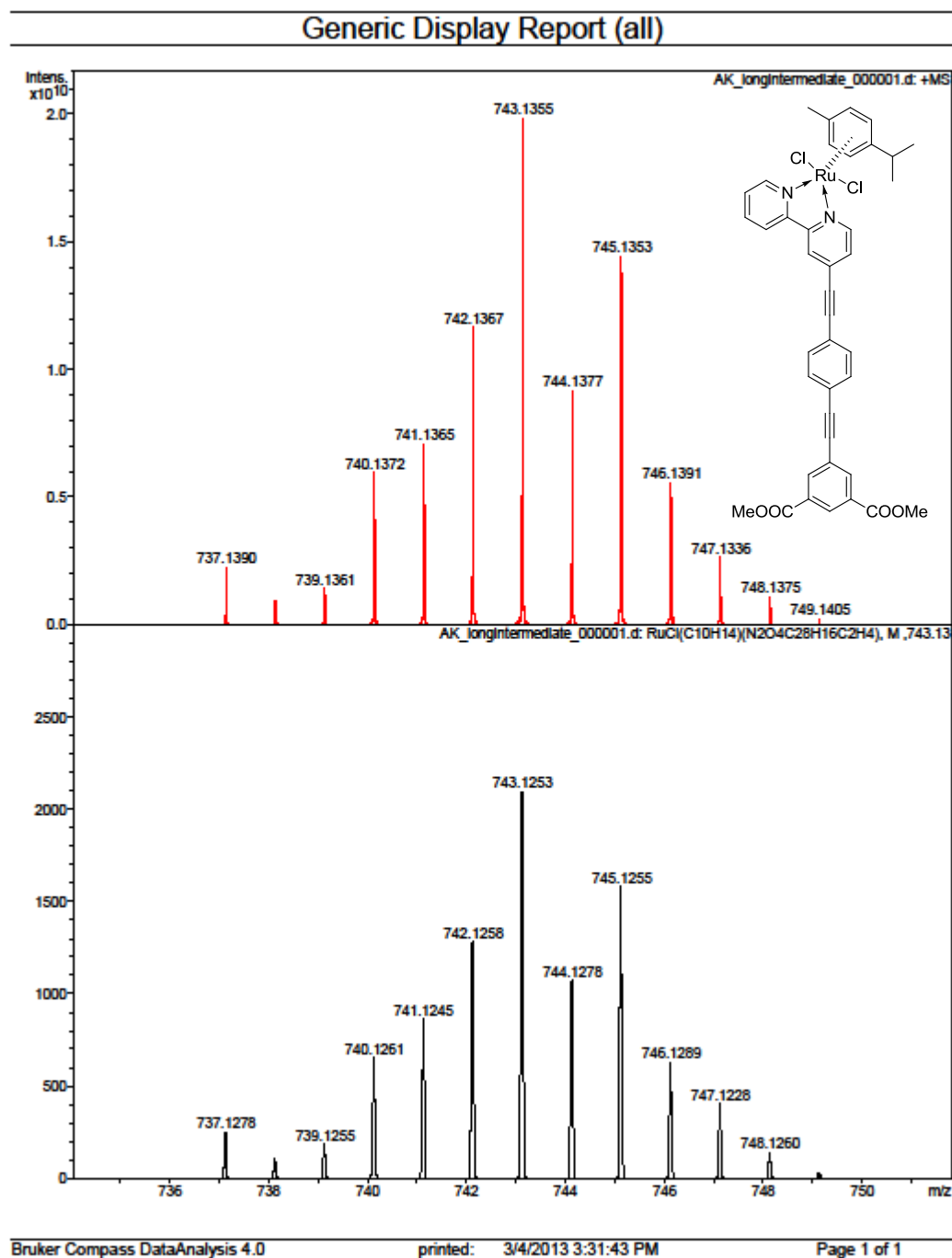


**Figure A 33** Top: Actual spectrum; bottom: calculated:  $[M-Cl]^+$

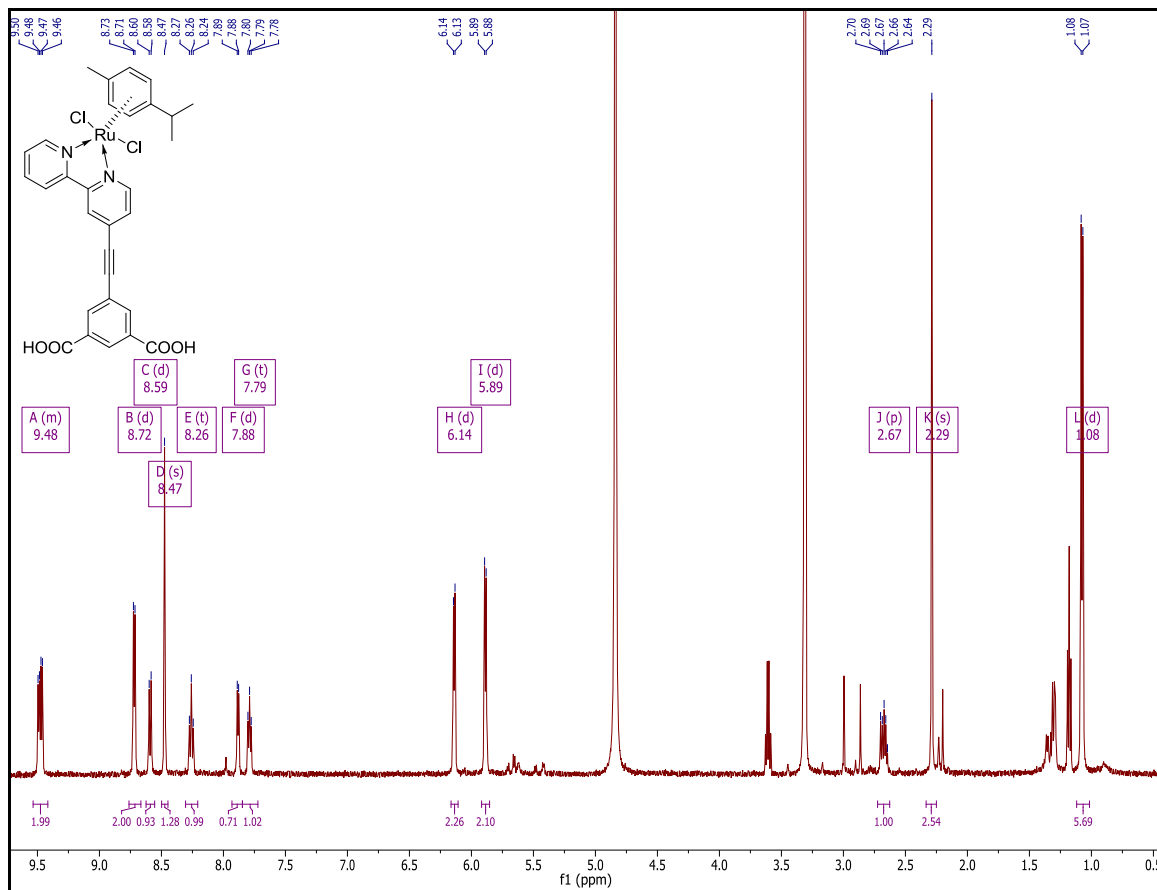
19.  $\text{RuCl}_2[p\text{-cymene}][7]$ :

**Figure A 34**  $^1\text{H}$  NMR ( $\text{CDCl}_3$ )  $\delta$  9.86 – 9.73 (m, 2H), 8.65 (s, 1H), 8.38 (t,  $J = 2.1$  Hz, 2H), 8.26 – 8.16 (m, 2H), 8.11 (t,  $J = 7.6$  Hz, 1H), 7.83 – 7.75 (m, 2H), 7.60 (d,  $J = 9.0$  Hz, 4H), 6.30 (dd,  $J = 15.2, 6.3$  Hz, 2H), 6.15 (d,  $J = 5.9$  Hz, 2H), 3.98 (s, 6H), 2.75 (p,  $J = 6.9$  Hz, 1H), 2.33 (s, 3H), 1.09 (d,  $J = 6.7$  Hz, 6H).

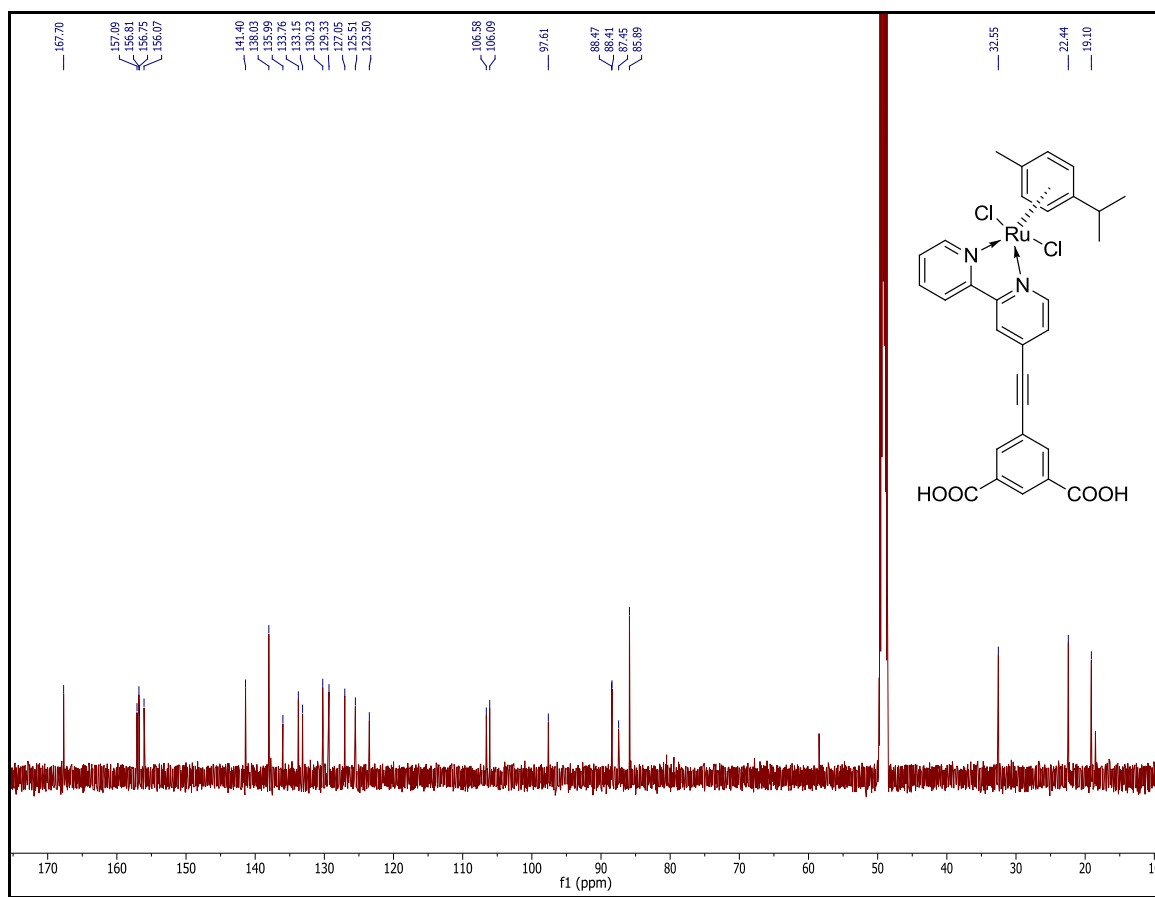




**Figure A 35** Top: Actual spectrum; bottom: calculated:  $[M-Cl]^+$

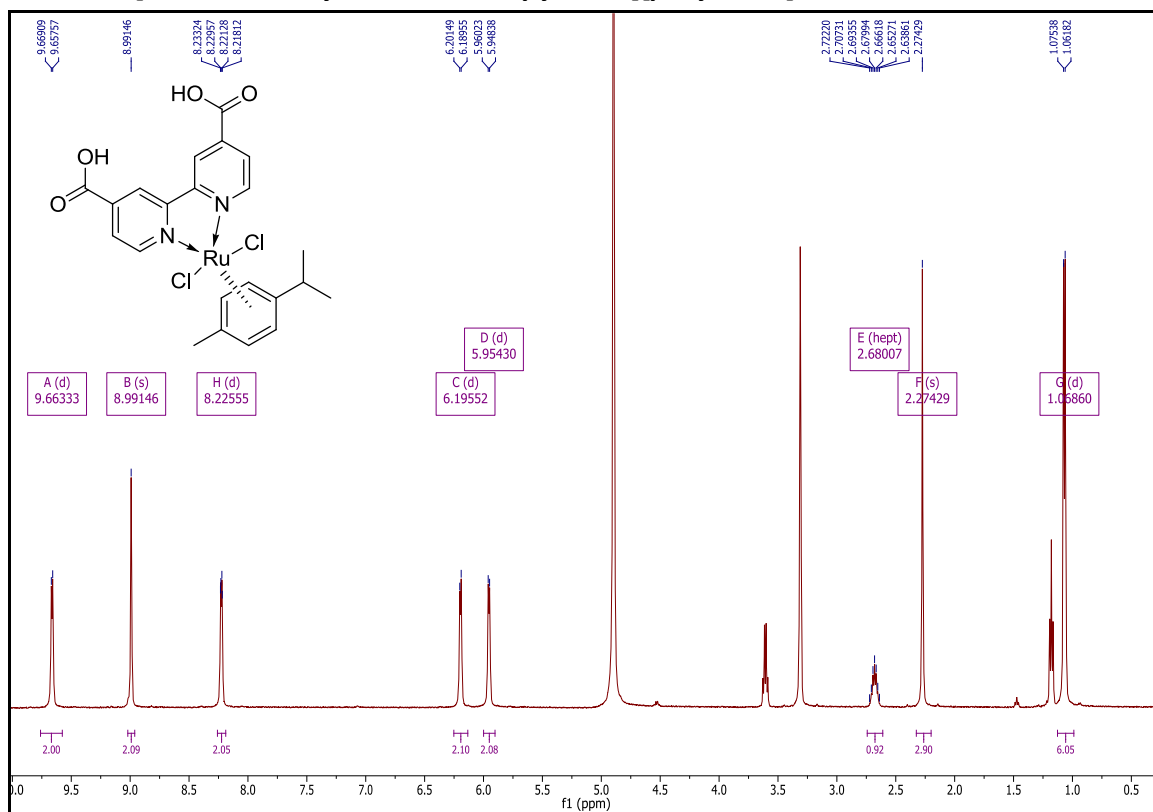
20.  $\text{RuCl}_2[\text{p-cymene}][\text{L1}]$ : 15

**Figure A 36**  $^1\text{H}$  NMR ( $\text{CD}_3\text{OD}$ )  $\delta$  9.53 – 9.42 (m, 2H), 8.72 (d,  $J$  = 6.3 Hz, 2H), 8.59 (d,  $J$  = 7.9 Hz, 1H), 8.47 (s, 2H), 8.26 (t,  $J$  = 7.7 Hz, 1H), 7.88 (d,  $J$  = 5.5 Hz, 1H), 7.79 (t,  $J$  = 6.6 Hz, 1H), 6.14 (d,  $J$  = 6.2 Hz, 2H), 5.89 (d,  $J$  = 6.3 Hz, 2H), 2.67 (p,  $J$  = 13.7, 6.9 Hz, 1H), 2.29 (s, 3H), 1.08 (d,  $J$  = 6.8 Hz, 6H).

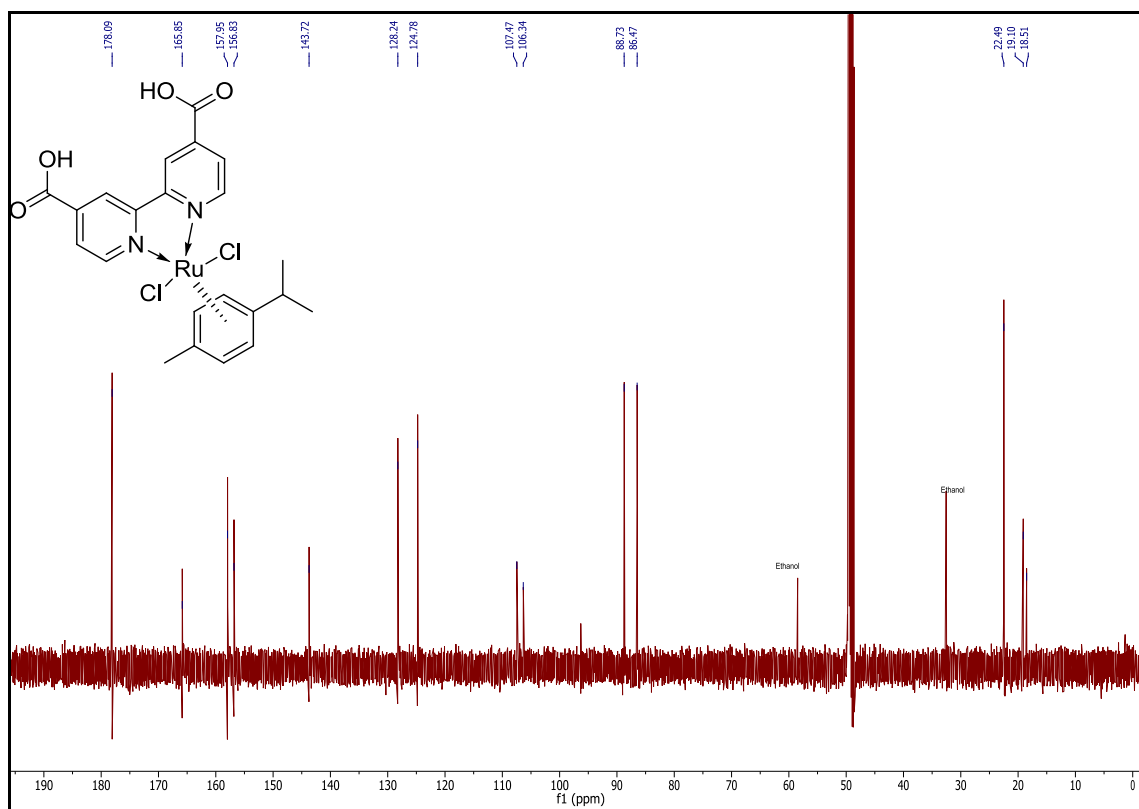


**Figure A 37**  $^{13}\text{C}$  NMR ( $\text{CD}_3\text{OD}$ )  $\delta$  167.70, 157.09, 156.81, 156.75, 156.07, 141.40, 138.03, 135.99, 133.76, 133.15, 130.23, 129.33, 127.05, 125.51, 123.50, 106.58, 106.09, 97.61, 88.47, 88.41, 87.45, 85.89, 32.55, 22.44, 19.10.

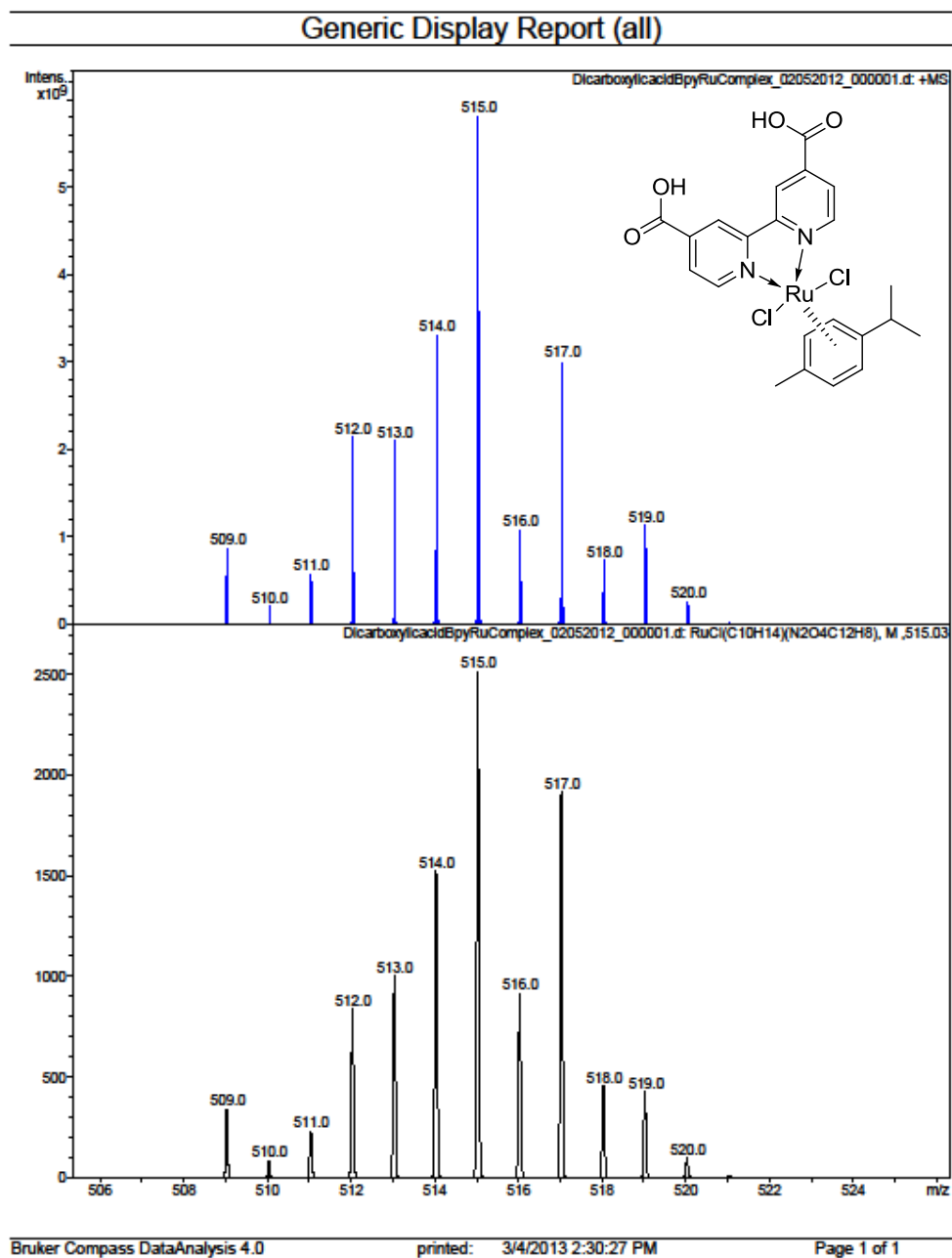
21.  $\text{RuCl}_2[4,4'\text{-Dicarboxylic acid-2,2'-Bipyridine}][p\text{-Cymene}]$ : **22**



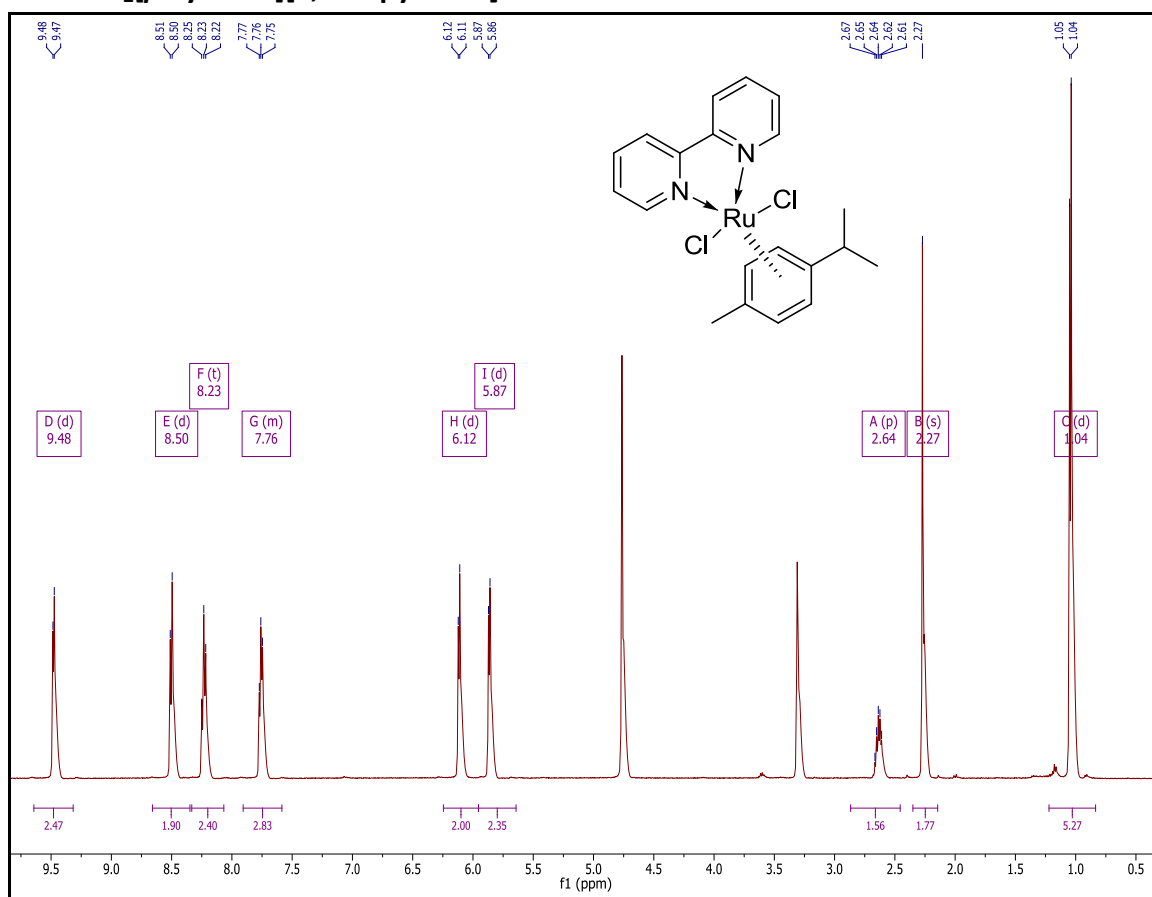
**Figure A 38**  $^1\text{H}$  NMR ( $\text{CD}_3\text{OD}$ )  $\delta$  9.66 (d,  $J$  = 5.8 Hz, 2H), 8.99 (s, 2H), 8.23 (d,  $J$  = 5.8 Hz, 2H), 6.20 (d,  $J$  = 5.9 Hz, 2H), 5.95 (d,  $J$  = 5.9 Hz, 2H), 2.68 (hept,  $J$  = 6.8 Hz, 1H), 2.27 (s, 3H), 1.07 (d,  $J$  = 6.8 Hz, 6H).



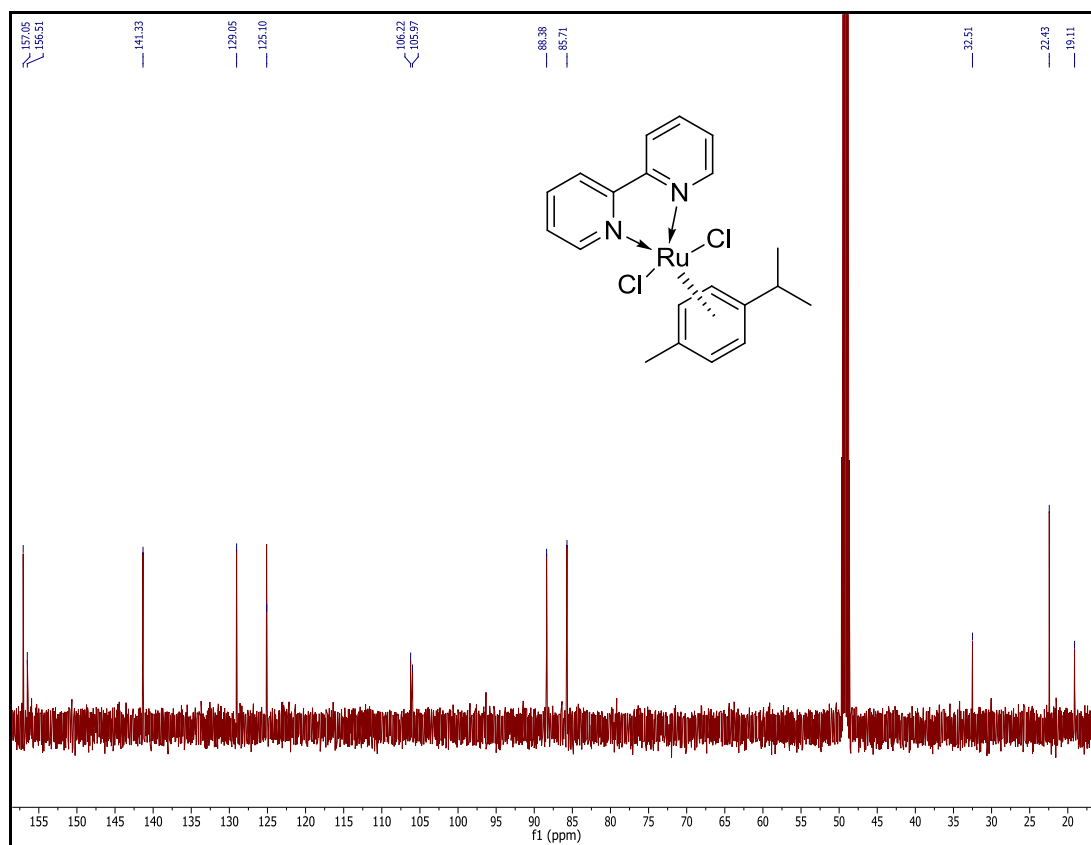
**Figure A 39**  $^{13}\text{C}$  NMR ( $\text{CD}_3\text{OD}$ )  $\delta$  178.09, 165.85, 157.95, 156.83, 143.72, 128.24, 124.78, 107.47, 106.34, 88.73, 86.47, 22.49, 19.10, 18.51.



**Figure A 40** Top: Actual spectrum; bottom: calculated:  $[M-Cl]^+$

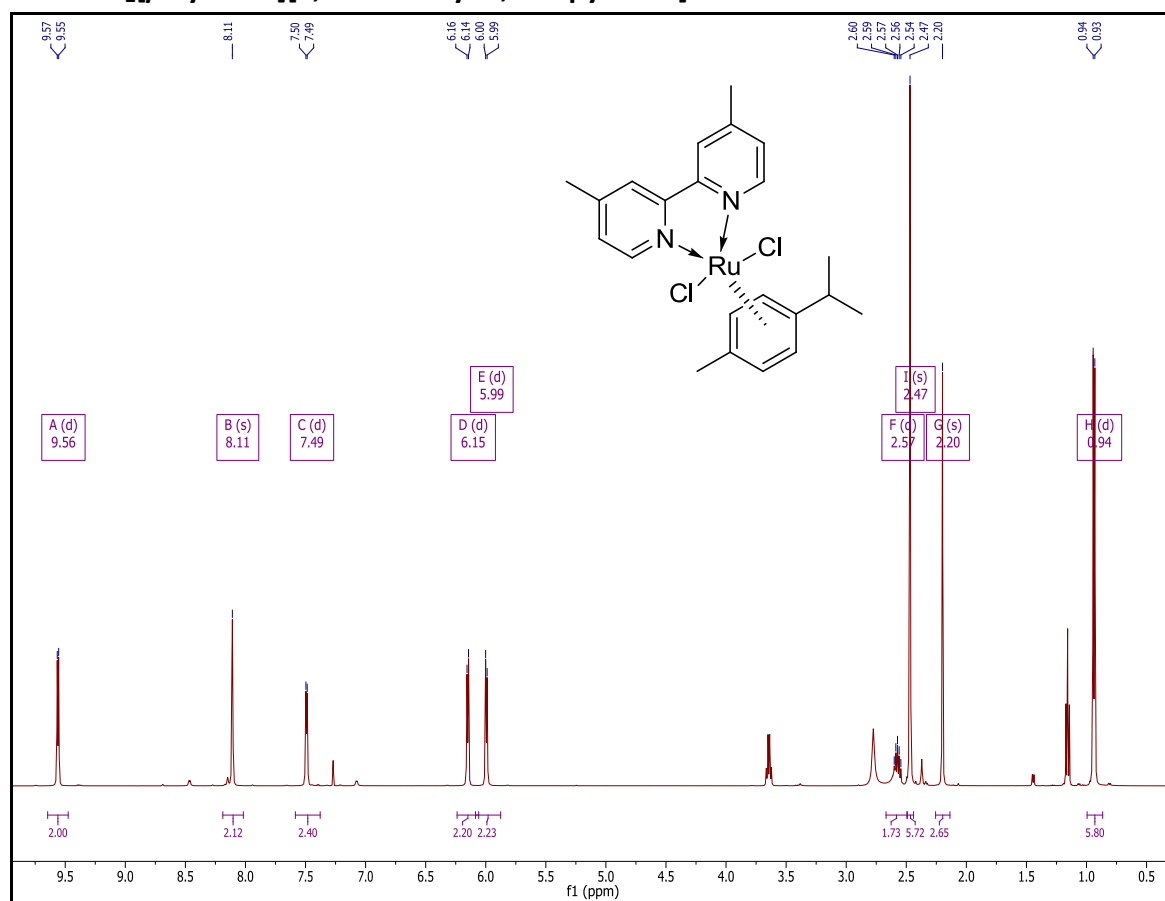
22.  $\text{RuCl}_2[p\text{-cymene}][2,2'\text{-bipyridine}]$ : 17

**Figure A 41**  $^1\text{H}$  NMR (CD<sub>3</sub>OD)  $\delta$  9.48 (d,  $J$  = 5.5 Hz, 2H), 8.50 (d,  $J$  = 8.1 Hz, 2H), 8.23 (t,  $J$  = 8.5 Hz, 2H), 7.91 – 7.59 (m, 2H), 6.12 (d,  $J$  = 6.3 Hz, 2H), 5.87 (d,  $J$  = 6.3 Hz, 2H), 2.64 (p,  $J$  = 13.7, 6.8 Hz, 1H), 2.27 (s, 3H), 1.04 (d,  $J$  = 6.9 Hz, 6H).

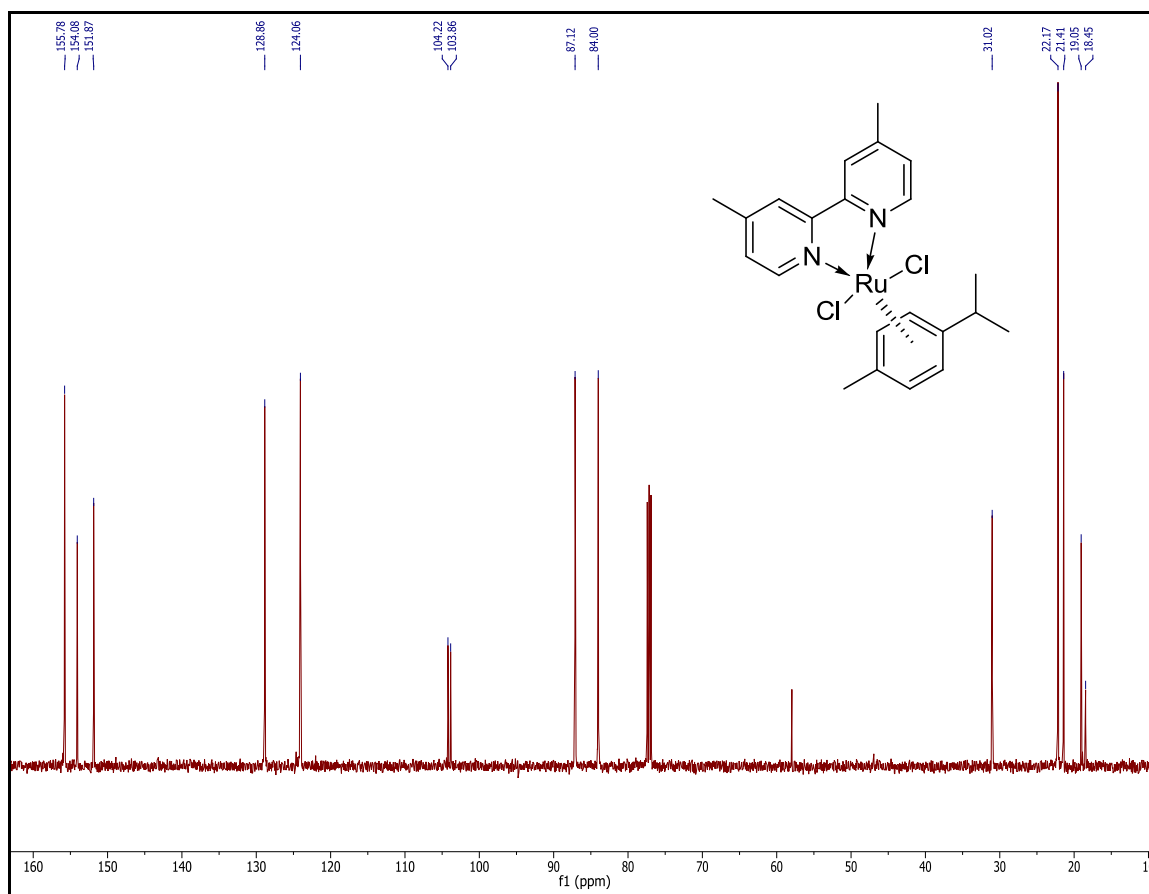


**Figure A 42**  $^{13}\text{C}$  NMR ( $\text{CD}_3\text{OD}$ )  $\delta$  157.05, 156.51, 141.33, 129.05, 125.10, 106.22, 105.97, 88.38, 85.71, 32.51, 22.43, 19.11

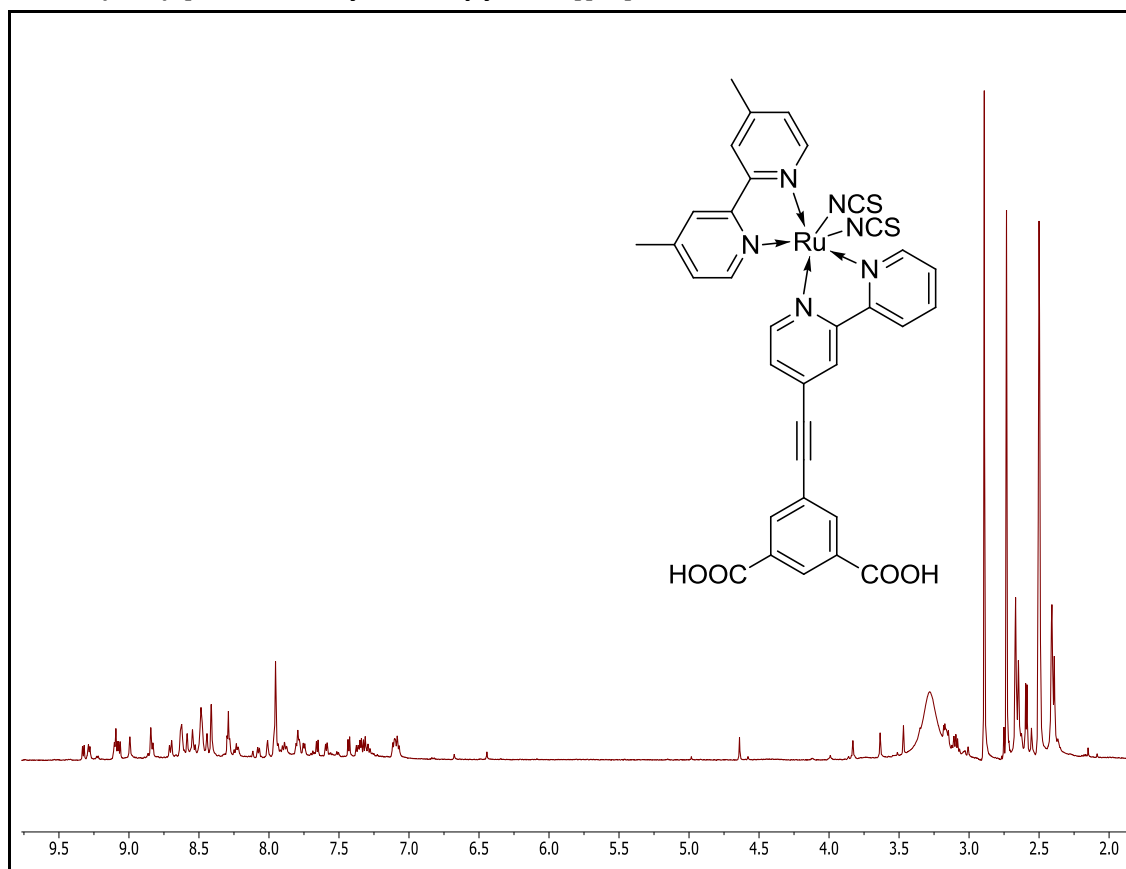


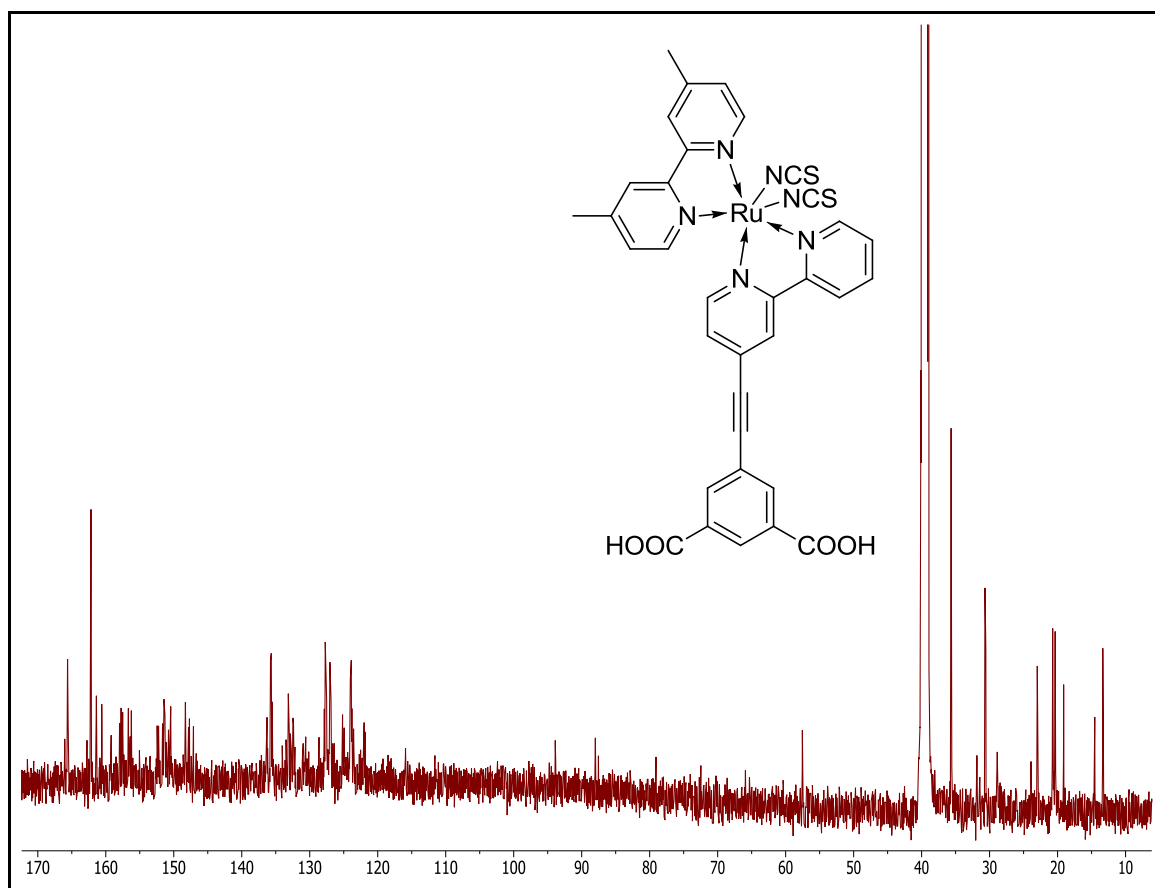
23.  $\text{RuCl}_2[p\text{-cymene}][4,4'\text{-dimethyl-2,2'-bipyridine}]$ : 18

**Figure A 43**  $^1\text{H}$  NMR ( $\text{CDCl}_3$ )  $\delta$  9.56 (d,  $J = 5.8$  Hz, 2H), 8.11 (s, 2H), 7.49 (d,  $J = 5.8$  Hz, 2H), 6.15 (d,  $J = 6.2$  Hz, 2H), 5.99 (d,  $J = 6.2$  Hz, 2H), 2.57 (d,  $J = 6.9$  Hz, 1H), 2.47 (s, 6H), 2.20 (s, 3H), 0.94 (d,  $J = 6.9$  Hz, 6H).

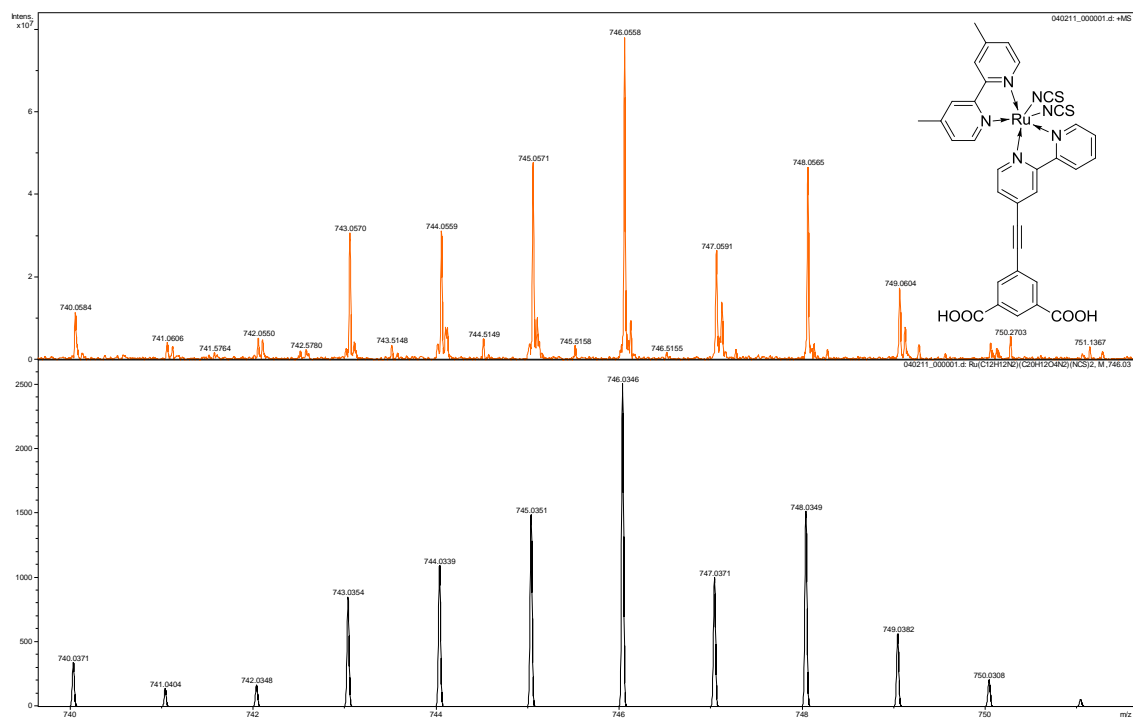


**Figure A 44**  $^{13}\text{C}$  NMR ( $\text{CDCl}_3$ )  $\delta$  155.78, 154.08, 151.87, 128.86, 124.06, 104.22, 103.86, 87.12, 84.00, 31.02, 22.17, 21.41, 19.05, 18.45.

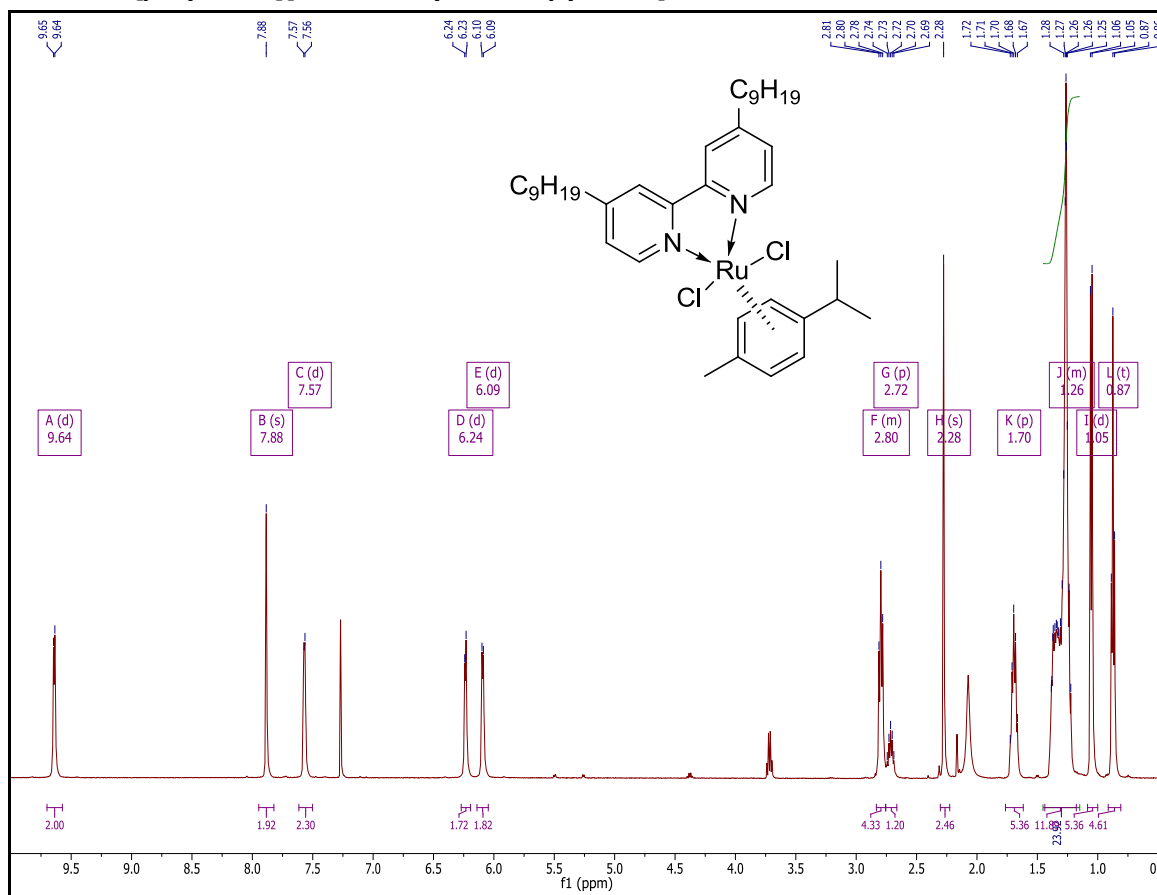
24.  $\text{Ru}(\text{NCS})_2[4,4'\text{-dimethyl-2,2'\text{-bipyridine}}][\text{L1}]$ : AK5**Figure A 45**  $^1\text{H}$  NMR in  $\text{DMSO-d}_6$



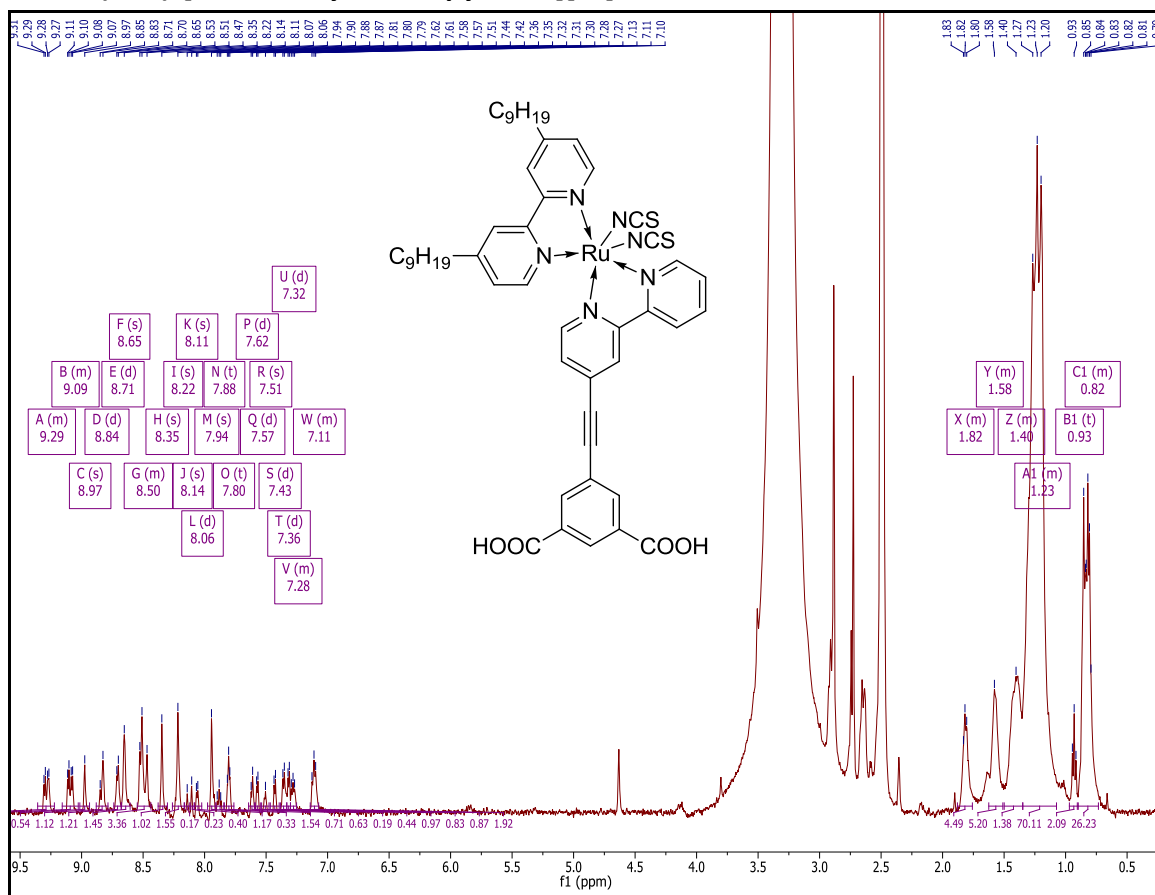
**Figure A 46**  $^{13}\text{C}$  NMR in  $\text{DMSO-d}_6$



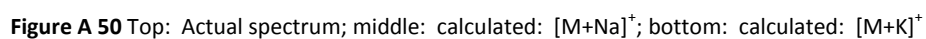
**Figure A 47** Top: Actual spectrum; bottom: calculated:  $[M+Na]^+$

25.  $\text{RuCl}_2[\textit{p}\text{-cymene}][4,4'\text{-dinonyl-2,2'-bipyridine}]$ : 12

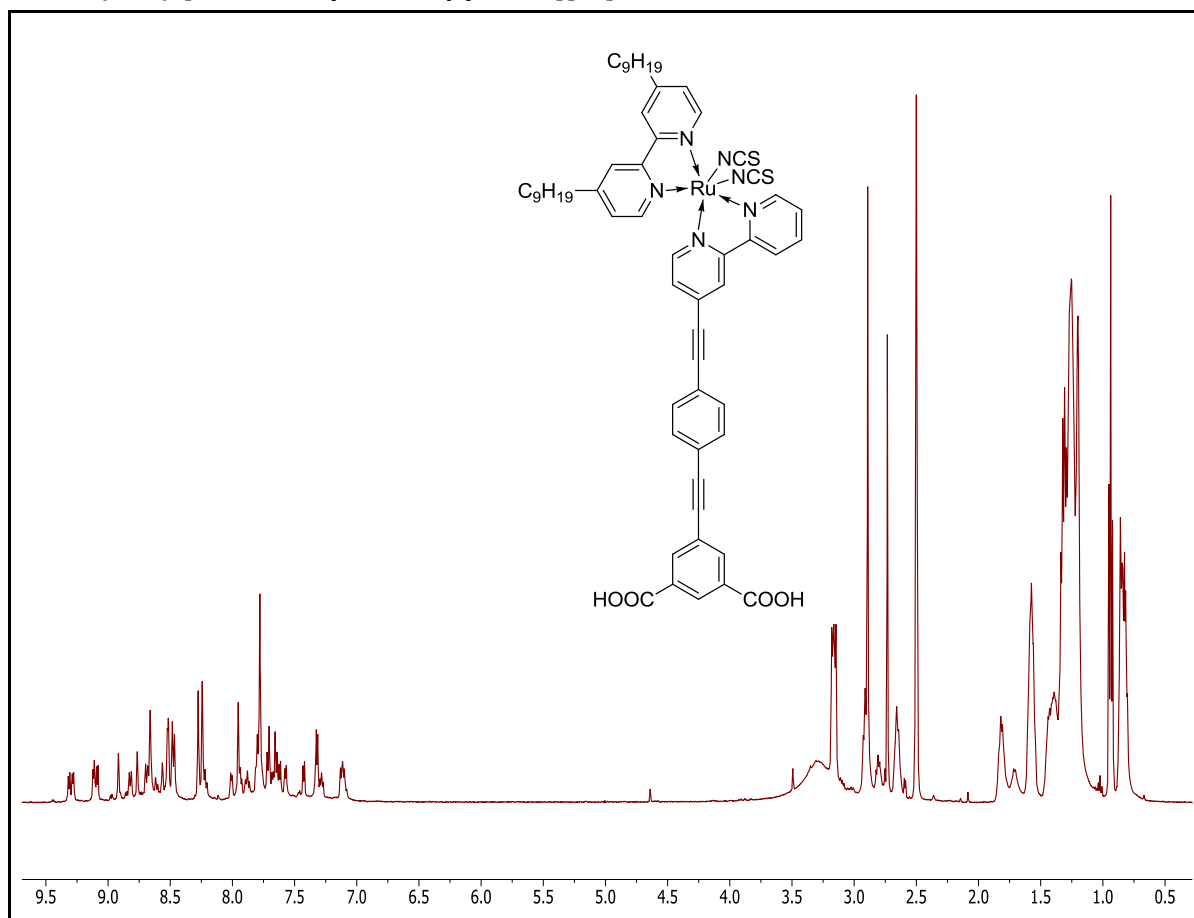
**Figure A 48**  $^1\text{H}$  NMR (CDCl<sub>3</sub>)  $\delta$  9.64 (d,  $J$  = 5.5 Hz, 2H), 7.88 (s, 2H), 7.57 (d,  $J$  = 4.9 Hz, 2H), 6.24 (d,  $J$  = 5.8 Hz, 2H), 6.09 (d,  $J$  = 5.8 Hz, 2H), 2.83 – 2.76 (m, 4H), 2.72 (p,  $J$  = 6.9 Hz, 1H), 2.28 (s, 3H), 1.70 (p,  $J$  = 7.6 Hz, 6H), 1.44 – 1.18 (m, 24H), 1.05 (d,  $J$  = 6.8 Hz, 6H), 0.87 (t,  $J$  = 6.7 Hz, 6H).

26. Ru(NCS)<sub>2</sub>[4,4'-dinonyl-2,2'-Bipyridine][L1]: AK3

**Figure A 49** <sup>1</sup>H NMR (DMSO-d<sub>6</sub>) δ 9.36 – 9.22 (m, 2H), 9.16 – 9.03 (m, 2H), 8.97 (s, 1H), 8.84 (d, *J* = 11.3 Hz, 1H), 8.71 (d, *J* = 6.2 Hz, 1H), 8.65 (s, 2H), 8.55 – 8.44 (m, 3H), 8.35 (s, 2H), 8.22 (s, 2H), 8.14 (s, 1H), 8.11 (s, 1H), 8.06 (d, *J* = 5.7 Hz, 1H), 7.94 (s, 2H), 7.88 (t, *J* = 7.1 Hz, 1H), 7.80 (t, *J* = 5.0 Hz, 1H), 7.62 (d, *J* = 5.9 Hz, 1H), 7.57 (d, *J* = 5.4 Hz, 1H), 7.51 (s, 1H), 7.43 (d, *J* = 5.8 Hz, 1H), 7.36 (d, *J* = 5.9 Hz, 1H), 7.32 (d, *J* = 5.3 Hz, 1H), 7.30 – 7.25 (m, 1H), 7.14 – 7.07 (m, 1H), 1.88 – 1.76 (m, 6H), 1.62 – 1.51 (m, 6H), 1.50 – 1.35 (m, 4H), 1.35 – 1.07 (m, 36H), 0.93 (t, *J* = 7.3 Hz, 4H), 0.90 – 0.73 (m, 24H).





**27. Ru(NCS)<sub>2</sub>[4,4'-dinonyl-2,2'-Bipyridine][L2]: AK4****Figure A 51** <sup>1</sup>H NMR in DMSO-d<sub>6</sub>

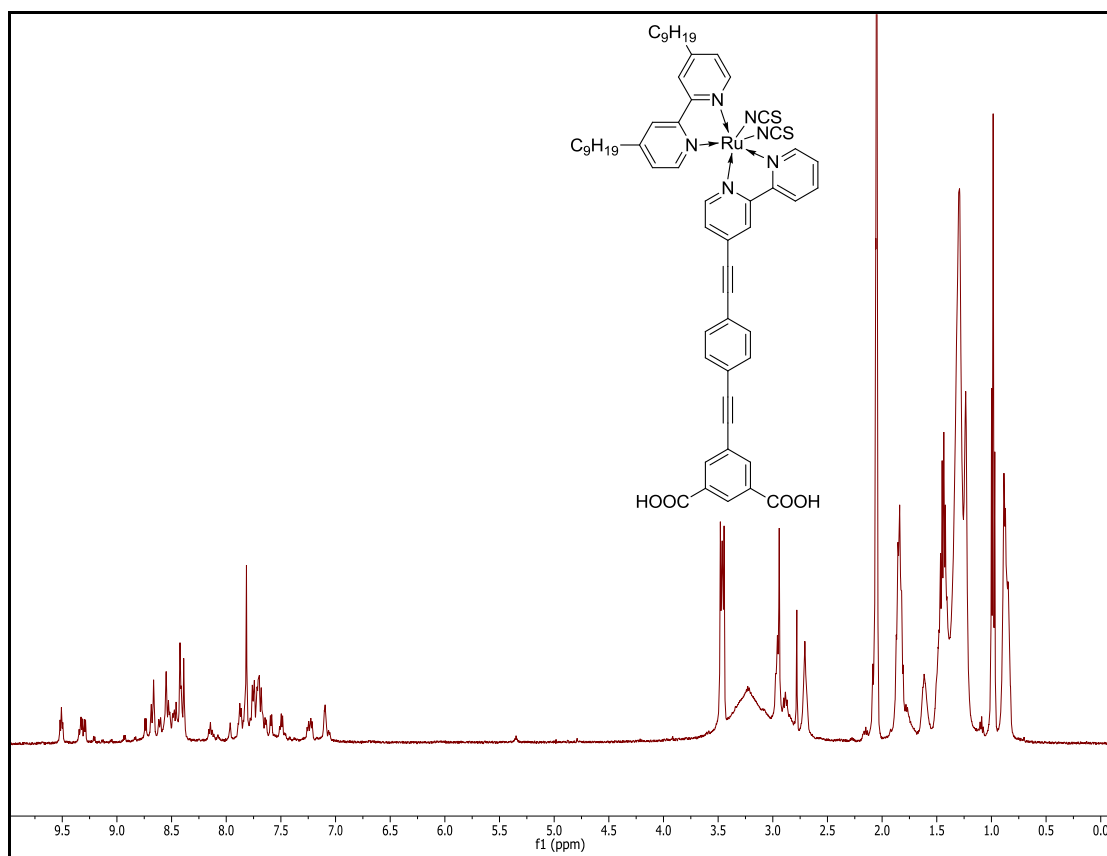


**Figure A 52**  $^1\text{H}$  NMR in Acetone- $\text{d}_6$

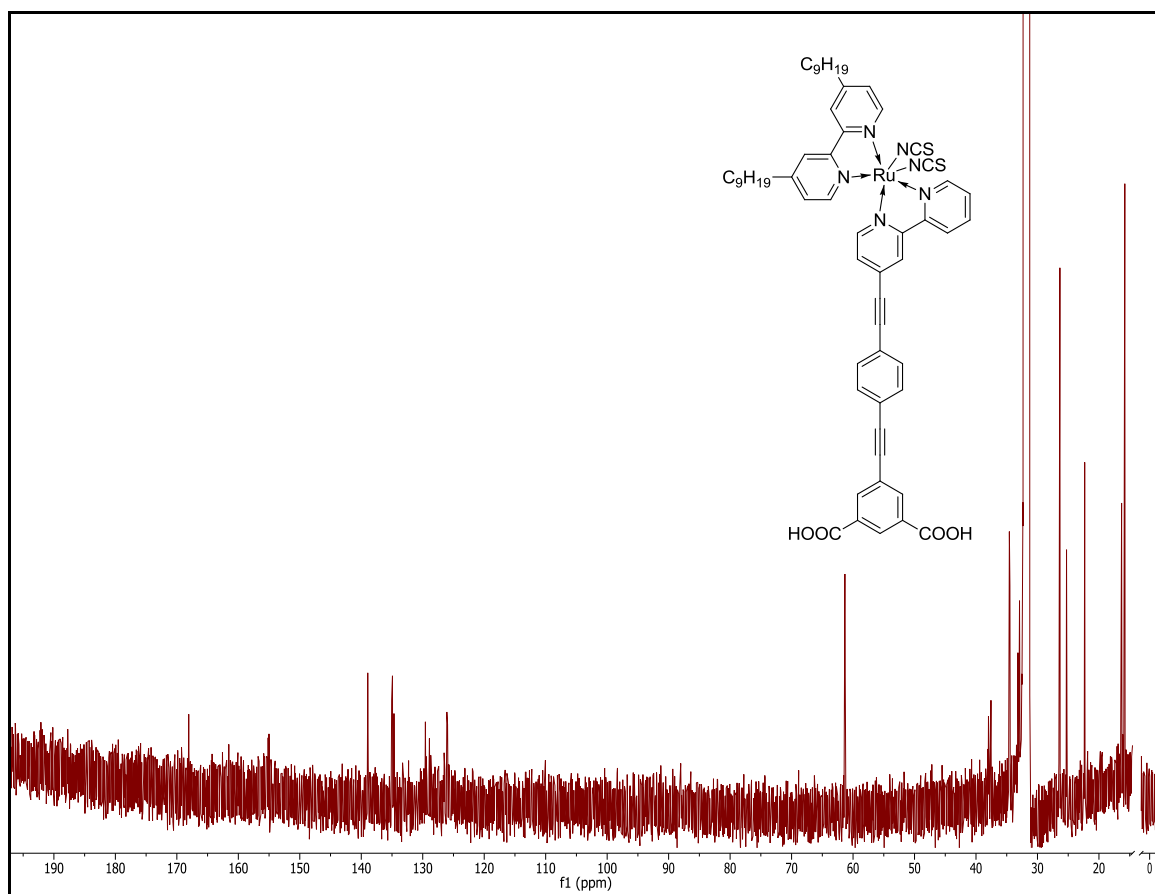
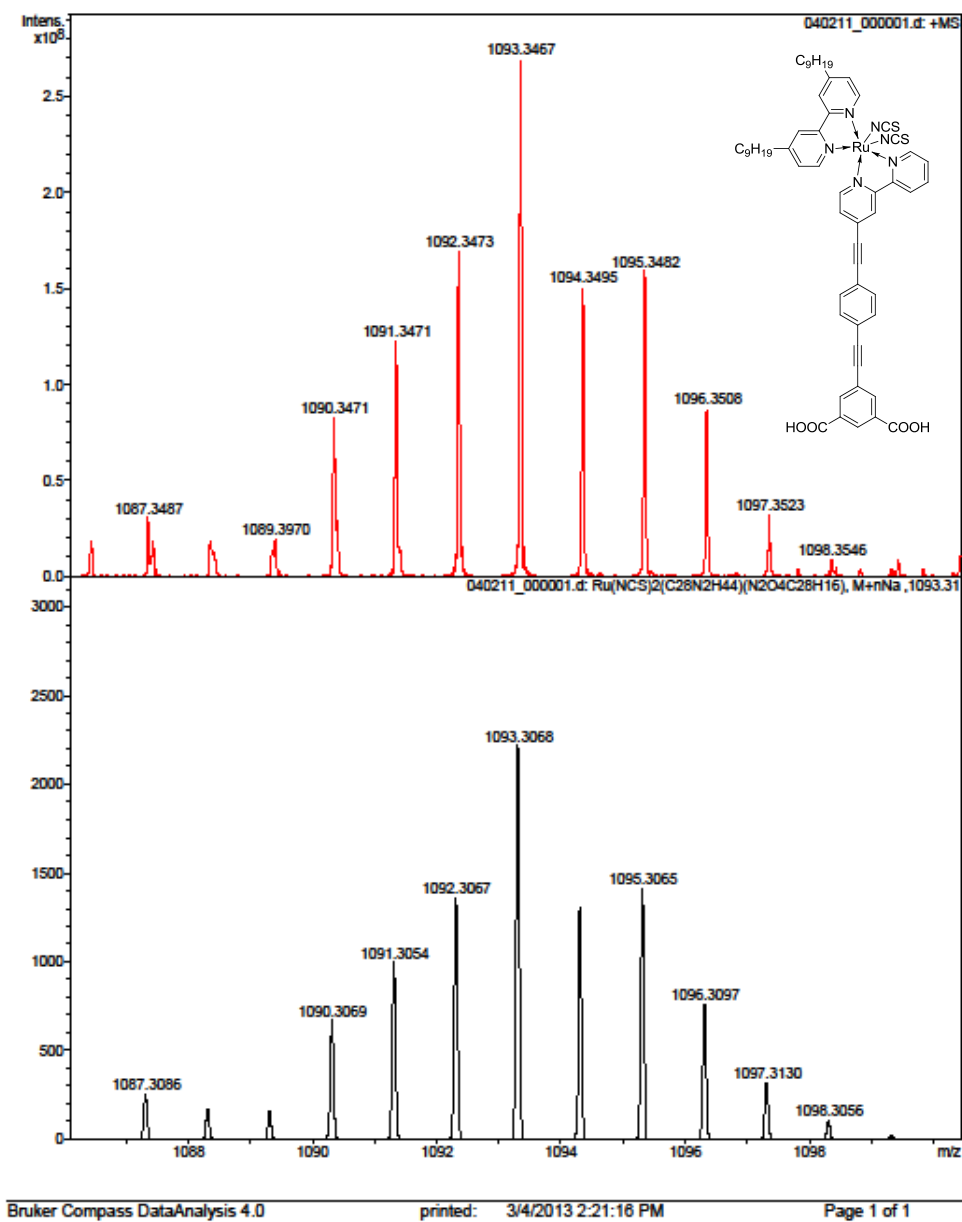
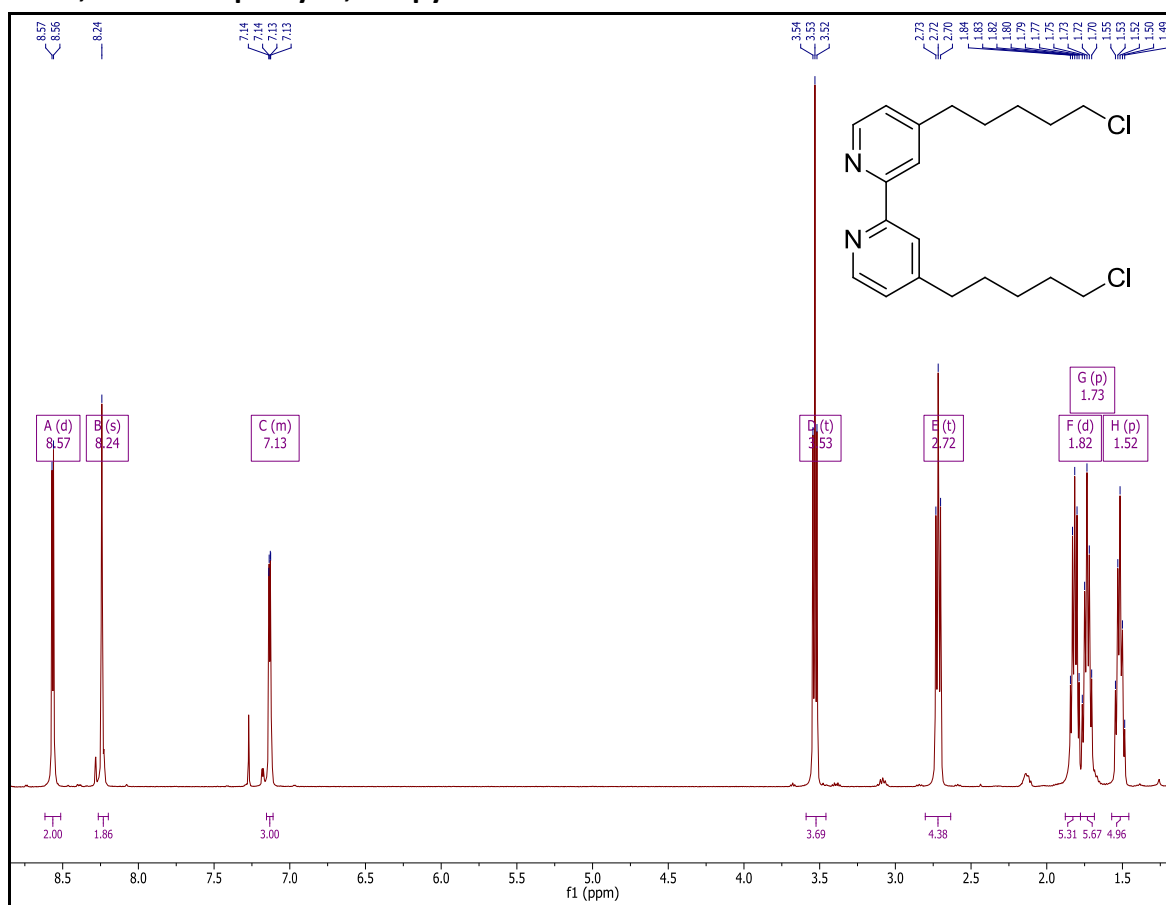


Figure A 53  $^{13}\text{C}$  NMR in Acetone- $\text{d}_6$

## Generic Display Report (all)



**Figure A 54** Top: Actual spectrum; bottom: calculated:  $[M+Na]^+$

28. 4,4'-Dichloropentyl-2,2'-bipyridine: **23**

**Figure A 55**  $^1\text{H}$  NMR ( $\text{CDCl}_3$ )  $\delta$  8.57 (d,  $J = 5.0$  Hz, 2H), 8.24 (s, 2H), 7.15 – 7.11 (m, 2H), 3.53 (t,  $J = 6.7$  Hz, 4H), 2.72 (t,  $J = 7.8$  Hz, 4H), 1.82 (d,  $J = 6.7$  Hz, 4H), 1.73 (p,  $J = 7.7$  Hz, 4H), 1.52 (p,  $J = 7.6$  Hz, 4H).

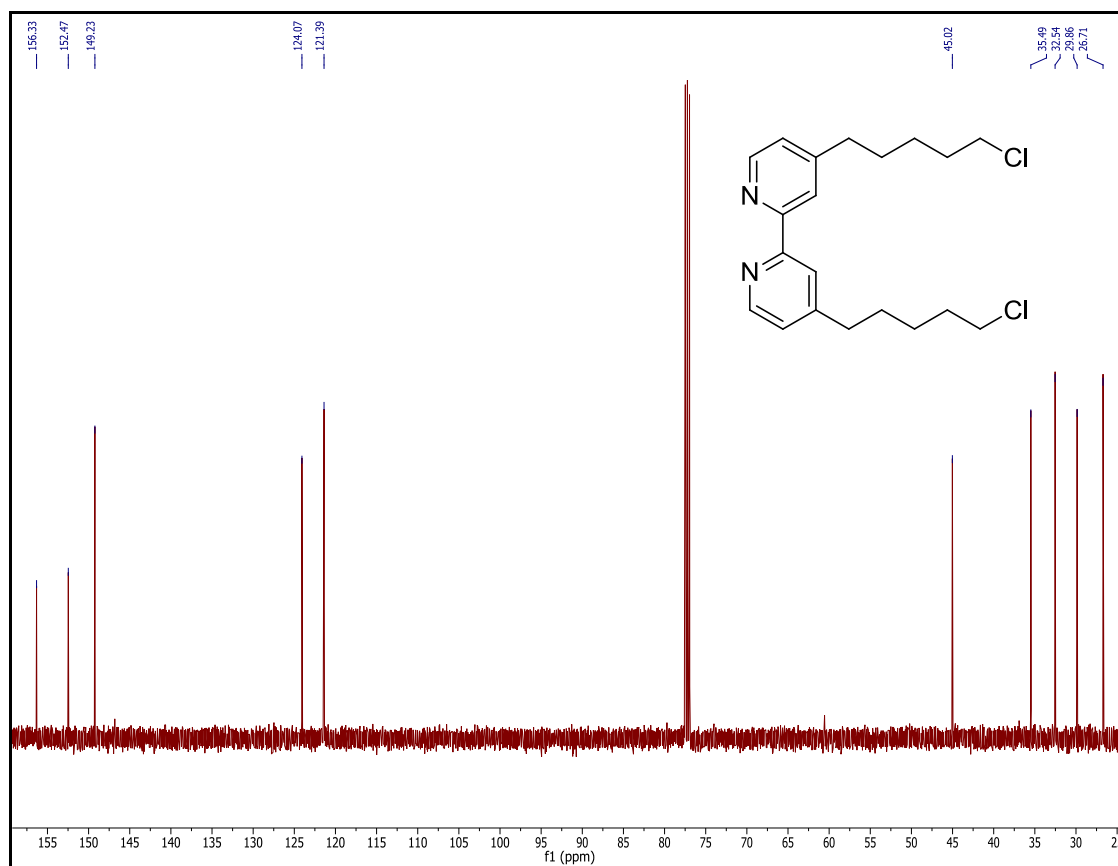
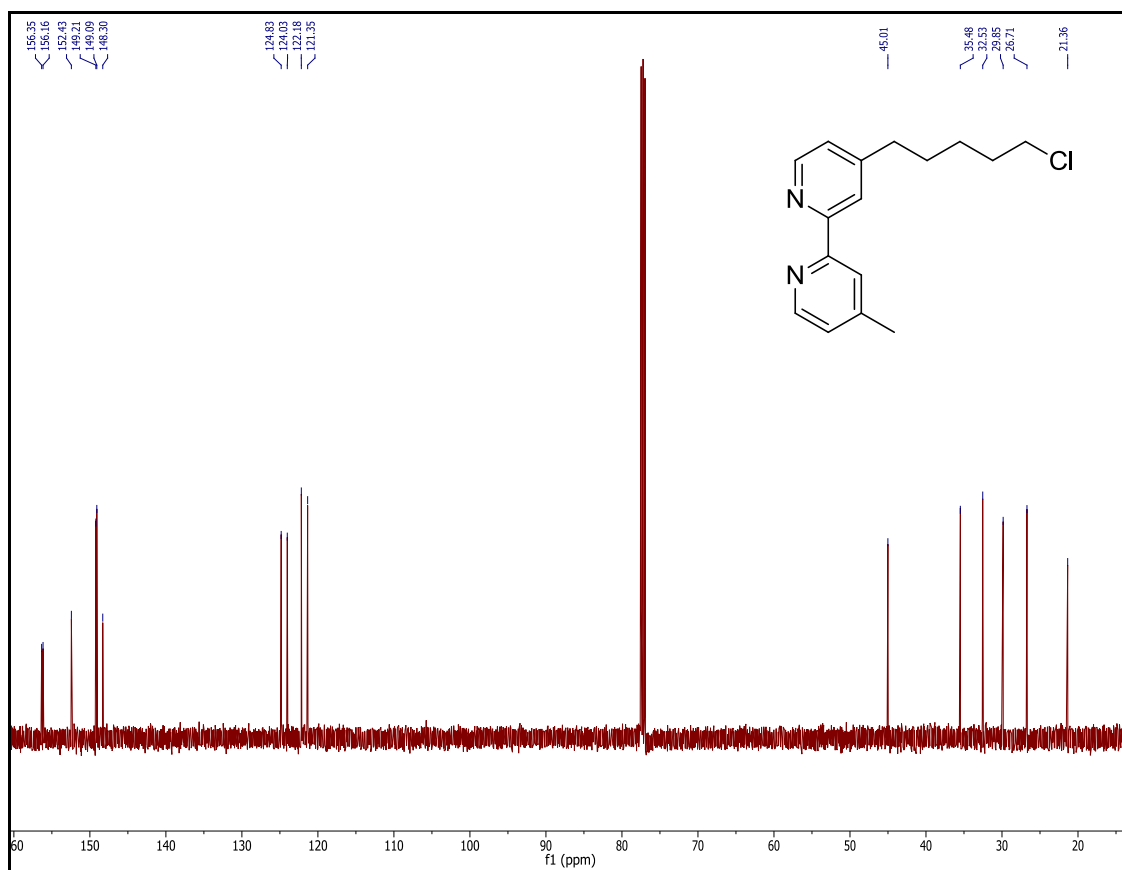


**Figure A 56**  $^{13}\text{C}$  NMR ( $\text{CDCl}_3$ )  $\delta$  156.33, 152.47, 149.23, 124.07, 121.39, 45.02, 35.49, 32.54, 29.86, 26.71

## 29. 4-Chloropentyl-4'-methyl-2,2'-bipyridine: 23a



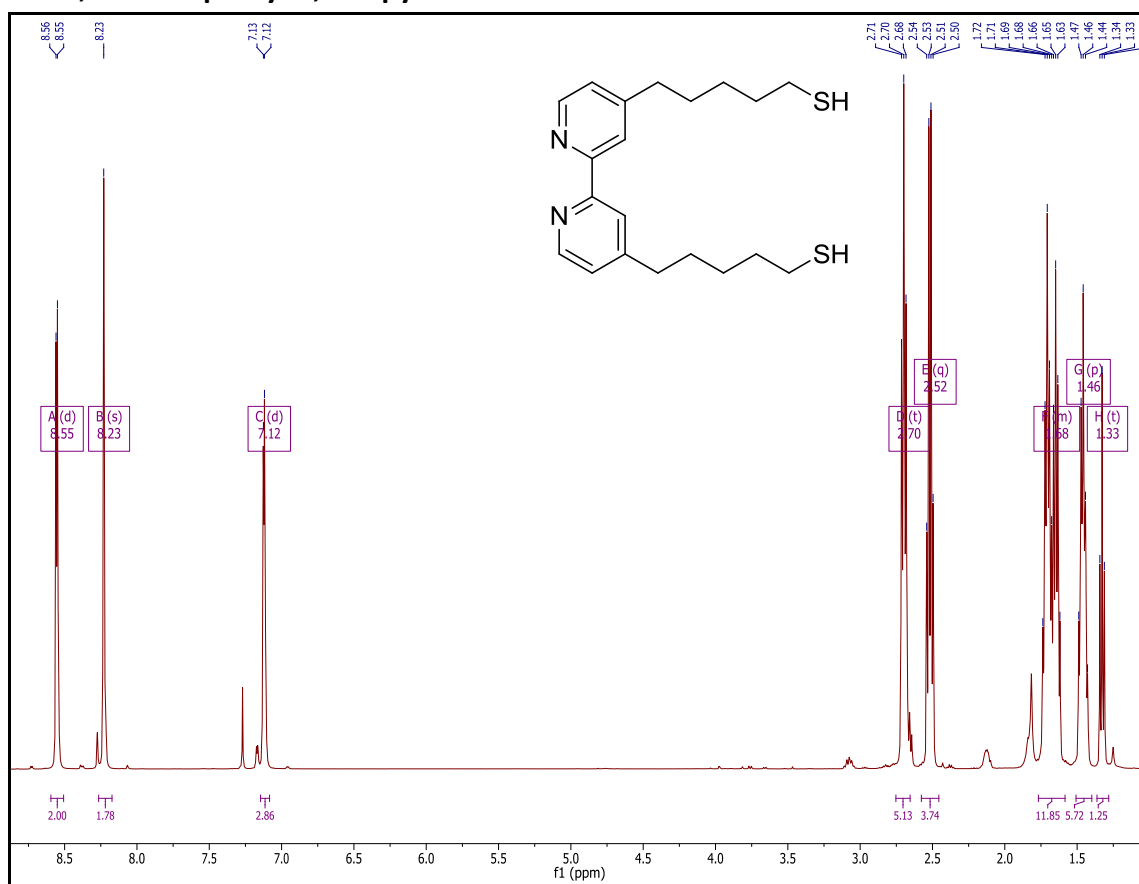
**Figure A 57** <sup>1</sup>H NMR (CDCl<sub>3</sub>) δ 8.55 (d, *J* = 4.9 Hz, 1H), 8.53 (d, *J* = 4.9 Hz, 1H), 8.22 (s, 2H), 7.12 (d, *J* = 4.7 Hz, 2H), 3.52 (t, *J* = 6.7 Hz, 2H), 2.70 (t, *J* = 7.8 Hz, 2H), 2.43 (s, 3H), 1.80 (p, *J* = 6.8 Hz, 2H), 1.72 (p, *J* = 7.8 Hz, 2H), 1.50 (p, *J* = 7.7 Hz, 2H).



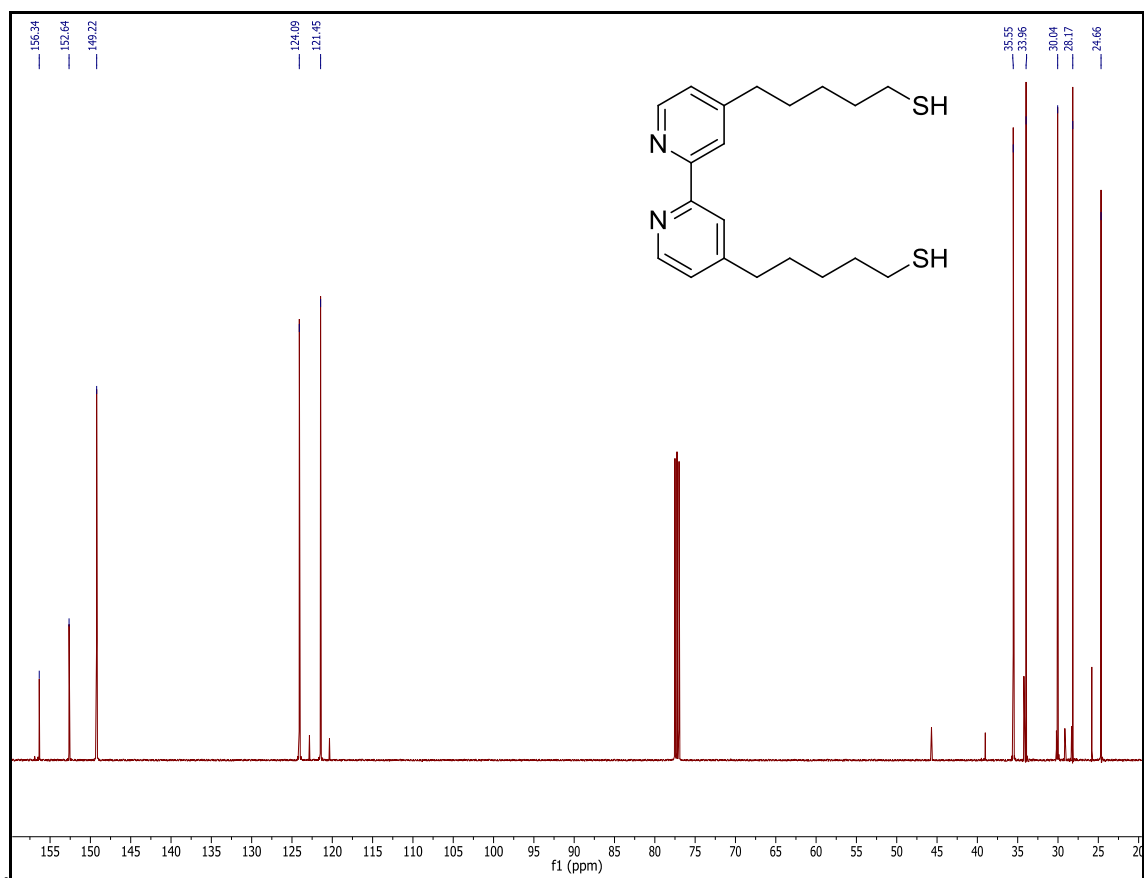
**Figure A 58**  $^{13}\text{C}$  NMR ( $\text{CDCl}_3$ )  $\delta$  156.35, 156.16, 152.43, 149.21, 149.09, 148.30, 124.83, 124.03, 122.18, 121.35, 45.01, 35.48, 32.53, 29.85, 26.71, 21.36.



## 30. 4,4'-Dithiopentyl-2,2'-bipyridine: 25

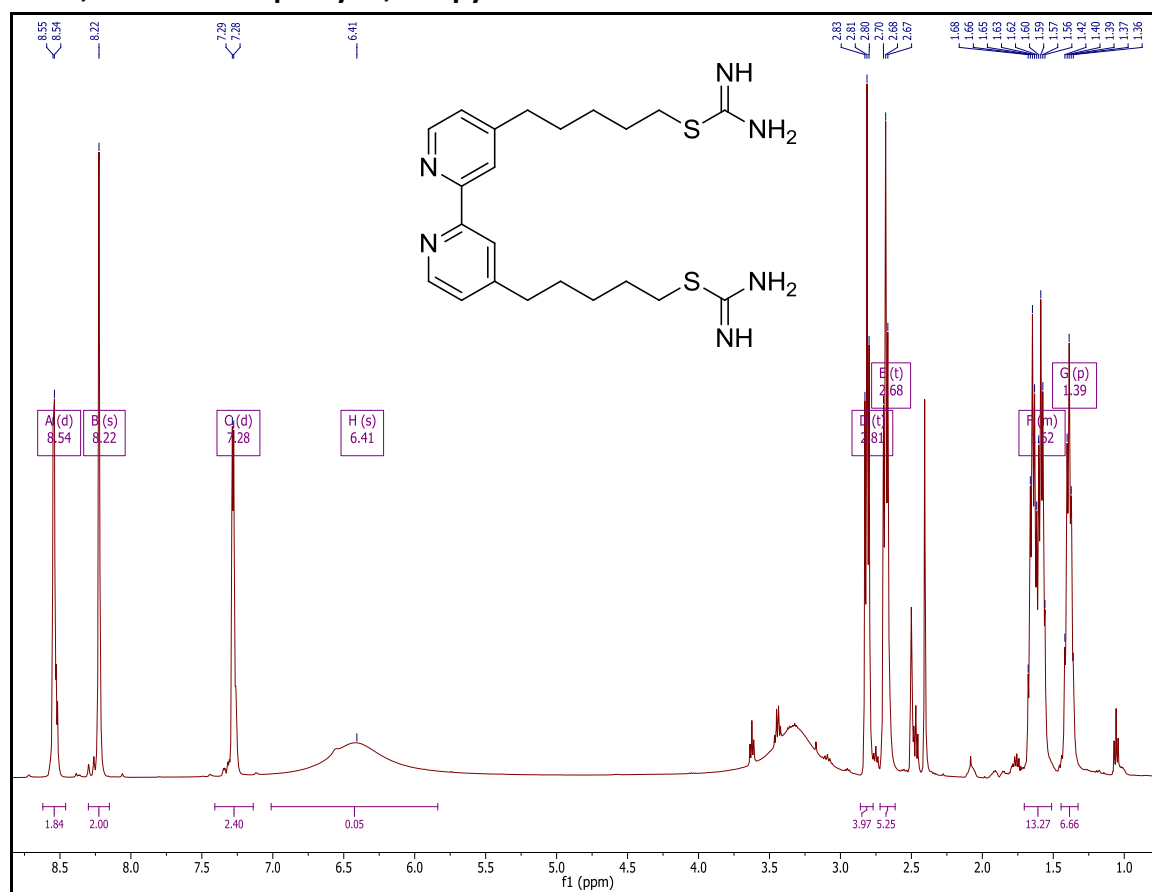


**Figure A 59**  $^1\text{H}$  NMR ( $\text{CDCl}_3$ )  $\delta$  8.55 (d,  $J = 4.9$  Hz, 2H), 8.23 (s, 2H), 7.12 (d,  $J = 3.6$  Hz, 2H), 2.70 (t,  $J = 7.7$  Hz, 4H), 2.52 (q,  $J = 7.4$  Hz, 4H), 1.77 – 1.58 (m, 8H), 1.46 (p,  $J = 7.5, 7.1$  Hz, 4H), 1.33 (t,  $J = 7.8$  Hz, 2H).

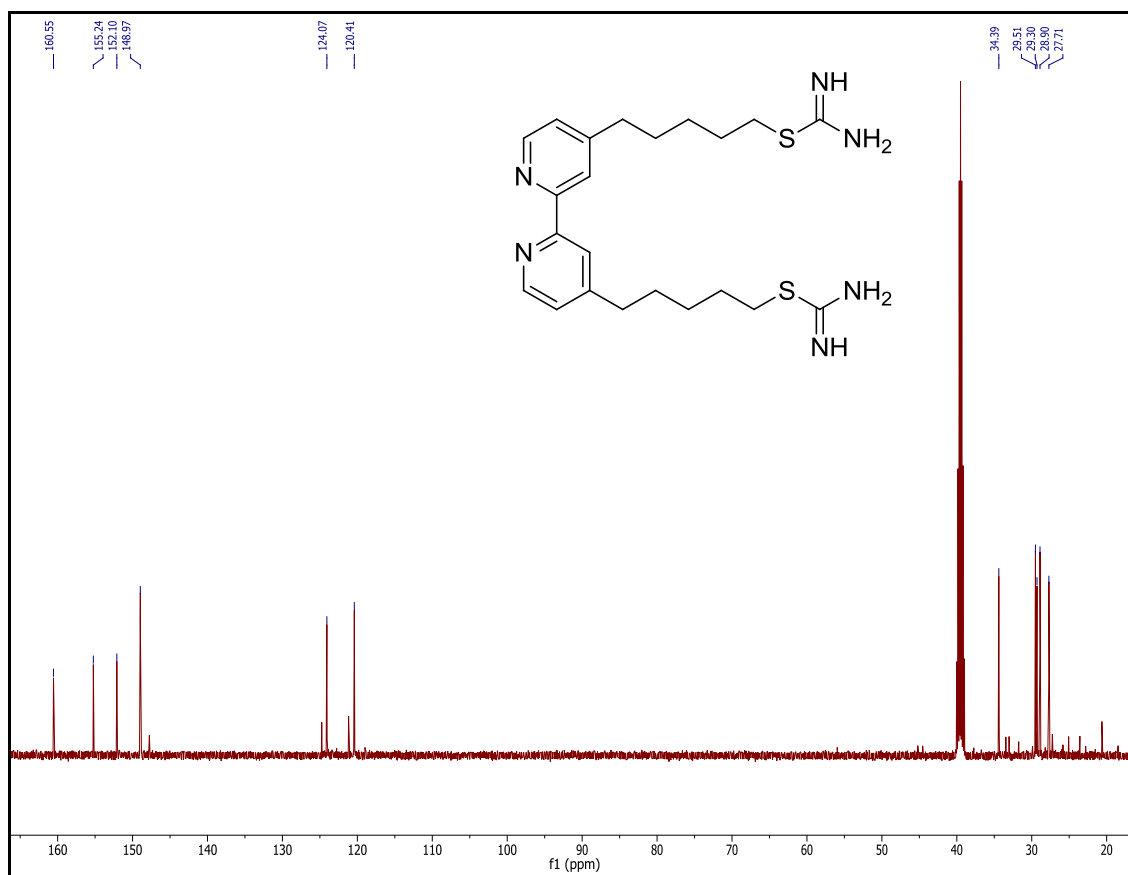


**Figure A 60**  $^{13}\text{C}$  NMR ( $\text{CDCl}_3$ )  $\delta$  156.34, 152.64, 149.22, 124.09, 121.45, 35.55, 33.96, 30.04, 28.17, 24.66.

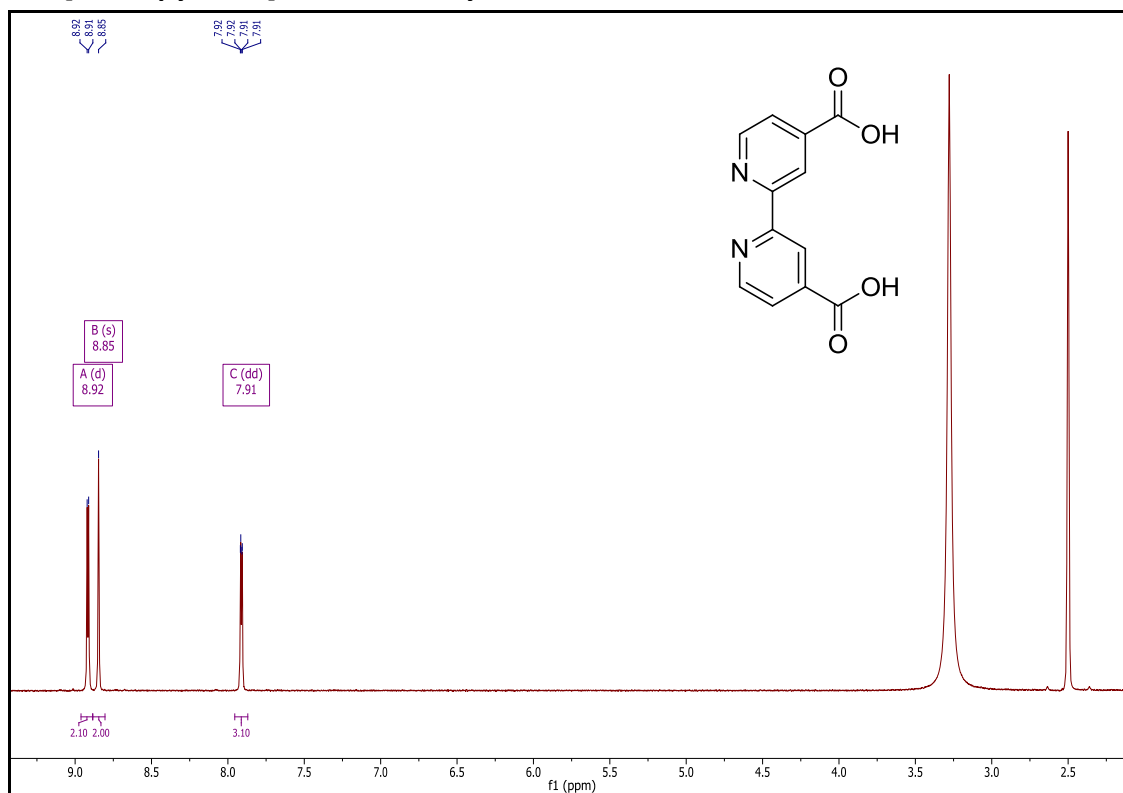
## 31. 4,4'-Dithioureapentyl-2,2'-bipyridine: 26



**Figure A 61** <sup>1</sup>H NMR (DMSO-d<sub>6</sub>) δ 8.54 (d, *J* = 4.9 Hz, 2H), 8.22 (s, 2H), 7.28 (d, *J* = 4.8 Hz, 2H), 6.41 (s, 6H), 2.81 (t, *J* = 7.2 Hz, 4H), 2.68 (t, *J* = 7.6 Hz, 4H), 1.70 – 1.51 (m, 8H), 1.39 (p, *J* = 7.5, 7.1 Hz, 4H).



**Figure A 62**  $^{13}\text{C}$  NMR ( $\text{DMSO-d}_6$ )  $\delta$  160.55, 155.24, 152.10, 148.97, 124.07, 120.41, 34.39, 29.51, 29.30, 28.90, 27.71.

32. [2,2'-bipyridine]-4,4'-Dicarboxylic acid: **11**

**Figure A 63** <sup>1</sup>H NMR (DMSO-d<sub>6</sub>) δ 8.92 (d, *J* = 4.9 Hz, 2H), 8.85 (s, 2H), 7.91 (dd, *J* = 4.9, 1.3 Hz, 2H).

## 33. [2,2'-bipyridine]-4,4'-Diethyl carboxylate: 19

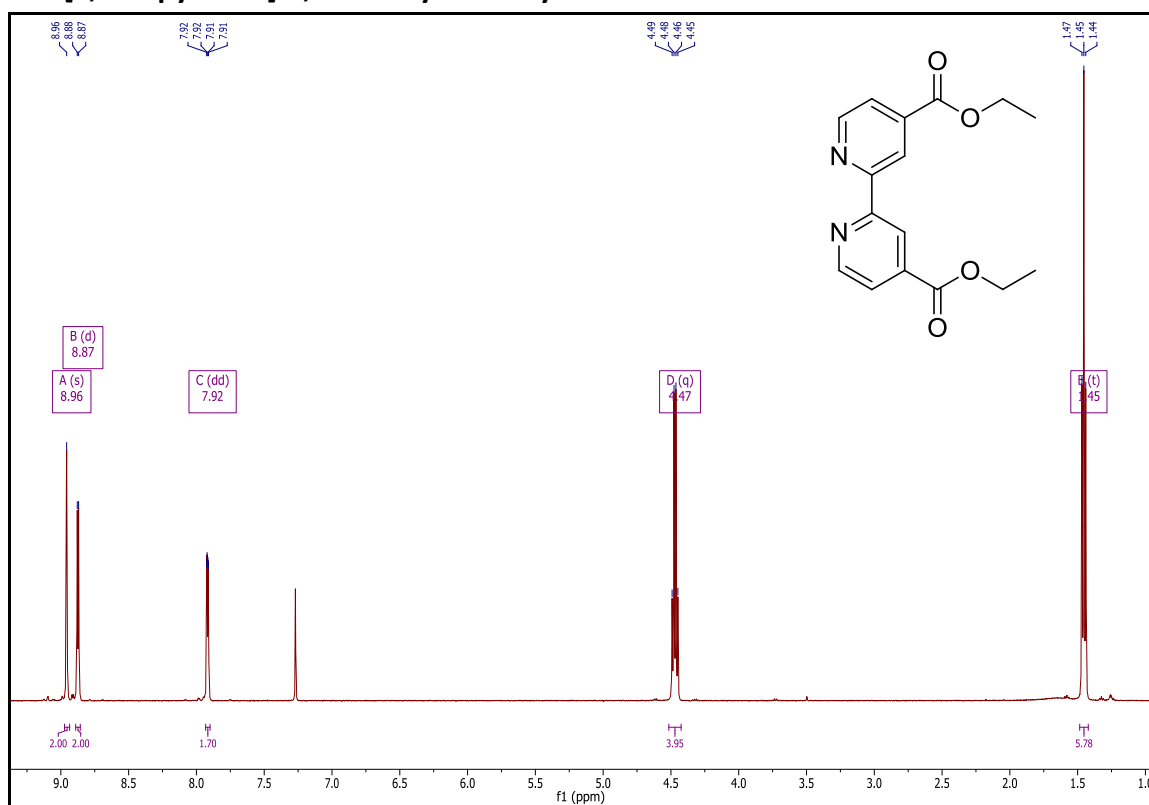


**Figure A 64**  $^1\text{H}$  NMR ( $\text{CDCl}_3$ )  $\delta$  8.96 (s, 2H), 8.87 (d,  $J = 4.9$  Hz, 2H), 7.92 (dd,  $J = 4.9, 1.6$  Hz, 2H), 4.47 (q,  $J = 7.1$  Hz, 4H), 1.45 (t,  $J = 7.1$  Hz, 6H).

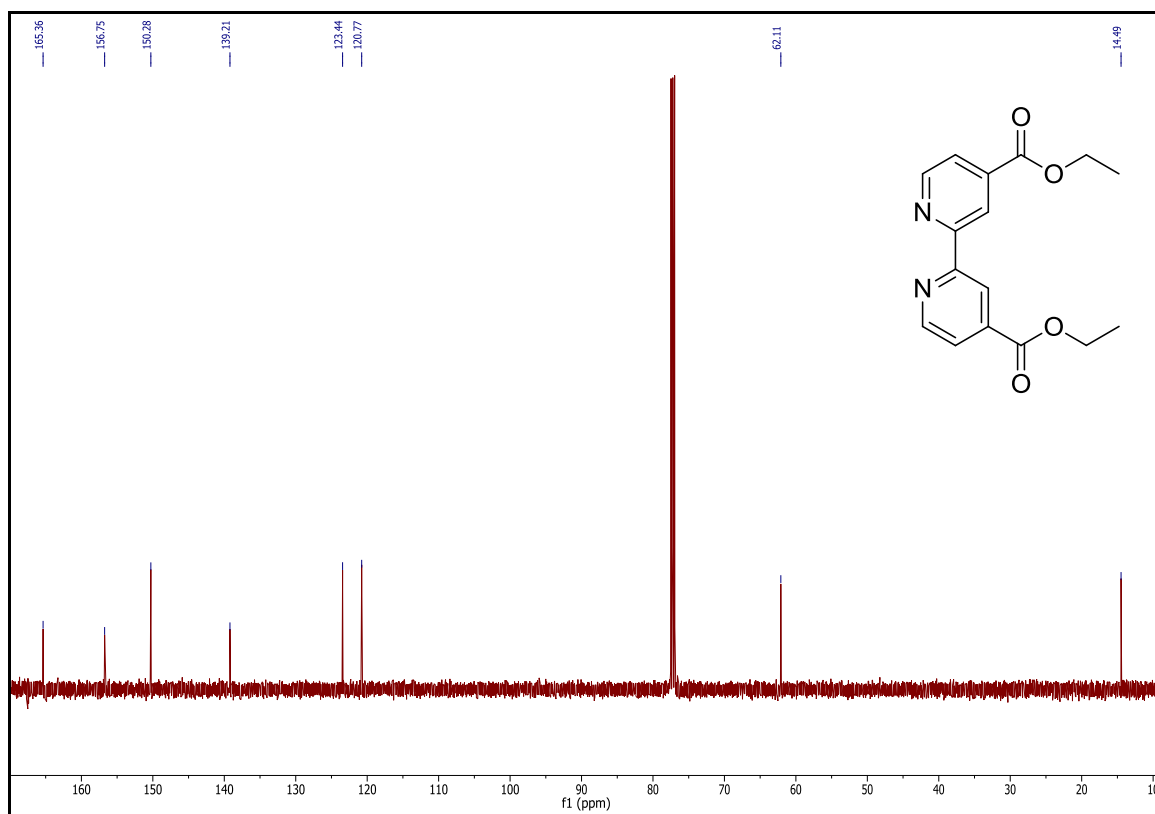
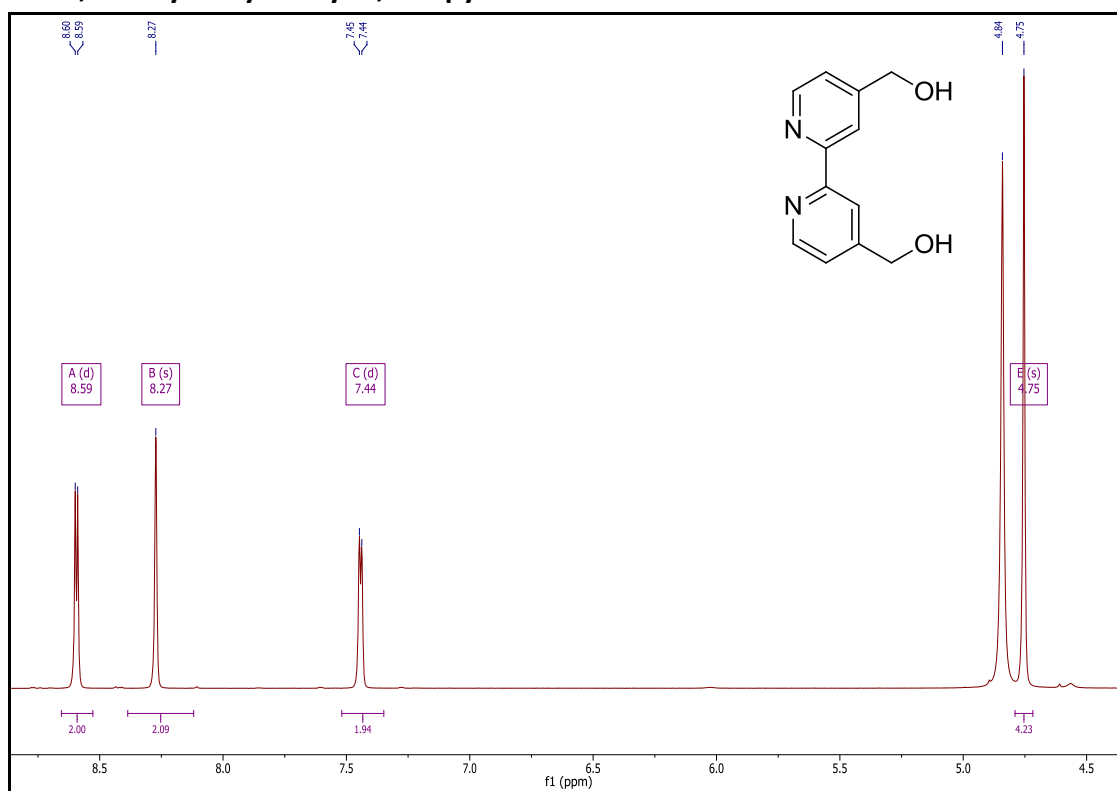
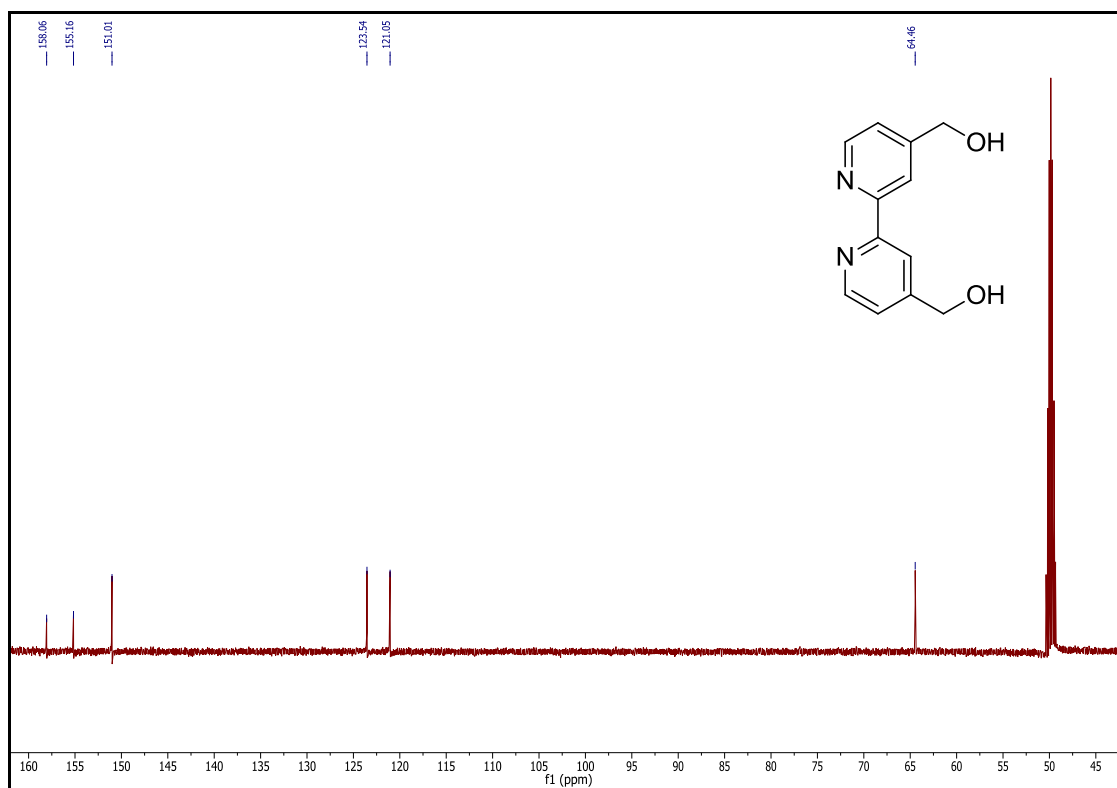


Figure A 65  $^{13}\text{C}$  NMR ( $\text{CDCl}_3$ )  $\delta$  165.36, 156.75, 150.28, 139.21, 123.44, 120.77, 62.11, 14.49.

34. 4,4'-Dihydroxymethyl-2,2'-bipyridine: **20**

**Figure A 66**  $^1\text{H}$  NMR ( $\text{CD}_3\text{OD}$ )  $\delta$  8.59 (d,  $J = 5.0$  Hz, 2H), 8.27 (s, 2H), 7.44 (d,  $J = 4.9$  Hz, 2H), 4.75 (s, 4H).





**Figure A 67**  $^{13}\text{C}$  NMR ( $\text{CD}_3\text{OD}$ )  $\delta$  158.06, 155.16, 151.01, 123.54, 121.05, 64.46.

## 35. 4-Methyl lipoate-4'-Hydroxymethyl-2,2'-bipyridine: 21

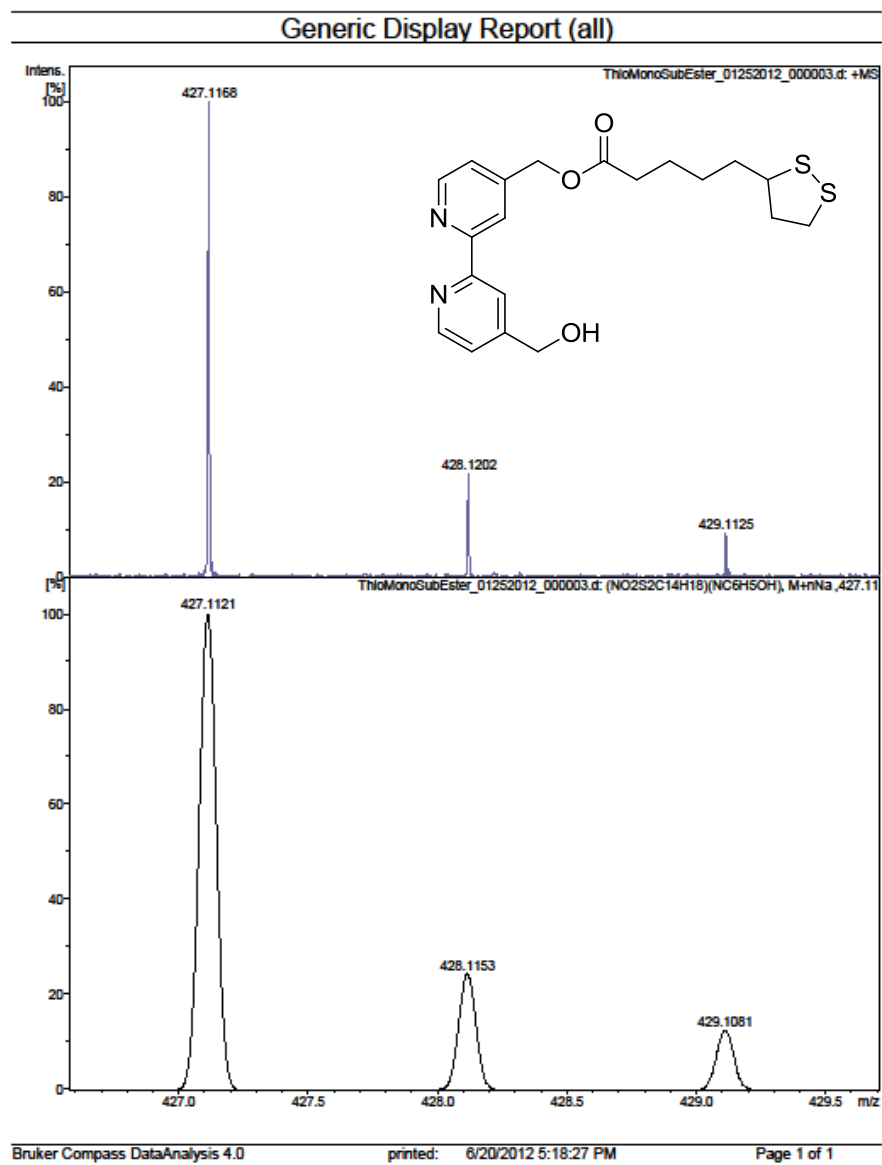
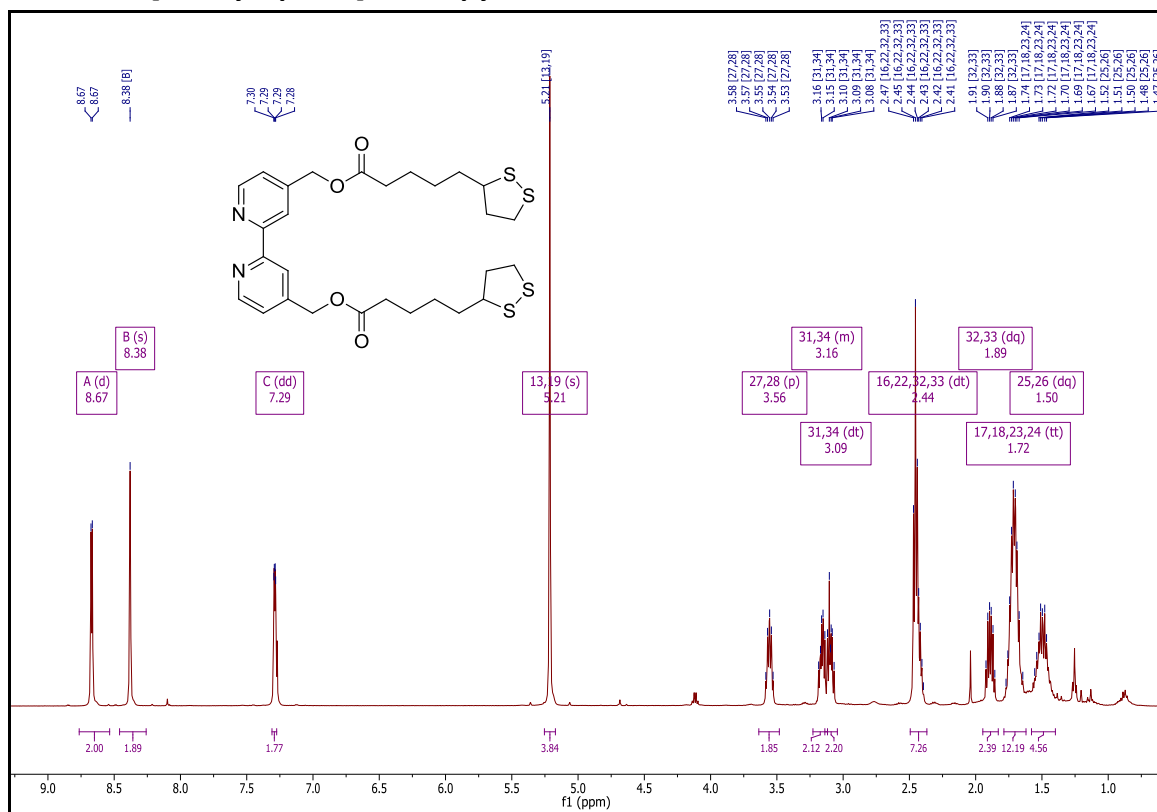
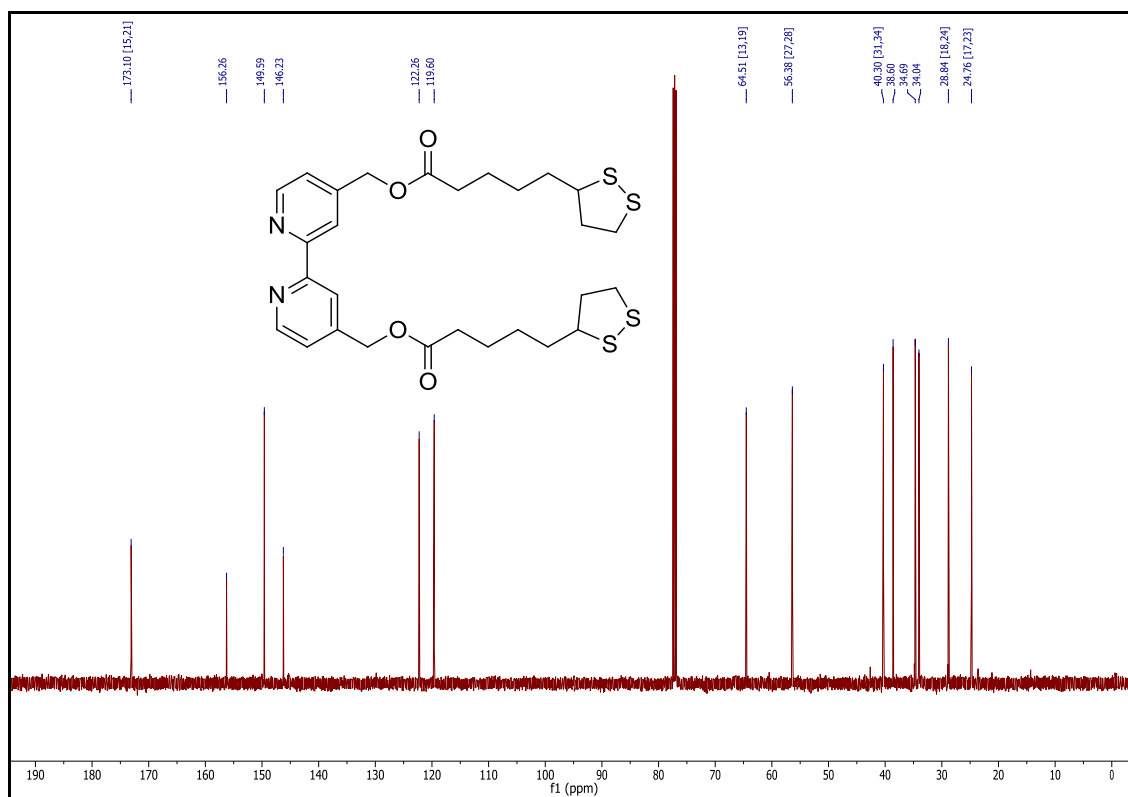


Figure A 68 Top: Actual spectrum; bottom: calculated:  $[M+Na]^+$

## 36. 4,4'-Di[Methyl lipoate]-2,2'-bipyridine: L3



**Figure A 69** <sup>1</sup>H NMR (CDCl<sub>3</sub>) δ 8.67 (d, *J* = 4.9 Hz, 2H), 8.38 (s, 2H), 7.29 (dd, *J* = 5.1, 1.7 Hz, 2H), 5.21 (s, 4H), 3.56 (p, *J* = 6.4 Hz, 2H), 3.23 – 3.12 (m, 2H), 3.09 (dt, *J* = 11.0, 6.9 Hz, 2H), 2.44 (dt, *J* = 17.3, 6.7 Hz, 7H), 1.89 (dq, *J* = 13.6, 6.9 Hz, 2H), 1.72 (tt, *J* = 14.6, 7.6 Hz, 12H), 1.50 (dq, *J* = 15.7, 7.7, 6.8 Hz, 5H).



**Figure A 70**  $^{13}\text{C}$  NMR (CDCl<sub>3</sub>)  $\delta$  173.10, 156.26, 149.59, 146.23, 122.26, 119.60, 64.51, 56.38, 40.30, 38.60, 34.69, 34.04, 28.84, 24.76.

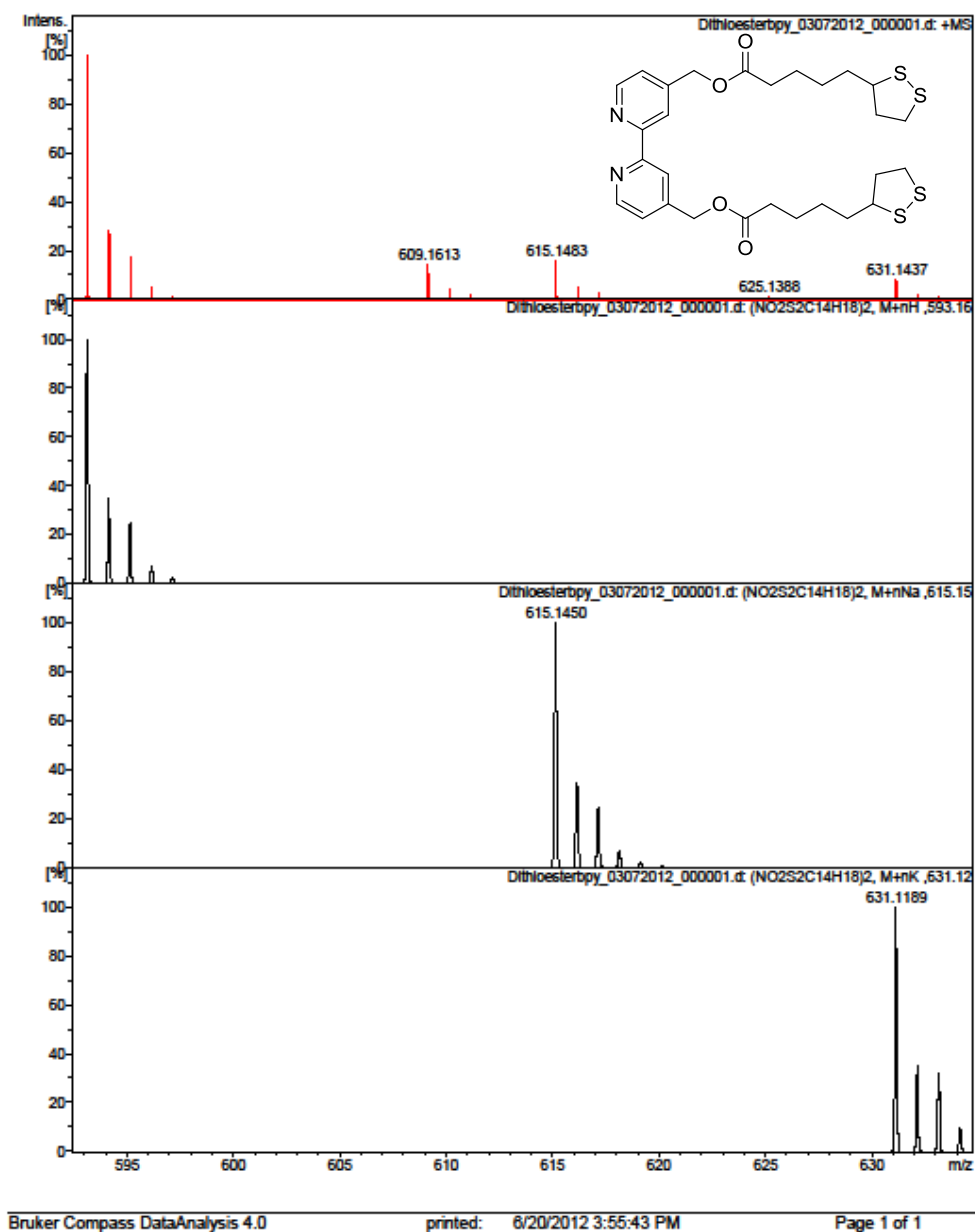


**Figure A 71** Top: Actual spectrum; Top mid: calculated:  $[M+H]^+$ ; bottom mid: calculated:  $[M+Na]^+$ ; bottom: calculated:  $[M+K]^+$

37.  $\text{Ru}(\text{NCS})_2[4,4'\text{-Dicarboxylic acid-2,2'-Bipyridine}][4,4'\text{-Dimethylipsoate-2,2'-Bipyridine}]$ : AK6

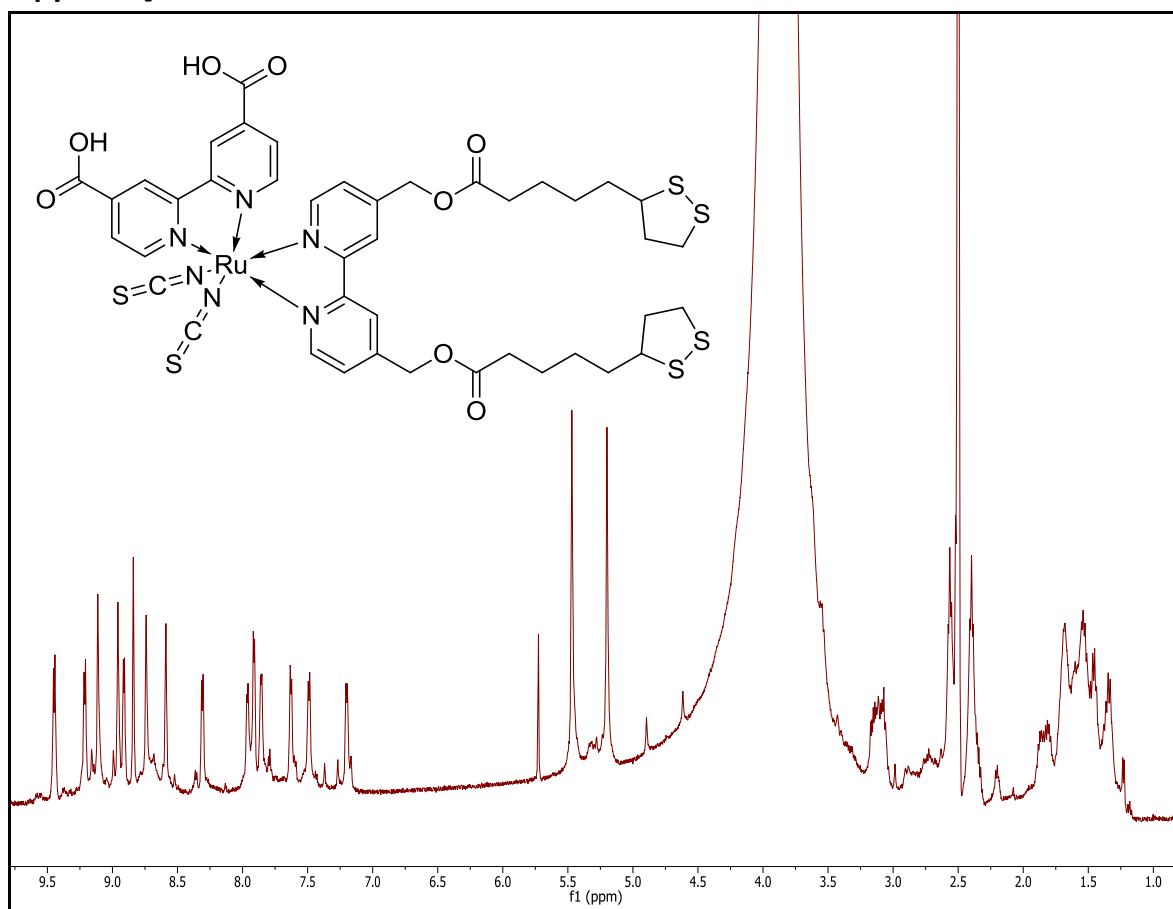
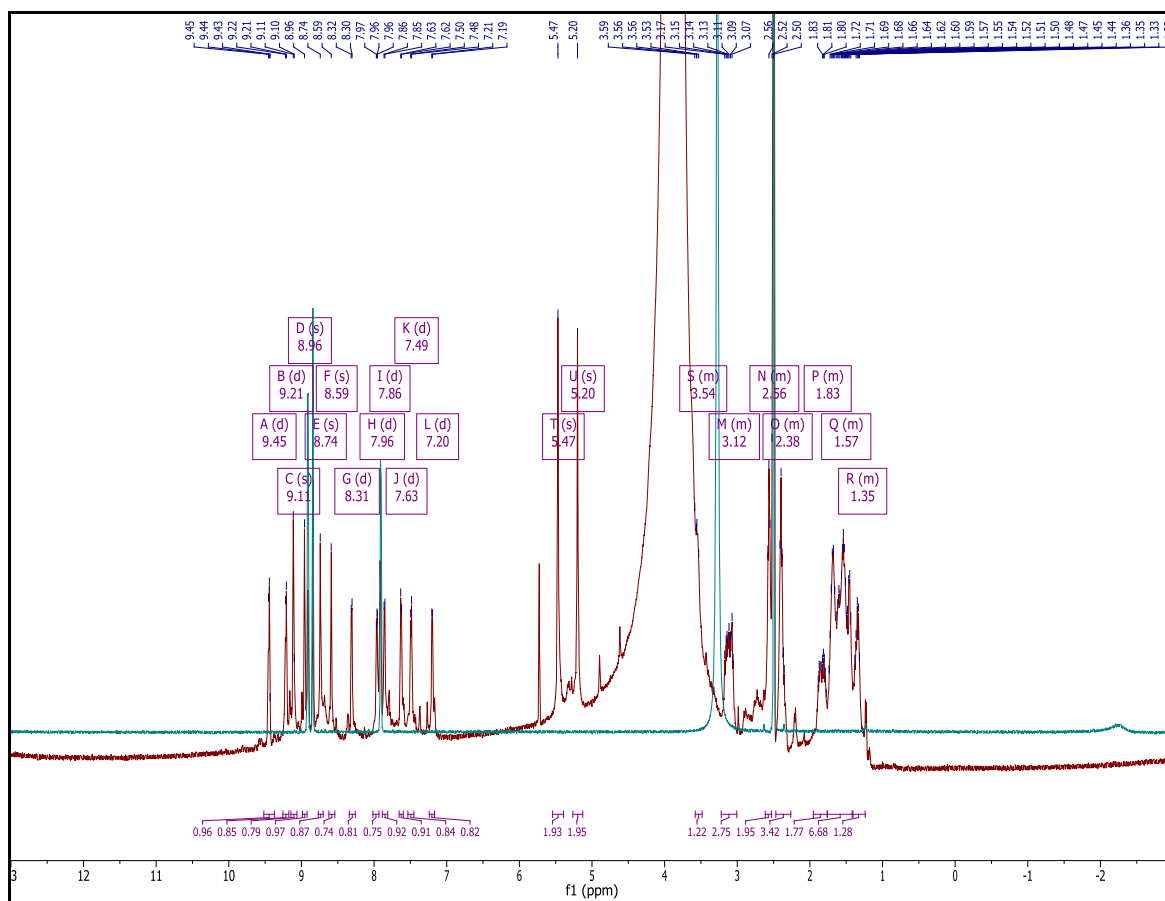
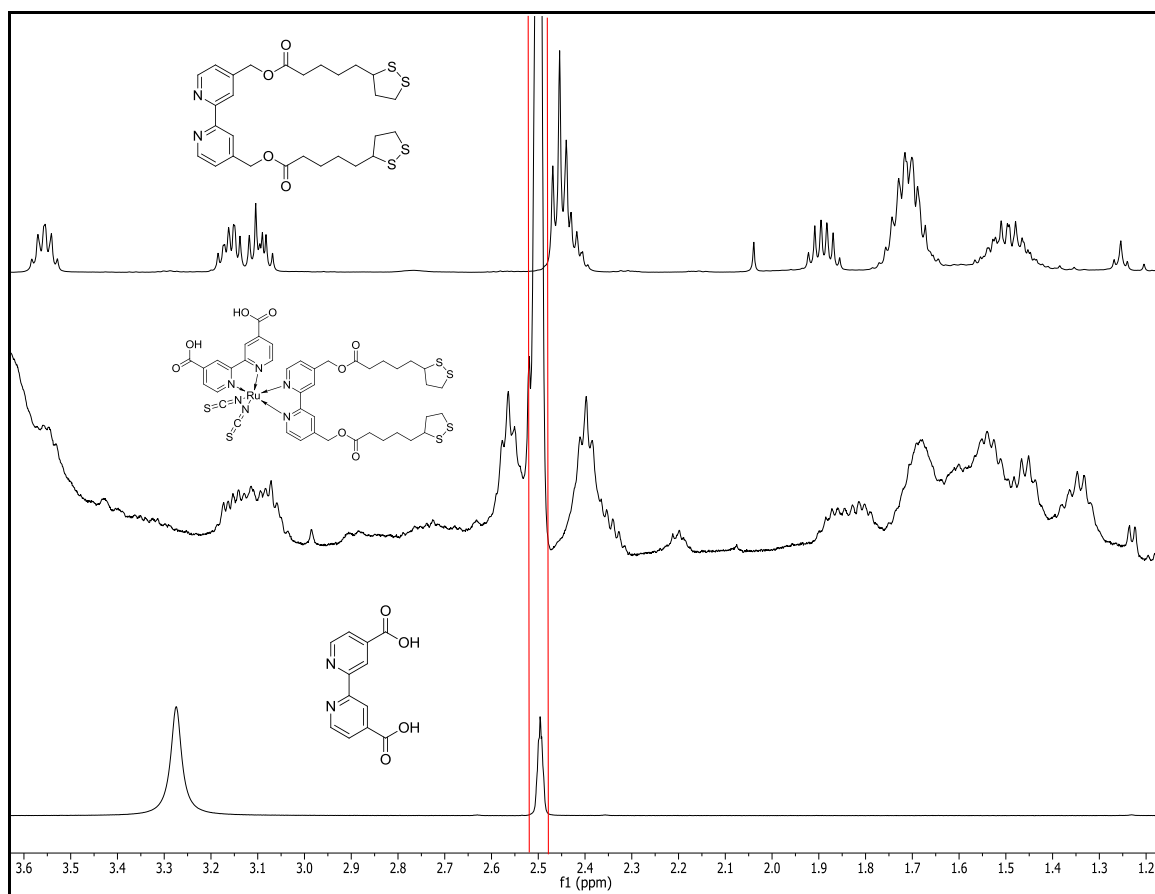


Figure A 72  $^1\text{H}$  NMR of AK6 in DMSO



**Figure A 73**  $^1\text{H}$  NMR of AK6 (red) and DicarboxylicBpy (green) in DMSO



**Figure A 74** Top: DithiocticBpy; Mid: AK6; Bottom: DicarboxylicBpy; red lines highlight DMSO solvent peak.



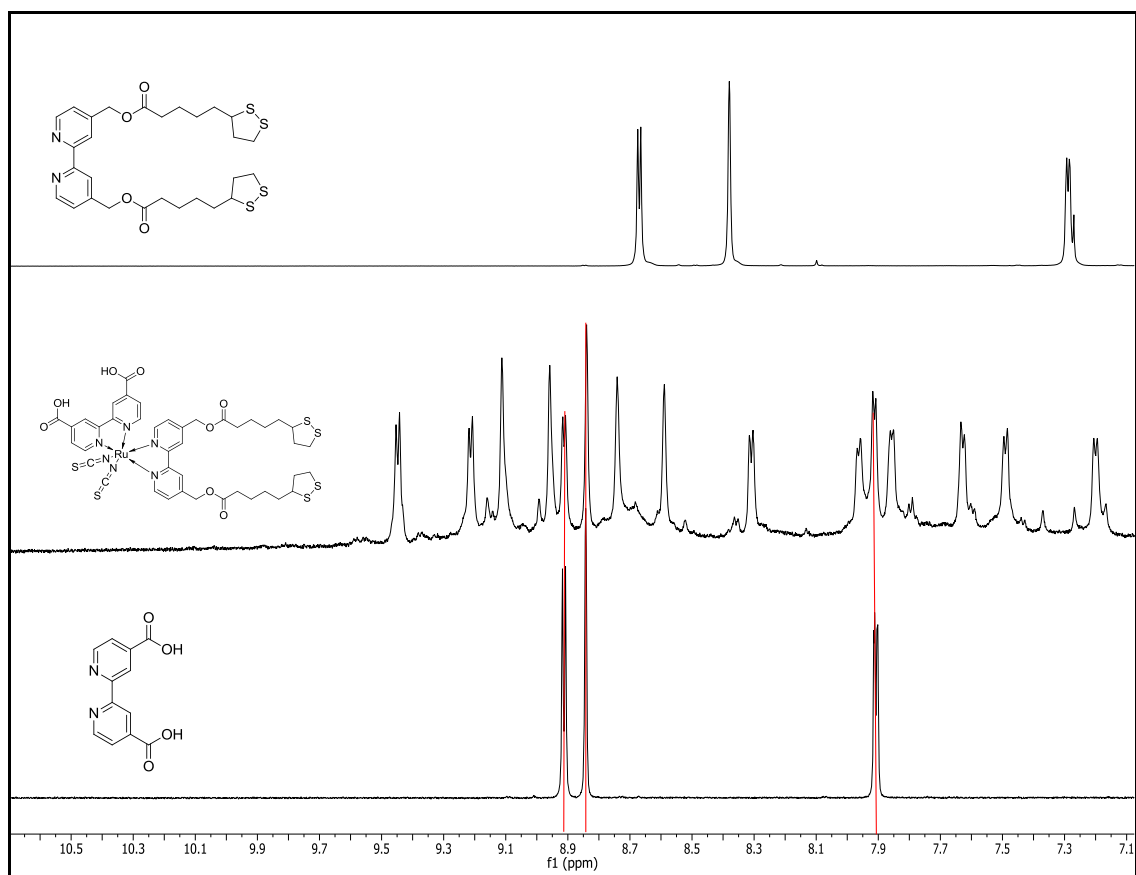


**Figure A 75** Top: Dithioctic Bpy; Mid: **AK6**; Bottom: DicarboxylicBpy; Red lines highlight peaks of dicarboxylic bpy present in **AK6** spectrum

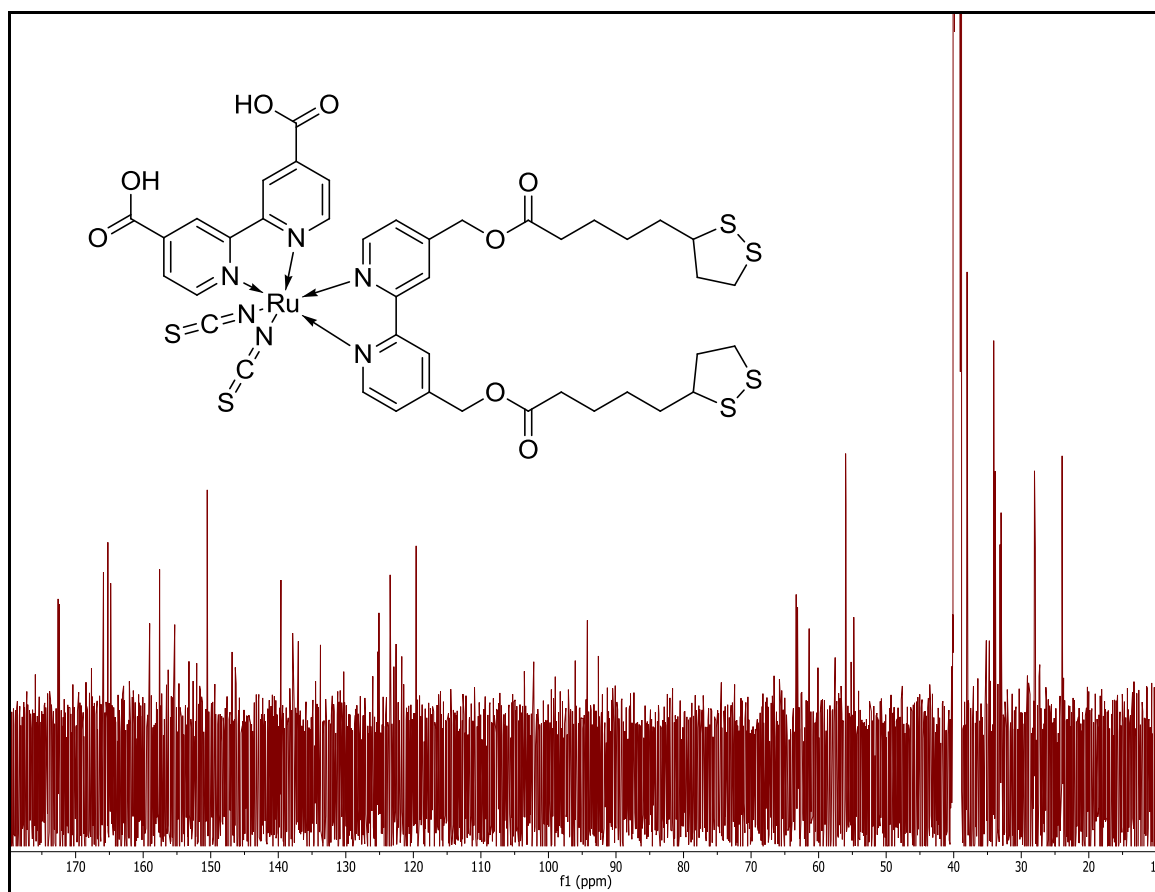


**Figure A 76**  $^{13}\text{C}$  NMR of AK6 in DMSO

### Generic Display Report (all)

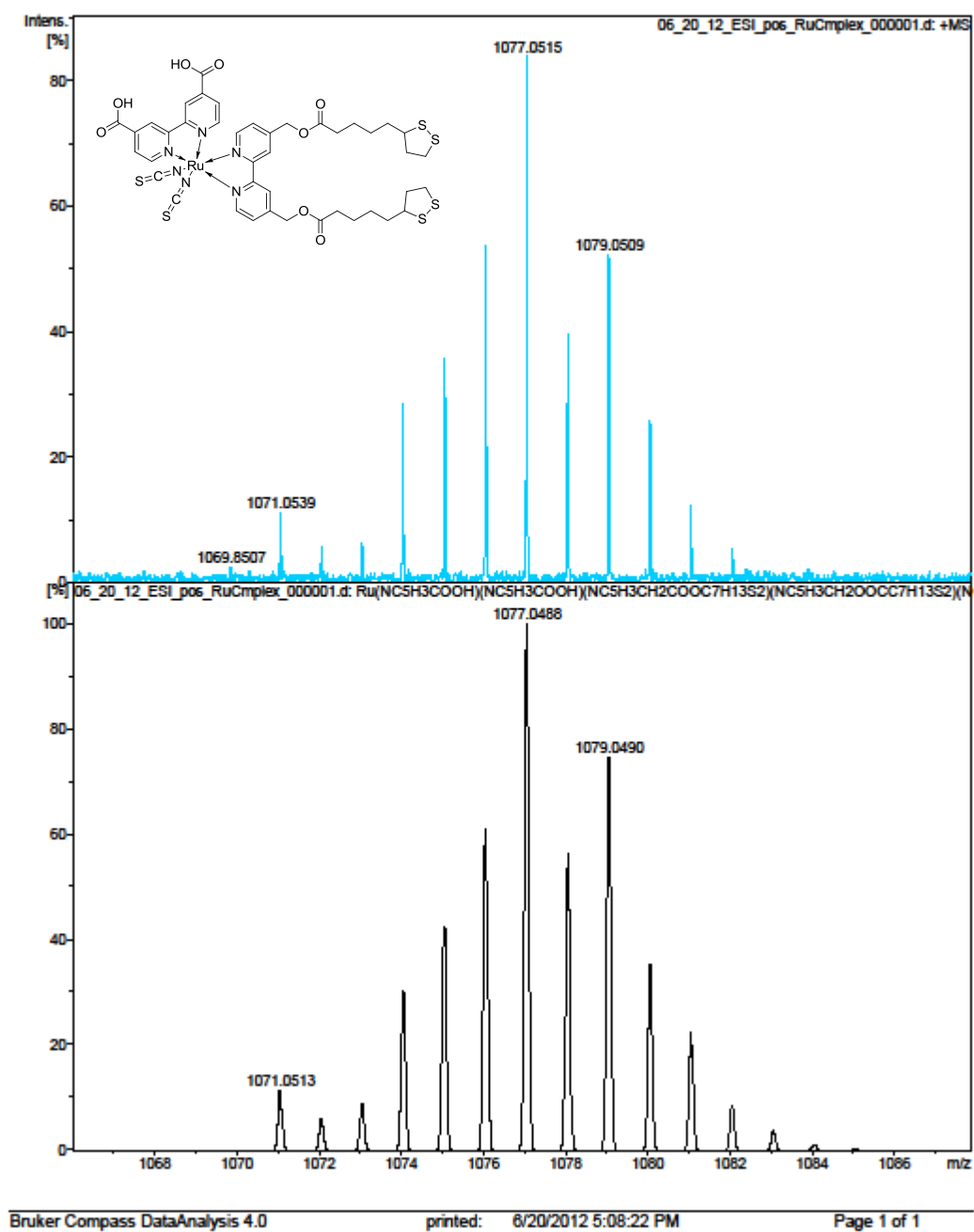


**Figure A 77** Top: actual spectrum; bottom: Calculated  $[M+Na]^+$

## Additional figures

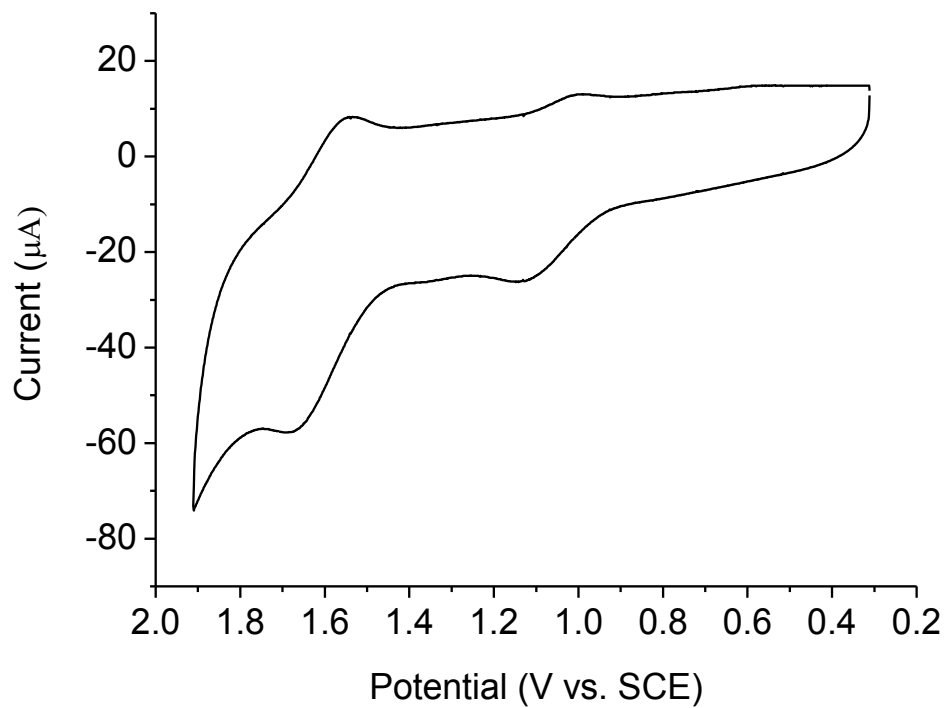


**Figure A 78** Cyclic voltammogram of **AK6** in acetonitrile solution ( $3 \times 10^{-4}$  M) with 0.1 M  $\text{LiClO}_4$  at a scan rate of 1 V/s.

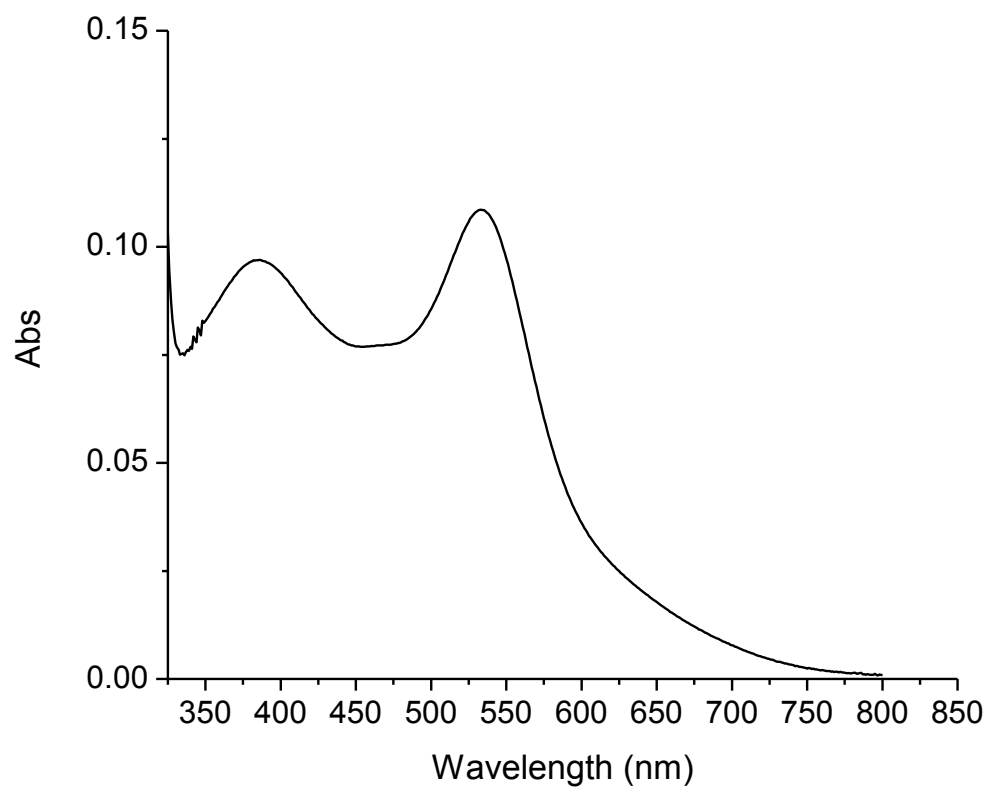


**Figure A 79** Absorption spectrum of **AK6** in acetonitrile.

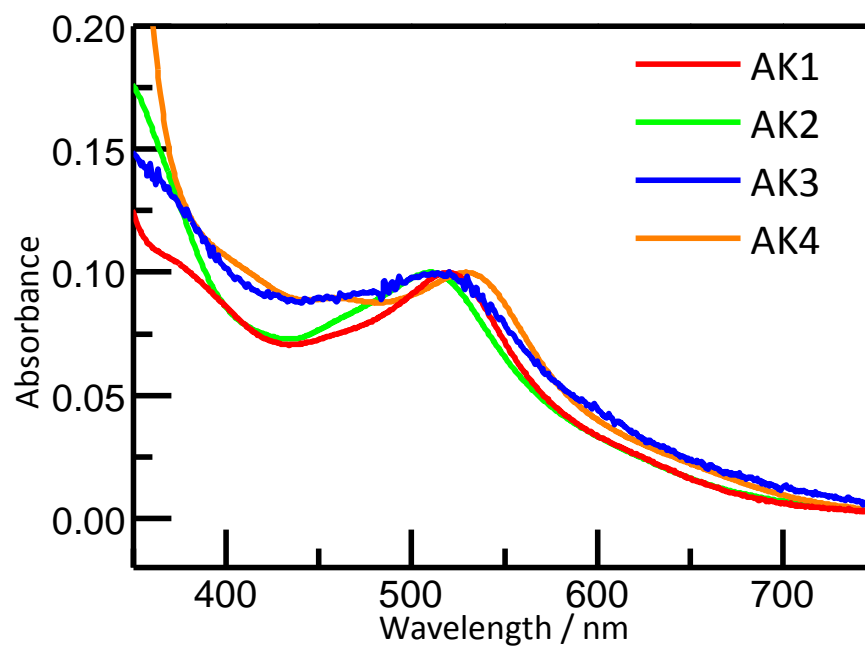
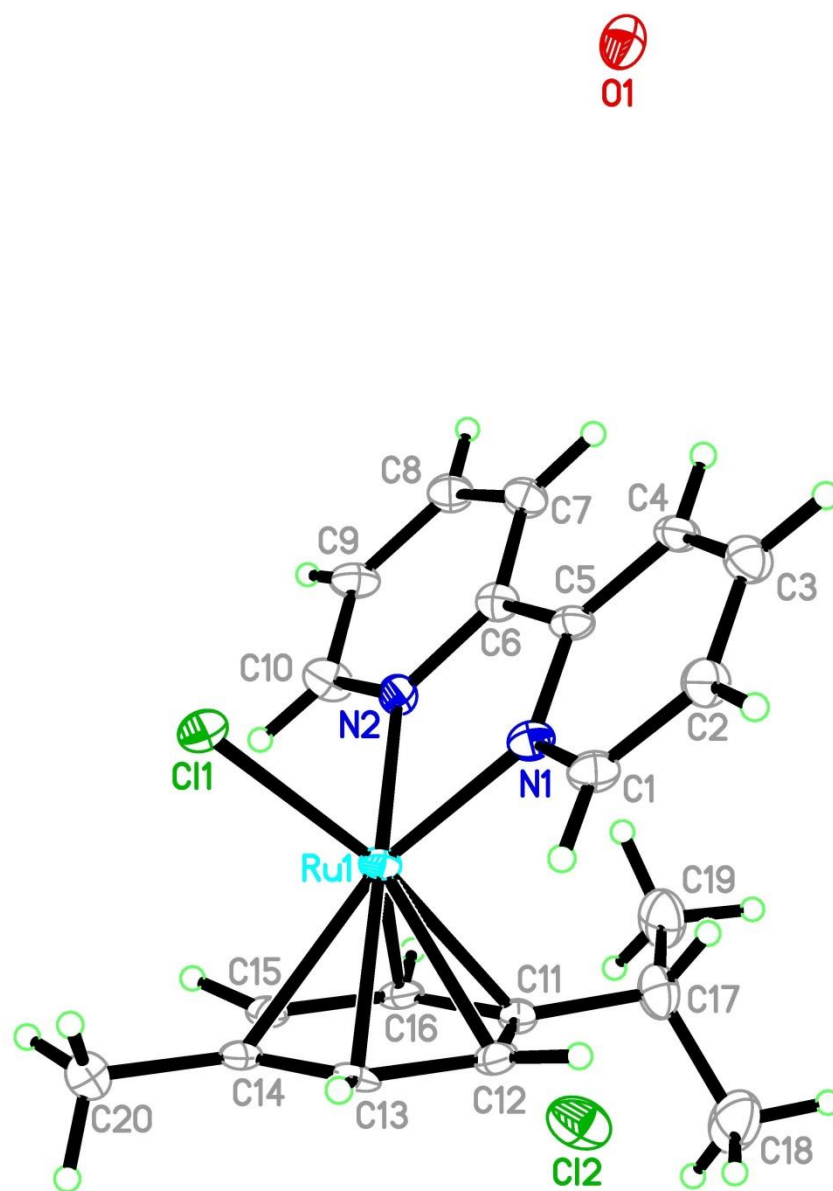


**Figure A 80** Absorbance spectra for **AK1-4**, showing characteristic MLCT absorbance band

**X-Ray Data:**Compound **17**

Image:



Data:

## supplementary materials

## supplementary materials

## Experimental

(080912ral\_ask\_final)

## Crystal data

 $C_{20}H_{22}ClN_2RuClO$  $M_r = 478.37$ Monoclinic,  $P2_1/c$ 

Hall symbol: -P 2ybc

 $a = 16.4921(6) \text{ \AA}$  $b = 17.3819(6) \text{ \AA}$  $c = 13.9299(5) \text{ \AA}$  $\beta = 91.191(2)^\circ$  $V = 3992.3(2) \text{ \AA}^3$  $Z = 8$  $F(000) = 1936$  $D_x = 1.592 \text{ Mg m}^{-3}$ Cu  $K\alpha$  radiation,  $\lambda = 1.54178 \text{ \AA}$ 

Cell parameters from 9912 reflections

 $\theta = 4.8\text{--}67.9^\circ$  $\mu = 8.91 \text{ mm}^{-1}$  $T = 100 \text{ K}$ 

Parallelepiped, Yellow

 $0.20 \times 0.15 \times 0.08 \text{ mm}$ 

## Data collection

Bruker SMART CCD Apex-II area-detector  
diffractometer

Radiation source: fine-focus sealed tube

Graphite monochromator

 $\phi$  and  $\omega$  scans

Absorption correction: Numerical

SADABS (Sheldrick, 2008a)

 $T_{\min} = 0.269$ ,  $T_{\max} = 0.536$ 

37304 measured reflections

7303 independent reflections

6555 reflections with  $I > 2\sigma(I)$  $R_{\text{int}} = 0.052$  $\theta_{\text{max}} = 71.9^\circ$ ,  $\theta_{\text{min}} = 2.7^\circ$  $h = -19 \rightarrow 19$  $k = -20 \rightarrow 20$  $l = -16 \rightarrow 17$ 

## Refinement

Refinement on  $F^2$ 

Least-squares matrix: Full

 $R[F^2 > 2\sigma(F^2)] = 0.065$  $wR(F^2) = 0.173$  $S = 1.20$ 

7303 reflections

475 parameters

0 restraints

Primary atom site location: Structure-invariant direct  
methods

Secondary atom site location: Difference Fourier map

Hydrogen site location: Inferred from neighbouring  
sites

H-atom parameters constrained

 $w = 1/[\sigma^2(F_o^2) + (0.0326P)^2 + 62.1699P]$ where  $P = (F_o^2 + 2F_c^2)/3$  $(\Delta/\sigma)_{\text{max}} < 0.001$  $\Delta\rho_{\text{max}} = 2.35 \text{ e \AA}^{-3}$  $\Delta\rho_{\text{min}} = -1.50 \text{ e \AA}^{-3}$ 

## Special details

Experimental. 'crystal mounted on a Cryoloop using Paratone-N'

**Geometry.** All esds (except the esd in the dihedral angle between two l.s. planes) are estimated using the full covariance matrix. The cell esds are taken into account individually in the estimation of esds in distances, angles and torsion angles; correlations between esds in cell parameters are only used when they are defined by crystal symmetry. An approximate (isotropic) treatment of cell esds is used for estimating esds involving l.s. planes.

**Refinement.** Refinement of  $F^2$  against ALL reflections. The weighted R-factor  $wR$  and goodness of fit  $S$  are based on  $F^2$ , conventional R-factors  $R$  are based on  $F$ , with  $F$  set to zero for negative  $F^2$ . The threshold expression of  $F^2 > 2\text{sigma}(F^2)$  is used only for calculating R-factors(gt) etc. and is not relevant to the choice of reflections for refinement. R-factors based on  $F^2$  are statistically about twice as large as those based on  $F$ , and R-factors based on ALL data will be even larger.



## supplementary materials

*Fractional atomic coordinates and isotropic or equivalent isotropic displacement parameters ( $\text{\AA}^2$ )*

	<i>x</i>	<i>y</i>	<i>z</i>	<i>U</i> <sub>iso</sub> */ <i>U</i> <sub>eq</sub>
Ru1	0.34558 (4)	0.22238 (4)	0.07683 (4)	0.02227 (17)
Cl1	0.27557 (12)	0.28769 (12)	0.20198 (14)	0.0304 (4)
N1	0.3264 (4)	0.1222 (4)	0.1556 (5)	0.0268 (15)
N2	0.4450 (4)	0.2197 (4)	0.1710 (5)	0.0248 (14)
C1	0.2596 (5)	0.0779 (5)	0.1467 (6)	0.0290 (18)
H1	0.2174	0.0935	0.1035	0.035*
C2	0.2502 (5)	0.0103 (5)	0.1985 (6)	0.0314 (19)
H2	0.2026	−0.0201	0.1906	0.038*
C3	0.3116 (5)	−0.0120 (5)	0.2622 (7)	0.034 (2)
H3	0.3071	−0.0582	0.2981	0.041*
C4	0.3796 (5)	0.0343 (5)	0.2724 (6)	0.0277 (18)
H4	0.4222	0.0201	0.3158	0.033*
C5	0.3854 (5)	0.1010 (5)	0.2195 (6)	0.0252 (17)
C6	0.4535 (5)	0.1549 (5)	0.2267 (6)	0.0266 (17)
C7	0.5217 (5)	0.1430 (5)	0.2863 (6)	0.0297 (18)
H7	0.5270	0.0981	0.3247	0.036*
C8	0.5814 (5)	0.1996 (5)	0.2872 (6)	0.0311 (19)
H8	0.6291	0.1929	0.3257	0.037*
C9	0.5719 (5)	0.2650 (6)	0.2329 (6)	0.033 (2)
H9	0.6124	0.3038	0.2345	0.039*
C10	0.5026 (5)	0.2741 (6)	0.1755 (7)	0.034 (2)
H10	0.4959	0.3197	0.1387	0.041*
C12	0.3041 (5)	0.1669 (5)	−0.0550 (6)	0.0268 (18)
H12	0.2778	0.1153	−0.0505	0.032*
C13	0.2557 (5)	0.2333 (5)	−0.0416 (6)	0.0261 (17)
H13	0.1966	0.2275	−0.0283	0.031*
C14	0.2931 (5)	0.3061 (5)	−0.0309 (6)	0.0279 (18)
C15	0.3780 (5)	0.3115 (5)	−0.0301 (6)	0.0271 (18)
H15	0.4048	0.3602	−0.0080	0.033*
C16	0.4252 (5)	0.2448 (5)	−0.0433 (5)	0.0258 (17)
H16	0.4849	0.2480	−0.0300	0.031*
C11	0.3897 (5)	0.1705 (5)	−0.0565 (6)	0.0262 (17)
C20	0.2423 (6)	0.3778 (6)	−0.0167 (7)	0.040 (2)
H20A	0.2142	0.3910	−0.0771	0.061*
H20B	0.2776	0.4205	0.0033	0.061*
H20C	0.2024	0.3681	0.0330	0.061*
C17	0.4383 (6)	0.0976 (6)	−0.0656 (8)	0.040 (2)
H17	0.4152	0.0597	−0.0195	0.048*
C18	0.4269 (7)	0.0641 (7)	−0.1636 (9)	0.059 (3)
H18A	0.3688	0.0586	−0.1783	0.088*
H18B	0.4529	0.0135	−0.1659	0.088*
H18C	0.4514	0.0982	−0.2109	0.088*
C19	0.5273 (6)	0.1052 (6)	−0.0402 (9)	0.051 (3)
H19A	0.5518	0.1438	−0.0819	0.076*
H19B	0.5542	0.0555	−0.0491	0.076*
H19C	0.5336	0.1214	0.0270	0.076*
Ru1A	0.14986 (4)	0.73004 (4)	0.05829 (4)	0.02257 (17)
Cl1A	0.21832 (12)	0.78909 (12)	0.19201 (14)	0.0295 (4)
N1A	0.1714 (4)	0.6273 (4)	0.1327 (5)	0.0243 (14)
N2A	0.0508 (4)	0.7213 (4)	0.1481 (5)	0.0268 (15)
C1A	0.2390 (5)	0.5843 (5)	0.1243 (6)	0.0273 (18)

## supplementary materials

H1A	0.2789	0.6001	0.0801	0.033*
C2A	0.2526 (5)	0.5182 (5)	0.1775 (6)	0.0315 (19)
H2A	0.3009	0.4893	0.1701	0.038*
C3A	0.1946 (5)	0.4948 (5)	0.2415 (6)	0.0307 (19)
H3A	0.2024	0.4495	0.2787	0.037*
C4A	0.1251 (5)	0.5386 (5)	0.2502 (7)	0.0320 (19)
H4A	0.0843	0.5234	0.2935	0.038*
C5A	0.1151 (5)	0.6049 (5)	0.1956 (6)	0.0233 (17)
C6A	0.0444 (5)	0.6562 (5)	0.2011 (6)	0.0257 (17)
C7A	-0.0225 (5)	0.6418 (5)	0.2574 (6)	0.0277 (18)
H7A	-0.0257	0.5960	0.2943	0.033*
C8A	-0.0844 (5)	0.6958 (6)	0.2585 (6)	0.0309 (19)
H8A	-0.1317	0.6867	0.2947	0.037*
C9A	-0.0767 (5)	0.7622 (5)	0.2068 (6)	0.0296 (19)
H9A	-0.1175	0.8007	0.2088	0.036*
C10A	-0.0084 (5)	0.7729 (5)	0.1513 (7)	0.0299 (19)
H10A	-0.0040	0.8187	0.1144	0.036*
C14A	0.2021 (5)	0.8226 (5)	-0.0378 (6)	0.0296 (19)
C13A	0.2408 (5)	0.7501 (5)	-0.0525 (6)	0.0299 (19)
H13A	0.2997	0.7443	-0.0355	0.036*
C12A	0.1956 (5)	0.6856 (5)	-0.0765 (6)	0.0308 (19)
H12A	0.2237	0.6346	-0.0753	0.037*
C11A	0.1090 (6)	0.6862 (5)	-0.0846 (6)	0.032 (2)
C15A	0.1166 (5)	0.8249 (5)	-0.0414 (6)	0.0279 (18)
H15A	0.0879	0.8712	-0.0164	0.033*
C17A	0.0602 (7)	0.6160 (6)	-0.1162 (8)	0.047 (3)
H17A	0.0545	0.6187	-0.1877	0.056*
C16A	0.0714 (5)	0.7584 (6)	-0.0673 (6)	0.031 (2)
H16A	0.0113	0.7594	-0.0585	0.037*
C19A	-0.0258 (7)	0.6178 (7)	-0.0767 (9)	0.053 (3)
H19D	-0.0563	0.5732	-0.1009	0.080*
H19E	-0.0531	0.6652	-0.0977	0.080*
H19F	-0.0231	0.6162	-0.0064	0.080*
C18A	0.1023 (8)	0.5419 (6)	-0.0931 (9)	0.056 (3)
H18D	0.1588	0.5447	-0.1136	0.084*
H18E	0.0747	0.4996	-0.1269	0.084*
H18F	0.1012	0.5327	-0.0237	0.084*
C20A	0.2498 (6)	0.8928 (6)	-0.0131 (7)	0.042 (2)
H20D	0.2128	0.9352	0.0009	0.063*
H20E	0.2836	0.9069	-0.0674	0.063*
H20F	0.2845	0.8825	0.0434	0.063*
O1	0.4399 (4)	0.0301 (4)	0.6006 (5)	0.0371 (15)
O2	0.9482 (4)	0.4753 (4)	0.3711 (5)	0.0385 (15)
Cl3	0.39853 (12)	0.60916 (12)	0.96742 (15)	0.0306 (4)
Cl2	0.10998 (13)	0.08498 (14)	0.96629 (18)	0.0405 (5)

Atomic displacement parameters ( $\text{\AA}^2$ )

	$U^{11}$	$U^{22}$	$U^{33}$	$U^{12}$	$U^{13}$	$U^{23}$
Ru1	0.0202 (3)	0.0263 (3)	0.0202 (3)	-0.0024 (2)	-0.0026 (2)	0.0023 (2)
Cl1	0.0304 (10)	0.0367 (11)	0.0241 (10)	-0.0041 (8)	0.0028 (8)	-0.0028 (8)
N1	0.024 (3)	0.033 (4)	0.023 (4)	-0.002 (3)	-0.001 (3)	-0.001 (3)
N2	0.023 (3)	0.022 (3)	0.030 (4)	-0.004 (3)	-0.005 (3)	0.000 (3)
Cl	0.022 (4)	0.038 (5)	0.026 (4)	-0.005 (4)	-0.005 (3)	0.000 (4)

## supplementary materials

C2	0.032 (4)	0.029 (5)	0.033 (5)	−0.009 (4)	0.000 (4)	0.002 (4)
C3	0.037 (5)	0.032 (5)	0.033 (5)	−0.004 (4)	0.001 (4)	0.005 (4)
C4	0.031 (4)	0.031 (5)	0.021 (4)	0.001 (4)	−0.004 (3)	0.004 (3)
C5	0.023 (4)	0.033 (4)	0.019 (4)	0.002 (3)	−0.005 (3)	0.001 (3)
C6	0.024 (4)	0.031 (4)	0.025 (4)	0.001 (3)	0.001 (3)	0.001 (3)
C7	0.025 (4)	0.034 (5)	0.030 (4)	0.002 (4)	−0.004 (4)	0.003 (4)
C8	0.026 (4)	0.038 (5)	0.029 (5)	−0.001 (4)	−0.006 (4)	0.000 (4)
C9	0.030 (4)	0.043 (5)	0.024 (4)	−0.008 (4)	−0.005 (4)	0.005 (4)
C10	0.025 (4)	0.038 (5)	0.038 (5)	−0.009 (4)	−0.006 (4)	0.009 (4)
C12	0.036 (5)	0.028 (4)	0.016 (4)	−0.003 (4)	−0.001 (3)	−0.001 (3)
C13	0.028 (4)	0.033 (5)	0.017 (4)	0.000 (3)	−0.007 (3)	0.010 (3)
C14	0.039 (5)	0.032 (5)	0.013 (4)	0.007 (4)	−0.004 (3)	0.001 (3)
C15	0.037 (5)	0.029 (4)	0.015 (4)	−0.002 (4)	0.000 (3)	0.005 (3)
C16	0.023 (4)	0.041 (5)	0.014 (4)	0.005 (3)	−0.002 (3)	−0.003 (3)
C11	0.036 (5)	0.025 (4)	0.018 (4)	0.002 (3)	0.001 (3)	0.002 (3)
C20	0.048 (6)	0.036 (5)	0.037 (5)	0.010 (4)	−0.003 (5)	0.001 (4)
C17	0.038 (5)	0.031 (5)	0.050 (6)	0.008 (4)	0.008 (5)	0.000 (4)
C18	0.058 (7)	0.055 (7)	0.064 (8)	0.011 (6)	0.004 (6)	−0.017 (6)
C19	0.041 (6)	0.045 (6)	0.066 (8)	0.012 (5)	0.000 (5)	−0.005 (6)
Ru1A	0.0205 (3)	0.0269 (3)	0.0203 (3)	0.0034 (2)	−0.0007 (2)	−0.0006 (2)
C11A	0.0282 (10)	0.0367 (11)	0.0234 (10)	0.0015 (8)	−0.0045 (8)	−0.0028 (8)
N1A	0.024 (3)	0.026 (4)	0.023 (3)	0.001 (3)	−0.001 (3)	−0.001 (3)
N2A	0.018 (3)	0.030 (4)	0.032 (4)	0.003 (3)	0.001 (3)	0.002 (3)
C1A	0.023 (4)	0.036 (5)	0.023 (4)	0.006 (3)	0.000 (3)	−0.007 (4)
C2A	0.029 (4)	0.037 (5)	0.029 (5)	0.010 (4)	−0.005 (4)	−0.007 (4)
C3A	0.033 (5)	0.027 (4)	0.031 (5)	0.007 (4)	−0.002 (4)	0.002 (4)
C4A	0.027 (4)	0.037 (5)	0.032 (5)	0.000 (4)	0.000 (4)	−0.001 (4)
C5A	0.026 (4)	0.022 (4)	0.022 (4)	0.001 (3)	−0.006 (3)	−0.006 (3)
C6A	0.021 (4)	0.036 (5)	0.020 (4)	−0.001 (3)	−0.005 (3)	−0.005 (3)
C7A	0.025 (4)	0.029 (4)	0.029 (4)	−0.001 (3)	−0.002 (3)	0.000 (4)
C8A	0.018 (4)	0.045 (5)	0.029 (5)	0.000 (4)	−0.001 (3)	−0.005 (4)
C9A	0.027 (4)	0.034 (5)	0.028 (4)	0.009 (4)	−0.004 (4)	0.000 (4)
C10A	0.024 (4)	0.029 (5)	0.036 (5)	0.006 (3)	−0.003 (4)	−0.003 (4)
C14A	0.036 (5)	0.029 (4)	0.024 (4)	−0.004 (4)	−0.001 (4)	0.010 (3)
C13A	0.025 (4)	0.046 (5)	0.019 (4)	0.003 (4)	0.000 (3)	0.005 (4)
C12A	0.039 (5)	0.036 (5)	0.018 (4)	0.009 (4)	0.004 (4)	0.001 (4)
C11A	0.042 (5)	0.039 (5)	0.015 (4)	0.001 (4)	−0.002 (4)	−0.002 (4)
C15A	0.036 (5)	0.024 (4)	0.024 (4)	0.006 (3)	−0.002 (4)	0.006 (3)
C17A	0.050 (6)	0.047 (6)	0.043 (6)	−0.008 (5)	−0.007 (5)	−0.007 (5)
C16A	0.029 (4)	0.048 (5)	0.016 (4)	0.003 (4)	−0.004 (3)	−0.015 (4)
C19A	0.058 (7)	0.046 (6)	0.056 (7)	−0.020 (5)	−0.014 (6)	0.007 (5)
C18A	0.081 (9)	0.032 (6)	0.054 (7)	−0.016 (5)	0.004 (6)	−0.007 (5)
C20A	0.041 (5)	0.047 (6)	0.038 (5)	−0.004 (5)	−0.004 (4)	0.002 (5)
O1	0.038 (3)	0.032 (3)	0.042 (4)	−0.002 (3)	0.009 (3)	−0.006 (3)
O2	0.036 (3)	0.037 (4)	0.043 (4)	0.002 (3)	−0.006 (3)	0.003 (3)
C13	0.0261 (10)	0.0381 (11)	0.0279 (10)	0.0036 (8)	0.0023 (8)	0.0009 (9)
C12	0.0298 (11)	0.0451 (13)	0.0461 (13)	−0.0090 (9)	−0.0116 (10)	0.0117 (10)

## Geometric parameters (Å, °)

Ru1—N2	2.079 (7)	Ru1A—N2A	2.084 (7)
Ru1—N1	2.085 (7)	Ru1A—N1A	2.092 (7)
Ru1—C12	2.172 (8)	Ru1A—C12A	2.180 (8)
Ru1—C16	2.184 (8)	Ru1A—C13A	2.202 (8)

# supplementary materials

Ru1—C11	2.201 (8)	Ru1A—C16A	2.210 (8)
Ru1—C13	2.203 (8)	Ru1A—C15A	2.218 (8)
Ru1—C15	2.223 (8)	Ru1A—C11A	2.223 (8)
Ru1—C14	2.251 (8)	Ru1A—C14A	2.274 (8)
Ru1—C11	2.397 (2)	Ru1A—C11A	2.390 (2)
N1—C1	1.348 (11)	N1A—C5A	1.348 (11)
N1—C5	1.355 (10)	N1A—C1A	1.350 (10)
N2—C10	1.340 (11)	N2A—C10A	1.328 (11)
N2—C6	1.374 (11)	N2A—C6A	1.356 (11)
C1—C2	1.390 (12)	C1A—C2A	1.383 (13)
C1—H1	0.9500	C1A—H1A	0.9500
C2—C3	1.387 (13)	C2A—C3A	1.381 (13)
C2—H2	0.9500	C2A—H2A	0.9500
C3—C4	1.385 (12)	C3A—C4A	1.385 (12)
C3—H3	0.9500	C3A—H3A	0.9500
C4—C5	1.378 (12)	C4A—C5A	1.389 (12)
C4—H4	0.9500	C4A—H4A	0.9500
C5—C6	1.466 (11)	C5A—C6A	1.469 (11)
C6—C7	1.399 (12)	C6A—C7A	1.389 (12)
C7—C8	1.391 (12)	C7A—C8A	1.387 (12)
C7—H7	0.9500	C7A—H7A	0.9500
C8—C9	1.372 (13)	C8A—C9A	1.368 (13)
C8—H8	0.9500	C8A—H8A	0.9500
C9—C10	1.390 (12)	C9A—C10A	1.392 (12)
C9—H9	0.9500	C9A—H9A	0.9500
C10—H10	0.9500	C10A—H10A	0.9500
C12—C11	1.413 (12)	C14A—C15A	1.409 (12)
C12—C13	1.418 (12)	C14A—C13A	1.429 (13)
C12—H12	1.0000	C14A—C20A	1.489 (13)
C13—C14	1.414 (12)	C13A—C12A	1.384 (13)
C13—H13	1.0000	C13A—H13A	1.0000
C14—C15	1.403 (12)	C12A—C11A	1.431 (13)
C14—C20	1.516 (12)	C12A—H12A	1.0000
C15—C16	1.411 (12)	C11A—C16A	1.423 (13)
C15—H15	1.0000	C11A—C17A	1.521 (13)
C16—C11	1.429 (12)	C15A—C16A	1.419 (12)
C16—H16	1.0000	C15A—H15A	1.0000
C11—C17	1.507 (12)	C17A—C18A	1.496 (16)
C20—H20A	0.9800	C17A—C19A	1.533 (16)
C20—H20B	0.9800	C17A—H17A	1.0000
C20—H20C	0.9800	C16A—H16A	1.0000
C17—C18	1.492 (15)	C19A—H19D	0.9800
C17—C19	1.508 (14)	C19A—H19E	0.9800
C17—H17	1.0000	C19A—H19F	0.9800
C18—H18A	0.9800	C18A—H18D	0.9800
C18—H18B	0.9800	C18A—H18E	0.9800
C18—H18C	0.9800	C18A—H18F	0.9800
C19—H19A	0.9800	C20A—H20D	0.9800
C19—H19B	0.9800	C20A—H20E	0.9800
C19—H19C	0.9800	C20A—H20F	0.9800
N2—Ru1—N1	77.0 (3)	N2A—Ru1A—N1A	76.5 (3)
N2—Ru1—C12	138.9 (3)	N2A—Ru1A—C12A	141.4 (3)
N1—Ru1—C12	91.5 (3)	N1A—Ru1A—C12A	93.8 (3)

## supplementary materials

N2—Ru1—C16	90.5 (3)	N2A—Ru1A—C13A	170.5 (3)
N1—Ru1—C16	130.7 (3)	N1A—Ru1A—C13A	111.8 (3)
C12—Ru1—C16	67.4 (3)	C12A—Ru1A—C13A	36.8 (3)
N2—Ru1—C11	104.6 (3)	N2A—Ru1A—C16A	92.2 (3)
N1—Ru1—C11	99.1 (3)	N1A—Ru1A—C16A	132.3 (3)
C12—Ru1—C11	37.7 (3)	C12A—Ru1A—C16A	66.7 (3)
C16—Ru1—C11	38.0 (3)	C13A—Ru1A—C16A	78.9 (3)
N2—Ru1—C13	169.7 (3)	N2A—Ru1A—C15A	104.1 (3)
N1—Ru1—C13	111.0 (3)	N1A—Ru1A—C15A	169.3 (3)
C12—Ru1—C13	37.8 (3)	C12A—Ru1A—C15A	79.0 (3)
C16—Ru1—C13	79.5 (3)	C13A—Ru1A—C15A	66.8 (3)
C11—Ru1—C13	68.4 (3)	C16A—Ru1A—C15A	37.4 (3)
N2—Ru1—C15	103.9 (3)	N2A—Ru1A—C11A	106.6 (3)
N1—Ru1—C15	167.4 (3)	N1A—Ru1A—C11A	101.3 (3)
C12—Ru1—C15	79.6 (3)	C12A—Ru1A—C11A	37.9 (3)
C16—Ru1—C15	37.3 (3)	C13A—Ru1A—C11A	68.0 (3)
C11—Ru1—C15	68.4 (3)	C16A—Ru1A—C11A	37.4 (3)
C13—Ru1—C15	66.7 (3)	C15A—Ru1A—C11A	68.1 (3)
N2—Ru1—C14	136.3 (3)	N2A—Ru1A—C14A	135.8 (3)
N1—Ru1—C14	146.1 (3)	N1A—Ru1A—C14A	146.5 (3)
C12—Ru1—C14	67.3 (3)	C12A—Ru1A—C14A	66.5 (3)
C16—Ru1—C14	66.6 (3)	C13A—Ru1A—C14A	37.2 (3)
C11—Ru1—C14	80.3 (3)	C16A—Ru1A—C14A	66.3 (3)
C13—Ru1—C14	37.0 (3)	C15A—Ru1A—C14A	36.5 (3)
C15—Ru1—C14	36.5 (3)	C11A—Ru1A—C14A	80.0 (3)
N2—Ru1—C11	86.4 (2)	N2A—Ru1A—C11A	85.8 (2)
N1—Ru1—C11	86.1 (2)	N1A—Ru1A—C11A	84.74 (19)
C12—Ru1—C11	132.6 (2)	C12A—Ru1A—C11A	131.1 (2)
C16—Ru1—C11	141.2 (2)	C13A—Ru1A—C11A	99.2 (2)
C11—Ru1—C11	168.6 (2)	C16A—Ru1A—C11A	141.3 (2)
C13—Ru1—C11	100.2 (2)	C15A—Ru1A—C11A	106.0 (2)
C15—Ru1—C11	106.5 (2)	C11A—Ru1A—C11A	167.1 (2)
C14—Ru1—C11	89.7 (2)	C14A—Ru1A—C11A	88.7 (2)
C1—N1—C5	118.6 (7)	C5A—N1A—C1A	118.6 (7)
C1—N1—Ru1	124.1 (6)	C5A—N1A—Ru1A	117.1 (5)
C5—N1—Ru1	117.3 (5)	C1A—N1A—Ru1A	124.2 (6)
C10—N2—C6	119.2 (7)	C10A—N2A—C6A	118.8 (7)
C10—N2—Ru1	124.2 (6)	C10A—N2A—Ru1A	123.8 (6)
C6—N2—Ru1	116.4 (5)	C6A—N2A—Ru1A	117.3 (5)
N1—C1—C2	122.4 (8)	N1A—C1A—C2A	122.5 (8)
N1—C1—H1	118.8	N1A—C1A—H1A	118.7
C2—C1—H1	118.8	C2A—C1A—H1A	118.7
C3—C2—C1	118.7 (8)	C3A—C2A—C1A	119.0 (8)
C3—C2—H2	120.7	C3A—C2A—H2A	120.5
C1—C2—H2	120.7	C1A—C2A—H2A	120.5
C4—C3—C2	118.9 (8)	C2A—C3A—C4A	118.7 (8)
C4—C3—H3	120.6	C2A—C3A—H3A	120.7
C2—C3—H3	120.6	C4A—C3A—H3A	120.7
C5—C4—C3	119.9 (8)	C3A—C4A—C5A	119.9 (8)
C5—C4—H4	120.1	C3A—C4A—H4A	120.1
C3—C4—H4	120.1	C5A—C4A—H4A	120.1
N1—C5—C4	121.6 (8)	N1A—C5A—C4A	121.3 (7)
N1—C5—C6	114.2 (7)	N1A—C5A—C6A	114.7 (7)
C4—C5—C6	124.2 (7)	C4A—C5A—C6A	124.0 (8)

## supplementary materials

N2—C6—C7	121.9 (8)	N2A—C6A—C7A	121.8 (8)
N2—C6—C5	114.6 (7)	N2A—C6A—C5A	114.0 (7)
C7—C6—C5	123.5 (8)	C7A—C6A—C5A	124.1 (8)
C8—C7—C6	117.4 (8)	C8A—C7A—C6A	118.6 (8)
C8—C7—H7	121.3	C8A—C7A—H7A	120.7
C6—C7—H7	121.3	C6A—C7A—H7A	120.7
C9—C8—C7	120.5 (8)	C9A—C8A—C7A	119.2 (8)
C9—C8—H8	119.7	C9A—C8A—H8A	120.4
C7—C8—H8	119.7	C7A—C8A—H8A	120.4
C8—C9—C10	119.7 (8)	C8A—C9A—C10A	119.4 (8)
C8—C9—H9	120.2	C8A—C9A—H9A	120.3
C10—C9—H9	120.2	C10A—C9A—H9A	120.3
N2—C10—C9	121.3 (8)	N2A—C10A—C9A	122.1 (8)
N2—C10—H10	119.3	N2A—C10A—H10A	119.0
C9—C10—H10	119.3	C9A—C10A—H10A	119.0
C11—C12—C13	122.1 (8)	C15A—C14A—C13A	118.1 (8)
C11—C12—Ru1	72.3 (5)	C15A—C14A—C20A	120.5 (8)
C13—C12—Ru1	72.3 (5)	C13A—C14A—C20A	121.3 (8)
C11—C12—H12	118.4	C15A—C14A—Ru1A	69.6 (5)
C13—C12—H12	118.4	C13A—C14A—Ru1A	68.7 (5)
Ru1—C12—H12	118.4	C20A—C14A—Ru1A	130.4 (6)
C14—C13—C12	119.8 (8)	C12A—C13A—C14A	120.5 (8)
C14—C13—Ru1	73.3 (5)	C12A—C13A—Ru1A	70.7 (5)
C12—C13—Ru1	69.9 (4)	C14A—C13A—Ru1A	74.1 (5)
C14—C13—H13	119.7	C12A—C13A—H13A	119.4
C12—C13—H13	119.7	C14A—C13A—H13A	119.4
Ru1—C13—H13	119.7	Ru1A—C13A—H13A	119.4
C15—C14—C13	119.6 (8)	C13A—C12A—C11A	123.1 (8)
C15—C14—C20	119.8 (8)	C13A—C12A—Ru1A	72.5 (5)
C13—C14—C20	120.5 (8)	C11A—C12A—Ru1A	72.7 (5)
C15—C14—Ru1	70.6 (5)	C13A—C12A—H12A	117.9
C13—C14—Ru1	69.7 (5)	C11A—C12A—H12A	117.9
C20—C14—Ru1	130.5 (6)	Ru1A—C12A—H12A	117.9
C14—C15—C16	119.8 (8)	C16A—C11A—C12A	115.5 (8)
C14—C15—Ru1	72.8 (5)	C16A—C11A—C17A	121.8 (8)
C16—C15—Ru1	69.8 (5)	C12A—C11A—C17A	122.6 (9)
C14—C15—H15	119.6	C16A—C11A—Ru1A	70.8 (5)
C16—C15—H15	119.6	C12A—C11A—Ru1A	69.4 (5)
Ru1—C15—H15	119.6	C17A—C11A—Ru1A	133.0 (7)
C15—C16—C11	122.2 (8)	C14A—C15A—C16A	120.4 (8)
C15—C16—Ru1	72.8 (5)	C14A—C15A—Ru1A	73.9 (5)
C11—C16—Ru1	71.6 (5)	C16A—C15A—Ru1A	71.0 (5)
C15—C16—H16	118.3	C14A—C15A—H15A	119.5
C11—C16—H16	118.3	C16A—C15A—H15A	119.5
Ru1—C16—H16	118.3	Ru1A—C15A—H15A	119.5
C12—C11—C16	116.5 (7)	C18A—C17A—C11A	112.9 (9)
C12—C11—C17	119.8 (8)	C18A—C17A—C19A	111.7 (10)
C16—C11—C17	123.6 (8)	C11A—C17A—C19A	111.6 (9)
C12—C11—Ru1	70.0 (5)	C18A—C17A—H17A	106.7
C16—C11—Ru1	70.3 (4)	C11A—C17A—H17A	106.7
C17—C11—Ru1	127.0 (6)	C19A—C17A—H17A	106.7
C14—C20—H20A	109.5	C15A—C16A—C11A	122.2 (8)
C14—C20—H20B	109.5	C15A—C16A—Ru1A	71.6 (5)
H20A—C20—H20B	109.5	C11A—C16A—Ru1A	71.8 (5)

## supplementary materials

C14—C20—H20C	109.5	C15A—C16A—H16A	118.2
H20A—C20—H20C	109.5	C11A—C16A—H16A	118.2
H20B—C20—H20C	109.5	Ru1A—C16A—H16A	118.2
C18—C17—C11	110.3 (9)	C17A—C19A—H19D	109.5
C18—C17—C19	110.7 (9)	C17A—C19A—H19E	109.5
C11—C17—C19	115.0 (8)	H19D—C19A—H19E	109.5
C18—C17—H17	106.8	C17A—C19A—H19F	109.5
C11—C17—H17	106.8	H19D—C19A—H19F	109.5
C19—C17—H17	106.8	H19E—C19A—H19F	109.5
C17—C18—H18A	109.5	C17A—C18A—H18D	109.5
C17—C18—H18B	109.5	C17A—C18A—H18E	109.5
H18A—C18—H18B	109.5	H18D—C18A—H18E	109.5
C17—C18—H18C	109.5	C17A—C18A—H18F	109.5
H18A—C18—H18C	109.5	H18D—C18A—H18F	109.5
H18B—C18—H18C	109.5	H18E—C18A—H18F	109.5
C17—C19—H19A	109.5	C14A—C20A—H20D	109.5
C17—C19—H19B	109.5	C14A—C20A—H20E	109.5
H19A—C19—H19B	109.5	H20D—C20A—H20E	109.5
C17—C19—H19C	109.5	C14A—C20A—H20F	109.5
H19A—C19—H19C	109.5	H20D—C20A—H20F	109.5
H19B—C19—H19C	109.5	H20E—C20A—H20F	109.5
N2—Ru1—N1—C1	175.1 (7)	N2A—Ru1A—N1A—C5A	1.7 (6)
C12—Ru1—N1—C1	−44.7 (7)	C12A—Ru1A—N1A—C5A	−140.4 (6)
C16—Ru1—N1—C1	−105.7 (7)	C13A—Ru1A—N1A—C5A	−173.5 (6)
C11—Ru1—N1—C1	−81.8 (7)	C16A—Ru1A—N1A—C5A	−78.8 (7)
C13—Ru1—N1—C1	−11.5 (8)	C15A—Ru1A—N1A—C5A	−93.1 (16)
C15—Ru1—N1—C1	−88.9 (15)	C11A—Ru1A—N1A—C5A	−102.9 (6)
C14—Ru1—N1—C1	4.3 (10)	C14A—Ru1A—N1A—C5A	168.2 (6)
C11—Ru1—N1—C1	87.9 (7)	C11A—Ru1A—N1A—C5A	88.6 (6)
N2—Ru1—N1—C5	−4.9 (6)	N2A—Ru1A—N1A—C1A	−175.5 (7)
C12—Ru1—N1—C5	135.3 (6)	C12A—Ru1A—N1A—C1A	42.4 (7)
C16—Ru1—N1—C5	74.3 (7)	C13A—Ru1A—N1A—C1A	9.3 (7)
C11—Ru1—N1—C5	98.2 (6)	C16A—Ru1A—N1A—C1A	104.1 (7)
C13—Ru1—N1—C5	168.5 (6)	C15A—Ru1A—N1A—C1A	89.8 (17)
C15—Ru1—N1—C5	91.0 (15)	C11A—Ru1A—N1A—C1A	80.0 (7)
C14—Ru1—N1—C5	−175.7 (6)	C14A—Ru1A—N1A—C1A	−8.9 (10)
C11—Ru1—N1—C5	−92.1 (6)	C11A—Ru1A—N1A—C1A	−88.5 (6)
N1—Ru1—N2—C10	−178.1 (8)	N1A—Ru1A—N2A—C10A	179.7 (7)
C12—Ru1—N2—C10	104.8 (8)	C12A—Ru1A—N2A—C10A	−101.3 (8)
C16—Ru1—N2—C10	50.0 (7)	C13A—Ru1A—N2A—C10A	−28 (2)
C11—Ru1—N2—C10	85.7 (8)	C16A—Ru1A—N2A—C10A	−47.2 (7)
C13—Ru1—N2—C10	39 (2)	C15A—Ru1A—N2A—C10A	−11.3 (8)
C15—Ru1—N2—C10	14.8 (8)	C11A—Ru1A—N2A—C10A	−82.3 (7)
C14—Ru1—N2—C10	−5.5 (9)	C14A—Ru1A—N2A—C10A	10.4 (9)
C11—Ru1—N2—C10	−91.3 (7)	C11A—Ru1A—N2A—C10A	94.1 (7)
N1—Ru1—N2—C6	6.4 (6)	N1A—Ru1A—N2A—C6A	−4.9 (6)
C12—Ru1—N2—C6	−70.7 (7)	C12A—Ru1A—N2A—C6A	74.0 (8)
C16—Ru1—N2—C6	−125.5 (6)	C13A—Ru1A—N2A—C6A	146.9 (18)
C11—Ru1—N2—C6	−89.8 (6)	C16A—Ru1A—N2A—C6A	128.2 (6)
C13—Ru1—N2—C6	−136.3 (16)	C15A—Ru1A—N2A—C6A	164.0 (6)
C15—Ru1—N2—C6	−160.7 (6)	C11A—Ru1A—N2A—C6A	93.0 (6)
C14—Ru1—N2—C6	179.0 (5)	C14A—Ru1A—N2A—C6A	−174.3 (5)
C11—Ru1—N2—C6	93.2 (6)	C11A—Ru1A—N2A—C6A	−90.5 (6)

## supplementary materials

C5—N1—C1—C2	−1.9 (13)	C5A—N1A—C1A—C2A	0.3 (12)
Ru1—N1—C1—C2	178.1 (7)	Ru1A—N1A—C1A—C2A	177.4 (6)
N1—C1—C2—C3	0.5 (14)	N1A—C1A—C2A—C3A	0.3 (13)
C1—C2—C3—C4	0.6 (13)	C1A—C2A—C3A—C4A	−0.2 (13)
C2—C3—C4—C5	−0.3 (13)	C2A—C3A—C4A—C5A	−0.4 (13)
C1—N1—C5—C4	2.3 (12)	C1A—N1A—C5A—C4A	−0.9 (12)
Ru1—N1—C5—C4	−177.7 (6)	Ru1A—N1A—C5A—C4A	−178.2 (6)
C1—N1—C5—C6	−177.3 (7)	C1A—N1A—C5A—C6A	178.8 (7)
Ru1—N1—C5—C6	2.8 (9)	Ru1A—N1A—C5A—C6A	1.5 (9)
C3—C4—C5—N1	−1.2 (13)	C3A—C4A—C5A—N1A	1.0 (13)
C3—C4—C5—C6	178.3 (8)	C3A—C4A—C5A—C6A	−178.7 (8)
C10—N2—C6—C7	−1.7 (13)	C10A—N2A—C6A—C7A	0.8 (12)
Ru1—N2—C6—C7	174.0 (6)	Ru1A—N2A—C6A—C7A	−174.8 (6)
C10—N2—C6—C5	177.3 (8)	C10A—N2A—C6A—C5A	−177.2 (7)
Ru1—N2—C6—C5	−6.9 (9)	Ru1A—N2A—C6A—C5A	7.2 (9)
N1—C5—C6—N2	2.7 (11)	N1A—C5A—C6A—N2A	−5.6 (10)
C4—C5—C6—N2	−176.8 (8)	C4A—C5A—C6A—N2A	174.1 (8)
N1—C5—C6—C7	−178.3 (8)	N1A—C5A—C6A—C7A	176.4 (8)
C4—C5—C6—C7	2.2 (13)	C4A—C5A—C6A—C7A	−3.9 (13)
N2—C6—C7—C8	−0.1 (13)	N2A—C6A—C7A—C8A	0.4 (12)
C5—C6—C7—C8	−179.1 (8)	C5A—C6A—C7A—C8A	178.2 (8)
C6—C7—C8—C9	1.4 (13)	C6A—C7A—C8A—C9A	−2.0 (13)
C7—C8—C9—C10	−1.0 (14)	C7A—C8A—C9A—C10A	2.6 (13)
C6—N2—C10—C9	2.2 (13)	C6A—N2A—C10A—C9A	−0.3 (13)
Ru1—N2—C10—C9	−173.2 (7)	Ru1A—N2A—C10A—C9A	175.0 (6)
C8—C9—C10—N2	−0.8 (15)	C8A—C9A—C10A—N2A	−1.4 (14)
N2—Ru1—C12—C11	−31.2 (7)	N2A—Ru1A—C14A—C15A	−37.0 (7)
N1—Ru1—C12—C11	−103.0 (5)	N1A—Ru1A—C14A—C15A	162.0 (5)
C16—Ru1—C12—C11	31.1 (5)	C12A—Ru1A—C14A—C15A	103.8 (6)
C13—Ru1—C12—C11	133.4 (7)	C13A—Ru1A—C14A—C15A	133.2 (8)
C15—Ru1—C12—C11	68.1 (5)	C16A—Ru1A—C14A—C15A	30.0 (5)
C14—Ru1—C12—C11	104.1 (5)	C11A—Ru1A—C14A—C15A	66.6 (5)
C11—Ru1—C12—C11	170.9 (4)	C11A—Ru1A—C14A—C15A	−119.6 (5)
N2—Ru1—C12—C13	−164.6 (5)	N2A—Ru1A—C14A—C13A	−170.2 (5)
N1—Ru1—C12—C13	123.6 (5)	N1A—Ru1A—C14A—C13A	28.8 (8)
C16—Ru1—C12—C13	−102.3 (5)	C12A—Ru1A—C14A—C13A	−29.4 (5)
C11—Ru1—C12—C13	−133.4 (7)	C16A—Ru1A—C14A—C13A	−103.2 (6)
C15—Ru1—C12—C13	−65.3 (5)	C15A—Ru1A—C14A—C13A	−133.2 (8)
C14—Ru1—C12—C13	−29.3 (5)	C11A—Ru1A—C14A—C13A	−66.6 (5)
C11—Ru1—C12—C13	37.5 (6)	C11A—Ru1A—C14A—C13A	107.2 (5)
C11—C12—C13—C14	1.1 (12)	N2A—Ru1A—C14A—C20A	76.3 (10)
Ru1—C12—C13—C14	55.8 (7)	N1A—Ru1A—C14A—C20A	−84.7 (10)
C11—C12—C13—Ru1	−54.8 (7)	C12A—Ru1A—C14A—C20A	−143.0 (10)
N2—Ru1—C13—C14	−53.9 (19)	C13A—Ru1A—C14A—C20A	−113.5 (10)
N1—Ru1—C13—C14	165.4 (5)	C16A—Ru1A—C14A—C20A	143.3 (9)
C12—Ru1—C13—C14	−131.4 (7)	C15A—Ru1A—C14A—C20A	113.3 (11)
C16—Ru1—C13—C14	−64.9 (5)	C11A—Ru1A—C14A—C20A	179.9 (9)
C11—Ru1—C13—C14	−102.9 (5)	C11A—Ru1A—C14A—C20A	−6.3 (8)
C15—Ru1—C13—C14	−28.0 (5)	C15A—C14A—C13A—C12A	4.8 (12)
C11—Ru1—C13—C14	75.6 (5)	C20A—C14A—C13A—C12A	−179.2 (8)
N2—Ru1—C13—C12	77.5 (18)	Ru1A—C14A—C13A—C12A	55.5 (7)
N1—Ru1—C13—C12	−63.2 (5)	C15A—C14A—C13A—Ru1A	−50.7 (7)
C16—Ru1—C13—C12	66.5 (5)	C20A—C14A—C13A—Ru1A	125.3 (8)
C11—Ru1—C13—C12	28.5 (5)	N2A—Ru1A—C13A—C12A	−85 (2)



## supplementary materials

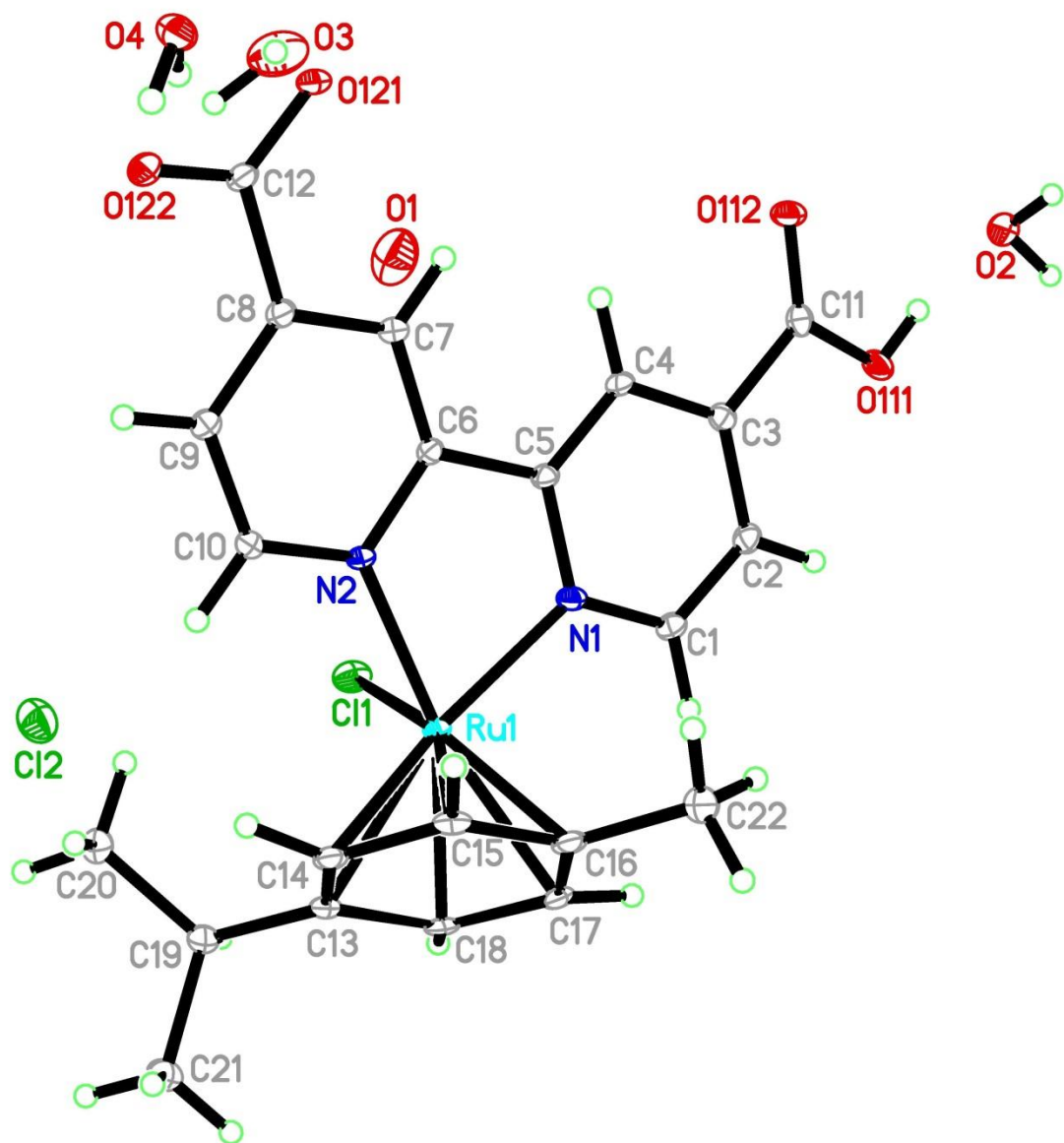
C15—Ru1—C13—C12	103.4 (5)	N1A—Ru1A—C13A—C12A	65.4 (6)
C14—Ru1—C13—C12	131.4 (7)	C16A—Ru1A—C13A—C12A	−65.9 (5)
C11—Ru1—C13—C12	−152.9 (4)	C15A—Ru1A—C13A—C12A	−103.1 (6)
C12—C13—C14—C15	−2.3 (11)	C11A—Ru1A—C13A—C12A	−28.4 (5)
Ru1—C13—C14—C15	51.9 (7)	C14A—Ru1A—C13A—C12A	−131.2 (8)
C12—C13—C14—C20	180.0 (8)	C11A—Ru1A—C13A—C12A	153.4 (5)
Ru1—C13—C14—C20	−125.9 (8)	N2A—Ru1A—C13A—C14A	46 (2)
C12—C13—C14—Ru1	−54.2 (7)	N1A—Ru1A—C13A—C14A	−163.3 (5)
N2—Ru1—C14—C15	34.5 (7)	C12A—Ru1A—C13A—C14A	131.2 (8)
N1—Ru1—C14—C15	−158.5 (5)	C16A—Ru1A—C13A—C14A	65.4 (5)
C12—Ru1—C14—C15	−103.6 (5)	C15A—Ru1A—C13A—C14A	28.2 (5)
C16—Ru1—C14—C15	−29.5 (5)	C11A—Ru1A—C13A—C14A	102.9 (6)
C11—Ru1—C14—C15	−66.6 (5)	C11A—Ru1A—C13A—C14A	−75.4 (5)
C13—Ru1—C14—C15	−133.5 (7)	C14A—C13A—C12A—C11A	−2.4 (13)
C11—Ru1—C14—C15	118.9 (5)	Ru1A—C13A—C12A—C11A	54.7 (7)
N2—Ru1—C14—C13	168.0 (5)	C14A—C13A—C12A—Ru1A	−57.1 (7)
N1—Ru1—C14—C13	−25.0 (8)	N2A—Ru1A—C12A—C13A	164.7 (5)
C12—Ru1—C14—C13	29.9 (5)	N1A—Ru1A—C12A—C13A	−122.2 (5)
C16—Ru1—C14—C13	104.1 (5)	C16A—Ru1A—C12A—C13A	102.9 (6)
C11—Ru1—C14—C13	66.9 (5)	C15A—Ru1A—C12A—C13A	65.8 (5)
C15—Ru1—C14—C13	133.5 (7)	C11A—Ru1A—C12A—C13A	134.2 (8)
C11—Ru1—C14—C13	−107.6 (5)	C14A—Ru1A—C12A—C13A	29.7 (5)
N2—Ru1—C14—C20	−78.7 (10)	C11A—Ru1A—C12A—C13A	−35.9 (6)
N1—Ru1—C14—C20	88.3 (10)	N2A—Ru1A—C12A—C11A	30.5 (8)
C12—Ru1—C14—C20	143.2 (9)	N1A—Ru1A—C12A—C11A	103.6 (5)
C16—Ru1—C14—C20	−142.6 (9)	C13A—Ru1A—C12A—C11A	−134.2 (8)
C11—Ru1—C14—C20	−179.8 (9)	C16A—Ru1A—C12A—C11A	−31.3 (5)
C13—Ru1—C14—C20	113.3 (11)	C15A—Ru1A—C12A—C11A	−68.4 (5)
C15—Ru1—C14—C20	−113.1 (11)	C14A—Ru1A—C12A—C11A	−104.5 (6)
C11—Ru1—C14—C20	5.8 (9)	C11A—Ru1A—C12A—C11A	−170.1 (4)
C13—C14—C15—C16	2.1 (11)	C13A—C12A—C11A—C16A	0.6 (12)
C20—C14—C15—C16	179.9 (8)	Ru1A—C12A—C11A—C16A	55.3 (7)
Ru1—C14—C15—C16	53.6 (7)	C13A—C12A—C11A—C17A	176.7 (9)
C13—C14—C15—Ru1	−51.5 (7)	Ru1A—C12A—C11A—C17A	−128.7 (9)
C20—C14—C15—Ru1	126.3 (8)	C13A—C12A—C11A—Ru1A	−54.6 (7)
N2—Ru1—C15—C14	−156.2 (5)	N2A—Ru1A—C11A—C16A	71.1 (6)
N1—Ru1—C15—C14	110.8 (13)	N1A—Ru1A—C11A—C16A	150.2 (5)
C12—Ru1—C15—C14	65.7 (5)	C12A—Ru1A—C11A—C16A	−128.2 (8)
C16—Ru1—C15—C14	131.9 (7)	C13A—Ru1A—C11A—C16A	−100.7 (6)
C11—Ru1—C15—C14	103.3 (5)	C15A—Ru1A—C11A—C16A	−27.8 (5)
C13—Ru1—C15—C14	28.4 (5)	C14A—Ru1A—C11A—C16A	−63.9 (5)
C11—Ru1—C15—C14	−65.9 (5)	C11A—Ru1A—C11A—C16A	−92.8 (12)
N2—Ru1—C15—C16	71.8 (5)	N2A—Ru1A—C11A—C12A	−160.7 (5)
N1—Ru1—C15—C16	−21.1 (16)	N1A—Ru1A—C11A—C12A	−81.5 (5)
C12—Ru1—C15—C16	−66.2 (5)	C13A—Ru1A—C11A—C12A	27.6 (5)
C11—Ru1—C15—C16	−28.6 (5)	C16A—Ru1A—C11A—C12A	128.2 (8)
C13—Ru1—C15—C16	−103.6 (5)	C15A—Ru1A—C11A—C12A	100.4 (6)
C14—Ru1—C15—C16	−131.9 (7)	C14A—Ru1A—C11A—C12A	64.4 (5)
C11—Ru1—C15—C16	162.2 (4)	C11A—Ru1A—C11A—C12A	35.4 (14)
C14—C15—C16—C11	−0.8 (12)	N2A—Ru1A—C11A—C17A	−44.8 (10)
Ru1—C15—C16—C11	54.2 (7)	N1A—Ru1A—C11A—C17A	34.3 (10)
C14—C15—C16—Ru1	−55.0 (7)	C12A—Ru1A—C11A—C17A	115.8 (11)
N2—Ru1—C16—C15	−112.8 (5)	C13A—Ru1A—C11A—C17A	143.4 (10)
N1—Ru1—C16—C15	174.1 (5)	C16A—Ru1A—C11A—C17A	−115.9 (11)

## supplementary materials

C12—Ru1—C16—C15	102.8 (5)	C15A—Ru1A—C11A—C17A	−143.7 (10)
C11—Ru1—C16—C15	133.7 (7)	C14A—Ru1A—C11A—C17A	−179.8 (10)
C13—Ru1—C16—C15	65.3 (5)	C11A—Ru1A—C11A—C17A	151.2 (8)
C14—Ru1—C16—C15	28.9 (5)	C13A—C14A—C15A—C16A	−5.5 (12)
C11—Ru1—C16—C15	−27.9 (6)	C20A—C14A—C15A—C16A	178.5 (8)
N2—Ru1—C16—C11	113.6 (5)	Ru1A—C14A—C15A—C16A	−55.8 (7)
N1—Ru1—C16—C11	40.4 (6)	C13A—C14A—C15A—Ru1A	50.3 (7)
C12—Ru1—C16—C11	−30.8 (5)	C20A—C14A—C15A—Ru1A	−125.7 (8)
C13—Ru1—C16—C11	−68.4 (5)	N2A—Ru1A—C15A—C14A	154.4 (5)
C15—Ru1—C16—C11	−133.7 (7)	N1A—Ru1A—C15A—C14A	−113.5 (15)
C14—Ru1—C16—C11	−104.8 (5)	C12A—Ru1A—C15A—C14A	−65.1 (5)
C11—Ru1—C16—C11	−161.6 (4)	C13A—Ru1A—C15A—C14A	−28.7 (5)
C13—C12—C11—C16	0.3 (11)	C16A—Ru1A—C15A—C14A	−131.0 (8)
Ru1—C12—C11—C16	−54.5 (6)	C11A—Ru1A—C15A—C14A	−103.1 (6)
C13—C12—C11—C17	176.7 (8)	C11A—Ru1A—C15A—C14A	64.7 (5)
Ru1—C12—C11—C17	122.0 (8)	N2A—Ru1A—C15A—C16A	−74.6 (5)
C13—C12—C11—Ru1	54.8 (7)	N1A—Ru1A—C15A—C16A	17.5 (18)
C15—C16—C11—C12	−0.5 (11)	C12A—Ru1A—C15A—C16A	65.9 (5)
Ru1—C16—C11—C12	54.3 (6)	C13A—Ru1A—C15A—C16A	102.4 (6)
C15—C16—C11—C17	−176.7 (8)	C11A—Ru1A—C15A—C16A	27.9 (5)
Ru1—C16—C11—C17	−122.0 (8)	C14A—Ru1A—C15A—C16A	131.0 (8)
C15—C16—C11—Ru1	−54.8 (7)	C11A—Ru1A—C15A—C16A	−164.3 (4)
N2—Ru1—C11—C12	159.4 (5)	C16A—C11A—C17A—C18A	−157.0 (9)
N1—Ru1—C11—C12	80.5 (5)	C12A—C11A—C17A—C18A	27.2 (13)
C16—Ru1—C11—C12	−129.3 (7)	Ru1A—C11A—C17A—C18A	−64.2 (13)
C13—Ru1—C11—C12	−28.6 (5)	C16A—C11A—C17A—C19A	−30.2 (13)
C15—Ru1—C11—C12	−101.1 (5)	C12A—C11A—C17A—C19A	154.0 (9)
C14—Ru1—C11—C12	−65.1 (5)	Ru1A—C11A—C17A—C19A	62.5 (13)
C11—Ru1—C11—C12	−35.9 (14)	C14A—C15A—C16A—C11A	4.0 (13)
N2—Ru1—C11—C16	−71.3 (5)	Ru1A—C15A—C16A—C11A	−53.2 (8)
N1—Ru1—C11—C16	−150.2 (5)	C14A—C15A—C16A—Ru1A	57.2 (7)
C12—Ru1—C11—C16	129.3 (7)	C12A—C11A—C16A—C15A	−1.4 (12)
C13—Ru1—C11—C16	100.7 (5)	C17A—C11A—C16A—C15A	−177.5 (8)
C15—Ru1—C11—C16	28.2 (5)	Ru1A—C11A—C16A—C15A	53.1 (7)
C14—Ru1—C11—C16	64.2 (5)	C12A—C11A—C16A—Ru1A	−54.5 (6)
C11—Ru1—C11—C16	93.4 (12)	C17A—C11A—C16A—Ru1A	129.3 (9)
N2—Ru1—C11—C17	46.5 (8)	N2A—Ru1A—C16A—C15A	110.7 (5)
N1—Ru1—C11—C17	−32.4 (8)	N1A—Ru1A—C16A—C15A	−175.7 (5)
C12—Ru1—C11—C17	−112.9 (10)	C12A—Ru1A—C16A—C15A	−102.8 (6)
C16—Ru1—C11—C17	117.8 (10)	C13A—Ru1A—C16A—C15A	−66.2 (5)
C13—Ru1—C11—C17	−141.5 (8)	C11A—Ru1A—C16A—C15A	−134.5 (8)
C15—Ru1—C11—C17	146.0 (9)	C14A—Ru1A—C16A—C15A	−29.4 (5)
C14—Ru1—C11—C17	−178.0 (8)	C11A—Ru1A—C16A—C15A	24.6 (7)
C11—Ru1—C11—C17	−148.8 (9)	N2A—Ru1A—C16A—C11A	−114.9 (5)
C12—C11—C17—C18	69.6 (11)	N1A—Ru1A—C16A—C11A	−41.2 (7)
C16—C11—C17—C18	−114.3 (10)	C12A—Ru1A—C16A—C11A	31.7 (5)
Ru1—C11—C17—C18	156.1 (8)	C13A—Ru1A—C16A—C11A	68.2 (6)
C12—C11—C17—C19	−164.4 (9)	C15A—Ru1A—C16A—C11A	134.5 (8)
C16—C11—C17—C19	11.8 (13)	C14A—Ru1A—C16A—C11A	105.1 (6)
Ru1—C11—C17—C19	−77.9 (11)	C11A—Ru1A—C16A—C11A	159.1 (4)

Compound 22

Image:



Data:

## supplementary materials

## supplementary materials

## Experimental

(081512ral\_ask\_0m)

## Crystal data

$C_{22}H_{21}ClN_2O_4Ru \cdot C_{22}H_{21}ClN_2O_4Ru \cdot Cl \cdot 2(H_2O) \cdot 2(O)$   
 $M_r = 1132.35$   
 Triclinic,  $P\bar{1}$   
 Hall symbol: -P 1  
 $a = 10.5814(1) \text{ \AA}$   
 $b = 15.1730(2) \text{ \AA}$   
 $c = 16.4293(2) \text{ \AA}$   
 $\alpha = 112.745(1)^\circ$   
 $\beta = 90.960(1)^\circ$   
 $\gamma = 108.402(1)^\circ$   
 $V = 2279.01(5) \text{ \AA}^3$

$Z = 2$   
 $F(000) = 1152$   
 $D_x = 1.653 \text{ Mg m}^{-3}$   
 Cu  $K\alpha$  radiation,  $\lambda = 1.54178 \text{ \AA}$   
 Cell parameters from 9974 reflections  
 $\theta = 3.0\text{--}72.0^\circ$   
 $\mu = 7.55 \text{ mm}^{-1}$   
 $T = 102 \text{ K}$   
 Parallelepiped, Orange  
 $0.21 \times 0.17 \times 0.14 \text{ mm}$

## Data collection

Bruker SMART CCD Apex-II area-detector  
 diffractometer  
 Radiation source: fine-focus sealed tube  
 Graphite monochromator  
 $\phi$  and  $\omega$  scans  
 Absorption correction: Numerical  
*SADABS* (Sheldrick, 2008a)  
 $T_{\min} = 0.279$ ,  $T_{\max} = 0.424$

21861 measured reflections  
 7664 independent reflections  
 6976 reflections with  $I > 2\sigma(I)$   
 $R_{\text{int}} = 0.022$   
 $\theta_{\max} = 71.9^\circ$ ,  $\theta_{\min} = 3.0^\circ$   
 $h = -12 \rightarrow 12$   
 $k = -15 \rightarrow 17$   
 $l = -19 \rightarrow 19$

## Refinement

Refinement on  $F^2$   
 Least-squares matrix: Full  
 $R[F^2 > 2\sigma(F^2)] = 0.033$   
 $wR(F^2) = 0.080$   
 $S = 1.03$   
 7664 reflections  
 619 parameters  
 0 restraints  
 Primary atom site location: Structure-invariant direct  
 methods

Secondary atom site location: Difference Fourier map  
 Hydrogen site location: Inferred from neighbouring  
 sites  
 H-atom parameters constrained  
 $w = 1/[\sigma^2(F_o^2) + (0.0326P)^2 + 6.9357P]$   
 where  $P = (F_o^2 + 2F_c^2)/3$   
 $(\Delta/\sigma)_{\max} < 0.001$   
 $\Delta\rho_{\max} = 1.92 \text{ e \AA}^{-3}$   
 $\Delta\rho_{\min} = -0.65 \text{ e \AA}^{-3}$

## Special details

*Experimental.* 'crystal mounted on a Cryoloop using Paratone-N'

*Geometry.* All esds (except the esd in the dihedral angle between two l.s. planes) are estimated using the full covariance matrix. The cell esds are taken into account individually in the estimation of esds in distances, angles and torsion angles; correlations between esds in cell parameters are only used when they are defined by crystal symmetry. An approximate (isotropic) treatment of cell esds is used for estimating esds involving l.s. planes.

*Refinement.* Refinement of  $F^2$  against ALL reflections. The weighted R-factor wR and goodness of fit S are based on  $F^2$ , conventional R-factors R are based on F, with F set to zero for negative  $F^2$ . The threshold expression of  $F^2 > 2\sigma(F^2)$  is used only for calculating R-factors(gt) etc. and is not relevant to the choice of reflections for refinement. R-factors based on  $F^2$  are statistically about twice as large as those based on F, and R- factors based on ALL data will be even larger.

## supplementary materials

Fractional atomic coordinates and isotropic or equivalent isotropic displacement parameters ( $\text{\AA}^2$ )

	<i>x</i>	<i>y</i>	<i>z</i>	<i>U</i> <sub>iso</sub> */ <i>U</i> <sub>eq</sub>
Ru1	0.13952 (3)	0.524119 (19)	0.266296 (16)	0.01357 (7)
Ru1A	0.57054 (3)	0.11435 (2)	0.283758 (16)	0.01367 (7)
Cl1	0.37247 (9)	0.63136 (7)	0.29910 (6)	0.02409 (19)
Cl1A	0.70922 (9)	0.29037 (7)	0.35573 (5)	0.0241 (2)
Cl2	0.09774 (10)	0.12899 (7)	0.17253 (6)	0.0287 (2)
O111	0.1224 (3)	0.85243 (19)	0.06587 (16)	0.0225 (6)
H3W	0.1242	0.8807	0.0307	0.034*
O112	0.1447 (3)	0.7256 (2)	−0.05506 (16)	0.0247 (6)
O121	0.2165 (3)	0.29338 (19)	−0.18192 (16)	0.0223 (6)
O122	0.2071 (3)	0.16556 (19)	−0.14237 (16)	0.0229 (6)
O11A	0.9344 (2)	0.0458 (2)	0.60253 (16)	0.0212 (5)
H11A	0.9529	0.0327	0.6455	0.032*
O11B	0.7571 (2)	0.06682 (19)	0.66899 (16)	0.0199 (5)
O12A	0.1347 (3)	0.2529 (2)	0.59640 (17)	0.0225 (6)
O12B	0.2642 (2)	0.20076 (19)	0.66435 (15)	0.0183 (5)
H12B	0.2276	0.2245	0.7087	0.027*
O1	0.4513 (4)	0.6136 (3)	1.0130 (3)	0.0550 (9)
O2	0.1455 (3)	0.9725 (2)	0.98732 (19)	0.0283 (6)
O3	0.4664 (4)	0.4552 (3)	0.8555 (2)	0.0522 (9)
O4	0.0184 (3)	0.0113 (2)	0.72808 (17)	0.0238 (6)
N1	0.1222 (3)	0.6025 (2)	0.18892 (18)	0.0160 (6)
N1A	0.6658 (3)	0.1032 (2)	0.38899 (18)	0.0173 (6)
N2	0.1792 (3)	0.4362 (2)	0.14275 (18)	0.0141 (6)
N2A	0.4497 (3)	0.1494 (2)	0.38199 (18)	0.0128 (6)
C1	0.0961 (4)	0.6896 (3)	0.2191 (2)	0.0185 (7)
H1	0.0751	0.7149	0.2778	0.022*
C2	0.0985 (4)	0.7439 (3)	0.1678 (2)	0.0178 (7)
H2	0.0787	0.8051	0.1908	0.021*
C3	0.1301 (3)	0.7081 (3)	0.0826 (2)	0.0161 (7)
C4	0.1586 (3)	0.6183 (3)	0.0508 (2)	0.0165 (7)
H4	0.1816	0.5927	−0.0073	0.020*
C5	0.1530 (3)	0.5663 (3)	0.1050 (2)	0.0149 (7)
C6	0.1786 (3)	0.4703 (3)	0.0774 (2)	0.0146 (7)
C7	0.1941 (3)	0.4145 (3)	−0.0087 (2)	0.0163 (7)
H7	0.1940	0.4401	−0.0531	0.020*
C8	0.2099 (3)	0.3214 (3)	−0.0302 (2)	0.0164 (7)
C9	0.2134 (4)	0.2879 (3)	0.0372 (2)	0.0177 (7)
H9	0.2252	0.2247	0.0249	0.021*
C10	0.1994 (4)	0.3478 (3)	0.1224 (2)	0.0171 (7)
H10	0.2044	0.3253	0.1685	0.021*
C11	0.1340 (3)	0.7628 (3)	0.0230 (2)	0.0181 (7)
C12	0.2123 (4)	0.2535 (3)	−0.1263 (2)	0.0182 (7)
C13	0.1586 (4)	0.4864 (3)	0.3829 (2)	0.0192 (8)
C14	0.0716 (4)	0.3996 (3)	0.3114 (2)	0.0188 (7)
H14	0.1015	0.3397	0.2835	0.023*
C15	−0.0406 (4)	0.4024 (3)	0.2649 (2)	0.0188 (7)
H15	−0.0881	0.3440	0.2067	0.023*
C16	−0.0701 (4)	0.4933 (3)	0.2914 (2)	0.0187 (7)
C17	0.0157 (4)	0.5815 (3)	0.3666 (2)	0.0192 (7)
H17	0.0078	0.6492	0.3786	0.023*
C18	0.1277 (4)	0.5785 (3)	0.4103 (2)	0.0187 (7)

## supplementary materials

H18	0.1970	0.6442	0.4527	0.022*
C19	0.2812 (4)	0.4855 (3)	0.4314 (2)	0.0217 (8)
H19	0.3456	0.5573	0.4615	0.026*
C20	0.3553 (4)	0.4216 (3)	0.3696 (3)	0.0284 (9)
H20A	0.2941	0.3507	0.3390	0.043*
H20B	0.4332	0.4244	0.4048	0.043*
H20C	0.3861	0.4487	0.3252	0.043*
C21	0.2347 (4)	0.4487 (3)	0.5041 (3)	0.0274 (9)
H21A	0.1974	0.4961	0.5466	0.041*
H21B	0.3116	0.4457	0.5357	0.041*
H21C	0.1652	0.3806	0.4766	0.041*
C1A	0.7803 (4)	0.0830 (3)	0.3878 (2)	0.0229 (8)
H1A	0.8238	0.0756	0.3366	0.027*
C2A	0.8376 (4)	0.0725 (3)	0.4580 (2)	0.0214 (8)
H2A	0.9187	0.0579	0.4551	0.026*
C3A	0.7746 (3)	0.0837 (3)	0.5326 (2)	0.0159 (7)
C4A	0.6602 (3)	0.1103 (3)	0.5364 (2)	0.0153 (7)
H4A	0.6184	0.1218	0.5884	0.018*
C5A	0.6072 (3)	0.1198 (2)	0.4638 (2)	0.0140 (7)
C6A	0.4863 (3)	0.1463 (2)	0.4601 (2)	0.0124 (7)
C7A	0.4139 (3)	0.1672 (2)	0.5304 (2)	0.0137 (7)
H7A	0.4422	0.1650	0.5845	0.016*
C8A	0.3006 (3)	0.1913 (2)	0.5215 (2)	0.0132 (7)
C9A	0.2630 (3)	0.1946 (3)	0.4414 (2)	0.0164 (7)
H9A	0.1856	0.2111	0.4333	0.020*
C10A	0.3394 (3)	0.1735 (3)	0.3738 (2)	0.0156 (7)
H10A	0.3132	0.1760	0.3194	0.019*
C11A	0.8221 (3)	0.0652 (3)	0.6091 (2)	0.0166 (7)
C12A	0.2229 (4)	0.2184 (3)	0.5986 (2)	0.0164 (7)
C13A	0.5412 (4)	0.1242 (3)	0.1534 (2)	0.0179 (7)
C14A	0.4178 (4)	0.0667 (3)	0.1673 (2)	0.0164 (7)
H14A	0.3430	0.0949	0.1763	0.020*
C15A	0.4065 (4)	-0.0171 (3)	0.1888 (2)	0.0168 (7)
H15A	0.3233	-0.0466	0.2112	0.020*
C16A	0.5179 (4)	-0.0487 (3)	0.1939 (2)	0.0190 (8)
C17A	0.6425 (4)	0.0078 (3)	0.1772 (2)	0.0209 (8)
H17A	0.7263	-0.0032	0.1929	0.025*
C18A	0.6553 (4)	0.0924 (3)	0.1590 (2)	0.0183 (7)
H18A	0.7477	0.1391	0.1614	0.022*
C19A	0.5584 (4)	0.2149 (3)	0.1327 (2)	0.0202 (8)
H19A	0.6561	0.2585	0.1492	0.024*
C20A	0.4779 (4)	0.2801 (3)	0.1828 (2)	0.0227 (8)
H20D	0.3816	0.2389	0.1671	0.034*
H20E	0.4942	0.3378	0.1662	0.034*
H20F	0.5060	0.3056	0.2472	0.034*
C21A	0.5190 (5)	0.1744 (3)	0.0304 (2)	0.0295 (9)
H21D	0.5721	0.1325	-0.0002	0.044*
H21E	0.5371	0.2320	0.0135	0.044*
H21F	0.4228	0.1330	0.0129	0.044*
C22A	0.5052 (4)	-0.1375 (3)	0.2170 (2)	0.0243 (8)
H22D	0.4306	-0.1472	0.2509	0.036*
H22E	0.5893	-0.1240	0.2531	0.036*
H22F	0.4873	-0.1993	0.1619	0.036*
H2W	0.074 (2)	0.941 (2)	0.9458 (17)	0.012 (9)*

## supplementary materials

H1W	0.125 (5)	1.024 (3)	1.025 (3)	0.057 (17)*
H4W	0.078 (3)	0.0683 (16)	0.7675 (19)	0.018 (10)*
H5W	-0.023 (4)	-0.024 (3)	0.757 (3)	0.047 (15)*
H8W	0.398 (13)	0.397 (8)	0.838 (15)	0.40 (13)*
H7W	0.49 (2)	0.428 (17)	0.890 (13)	0.44 (15)*
C22	-0.1871 (4)	0.4980 (3)	0.2423 (3)	0.0249 (8)
H22A	-0.2050	0.4486	0.1798	0.037*
H22B	-0.1655	0.5668	0.2447	0.037*
H22C	-0.2672	0.4817	0.2703	0.037*

Atomic displacement parameters ( $\text{\AA}^2$ )

	$U^{11}$	$U^{22}$	$U^{33}$	$U^{12}$	$U^{13}$	$U^{23}$
Ru1	0.01759 (14)	0.01487 (13)	0.00828 (13)	0.00743 (10)	0.00366 (10)	0.00336 (10)
Ru1A	0.01576 (14)	0.01950 (14)	0.00573 (13)	0.00837 (10)	0.00311 (10)	0.00339 (10)
Cl1	0.0201 (4)	0.0263 (4)	0.0183 (4)	0.0031 (3)	0.0012 (3)	0.0055 (4)
Cl1A	0.0279 (5)	0.0236 (4)	0.0118 (4)	-0.0001 (4)	0.0010 (3)	0.0054 (3)
Cl2	0.0333 (5)	0.0252 (5)	0.0295 (5)	0.0107 (4)	0.0024 (4)	0.0131 (4)
O111	0.0358 (16)	0.0194 (13)	0.0167 (13)	0.0145 (11)	0.0025 (11)	0.0082 (11)
O112	0.0384 (16)	0.0266 (14)	0.0139 (14)	0.0176 (12)	0.0079 (11)	0.0081 (11)
O121	0.0339 (15)	0.0269 (14)	0.0126 (13)	0.0180 (12)	0.0092 (11)	0.0087 (11)
O122	0.0344 (16)	0.0197 (13)	0.0163 (13)	0.0157 (11)	0.0053 (11)	0.0041 (11)
O11A	0.0207 (13)	0.0332 (15)	0.0190 (14)	0.0157 (11)	0.0049 (11)	0.0150 (12)
O11B	0.0224 (14)	0.0259 (14)	0.0157 (13)	0.0122 (11)	0.0056 (11)	0.0099 (11)
O12A	0.0296 (15)	0.0283 (14)	0.0212 (14)	0.0230 (12)	0.0112 (11)	0.0115 (11)
O12B	0.0224 (13)	0.0286 (14)	0.0082 (12)	0.0162 (11)	0.0065 (10)	0.0060 (11)
O1	0.048 (2)	0.050 (2)	0.076 (3)	0.0218 (17)	0.0216 (19)	0.031 (2)
O2	0.0347 (17)	0.0320 (16)	0.0257 (16)	0.0200 (13)	0.0082 (13)	0.0127 (13)
O3	0.043 (2)	0.055 (2)	0.041 (2)	0.0058 (17)	0.0114 (17)	0.0111 (17)
O4	0.0251 (15)	0.0301 (15)	0.0192 (14)	0.0107 (12)	0.0029 (11)	0.0124 (12)
N1	0.0198 (15)	0.0179 (15)	0.0105 (14)	0.0073 (12)	0.0037 (12)	0.0054 (12)
N1A	0.0189 (16)	0.0271 (16)	0.0094 (14)	0.0129 (13)	0.0048 (12)	0.0070 (12)
N2	0.0176 (15)	0.0154 (14)	0.0090 (14)	0.0075 (11)	0.0035 (11)	0.0034 (11)
N2A	0.0163 (15)	0.0128 (13)	0.0086 (14)	0.0065 (11)	0.0031 (11)	0.0026 (11)
C1	0.0223 (19)	0.0185 (18)	0.0136 (18)	0.0100 (15)	0.0041 (14)	0.0031 (14)
C2	0.0205 (19)	0.0149 (17)	0.0171 (18)	0.0085 (14)	0.0030 (15)	0.0040 (14)
C3	0.0147 (17)	0.0171 (17)	0.0143 (18)	0.0050 (14)	-0.0006 (14)	0.0048 (14)
C4	0.0193 (18)	0.0193 (17)	0.0099 (16)	0.0097 (14)	0.0032 (14)	0.0027 (14)
C5	0.0146 (17)	0.0173 (17)	0.0109 (17)	0.0064 (13)	0.0017 (13)	0.0034 (14)
C6	0.0137 (17)	0.0177 (17)	0.0132 (17)	0.0072 (13)	0.0033 (13)	0.0059 (14)
C7	0.0183 (18)	0.0186 (17)	0.0130 (17)	0.0078 (14)	0.0042 (14)	0.0064 (14)
C8	0.0166 (18)	0.0189 (17)	0.0137 (18)	0.0078 (14)	0.0030 (14)	0.0053 (14)
C9	0.0214 (19)	0.0167 (17)	0.0152 (18)	0.0091 (14)	0.0034 (14)	0.0048 (14)
C10	0.0219 (19)	0.0194 (18)	0.0142 (18)	0.0107 (14)	0.0040 (14)	0.0082 (15)
C11	0.0146 (18)	0.0184 (18)	0.020 (2)	0.0052 (14)	-0.0005 (14)	0.0076 (15)
C12	0.0179 (18)	0.0239 (19)	0.0138 (18)	0.0116 (15)	0.0048 (14)	0.0052 (15)
C13	0.027 (2)	0.0245 (19)	0.0128 (18)	0.0134 (16)	0.0091 (15)	0.0104 (15)
C14	0.025 (2)	0.0205 (18)	0.0162 (18)	0.0107 (15)	0.0117 (15)	0.0104 (15)
C15	0.0213 (19)	0.0201 (18)	0.0132 (17)	0.0034 (14)	0.0074 (14)	0.0080 (15)
C16	0.0178 (18)	0.0261 (19)	0.0145 (18)	0.0084 (15)	0.0090 (15)	0.0097 (15)
C17	0.026 (2)	0.0231 (19)	0.0150 (18)	0.0146 (15)	0.0131 (15)	0.0092 (15)
C18	0.025 (2)	0.0242 (19)	0.0078 (16)	0.0104 (15)	0.0083 (14)	0.0057 (14)
C19	0.029 (2)	0.0260 (19)	0.0146 (18)	0.0149 (16)	0.0053 (16)	0.0087 (16)
C20	0.032 (2)	0.039 (2)	0.024 (2)	0.0229 (19)	0.0073 (17)	0.0146 (18)

## supplementary materials

C21	0.040 (2)	0.031 (2)	0.019 (2)	0.0188 (18)	0.0078 (17)	0.0127 (17)
C1A	0.0203 (19)	0.038 (2)	0.0159 (19)	0.0170 (17)	0.0087 (15)	0.0107 (17)
C2A	0.0185 (19)	0.032 (2)	0.0173 (19)	0.0158 (16)	0.0060 (15)	0.0086 (16)
C3A	0.0162 (17)	0.0170 (17)	0.0119 (17)	0.0056 (13)	0.0013 (14)	0.0034 (14)
C4A	0.0184 (18)	0.0162 (17)	0.0104 (17)	0.0072 (13)	0.0052 (14)	0.0037 (14)
C5A	0.0154 (17)	0.0140 (16)	0.0103 (16)	0.0052 (13)	0.0029 (13)	0.0027 (13)
C6A	0.0176 (17)	0.0112 (15)	0.0059 (15)	0.0058 (13)	0.0027 (13)	0.0004 (13)
C7A	0.0180 (18)	0.0127 (16)	0.0083 (16)	0.0053 (13)	−0.0010 (13)	0.0024 (13)
C8A	0.0159 (17)	0.0122 (16)	0.0100 (16)	0.0059 (13)	0.0038 (13)	0.0023 (13)
C9A	0.0199 (18)	0.0171 (17)	0.0153 (18)	0.0116 (14)	0.0025 (14)	0.0060 (14)
C10A	0.0211 (18)	0.0167 (17)	0.0107 (17)	0.0091 (14)	0.0027 (14)	0.0055 (14)
C11A	0.0178 (18)	0.0148 (17)	0.0147 (18)	0.0062 (14)	−0.0007 (14)	0.0031 (14)
C12A	0.0195 (18)	0.0136 (16)	0.0150 (18)	0.0066 (14)	0.0050 (14)	0.0040 (14)
C13A	0.029 (2)	0.0203 (18)	0.0036 (16)	0.0104 (15)	0.0032 (14)	0.0032 (14)
C14A	0.0211 (19)	0.0214 (18)	0.0023 (15)	0.0095 (14)	−0.0014 (13)	−0.0013 (13)
C15A	0.0199 (19)	0.0178 (17)	0.0054 (16)	0.0057 (14)	0.0014 (14)	−0.0018 (13)
C16A	0.030 (2)	0.0174 (17)	0.0083 (17)	0.0130 (15)	0.0036 (15)	0.0009 (14)
C17A	0.027 (2)	0.028 (2)	0.0084 (17)	0.0173 (16)	0.0054 (15)	0.0023 (15)
C18A	0.024 (2)	0.0243 (19)	0.0055 (16)	0.0116 (15)	0.0059 (14)	0.0030 (14)
C19A	0.026 (2)	0.0237 (19)	0.0110 (17)	0.0094 (15)	0.0032 (15)	0.0067 (15)
C20A	0.031 (2)	0.0231 (19)	0.0205 (19)	0.0143 (16)	0.0060 (16)	0.0113 (16)
C21A	0.045 (3)	0.031 (2)	0.0140 (19)	0.0138 (19)	0.0037 (18)	0.0105 (17)
C22A	0.036 (2)	0.025 (2)	0.0168 (19)	0.0174 (17)	0.0080 (16)	0.0076 (16)
C22	0.023 (2)	0.030 (2)	0.024 (2)	0.0108 (16)	0.0040 (16)	0.0119 (17)

## Geometric parameters (Å, °)

Ru1—N1	2.088 (3)	C14—C15	1.422 (5)
Ru1—N2	2.089 (3)	C14—H14	1.0000
Ru1—C15	2.188 (3)	C15—C16	1.415 (5)
Ru1—C16	2.199 (4)	C15—H15	1.0000
Ru1—C18	2.204 (3)	C16—C17	1.434 (5)
Ru1—C17	2.207 (3)	C16—C22	1.501 (5)
Ru1—C14	2.209 (3)	C17—C18	1.398 (5)
Ru1—C13	2.224 (3)	C17—H17	1.0000
Ru1—C11	2.3998 (9)	C18—H18	1.0000
Ru1A—N1A	2.076 (3)	C19—C20	1.526 (5)
Ru1A—N2A	2.087 (3)	C19—C21	1.530 (5)
Ru1A—C15A	2.178 (3)	C19—H19	1.0000
Ru1A—C18A	2.200 (3)	C20—H20A	0.9800
Ru1A—C14A	2.210 (3)	C20—H20B	0.9800
Ru1A—C16A	2.211 (3)	C20—H20C	0.9800
Ru1A—C17A	2.212 (3)	C21—H21A	0.9800
Ru1A—C13A	2.226 (3)	C21—H21B	0.9800
Ru1A—C11A	2.3895 (9)	C21—H21C	0.9800
O111—C11	1.315 (4)	C1A—C2A	1.379 (5)
O111—H3W	0.8400	C1A—H1A	0.9500
O112—C11	1.209 (4)	C2A—C3A	1.383 (5)
O121—C12	1.272 (4)	C2A—H2A	0.9500
O122—C12	1.237 (4)	C3A—C4A	1.387 (5)
O11A—C11A	1.309 (4)	C3A—C11A	1.500 (5)
O11A—H11A	0.8400	C4A—C5A	1.386 (5)
O11B—C11A	1.207 (4)	C4A—H4A	0.9500
O12A—C12A	1.212 (4)	C5A—C6A	1.464 (5)



## supplementary materials

O12B—C12A	1.308 (4)	C6A—C7A	1.385 (5)
O12B—H12B	0.8400	C7A—C8A	1.381 (5)
O2—H2W	0.880 (2)	C7A—H7A	0.9500
O2—H1W	0.880 (2)	C8A—C9A	1.392 (5)
O3—H8W	0.880 (3)	C8A—C12A	1.515 (5)
O3—H7W	0.880 (2)	C9A—C10A	1.382 (5)
O4—H4W	0.880 (2)	C9A—H9A	0.9500
O4—H5W	0.880 (2)	C10A—H10A	0.9500
N1—C1	1.341 (4)	C13A—C14A	1.401 (5)
N1—C5	1.361 (4)	C13A—C18A	1.449 (5)
N1A—C1A	1.339 (5)	C13A—C19A	1.500 (5)
N1A—C5A	1.357 (4)	C14A—C15A	1.417 (5)
N2—C10	1.339 (4)	C14A—H14A	1.0000
N2—C6	1.361 (4)	C15A—C16A	1.418 (5)
N2A—C10A	1.348 (4)	C15A—H15A	1.0000
N2A—C6A	1.357 (4)	C16A—C17A	1.424 (5)
C1—C2	1.384 (5)	C16A—C22A	1.504 (5)
C1—H1	0.9500	C17A—C18A	1.393 (5)
C2—C3	1.381 (5)	C17A—H17A	1.0000
C2—H2	0.9500	C18A—H18A	1.0000
C3—C4	1.391 (5)	C19A—C20A	1.519 (5)
C3—C11	1.502 (5)	C19A—C21A	1.547 (5)
C4—C5	1.390 (5)	C19A—H19A	1.0000
C4—H4	0.9500	C20A—H20D	0.9800
C5—C6	1.464 (5)	C20A—H20E	0.9800
C6—C7	1.384 (5)	C20A—H20F	0.9800
C7—C8	1.384 (5)	C21A—H21D	0.9800
C7—H7	0.9500	C21A—H21E	0.9800
C8—C9	1.390 (5)	C21A—H21F	0.9800
C8—C12	1.521 (5)	C22A—H22D	0.9800
C9—C10	1.385 (5)	C22A—H22E	0.9800
C9—H9	0.9500	C22A—H22F	0.9800
C10—H10	0.9500	C22—H22A	0.9800
C13—C14	1.400 (5)	C22—H22B	0.9800
C13—C18	1.439 (5)	C22—H22C	0.9800
C13—C19	1.518 (5)		
N1—Ru1—N2	77.24 (11)	C16—C15—H15	119.2
N1—Ru1—C15	118.03 (12)	C14—C15—H15	119.2
N2—Ru1—C15	94.71 (12)	Ru1—C15—H15	119.2
N1—Ru1—C16	94.15 (12)	C15—C16—C17	117.9 (3)
N2—Ru1—C16	119.33 (12)	C15—C16—C22	121.3 (3)
C15—Ru1—C16	37.64 (13)	C17—C16—C22	120.7 (3)
N1—Ru1—C18	124.18 (12)	C15—C16—Ru1	70.8 (2)
N2—Ru1—C18	158.04 (12)	C17—C16—Ru1	71.3 (2)
C15—Ru1—C18	79.77 (13)	C22—C16—Ru1	128.8 (3)
C16—Ru1—C18	68.06 (13)	C18—C17—C16	120.9 (3)
N1—Ru1—C17	97.86 (12)	C18—C17—Ru1	71.4 (2)
N2—Ru1—C17	157.03 (13)	C16—C17—Ru1	70.68 (19)
C15—Ru1—C17	67.49 (13)	C18—C17—H17	118.8
C16—Ru1—C17	37.99 (13)	C16—C17—H17	118.8
C18—Ru1—C17	36.94 (13)	Ru1—C17—H17	118.8
N1—Ru1—C14	154.95 (13)	C17—C18—C13	121.1 (3)
N2—Ru1—C14	95.85 (12)	C17—C18—Ru1	71.64 (19)

# supplementary materials

C15—Ru1—C14	37.72 (13)	C13—C18—Ru1	71.76 (19)
C16—Ru1—C14	67.98 (13)	C17—C18—H18	118.9
C18—Ru1—C14	66.79 (13)	C13—C18—H18	118.9
C17—Ru1—C14	79.06 (13)	Ru1—C18—H18	118.9
N1—Ru1—C13	161.87 (12)	C13—C19—C20	113.5 (3)
N2—Ru1—C13	120.34 (12)	C13—C19—C21	107.7 (3)
C15—Ru1—C13	67.94 (13)	C20—C19—C21	111.8 (3)
C16—Ru1—C13	81.24 (13)	C13—C19—H19	107.9
C18—Ru1—C13	37.93 (13)	C20—C19—H19	107.9
C17—Ru1—C13	67.78 (13)	C21—C19—H19	107.9
C14—Ru1—C13	36.83 (13)	C19—C20—H20A	109.5
N1—Ru1—C11	83.44 (8)	C19—C20—H20B	109.5
N2—Ru1—C11	87.38 (8)	H20A—C20—H20B	109.5
C15—Ru1—C11	158.38 (10)	C19—C20—H20C	109.5
C16—Ru1—C11	152.08 (10)	H20A—C20—H20C	109.5
C18—Ru1—C11	90.27 (10)	H20B—C20—H20C	109.5
C17—Ru1—C11	114.60 (10)	C19—C21—H21A	109.5
C14—Ru1—C11	120.66 (10)	C19—C21—H21B	109.5
C13—Ru1—C11	92.44 (10)	H21A—C21—H21B	109.5
N1A—Ru1A—N2A	77.53 (11)	C19—C21—H21C	109.5
N1A—Ru1A—C15A	119.98 (13)	H21A—C21—H21C	109.5
N2A—Ru1A—C15A	93.71 (12)	H21B—C21—H21C	109.5
N1A—Ru1A—C18A	120.70 (12)	N1A—C1A—C2A	122.5 (3)
N2A—Ru1A—C18A	161.60 (12)	N1A—C1A—H1A	118.8
C15A—Ru1A—C18A	79.54 (13)	C2A—C1A—H1A	118.8
N1A—Ru1A—C14A	157.33 (13)	C1A—C2A—C3A	118.8 (3)
N2A—Ru1A—C14A	97.24 (12)	C1A—C2A—H2A	120.6
C15A—Ru1A—C14A	37.68 (13)	C3A—C2A—H2A	120.6
C18A—Ru1A—C14A	66.98 (13)	C2A—C3A—C4A	119.0 (3)
N1A—Ru1A—C16A	94.25 (12)	C2A—C3A—C11A	122.9 (3)
N2A—Ru1A—C16A	116.52 (12)	C4A—C3A—C11A	118.0 (3)
C15A—Ru1A—C16A	37.69 (13)	C5A—C4A—C3A	119.6 (3)
C18A—Ru1A—C16A	67.69 (13)	C5A—C4A—H4A	120.2
C14A—Ru1A—C16A	68.07 (13)	C3A—C4A—H4A	120.2
N1A—Ru1A—C17A	95.73 (12)	N1A—C5A—C4A	120.8 (3)
N2A—Ru1A—C17A	153.40 (13)	N1A—C5A—C6A	115.1 (3)
C15A—Ru1A—C17A	67.12 (13)	C4A—C5A—C6A	124.1 (3)
C18A—Ru1A—C17A	36.82 (13)	N2A—C6A—C7A	121.9 (3)
C14A—Ru1A—C17A	79.02 (13)	N2A—C6A—C5A	114.7 (3)
C16A—Ru1A—C17A	37.56 (14)	C7A—C6A—C5A	123.4 (3)
N1A—Ru1A—C13A	158.45 (13)	C8A—C7A—C6A	119.8 (3)
N2A—Ru1A—C13A	123.41 (12)	C8A—C7A—H7A	120.1
C15A—Ru1A—C13A	67.75 (13)	C6A—C7A—H7A	120.1
C18A—Ru1A—C13A	38.20 (13)	C7A—C8A—C9A	118.4 (3)
C14A—Ru1A—C13A	36.81 (13)	C7A—C8A—C12A	120.7 (3)
C16A—Ru1A—C13A	81.13 (13)	C9A—C8A—C12A	120.8 (3)
C17A—Ru1A—C13A	67.83 (13)	C10A—C9A—C8A	119.3 (3)
N1A—Ru1A—C11A	83.87 (9)	C10A—C9A—H9A	120.4
N2A—Ru1A—C11A	85.87 (8)	C8A—C9A—H9A	120.4
C15A—Ru1A—C11A	155.53 (9)	N2A—C10A—C9A	122.5 (3)
C18A—Ru1A—C11A	93.25 (10)	N2A—C10A—H10A	118.7
C14A—Ru1A—C11A	118.04 (9)	C9A—C10A—H10A	118.7
C16A—Ru1A—C11A	156.68 (10)	O11B—C11A—O11A	125.3 (3)
C17A—Ru1A—C11A	119.34 (10)	O11B—C11A—C3A	120.6 (3)

## supplementary materials

C13A—Ru1A—C11A	92.10 (9)	O11A—C11A—C3A	114.1 (3)
C11—O111—H3W	109.5	O12A—C12A—O12B	126.6 (3)
C11A—O11A—H11A	109.5	O12A—C12A—C8A	121.6 (3)
C12A—O12B—H12B	109.5	O12B—C12A—C8A	111.9 (3)
H2W—O2—H1W	101 (4)	C14A—C13A—C18A	117.3 (3)
H8W—O3—H7W	79 (10)	C14A—C13A—C19A	122.9 (3)
H4W—O4—H5W	107 (4)	C18A—C13A—C19A	119.8 (3)
C1—N1—C5	118.9 (3)	C14A—C13A—Ru1A	70.97 (19)
C1—N1—Ru1	124.6 (2)	C18A—C13A—Ru1A	69.89 (18)
C5—N1—Ru1	116.2 (2)	C19A—C13A—Ru1A	130.5 (2)
C1A—N1A—C5A	119.2 (3)	C13A—C14A—C15A	121.2 (3)
C1A—N1A—Ru1A	124.4 (2)	C13A—C14A—Ru1A	72.22 (19)
C5A—N1A—Ru1A	116.4 (2)	C15A—C14A—Ru1A	69.90 (18)
C10—N2—C6	118.2 (3)	C13A—C14A—H14A	118.6
C10—N2—Ru1	125.1 (2)	C15A—C14A—H14A	118.6
C6—N2—Ru1	116.7 (2)	Ru1A—C14A—H14A	118.6
C10A—N2A—C6A	118.1 (3)	C14A—C15A—C16A	121.6 (3)
C10A—N2A—Ru1A	125.7 (2)	C14A—C15A—Ru1A	72.42 (19)
C6A—N2A—Ru1A	116.2 (2)	C16A—C15A—Ru1A	72.4 (2)
N1—C1—C2	122.4 (3)	C14A—C15A—H15A	118.8
N1—C1—H1	118.8	C16A—C15A—H15A	118.8
C2—C1—H1	118.8	Ru1A—C15A—H15A	118.8
C3—C2—C1	119.2 (3)	C15A—C16A—C17A	117.3 (3)
C3—C2—H2	120.4	C15A—C16A—C22A	121.3 (3)
C1—C2—H2	120.4	C17A—C16A—C22A	121.4 (3)
C2—C3—C4	119.0 (3)	C15A—C16A—Ru1A	69.89 (19)
C2—C3—C11	122.1 (3)	C17A—C16A—Ru1A	71.3 (2)
C4—C3—C11	118.9 (3)	C22A—C16A—Ru1A	129.2 (2)
C5—C4—C3	119.3 (3)	C18A—C17A—C16A	121.3 (3)
C5—C4—H4	120.4	C18A—C17A—Ru1A	71.1 (2)
C3—C4—H4	120.4	C16A—C17A—Ru1A	71.2 (2)
N1—C5—C4	121.3 (3)	C18A—C17A—H17A	118.5
N1—C5—C6	115.0 (3)	C16A—C17A—H17A	118.5
C4—C5—C6	123.7 (3)	Ru1A—C17A—H17A	118.5
N2—C6—C7	121.6 (3)	C17A—C18A—C13A	121.2 (3)
N2—C6—C5	114.5 (3)	C17A—C18A—Ru1A	72.1 (2)
C7—C6—C5	123.8 (3)	C13A—C18A—Ru1A	71.90 (19)
C8—C7—C6	120.0 (3)	C17A—C18A—H18A	118.9
C8—C7—H7	120.0	C13A—C18A—H18A	118.9
C6—C7—H7	120.0	Ru1A—C18A—H18A	118.9
C7—C8—C9	118.2 (3)	C13A—C19A—C20A	113.9 (3)
C7—C8—C12	121.0 (3)	C13A—C19A—C21A	107.1 (3)
C9—C8—C12	120.6 (3)	C20A—C19A—C21A	111.2 (3)
C10—C9—C8	119.1 (3)	C13A—C19A—H19A	108.1
C10—C9—H9	120.4	C20A—C19A—H19A	108.1
C8—C9—H9	120.4	C21A—C19A—H19A	108.1
N2—C10—C9	122.8 (3)	C19A—C20A—H20D	109.5
N2—C10—H10	118.6	C19A—C20A—H20E	109.5
C9—C10—H10	118.6	H20D—C20A—H20E	109.5
O112—C11—O111	125.8 (3)	C19A—C20A—H20F	109.5
O112—C11—C3	122.3 (3)	H20D—C20A—H20F	109.5
O111—C11—C3	111.8 (3)	H20E—C20A—H20F	109.5
O122—C12—O121	127.1 (3)	C19A—C21A—H21D	109.5
O122—C12—C8	117.3 (3)	C19A—C21A—H21E	109.5

## supplementary materials

O121—C12—C8	115.6 (3)	H21D—C21A—H21E	109.5
C14—C13—C18	117.6 (3)	C19A—C21A—H21F	109.5
C14—C13—C19	122.4 (3)	H21D—C21A—H21F	109.5
C18—C13—C19	120.0 (3)	H21E—C21A—H21F	109.5
C14—C13—Ru1	71.01 (19)	C16A—C22A—H22D	109.5
C18—C13—Ru1	70.30 (18)	C16A—C22A—H22E	109.5
C19—C13—Ru1	130.1 (3)	H22D—C22A—H22E	109.5
C13—C14—C15	121.8 (3)	C16A—C22A—H22F	109.5
C13—C14—Ru1	72.2 (2)	H22D—C22A—H22F	109.5
C15—C14—Ru1	70.3 (2)	H22E—C22A—H22F	109.5
C13—C14—H14	118.3	C16—C22—H22A	109.5
C15—C14—H14	118.3	C16—C22—H22B	109.5
Ru1—C14—H14	118.3	H22A—C22—H22B	109.5
C16—C15—C14	120.6 (3)	C16—C22—H22C	109.5
C16—C15—Ru1	71.6 (2)	H22A—C22—H22C	109.5
C14—C15—Ru1	71.9 (2)	H22B—C22—H22C	109.5
N2—Ru1—N1—C1	−178.0 (3)	C18—Ru1—C17—C16	−133.8 (3)
C15—Ru1—N1—C1	93.4 (3)	C14—Ru1—C17—C16	−68.1 (2)
C16—Ru1—N1—C1	62.8 (3)	C13—Ru1—C17—C16	−104.8 (2)
C18—Ru1—N1—C1	−3.4 (3)	C11—Ru1—C17—C16	173.03 (17)
C17—Ru1—N1—C1	24.8 (3)	C16—C17—C18—C13	−1.6 (5)
C14—Ru1—N1—C1	105.8 (4)	Ru1—C17—C18—C13	−54.2 (3)
C13—Ru1—N1—C1	−11.5 (6)	C16—C17—C18—Ru1	52.5 (3)
C11—Ru1—N1—C1	−89.2 (3)	C14—C13—C18—C17	−0.6 (5)
N2—Ru1—N1—C5	−4.7 (2)	C19—C13—C18—C17	179.8 (3)
C15—Ru1—N1—C5	−93.3 (3)	Ru1—C13—C18—C17	54.1 (3)
C16—Ru1—N1—C5	−123.8 (3)	C14—C13—C18—Ru1	−54.7 (3)
C18—Ru1—N1—C5	170.0 (2)	C19—C13—C18—Ru1	125.7 (3)
C17—Ru1—N1—C5	−161.9 (2)	N1—Ru1—C18—C17	51.1 (3)
C14—Ru1—N1—C5	−80.9 (4)	N2—Ru1—C18—C17	−143.0 (3)
C13—Ru1—N1—C5	161.8 (4)	C15—Ru1—C18—C17	−66.0 (2)
C11—Ru1—N1—C5	84.1 (2)	C16—Ru1—C18—C17	−28.6 (2)
N2A—Ru1A—N1A—C1A	−177.1 (3)	C14—Ru1—C18—C17	−103.1 (2)
C15A—Ru1A—N1A—C1A	95.9 (3)	C13—Ru1—C18—C17	−133.0 (3)
C18A—Ru1A—N1A—C1A	0.2 (4)	C11—Ru1—C18—C17	133.3 (2)
C14A—Ru1A—N1A—C1A	104.2 (4)	N1—Ru1—C18—C13	−175.86 (19)
C16A—Ru1A—N1A—C1A	66.7 (3)	N2—Ru1—C18—C13	−9.9 (4)
C17A—Ru1A—N1A—C1A	29.0 (3)	C15—Ru1—C18—C13	67.1 (2)
C13A—Ru1A—N1A—C1A	−9.8 (5)	C16—Ru1—C18—C13	104.5 (2)
C11A—Ru1A—N1A—C1A	−90.0 (3)	C17—Ru1—C18—C13	133.0 (3)
N2A—Ru1A—N1A—C5A	1.6 (2)	C14—Ru1—C18—C13	29.9 (2)
C15A—Ru1A—N1A—C5A	−85.5 (3)	C11—Ru1—C18—C13	−93.6 (2)
C18A—Ru1A—N1A—C5A	178.8 (2)	C14—C13—C19—C20	38.7 (5)
C14A—Ru1A—N1A—C5A	−77.2 (4)	C18—C13—C19—C20	−141.7 (3)
C16A—Ru1A—N1A—C5A	−114.7 (3)	Ru1—C13—C19—C20	−53.0 (5)
C17A—Ru1A—N1A—C5A	−152.4 (3)	C14—C13—C19—C21	−85.6 (4)
C13A—Ru1A—N1A—C5A	168.8 (3)	C18—C13—C19—C21	93.9 (4)
C11A—Ru1A—N1A—C5A	88.7 (2)	Ru1—C13—C19—C21	−177.4 (3)
N1—Ru1—N2—C10	−175.5 (3)	C5A—N1A—C1A—C2A	3.9 (6)
C15—Ru1—N2—C10	−57.8 (3)	Ru1A—N1A—C1A—C2A	−177.5 (3)
C16—Ru1—N2—C10	−87.9 (3)	N1A—C1A—C2A—C3A	−0.3 (6)
C18—Ru1—N2—C10	16.4 (5)	C1A—C2A—C3A—C4A	−3.3 (5)
C17—Ru1—N2—C10	−95.6 (4)	C1A—C2A—C3A—C11A	174.8 (3)

## supplementary materials

C14—Ru1—N2—C10	-19.9 (3)	C2A—C3A—C4A—C5A	3.4 (5)
C13—Ru1—N2—C10	9.3 (3)	C11A—C3A—C4A—C5A	-174.8 (3)
C11—Ru1—N2—C10	100.6 (3)	C1A—N1A—C5A—C4A	-3.8 (5)
N1—Ru1—N2—C6	1.6 (2)	Ru1A—N1A—C5A—C4A	177.5 (3)
C15—Ru1—N2—C6	119.3 (2)	C1A—N1A—C5A—C6A	177.1 (3)
C16—Ru1—N2—C6	89.2 (3)	Ru1A—N1A—C5A—C6A	-1.6 (4)
C18—Ru1—N2—C6	-166.5 (3)	C3A—C4A—C5A—N1A	0.2 (5)
C17—Ru1—N2—C6	81.5 (4)	C3A—C4A—C5A—C6A	179.3 (3)
C14—Ru1—N2—C6	157.2 (2)	C10A—N2A—C6A—C7A	-0.2 (5)
C13—Ru1—N2—C6	-173.6 (2)	Ru1A—N2A—C6A—C7A	-179.5 (2)
C11—Ru1—N2—C6	-82.3 (2)	C10A—N2A—C6A—C5A	-179.8 (3)
N1A—Ru1A—N2A—C10A	179.4 (3)	Ru1A—N2A—C6A—C5A	0.8 (4)
C15A—Ru1A—N2A—C10A	-60.7 (3)	N1A—C5A—C6A—N2A	0.5 (4)
C18A—Ru1A—N2A—C10A	6.9 (5)	C4A—C5A—C6A—N2A	-178.5 (3)
C14A—Ru1A—N2A—C10A	-23.0 (3)	N1A—C5A—C6A—C7A	-179.1 (3)
C16A—Ru1A—N2A—C10A	-92.0 (3)	C4A—C5A—C6A—C7A	1.8 (5)
C17A—Ru1A—N2A—C10A	-102.9 (4)	N2A—C6A—C7A—C8A	0.5 (5)
C13A—Ru1A—N2A—C10A	5.0 (3)	C5A—C6A—C7A—C8A	-179.9 (3)
C11A—Ru1A—N2A—C10A	94.8 (3)	C6A—C7A—C8A—C9A	-0.5 (5)
N1A—Ru1A—N2A—C6A	-1.3 (2)	C6A—C7A—C8A—C12A	-177.7 (3)
C15A—Ru1A—N2A—C6A	118.6 (2)	C7A—C8A—C9A—C10A	0.2 (5)
C18A—Ru1A—N2A—C6A	-173.8 (3)	C12A—C8A—C9A—C10A	177.3 (3)
C14A—Ru1A—N2A—C6A	156.3 (2)	C6A—N2A—C10A—C9A	-0.2 (5)
C16A—Ru1A—N2A—C6A	87.3 (3)	Ru1A—N2A—C10A—C9A	179.1 (2)
C17A—Ru1A—N2A—C6A	76.4 (4)	C8A—C9A—C10A—N2A	0.2 (5)
C13A—Ru1A—N2A—C6A	-175.7 (2)	C2A—C3A—C11A—O11B	-173.2 (3)
C11A—Ru1A—N2A—C6A	-85.9 (2)	C4A—C3A—C11A—O11B	4.9 (5)
C5—N1—C1—C2	0.4 (5)	C2A—C3A—C11A—O11A	5.3 (5)
Ru1—N1—C1—C2	173.5 (3)	C4A—C3A—C11A—O11A	-176.6 (3)
N1—C1—C2—C3	-0.6 (5)	C7A—C8A—C12A—O12A	169.9 (3)
C1—C2—C3—C4	0.0 (5)	C9A—C8A—C12A—O12A	-7.2 (5)
C1—C2—C3—C11	179.7 (3)	C7A—C8A—C12A—O12B	-9.5 (4)
C2—C3—C4—C5	0.7 (5)	C9A—C8A—C12A—O12B	173.3 (3)
C11—C3—C4—C5	-179.0 (3)	N1A—Ru1A—C13A—C14A	144.0 (3)
C1—N1—C5—C4	0.4 (5)	N2A—Ru1A—C13A—C14A	-51.0 (2)
Ru1—N1—C5—C4	-173.3 (3)	C15A—Ru1A—C13A—C14A	28.3 (2)
C1—N1—C5—C6	-179.4 (3)	C18A—Ru1A—C13A—C14A	130.0 (3)
Ru1—N1—C5—C6	6.9 (4)	C16A—Ru1A—C13A—C14A	65.0 (2)
C3—C4—C5—N1	-0.9 (5)	C17A—Ru1A—C13A—C14A	101.6 (2)
C3—C4—C5—C6	178.8 (3)	C11A—Ru1A—C13A—C14A	-137.4 (2)
C10—N2—C6—C7	1.9 (5)	N1A—Ru1A—C13A—C18A	14.0 (4)
Ru1—N2—C6—C7	-175.4 (3)	N2A—Ru1A—C13A—C18A	179.02 (19)
C10—N2—C6—C5	178.8 (3)	C15A—Ru1A—C13A—C18A	-101.7 (2)
Ru1—N2—C6—C5	1.5 (4)	C14A—Ru1A—C13A—C18A	-130.0 (3)
N1—C5—C6—N2	-5.5 (4)	C16A—Ru1A—C13A—C18A	-65.0 (2)
C4—C5—C6—N2	174.8 (3)	C17A—Ru1A—C13A—C18A	-28.4 (2)
N1—C5—C6—C7	171.3 (3)	C11A—Ru1A—C13A—C18A	92.6 (2)
C4—C5—C6—C7	-8.4 (5)	N1A—Ru1A—C13A—C19A	-98.5 (4)
N2—C6—C7—C8	0.5 (5)	N2A—Ru1A—C13A—C19A	66.5 (4)
C5—C6—C7—C8	-176.1 (3)	C15A—Ru1A—C13A—C19A	145.8 (4)
C6—C7—C8—C9	-1.8 (5)	C18A—Ru1A—C13A—C19A	-112.5 (4)
C6—C7—C8—C12	173.5 (3)	C14A—Ru1A—C13A—C19A	117.5 (4)
C7—C8—C9—C10	0.8 (5)	C16A—Ru1A—C13A—C19A	-177.5 (4)
C12—C8—C9—C10	-174.5 (3)	C17A—Ru1A—C13A—C19A	-140.9 (4)

## supplementary materials

C6—N2—C10—C9	−3.0 (5)	C11A—Ru1A—C13A—C19A	−19.9 (3)
Ru1—N2—C10—C9	174.0 (3)	C18A—C13A—C14A—C15A	2.1 (5)
C8—C9—C10—N2	1.7 (5)	C19A—C13A—C14A—C15A	−178.5 (3)
C2—C3—C11—O112	−170.4 (3)	Ru1A—C13A—C14A—C15A	−52.0 (3)
C4—C3—C11—O112	9.3 (5)	C18A—C13A—C14A—Ru1A	54.1 (3)
C2—C3—C11—O111	8.6 (5)	C19A—C13A—C14A—Ru1A	−126.5 (3)
C4—C3—C11—O111	−171.8 (3)	N1A—Ru1A—C14A—C13A	−145.9 (3)
C7—C8—C12—O122	−169.8 (3)	N2A—Ru1A—C14A—C13A	139.2 (2)
C9—C8—C12—O122	5.4 (5)	C15A—Ru1A—C14A—C13A	−134.1 (3)
C7—C8—C12—O121	8.7 (5)	C18A—Ru1A—C14A—C13A	−31.0 (2)
C9—C8—C12—O121	−176.2 (3)	C16A—Ru1A—C14A—C13A	−105.1 (2)
N1—Ru1—C13—C14	141.1 (4)	C17A—Ru1A—C14A—C13A	−67.5 (2)
N2—Ru1—C13—C14	−54.2 (2)	C11A—Ru1A—C14A—C13A	50.0 (2)
C15—Ru1—C13—C14	28.0 (2)	N1A—Ru1A—C14A—C15A	−11.8 (4)
C16—Ru1—C13—C14	64.7 (2)	N2A—Ru1A—C14A—C15A	−86.7 (2)
C18—Ru1—C13—C14	130.1 (3)	C18A—Ru1A—C14A—C15A	103.1 (2)
C17—Ru1—C13—C14	101.7 (2)	C16A—Ru1A—C14A—C15A	29.0 (2)
C11—Ru1—C13—C14	−142.6 (2)	C17A—Ru1A—C14A—C15A	66.6 (2)
N1—Ru1—C13—C18	11.1 (5)	C13A—Ru1A—C14A—C15A	134.1 (3)
N2—Ru1—C13—C18	175.71 (19)	C11A—Ru1A—C14A—C15A	−175.86 (17)
C15—Ru1—C13—C18	−102.0 (2)	C13A—C14A—C15A—C16A	−2.5 (5)
C16—Ru1—C13—C18	−65.3 (2)	Ru1A—C14A—C15A—C16A	−55.5 (3)
C17—Ru1—C13—C18	−28.3 (2)	C13A—C14A—C15A—Ru1A	53.0 (3)
C14—Ru1—C13—C18	−130.1 (3)	N1A—Ru1A—C15A—C14A	174.78 (19)
C11—Ru1—C13—C18	87.3 (2)	N2A—Ru1A—C15A—C14A	97.0 (2)
N1—Ru1—C13—C19	−102.1 (5)	C18A—Ru1A—C15A—C14A	−65.7 (2)
N2—Ru1—C13—C19	62.6 (4)	C16A—Ru1A—C15A—C14A	−132.6 (3)
C15—Ru1—C13—C19	144.9 (4)	C17A—Ru1A—C15A—C14A	−102.0 (2)
C16—Ru1—C13—C19	−178.5 (3)	C13A—Ru1A—C15A—C14A	−27.7 (2)
C18—Ru1—C13—C19	−113.1 (4)	C11A—Ru1A—C15A—C14A	8.9 (4)
C17—Ru1—C13—C19	−141.4 (4)	N1A—Ru1A—C15A—C16A	−52.6 (2)
C14—Ru1—C13—C19	116.8 (4)	N2A—Ru1A—C15A—C16A	−130.4 (2)
C11—Ru1—C13—C19	−25.8 (3)	C18A—Ru1A—C15A—C16A	66.9 (2)
C18—C13—C14—C15	2.3 (5)	C14A—Ru1A—C15A—C16A	132.6 (3)
C19—C13—C14—C15	−178.1 (3)	C17A—Ru1A—C15A—C16A	30.6 (2)
Ru1—C13—C14—C15	−52.1 (3)	C13A—Ru1A—C15A—C16A	104.9 (2)
C18—C13—C14—Ru1	54.4 (3)	C11A—Ru1A—C15A—C16A	141.4 (2)
C19—C13—C14—Ru1	−126.0 (3)	C14A—C15A—C16A—C17A	0.5 (5)
N1—Ru1—C14—C13	−152.5 (3)	Ru1A—C15A—C16A—C17A	−55.0 (3)
N2—Ru1—C14—C13	135.3 (2)	C14A—C15A—C16A—C22A	179.9 (3)
C15—Ru1—C14—C13	−134.6 (3)	Ru1A—C15A—C16A—C22A	124.4 (3)
C16—Ru1—C14—C13	−105.4 (2)	C14A—C15A—C16A—Ru1A	55.5 (3)
C18—Ru1—C14—C13	−30.8 (2)	N1A—Ru1A—C16A—C15A	136.3 (2)
C17—Ru1—C14—C13	−67.4 (2)	N2A—Ru1A—C16A—C15A	58.2 (2)
C11—Ru1—C14—C13	44.8 (2)	C18A—Ru1A—C16A—C15A	−102.1 (2)
N1—Ru1—C14—C15	−17.9 (4)	C14A—Ru1A—C16A—C15A	−29.0 (2)
N2—Ru1—C14—C15	−90.1 (2)	C17A—Ru1A—C16A—C15A	−129.8 (3)
C16—Ru1—C14—C15	29.2 (2)	C13A—Ru1A—C16A—C15A	−64.9 (2)
C18—Ru1—C14—C15	103.8 (2)	C11A—Ru1A—C16A—C15A	−139.3 (2)
C17—Ru1—C14—C15	67.2 (2)	N1A—Ru1A—C16A—C17A	−93.9 (2)
C13—Ru1—C14—C15	134.6 (3)	N2A—Ru1A—C16A—C17A	−172.05 (19)
C11—Ru1—C14—C15	179.43 (17)	C15A—Ru1A—C16A—C17A	129.8 (3)
C13—C14—C15—C16	−1.8 (5)	C18A—Ru1A—C16A—C17A	27.6 (2)
Ru1—C14—C15—C16	−54.6 (3)	C14A—Ru1A—C16A—C17A	100.8 (2)

# supplementary materials

C13—C14—C15—Ru1	52.9 (3)	C13A—Ru1A—C16A—C17A	64.9 (2)
N1—Ru1—C15—C16	−56.2 (2)	C11A—Ru1A—C16A—C17A	−9.5 (4)
N2—Ru1—C15—C16	−134.3 (2)	N1A—Ru1A—C16A—C22A	21.9 (3)
C18—Ru1—C15—C16	67.2 (2)	N2A—Ru1A—C16A—C22A	−56.3 (4)
C17—Ru1—C15—C16	30.7 (2)	C15A—Ru1A—C16A—C22A	−114.5 (4)
C14—Ru1—C15—C16	132.3 (3)	C18A—Ru1A—C16A—C22A	143.4 (4)
C13—Ru1—C15—C16	104.9 (2)	C14A—Ru1A—C16A—C22A	−143.5 (4)
C11—Ru1—C15—C16	131.0 (2)	C17A—Ru1A—C16A—C22A	115.7 (4)
N1—Ru1—C15—C14	171.51 (19)	C13A—Ru1A—C16A—C22A	−179.3 (4)
N2—Ru1—C15—C14	93.5 (2)	C11A—Ru1A—C16A—C22A	106.2 (4)
C16—Ru1—C15—C14	−132.3 (3)	C15A—C16A—C17A—C18A	1.8 (5)
C18—Ru1—C15—C14	−65.1 (2)	C22A—C16A—C17A—C18A	−177.6 (3)
C17—Ru1—C15—C14	−101.5 (2)	Ru1A—C16A—C17A—C18A	−52.5 (3)
C13—Ru1—C15—C14	−27.4 (2)	C15A—C16A—C17A—Ru1A	54.3 (3)
C11—Ru1—C15—C14	−1.3 (4)	C22A—C16A—C17A—Ru1A	−125.1 (3)
C14—C15—C16—C17	−0.6 (5)	N1A—Ru1A—C17A—C18A	−136.2 (2)
Ru1—C15—C16—C17	−55.3 (3)	N2A—Ru1A—C17A—C18A	150.3 (2)
C14—C15—C16—C22	179.2 (3)	C15A—Ru1A—C17A—C18A	103.6 (2)
Ru1—C15—C16—C22	124.4 (3)	C14A—Ru1A—C17A—C18A	66.1 (2)
C14—C15—C16—Ru1	54.8 (3)	C16A—Ru1A—C17A—C18A	134.3 (3)
N1—Ru1—C16—C15	132.6 (2)	C13A—Ru1A—C17A—C18A	29.4 (2)
N2—Ru1—C16—C15	55.0 (2)	C11A—Ru1A—C17A—C18A	−50.0 (2)
C18—Ru1—C16—C15	−102.0 (2)	N1A—Ru1A—C17A—C16A	89.5 (2)
C17—Ru1—C16—C15	−129.9 (3)	N2A—Ru1A—C17A—C16A	16.0 (4)
C14—Ru1—C16—C15	−29.2 (2)	C15A—Ru1A—C17A—C16A	−30.7 (2)
C13—Ru1—C16—C15	−65.0 (2)	C18A—Ru1A—C17A—C16A	−134.3 (3)
C11—Ru1—C16—C15	−143.53 (19)	C14A—Ru1A—C17A—C16A	−68.2 (2)
N1—Ru1—C16—C17	−97.5 (2)	C13A—Ru1A—C17A—C16A	−104.9 (2)
N2—Ru1—C16—C17	−175.14 (18)	C11A—Ru1A—C17A—C16A	175.70 (17)
C15—Ru1—C16—C17	129.9 (3)	C16A—C17A—C18A—C13A	−2.2 (5)
C18—Ru1—C16—C17	27.9 (2)	Ru1A—C17A—C18A—C13A	−54.7 (3)
C14—Ru1—C16—C17	100.7 (2)	C16A—C17A—C18A—Ru1A	52.5 (3)
C13—Ru1—C16—C17	64.9 (2)	C14A—C13A—C18A—C17A	0.2 (5)
C11—Ru1—C16—C17	−13.6 (3)	C19A—C13A—C18A—C17A	−179.3 (3)
N1—Ru1—C16—C22	17.4 (3)	Ru1A—C13A—C18A—C17A	54.8 (3)
N2—Ru1—C16—C22	−60.3 (4)	C14A—C13A—C18A—Ru1A	−54.6 (3)
C15—Ru1—C16—C22	−115.2 (4)	C19A—C13A—C18A—Ru1A	126.0 (3)
C18—Ru1—C16—C22	142.7 (4)	N1A—Ru1A—C18A—C17A	53.2 (3)
C17—Ru1—C16—C22	114.9 (4)	N2A—Ru1A—C18A—C17A	−135.3 (4)
C14—Ru1—C16—C22	−144.5 (4)	C15A—Ru1A—C18A—C17A	−65.6 (2)
C13—Ru1—C16—C22	179.8 (4)	C14A—Ru1A—C18A—C17A	−102.8 (2)
C11—Ru1—C16—C22	101.2 (3)	C16A—Ru1A—C18A—C17A	−28.2 (2)
C15—C16—C17—C18	2.2 (5)	C13A—Ru1A—C18A—C17A	−132.8 (3)
C22—C16—C17—C18	−177.5 (3)	C11A—Ru1A—C18A—C17A	138.0 (2)
Ru1—C16—C17—C18	−52.8 (3)	N1A—Ru1A—C18A—C13A	−174.06 (19)
C15—C16—C17—Ru1	55.1 (3)	N2A—Ru1A—C18A—C13A	−2.6 (5)
C22—C16—C17—Ru1	−124.7 (3)	C15A—Ru1A—C18A—C13A	67.2 (2)
N1—Ru1—C17—C18	−139.5 (2)	C14A—Ru1A—C18A—C13A	29.9 (2)
N2—Ru1—C17—C18	144.8 (3)	C16A—Ru1A—C18A—C13A	104.6 (2)
C15—Ru1—C17—C18	103.4 (2)	C17A—Ru1A—C18A—C13A	132.8 (3)
C16—Ru1—C17—C18	133.8 (3)	C11A—Ru1A—C18A—C13A	−89.3 (2)
C14—Ru1—C17—C18	65.7 (2)	C14A—C13A—C19A—C20A	37.7 (5)
C13—Ru1—C17—C18	29.0 (2)	C18A—C13A—C19A—C20A	−142.8 (3)
C11—Ru1—C17—C18	−53.1 (2)	Ru1A—C13A—C19A—C20A	−54.7 (4)

**supplementary materials**

---

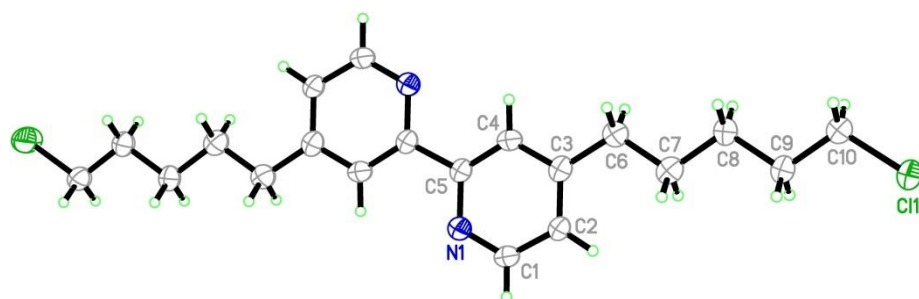
N1—Ru1—C17—C16	86.7 (2)	C14A—C13A—C19A—C21A	−85.7 (4)
N2—Ru1—C17—C16	10.9 (4)	C18A—C13A—C19A—C21A	93.7 (4)
C15—Ru1—C17—C16	−30.5 (2)	Ru1A—C13A—C19A—C21A	−178.2 (3)

---



Compound **23**

Image:



Data:

## supplementary materials

## supplementary materials

## Experimental

## (triclinic)

## Crystal data

$C_{20}H_{20}Cl_2N_2$   
 $M_r = 365.33$   
 Monoclinic,  $C2/m$   
 Hall symbol:  $-C\ 2y$   
 $a = 11.8915\ (14)\ \text{\AA}$   
 $b = 7.2248\ (9)\ \text{\AA}$   
 $c = 11.5664\ (13)\ \text{\AA}$   
 $\beta = 94.649\ (7)^\circ$   
 $V = 990.4\ (2)\ \text{\AA}^3$   
 $Z = 2$

$F(000) = 388$   
 $D_x = 1.225\ \text{Mg m}^{-3}$   
 Cu  $K\alpha$  radiation,  $\lambda = 1.54178\ \text{\AA}$   
 Cell parameters from 2198 reflections  
 $\theta = 3.8\text{--}65.8^\circ$   
 $\mu = 2.96\ \text{mm}^{-1}$   
 $T = 293\ \text{K}$   
 Plate, Colourless  
 $0.24 \times 0.14 \times 0.05\ \text{mm}$

## Data collection

Bruker SMART CCD Apex-II area-detector  
 diffractometer  
 Radiation source: fine-focus sealed tube  
 Graphite monochromator  
 $\phi$  and  $\omega$  scans  
 Absorption correction: Numerical  
 SADABS (Sheldrick, 2008a)  
 $T_{\min} = 0.537$ ,  $T_{\max} = 0.866$

3256 measured reflections  
 893 independent reflections  
 646 reflections with  $I > 2\sigma(I)$   
 $R_{\text{int}} = 0.049$   
 $\theta_{\text{max}} = 66.2^\circ$ ,  $\theta_{\text{min}} = 3.8^\circ$   
 $h = -14 \rightarrow 13$   
 $k = -8 \rightarrow 8$   
 $l = -13 \rightarrow 13$

## Refinement

Refinement on  $F^2$   
 Least-squares matrix: Full  
 $R[F^2 > 2\sigma(F^2)] = 0.115$   
 $wR(F^2) = 0.268$   
 $S = 1.12$   
 893 reflections  
 73 parameters  
 0 restraints  
 Primary atom site location: Structure-invariant direct  
 methods

Secondary atom site location: Difference Fourier map  
 Hydrogen site location: Inferred from neighbouring  
 sites  
 H-atom parameters constrained  
 $w = 1/[\sigma^2(F_o^2) + (0.0701P)^2 + 7.7288P]$   
 where  $P = (F_o^2 + 2F_c^2)/3$   
 $(\Delta/\sigma)_{\text{max}} < 0.001$   
 $\Delta\rho_{\text{max}} = 0.35\ \text{e \AA}^{-3}$   
 $\Delta\rho_{\text{min}} = -0.27\ \text{e \AA}^{-3}$

## Special details

*Experimental.* 'crystal mounted on a Cryoloop using Paratone-N'

*Geometry.* All esds (except the esd in the dihedral angle between two *Ls.* planes) are estimated using the full covariance matrix. The cell esds are taken into account individually in the estimation of esds in distances, angles and torsion angles; correlations between esds in cell parameters are only used when they are defined by crystal symmetry. An approximate (isotropic) treatment of cell esds is used for estimating esds involving *Ls.* planes.

*Refinement.* Refinement of  $F^2$  against ALL reflections. The weighted *R*-factor *wR* and goodness of fit *S* are based on  $F^2$ , conventional *R*-factors *R* are based on *F*, with *F* set to zero for negative  $F^2$ . The threshold expression of  $F^2 > 2\text{sigma}(F^2)$  is used only for calculating *R*-factors(gt) etc. and is not relevant to the choice of reflections for refinement. *R*-factors based on  $F^2$  are statistically about twice as large as those based on *F*, and *R*-factors based on ALL data will be even larger.

## supplementary materials

Fractional atomic coordinates and isotropic or equivalent isotropic displacement parameters ( $\text{\AA}^2$ )

	x	y	z	$U_{\text{eq}}$	Occ. (<1)
C11	1.3439 (2)	0.5000	0.9442 (2)	0.1255 (18)	
N1	0.4988 (6)	0.5000	0.6549 (6)	0.0565 (19)	
C1	0.5702 (7)	0.5000	0.7478 (7)	0.057 (2)	
H1	0.5411	0.5000	0.8200	0.069*	
C2	0.6890 (7)	0.5000	0.7442 (6)	0.053 (2)	
H2	0.7361	0.5000	0.8124	0.063*	
C3	0.7329 (7)	0.5000	0.6395 (7)	0.054 (2)	
C4	0.6574 (7)	0.5000	0.5419 (7)	0.054 (2)	
H4	0.6846	0.5000	0.4687	0.064*	
C5	0.5425 (7)	0.5000	0.5516 (6)	0.0497 (19)	
C6	0.8588 (7)	0.5000	0.6272 (7)	0.064 (2)	
H6A	0.8770	0.3918	0.5827	0.076*	0.50
H6B	0.8770	0.6082	0.5827	0.076*	0.50
C7	0.9322 (8)	0.5000	0.7383 (7)	0.065 (3)	
H7B	0.9152	0.3915	0.7831	0.078*	0.50
H7A	0.9152	0.6085	0.7831	0.078*	0.50
C8	1.0578 (7)	0.5000	0.7187 (7)	0.058 (2)	
H8B	1.0749	0.3915	0.6739	0.070*	0.50
H8A	1.0749	0.6085	0.6739	0.070*	0.50
C9	1.1324 (7)	0.5000	0.8322 (7)	0.065 (2)	
H9B	1.1155	0.6086	0.8771	0.078*	0.50
H9A	1.1155	0.3914	0.8771	0.078*	0.50
C10	1.2555 (7)	0.5000	0.8123 (7)	0.068 (3)	
H10A	1.2722	0.6085	0.7674	0.082*	0.50
H10B	1.2722	0.3915	0.7674	0.082*	0.50

Atomic displacement parameters ( $\text{\AA}^2$ )

	$U^{11}$	$U^{22}$	$U^{33}$	$U^{12}$	$U^{13}$	$U^{23}$
C11	0.0560 (16)	0.257 (5)	0.0616 (16)	0.000	-0.0075 (11)	0.000
N1	0.049 (4)	0.071 (5)	0.049 (4)	0.000	0.004 (3)	0.000
C1	0.059 (5)	0.071 (6)	0.042 (4)	0.000	0.008 (4)	0.000
C2	0.049 (5)	0.064 (5)	0.044 (4)	0.000	-0.003 (4)	0.000
C3	0.058 (5)	0.050 (5)	0.053 (5)	0.000	-0.005 (4)	0.000
C4	0.058 (5)	0.062 (5)	0.042 (4)	0.000	0.009 (4)	0.000
C5	0.050 (5)	0.053 (5)	0.046 (4)	0.000	-0.003 (4)	0.000
C6	0.059 (5)	0.075 (6)	0.057 (5)	0.000	0.004 (4)	0.000
C7	0.070 (6)	0.067 (6)	0.058 (5)	0.000	0.000 (4)	0.000
C8	0.051 (5)	0.061 (5)	0.061 (5)	0.000	-0.003 (4)	0.000
C9	0.054 (5)	0.082 (7)	0.057 (5)	0.000	-0.005 (4)	0.000
C10	0.059 (6)	0.090 (7)	0.054 (5)	0.000	0.001 (4)	0.000

Geometric parameters ( $\text{\AA}$ ,  $^\circ$ )

C11—C10	1.781 (8)	C6—H6A	0.9700
N1—C1	1.315 (10)	C6—H6B	0.9700
N1—C5	1.341 (10)	C7—C8	1.529 (12)
C1—C2	1.416 (11)	C7—H7B	0.9700
C1—H1	0.9300	C7—H7A	0.9700
C2—C3	1.357 (11)	C8—C9	1.524 (10)
C2—H2	0.9300	C8—H8B	0.9700

## supplementary materials

C3—C4	1.384 (11)	C8—H8A	0.9700
C3—C6	1.515 (12)	C9—C10	1.500 (12)
C4—C5	1.380 (11)	C9—H9B	0.9700
C4—H4	0.9300	C9—H9A	0.9700
C5—C5 <sup>i</sup>	1.501 (14)	C10—H10A	0.9700
C6—C7	1.494 (11)	C10—H10B	0.9700
C1—N1—C5	117.1 (7)	C6—C7—H7B	109.1
N1—C1—C2	123.8 (7)	C8—C7—H7B	109.1
N1—C1—H1	118.1	C6—C7—H7A	109.1
C2—C1—H1	118.1	C8—C7—H7A	109.1
C3—C2—C1	118.9 (7)	H7B—C7—H7A	107.8
C3—C2—H2	120.6	C9—C8—C7	112.3 (7)
C1—C2—H2	120.6	C9—C8—H8B	109.1
C2—C3—C4	117.2 (8)	C7—C8—H8B	109.1
C2—C3—C6	122.6 (7)	C9—C8—H8A	109.1
C4—C3—C6	120.2 (8)	C7—C8—H8A	109.1
C5—C4—C3	120.9 (8)	H8B—C8—H8A	107.9
C5—C4—H4	119.5	C10—C9—C8	112.0 (7)
C3—C4—H4	119.5	C10—C9—H9B	109.2
N1—C5—C4	122.1 (7)	C8—C9—H9B	109.2
N1—C5—C5 <sup>i</sup>	115.0 (9)	C10—C9—H9A	109.2
C4—C5—C5 <sup>i</sup>	122.9 (9)	C8—C9—H9A	109.2
C7—C6—C3	115.6 (7)	H9B—C9—H9A	107.9
C7—C6—H6A	108.4	C9—C10—C11	112.6 (6)
C3—C6—H6A	108.4	C9—C10—H10A	109.1
C7—C6—H6B	108.4	C11—C10—H10A	109.1
C3—C6—H6B	108.4	C9—C10—H10B	109.1
H6A—C6—H6B	107.4	C11—C10—H10B	109.1
C6—C7—C8	112.5 (7)	H10A—C10—H10B	107.8
C5—N1—C1—C2	0.000 (2)	C3—C4—C5—N1	0.000 (2)
N1—C1—C2—C3	0.000 (3)	C3—C4—C5—C5 <sup>i</sup>	180.000 (2)
C1—C2—C3—C4	0.000 (2)	C2—C3—C6—C7	0.000 (2)
C1—C2—C3—C6	180.000 (2)	C4—C3—C6—C7	180.000 (2)
C2—C3—C4—C5	0.000 (2)	C3—C6—C7—C8	180.000 (2)
C6—C3—C4—C5	180.000 (2)	C6—C7—C8—C9	180.000 (2)
C1—N1—C5—C4	0.000 (2)	C7—C8—C9—C10	180.000 (2)
C1—N1—C5—C5 <sup>i</sup>	180.000 (2)	C8—C9—C10—C11	180.000 (1)

Symmetry code: (i)  $-x+1, -y+1, -z+1$ .

## References

- (1) Caldeira, K.; Jain, A. K.; Hoffert, M. I. *Science* **2003**, 299, 2052.
- (2) Perlin, J. *New York* **2004**, 1.
- (3) O'Regan, B.; Grätzel, M. *Nature* **1991**, 353, 737.
- (4) Nazeeruddin, M. K.; Kay, A.; Rodicio, I.; Humphry-Baker, R.; Mueller, E.; Liska, P.; Vlachopoulos, N.; Graetzel, M. *Journal of the American Chemical Society* **1993**, 115, 6382.
- (5) Gratzel, M. *Nature* **2001**, 414, 338.
- (6) Gratzel, M. *Inorg Chem* **2005**, 44, 6841.
- (7) Kopecky, A. G., E. In *Photochemistry*; Albini, A., Ed.; Royal Society of Chemistry: 2009; Vol. 37, p 362.
- (8) Nissha Printing Co., L. 1996; Vol. 2012, p Diagram of DSSC; ; [http://www.nissha.co.jp/english/company/r\\_and\\_d/dsc/dsc\\_1.html](http://www.nissha.co.jp/english/company/r_and_d/dsc/dsc_1.html).
- (9) Argazzi, R.; Bignozzi, C. A.; Heimer, T. A.; Castellano, F. N.; Meyer, G. J. *Inorganic Chemistry* **1994**, 33, 5741.
- (10) Zaban, A.; Ferrere, S.; Gregg, B. A. *Journal of Physical Chemistry B* **1998**, 102, 452.
- (11) Saupe, G. B.; Mallouk, T. E.; Kim, W.; Schmehl, R. H. *Journal of Physical Chemistry B* **1997**, 101, 2508.
- (12) Trammell, S. A.; Wimbish, J. C.; Odobel, F.; Gallagher, L. A.; Narula, P. M.; Meyer, T. J. *Journal of the American Chemical Society* **1998**, 120, 13248.
- (13) Li, G.; Sproviero, E. M.; McNamara, W. R.; Snoeberger, R. C., 3rd; Crabtree, R. H.; Brudvig, G. W.; Batista, V. S. *The journal of physical chemistry. B* **2010**, 114, 14214.
- (14) Nelson, I. V.; Iwamoto, R. T. *Journal of Electroanalytical Chemistry (1959)* **1964**, 7, 218.
- (15) Richards, C. E.; Anderson, A. Y.; Martiniani, S.; Law, C. H.; O'Regan, B. C. *Journal of Physical Chemistry Letters* **2012**, 3, 1980.
- (16) Hagfeldt, A.; Boschloo, G.; Sun, L.; Kloo, L.; Pettersson, H. *Chem Rev* **2010**, 110, 6595.
- (17) Fitzmaurice, D. *Solar Energy Materials and Solar Cells* **1994**, 32, 289.
- (18) Ardo, S.; Meyer, G. J. *Chem Soc Rev* **2009**, 38, 115.
- (19) Li, X.; Reynal, A.; Barnes, P.; Humphry-Baker, R.; Zakeeruddin, S. M.; De Angelis, F.; O'Regan, B. C. *Physical chemistry chemical physics : PCCP* **2012**, 14, 15421.
- (20) Wei, Q.; Galoppini, E. *Tetrahedron* **2004**, 60, 8497.
- (21) Clark, C. C.; Meyer, G. J.; Wei, Q.; Galoppini, E. *The journal of physical chemistry. B* **2006**, 110, 11044.
- (22) Hagberg, D. P.; Marinado, T.; Karlsson, K. M.; Nonomura, K.; Qin, P.; Boschloo, G.; Brinck, T.; Hagfeldt, A.; Sun, L. *J Org Chem* **2007**, 72, 9550.
- (23) Wiberg, J.; Marinado, T.; Hagberg, D. P.; Sun, L.; Hagfeldt, A.; Albinsson, B. *The journal of physical chemistry. B* **2010**, 114, 14358.
- (24) Spokoyny, A. M.; Li, T. C.; Farha, O. K.; Machan, C. W.; She, C.; Stern, C. L.; Marks, T. J.; Hupp, J. T.; Mirkin, C. A. *Angew Chem Int Ed Engl* **2010**, 49, 5339.
- (25) DeVries, M. J.; Pellin, M. J.; Hupp, J. T. *Langmuir* **2010**, 26, 9082.

- (26) Wang, P.; Zakeeruddin, S. M.; Moser, J. E.; Nazeeruddin, M. K.; Sekiguchi, T.; Gratzel, M. *Nat Mater* **2003**, 2, 402.
- (27) Nazeeruddin, M. K.; Zakeeruddin, S. M.; Lagref, J. J.; Liska, P.; Comte, P.; Barolo, C.; Viscardi, G.; Schenk, K.; Graetzel, M. *Coordination Chemistry Reviews* **2004**, 248, 1317.
- (28) Jang, S. R.; Yum, J. H.; Klein, C.; Kim, K. J.; Wagner, P.; Officer, D.; Gratzel, M.; Nazeeruddin, M. K. *J Phys Chem C* **2009**, 113, 1998.
- (29) Nazeeruddin, M. K.; Klein, C.; Liska, P.; Grätzel, M. *Coordination Chemistry Reviews* **2005**, 249, 1460.
- (30) Klein, C.; Nazeeruddin, M. K.; Liska, P.; Di Censo, D.; Hirata, N.; Palomares, E.; Durrant, J. R.; Gratzel, M. *Inorg Chem* **2005**, 44, 178.
- (31) Thyagarajan, S.; Galoppini, E.; Persson, P.; Giaimuccio, J. M.; Meyer, G. J. *Langmuir* **2009**, 25, 9219.
- (32) Rochford, J.; Galoppini, E. *Langmuir* **2008**, 24, 5366.
- (33) Wang, D.; Mendelsohn, R.; Galoppini, E.; Hoertz, P. G.; Carlisle, R. A.; Meyer, G. J. *Journal of Physical Chemistry B* **2004**, 108, 16642.
- (34) Boixel, J.; Fortage, J.; Blart, E.; Pellegrin, Y.; Hammarstrom, L.; Becker, H. C.; Odobel, F. *Dalton Trans* **2010**, 39, 1450.
- (35) Meier, H.; Muhling, B.; Gerold, J.; Jacob, D.; Oehlhof, A. *European Journal of Organic Chemistry* **2007**, 2007, 625.
- (36) Galoppini, E. *Coordination Chemistry Reviews* **2004**, 248, 1283.
- (37) He, S.; Buel, A. A.; Hanley, J. M.; Morgan, B. P.; Tennyson, A. G.; Smith, R. C. *Macromolecules* **2012**, 45, 6344.
- (38) Vokata, T.; Moon, J. H. *Macromolecules* **2013**, 46, 1253.
- (39) Chu, C. C.; Wang, X.; Li, S.; Ge, S. G.; Ge, L.; Yu, J. H.; Yan, M. *Analytical Methods* **2012**, 4, 4339.
- (40) Santella, M.; Mazzanti, V.; Jevric, M.; Parker, C. R.; Broman, S. L.; Bond, A. D.; Nielsen, M. B. *J Org Chem* **2012**, 77, 8922.
- (41) Jeschke, G.; Sajid, M.; Schulte, M.; Ramezani, N.; Volkov, A.; Zimmermann, H.; Godt, A. *J Am Chem Soc* **2010**, 132, 10107.
- (42) Zhang, Y. Y.; Galoppini, E.; Johansson, P. G.; Meyer, G. J. *Pure and Applied Chemistry* **2011**, 83, 861.
- (43) Wang, H. Y.; He, G.; Chen, X. L.; Liu, T. H.; Ding, L. P.; Fang, Y. *Journal of Materials Chemistry* **2012**, 22, 7529.
- (44) James, P. V.; Yoosaf, K.; Kumar, J.; Thomas, K. G.; Listorti, A.; Accorsi, G.; Armaroli, N. *Photochemical & photobiological sciences : Official journal of the European Photochemistry Association and the European Society for Photobiology* **2009**, 8, 1432.
- (45) Albinsson, B.; Eng, M. P.; Pettersson, K.; Winters, M. U. *Physical Chemistry Chemical Physics* **2007**, 9, 5847.
- (46) Duvanel, G.; Grilj, J.; Vauthey, E. *The journal of physical chemistry. A* **2013**, 117, 918.
- (47) Soler, M. A.; Roitberg, A. E.; Nelson, T.; Tretiak, S.; Fernandez-Alberti, S. *The journal of physical chemistry. A* **2012**, 116, 9802.
- (48) Wielopolski, M.; Atienza, C.; Clark, T.; Guldi, D. M.; Martin, N. *Chemistry* **2008**, 14, 6379.
- (49) Colvin, M. T.; Ricks, A. B.; Wasielewski, M. R. *The journal of physical chemistry. A* **2012**, 116, 2184.
- (50) Pettersson, K.; Kyrychenko, A.; Ronnow, E.; Ljungdahl, T.; Martensson, J.; Albinsson, B. *The journal of physical chemistry. A* **2006**, 110, 310.

- (51) Myahkostupov, M.; Piotrowiak, P.; Wang, D.; Galoppini, E. *J Phys Chem C* **2007**, *111*, 2827.
- (52) Lundqvist, M. J.; Galoppini, E.; Meyer, G. J.; Persson, P. *The journal of physical chemistry. A* **2007**, *111*, 1487.
- (53) Persson, P.; Knitter, M.; Galoppini, E. *RSC Advances* **2012**, *2*, 7868.
- (54) Zakeeruddin, S. M.; Nazeeruddin, M. K.; Humphry-Baker, R.; Gratzel, M.; Shklover, V. *Inorganic Chemistry* **1998**, *37*, 5251.
- (55) Zakeeruddin, S. M.; Nazeeruddin, M. K.; Humphry-Baker, R.; Pechy, P.; Quagliotto, P.; Barolo, C.; Viscardi, G.; Gratzel, M. *Langmuir* **2002**, *18*, 952.
- (56) Rajesh, K.; Somasundaram, M.; Saiganesh, R.; Balasubramanian, K. K. *J Org Chem* **2007**, *72*, 5867.
- (57) Grosshenny, V.; Romero, F. M.; Ziessel, R. *Journal of Organic Chemistry* **1997**, *62*, 1491.
- (58) Orsini, A.; Viterisi, A.; Bodlenner, A.; Weibel, J. M.; Pale, P. *Tetrahedron Letters* **2005**, *46*, 2259.
- (59) Theodorou, V.; Skobridis, K.; Tzakos, A. G.; Ragoussis, V. *Tetrahedron Letters* **2007**, *48*, 8230.
- (60) Bair, J. S.; Harrison, R. G. *J Org Chem* **2007**, *72*, 6653.
- (61) Jones, R. A.; Roney, B. D.; Sasse, W. H. F.; Wade, K. O. *Journal of the Chemical Society* **1967**, *2*, 106.
- (62) Sprecher, M.; Breslow, R.; Uziel, O.; Link, T. M. *Org Prep Proced Int* **1994**, *26*, 696.
- (63) Julemont, F.; de Leval, X.; Michaux, C.; Renard, J. F.; Winum, J. Y.; Montero, J. L.; Damas, J.; Dogne, J. M.; Pirotte, B. *J Med Chem* **2004**, *47*, 6749.
- (64) Lee, C. H.; Galoppini, E. *J Org Chem* **2010**, *75*, 3692.
- (65) Kochi, J. K. *Journal of the American Chemical Society* **1957**, *79*, 2942.
- (66) Lee, C. H.; Zhang, Y. Y.; Romayanantakit, A.; Galoppini, E. *Tetrahedron* **2010**, *66*, 3897.
- (67) Kuang, D.; Ito, S.; Wenger, B.; Klein, C.; Moser, J. E.; Humphry-Baker, R.; Zakeeruddin, S. M.; Gratzel, M. *J Am Chem Soc* **2006**, *128*, 4146.
- (68) Barder, T. E.; Walker, S. D.; Martinelli, J. R.; Buchwald, S. L. *J Am Chem Soc* **2005**, *127*, 4685.
- (69) Sonogashira, K. *Journal of Organometallic Chemistry* **2002**, *653*, 46.
- (70) Zastrow, M.; Thyagarajan, S.; Ahmed, S. A.; Haase, P.; Seedorff, S.; Gelman, D.; Wachtveitl, J.; Galoppini, E.; Ruck-Braun, K. *Chemistry, an Asian journal* **2010**, *5*, 1202.
- (71) Wang, D., Rutgers University - Newark, 2004.
- (72) Hara, K.; Sugihara, H.; Tachibana, Y.; Islam, A.; Yanagida, M.; Sayama, K.; Arakawa, H.; Fujihashi, G.; Horiguchi, T.; Kinoshita, T. *Langmuir* **2001**, *17*, 5992.
- (73) Bora, T.; Singh, M. M. *Transition Met Chem* **1978**, *3*, 27.
- (74) Bennett, M. A.; Matheson, T. W.; Robertson, G. B.; Steffen, W. L.; Turney, T. W. *Journal of the Chemical Society, Chemical Communications* **1979**, *0*, 32.
- (75) Thamapipol, S.; Bernardinelli, G.; Besnard, C.; Kundig, E. P. *Org Lett* **2010**, *12*, 5604.
- (76) De Angelis, F.; Fantacci, S.; Selloni, A.; Nazeeruddin, M. K. *Chemical Physics Letters* **2005**, *415*, 115.
- (77) Qu, P.; Meyer, G. J. *Langmuir* **2001**, *17*, 6720.
- (78) Kelly, C. A.; Farzad, F.; Thompson, D. W.; Stipkala, J. M.; Meyer, G. J. *Langmuir* **1999**, *15*, 7047.

- (79) Bergeron, B. V.; Meyer, G. J. *The Journal of Physical Chemistry B* **2003**, *107*, 245.
- (80) Abrahamsson, M.; Johansson, P. G.; Ardo, S.; Kopecky, A.; Galoppini, E.; Meyer, G. J. *Journal of Physical Chemistry Letters* **2010**, *1*, 1725.
- (81) Haque, S. A.; Tachibana, Y.; Klug, D. R.; Durrant, J. R. *The journal of physical chemistry. B* **1998**, *102*, 1745.
- (82) Boschloo, G.; Fitzmaurice, D. *Journal of Physical Chemistry B* **1999**, *103*, 7860.
- (83) Williams, G.; Watts, D. C. *Transactions of the Faraday Society* **1970**, *66*, 80.
- (84) Soeder gren, S.; Hagfeldt, A.; Olsson, J.; Lindquist, S.-E. *The Journal of Physical Chemistry* **1994**, *98*, 5552.
- (85) Katoh, R.; Furube, A. *Journal of Physical Chemistry Letters* **2011**, *2*, 1888.
- (86) O'Regan, B.; Moser, J.; Anderson, M.; Graetzel, M. *J Phys Chem* **1990**, *94*, 8720.
- (87) O'Regan, B. C.; Durrant, J. R. *Acc Chem Res* **2009**, *42*, 1799.
- (88) Vargas-Florencia, D.; Petrov, O. V.; Furo, I. *Journal of colloid and interface science* **2007**, *305*, 280.
- (89) Stanbury, D. M. In *Advances in Inorganic Chemistry*; Sykes, A. G., Ed.; Academic Press: 1989; Vol. Volume 33, p 69.
- (90) Wilmarth, W. K.; Stanbury, D. M.; Byrd, J. E.; Po, H. N.; Chua, C.-P. *Coordination Chemistry Reviews* **1983**, *51*, 155.
- (91) Boschloo, G.; Hagfeldt, A. *Acc Chem Res* **2009**, *42*, 1819.
- (92) Sauvé, G.; Cass, M. E.; Coia, G.; Doig, S. J.; Lauermann, I.; Pomykal, K. E.; Lewis, N. S. *The Journal of Physical Chemistry B* **2000**, *104*, 6821.
- (93) Kuciauskas, D.; Freund, M. S.; Gray, H. B.; Winkler, J. R.; Lewis, N. S. *The Journal of Physical Chemistry B* **2001**, *105*, 392.
- (94) Daenke, T.; Kwon, T. H.; Holmes, A. B.; Duffy, N. W.; Bach, U.; Spiccia, L. *Nat Chem* **2011**, *3*, 211.
- (95) Nusbaumer, H.; Moser, J.-E.; Zakeeruddin, S. M.; Nazeeruddin, M. K.; Grätzel, M. *The Journal of Physical Chemistry B* **2001**, *105*, 10461.
- (96) Klahr, B. M.; Hamann, T. W. *J Phys Chem C* **2009**, *113*, 14040.
- (97) Kuwahara, Y.; Akiyama, T.; Yamada, S. *Langmuir* **2001**, *17*, 5714.
- (98) Akiyama, T.; Nitahara, S.; Inoue, S.; Yamada, S. *Photochemical & photobiological sciences : Official journal of the European Photochemistry Association and the European Society for Photobiology* **2004**, *3*, 26.
- (99) Nitahara, S.; Akiyama, T.; Inoue, S.; Yamada, S. *The journal of physical chemistry. B* **2005**, *109*, 3944.
- (100) Ipe, B. I.; Yoosaf, K.; Thomas, K. G. *J Am Chem Soc* **2006**, *128*, 1907.
- (101) Luo, J.; Isied, S. S. *Langmuir* **1998**, *14*, 3602.
- (102) Montgomery, H. J.; Pelleteret, D.; Bell, S. E.; Fletcher, N. C. *Inorg Chem* **2011**, *50*, 2738.
- (103) Friederici, M.; Angurell, I.; Rossell, O.; Seco, M.; Divins, N. J.; Llorca, J. *Organometallics* **2012**, *31*, 722.
- (104) Zhu, L.; Yan, H.; Nguyen, K. T.; Tian, H.; Zhao, Y. *Chem Commun (Camb)* **2012**, *48*, 4290.
- (105) Chen, D. T.; De, R.; Mohler, D. L. *Synthesis-Stuttgart* **2009**, *2009*, 211.
- (106) Maskus, M.; Abruna, H. D. *Langmuir* **1996**, *12*, 4455.
- (107) Hu, J.; Fox, M. A. *J Org Chem* **1999**, *64*, 4959.
- (108) Fuldner, S.; Mild, R.; Siegmund, H. I.; Schroeder, J. A.; Gruberc, M.; Konig, B. *Green Chemistry* **2010**, *12*, 400.



- (109) Gillaizeau-Gauthier, I.; Odobel, F.; Alebbi, M.; Argazzi, R.; Costa, E.; Bignozzi, C. A.; Qu, P.; Meyer, G. J. *Inorg Chem* **2001**, *40*, 6073.
- (110) Klein, C.; Baranoff, E.; Nazeeruddin, M. K.; Gratzel, M. *Tetrahedron Letters* **2010**, *51*, 6161.
- (111) Zhang, S.-J.; Ge, Q.-F.; Guo, D.-W.; Hu, W.-X.; Liu, H.-Z. *Bioorganic & Medicinal Chemistry Letters* **2010**, *20*, 3078.
- (112) Cabeza, J. A.; del Rio, I.; Martinez-Mendez, L.; Miguel, D. *Journal of Organometallic Chemistry* **2007**, *692*, 4407.
- (113) Cooke, M. W.; Murphy, C. A.; Cameron, T. S.; Beck, E. J.; Vamvounis, G.; Aquino, M. A. S. *Polyhedron* **2002**, *21*, 1235.
- (114) Marin, V.; Wouters, D.; Hoeppener, S.; Holder, E.; Schubert, U. S. *Australian Journal of Chemistry* **2007**, *60*, 414.
- (115) T. W. Green, P. G. M. W. *Protective Groups in Organic Synthesis*; Wiley-Interscience, 1999.

April 2013

**Curriculum Vitae****Andrew Kopecky**

Belleville NJ 07109

973-568-7712

andrew.kopecky@gmail.com

**Education Experiences**

- Sept 2006-May 2013      Ph.D., Chemistry – *N3-Type Ruthenium Rigid Rod Dyes for Studying Solar Cell Properties*  
 Rutgers University – Newark; Advisor: Elena Galoppini  
 Anticipated Graduation May 2013
- Sept 2001-Dec 2005      B.S. Mathematics  
 University of Maryland – College Park

**Publications**

1. *Synthesis of Bifunctional Ru Complexes with 1,2-Dithiolane and Carboxylate-Substituted Ligands.* Kopecky, A.; Liu, G.; Agushi, A.; Agrios, A. G.; Galoppini, E. *Eur. J. Inorg. Chem.* Submitted March **2013**.
2. *Distance Dependent Electron Transfer at TiO<sub>2</sub> Interfaces Sensitized with Phenyleneethynylene Bridged RuII-Isothiocyanate Compounds.* Johansson, P. G.; Kopecky, A.; Galoppini, E.; Meyer, G. J. *J. Am. Chem Soc.* Submitted March **2013**.
3. *Decreased Interfacial Charge Recombination Rate Constants with N3-Type Sensitizers.* Abrahamsson, M.; Johansson, P. G.; Ardo, S.; Kopecky, A.; Galoppini, E.; Meyer, G. J. *J. Phys. Chem. Letters.* **2010** 1 1725-1728. DOI: 10.1021/jz100546y
4. *Multi-component arrays for interfacial electronic processes on the surface of nanostructured metal oxide semiconductors.* Kopecky, A.; Galoppini, E. *Photochemistry.* **2009** 37 362-392. DOI: 10.1039/B813865F

**Contributed Presentations at Conferences and Meetings**

- May 29-June 2, 2012      Mid-Atlantic Regional Meeting, ACS, Baltimore, MD (talk: *Molecular Level Control for Excited State Electron Injection and Charge Recombination at Sensitized TiO<sub>2</sub> Interfaces*)
- May 21-24, 2011      Mid-Atlantic Regional Meeting, ACS, College Park, MD  
 (poster: *N3-type dyes for Open-Circuit Photovoltage Studies*)
- July 2011      Gordon Research Symposium, MA (talk: *N3-type dyes for Open-Circuit Photovoltage Studies*)

November 16, 2011      Annual Chemistry Graduate Students Poster Session (poster:  
*N3-type dyes for Open-Circuit Photovoltage Studies*)

### Teaching and Tutoring

Jan 2007-May 2011	World of Chemistry Laboratory for Nursing Students
Mar 2009-May 2009	Tutoring for Organic Biochemistry
Sept 2007-Dec 2007	General Chemistry Laboratory

### Other Activities

Research Volunteer – July 2011-March 2013

- Research volunteer at Newark's Beth Israel Medical Center in Pediatric Emergency Department
- Assisted graduate fellows on research project detecting prevalence of sexually-transmitted disease in urban population
- Assisted ED staff as needed
- Maintained patient confidentiality while obtaining consent for study
- Prepared urine sample for study

Chemistry Graduate Student Group – August 2011-May 2013

- Organized First Annual Chemistry Graduate Student Poster Session – November 2011
- Organized Second Annual Chemistry Graduate Student Poster Session – November 2012
- President and founding member

Lab Supervision – June 2009-May 2013

- Supervision and guidance of four undergraduate students and one high school student for research towards N3-type dye synthesis
- Rutgers University – Newark, Dr. Elena Galoppini's Lab

Ballroom Dance Club – Sep 2004-Dec 2005

- University of Maryland, College Park
- Participated in DCDI Ballroom Competition, 2005